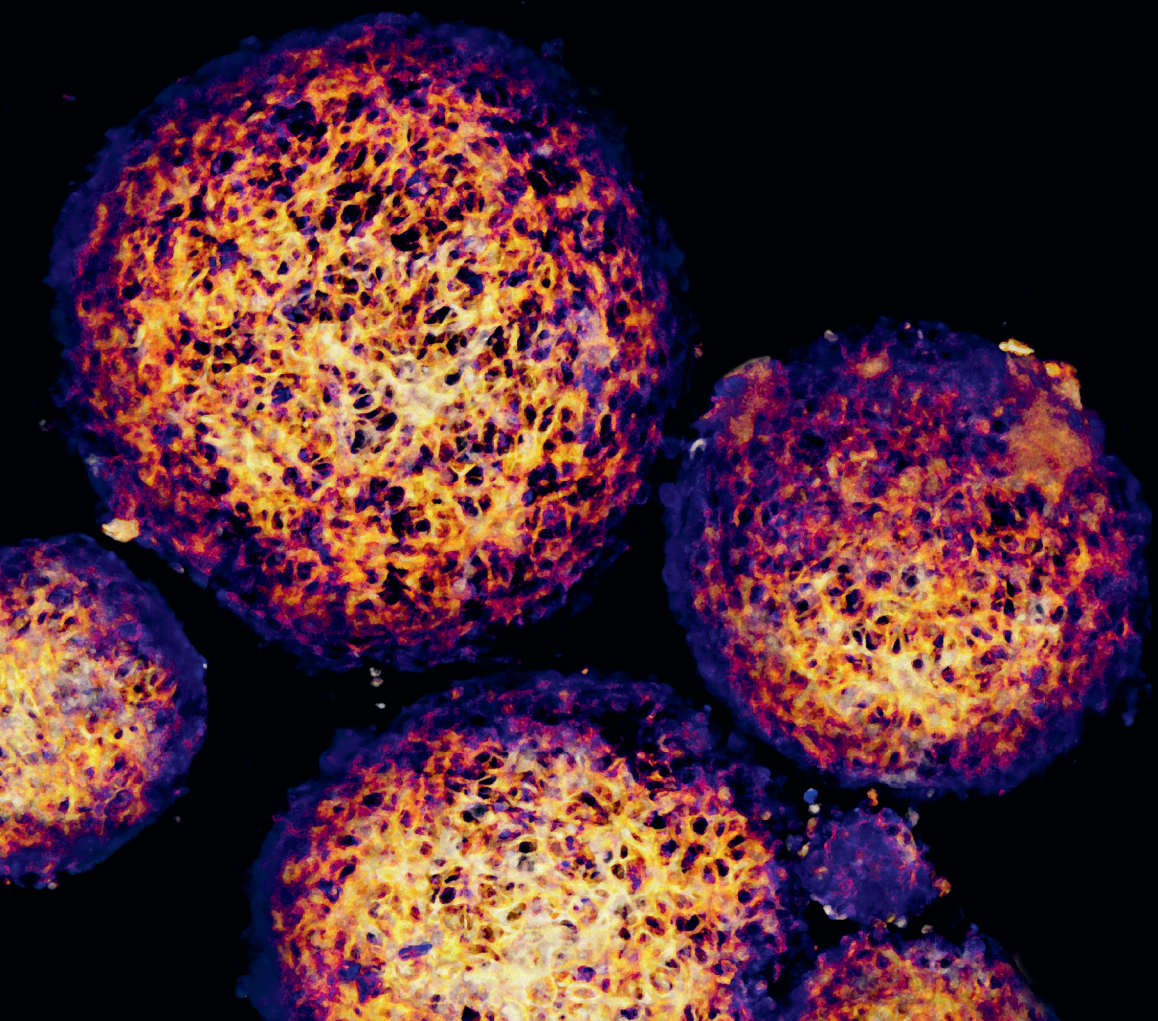


Improving surgery in pediatric oncology by fluorescence- and 3D imaging

LIANNE WELLENS



Improving surgery in pediatric
oncology by fluorescence-
and 3D imaging

LIANNE WELLENS

Improving surgery in pediatric oncology by fluorescence- and 3D imaging
PhD Thesis, Utrecht University, The Netherlands
©Lianne Wellens, Utrecht, 2022

All rights reserved. No part of this thesis may be reproduced or transmitted in any form or by any means without prior written permission from the author. The copyright of the papers that have been published or have been accepted for publication has been transferred to the respective journals.

Funding for this thesis was provided by the Villa Joep Foundation and the Children Cancer Free foundation (KiKa).

The printing of this thesis was financially supported by The Princess Máxima Center for Pediatric Oncology, Pfizer Biopharmaceuticals Group, Quest Medical Imaging and RVC Medical IT B.V..

Provided by thesis specialist Ridderprint, www.ridderprint.nl

Printing: Ridderprint

Cover: Lianne Wellens & Ravian van Ineveld

Lay out and design: Dagmar van Schaik, persoonlijkproefschrift.nl

ISBN: 978-94-6458-088-4

Proefschrift

ter verkrijging van de graad van doctor aan de Universiteit Utrecht
op gezag van de rector magnificus, prof.dr. H.R.B.M. Kummeling,
ingevolge het besluit van het college voor promoties
in het openbaar te verdedigen
op vrijdag 11 maart 2022 des middags te 2.15 uur

door

Lianneke Marline Wellens

geboren op 26 mei 1991
te Rijsenhout

Promotor: Prof.dr. M.H.W.A. Wijnen

Copromotoren: Dr. A.C. Rios
Dr. A.L. Vahrmeijer

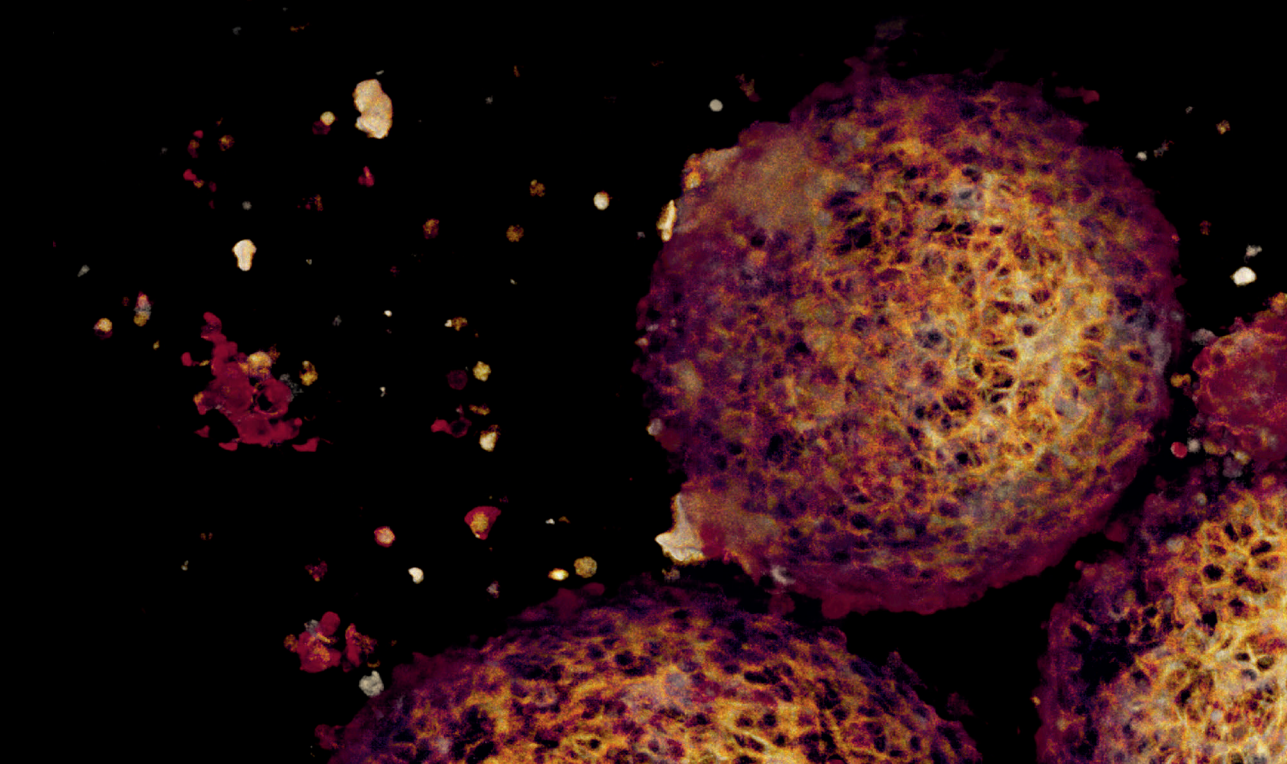
TABLE OF CONTENT

1) General introduction and outline of this thesis	7
<hr/>	
PART I - Facing Complications in Pediatric Surgery	19
<hr/>	
2) Comparison of 3-dimensional and augmented reality kidney models with conventional imaging data in the preoperative assessment of children with Wilms tumors	21
3) Complications of neuroblastoma surgery - a systematic review	41
<hr/>	
PART II - Translational Science for Image-guided Surgery	91
<hr/>	
4) Preclinical validation establishes anti-GD2-IRDye800CW as a fluorescence guided surgery probe for high-risk neuroblastoma	93
5) High-resolution 3D imaging of fixed and cleared organoids	119
6) Tumor organoids and 3D imaging offer a patient-specific screening tool for FGS probes	145
<hr/>	
PART III - Bridging the Gap between Translational Science and Surgery in Pediatric Oncology	169
<hr/>	
7) Trial design: a phase I first-in-human imaging study of anti-GD2-IRDye800CW in patients with high-risk neuroblastoma	171
<hr/>	
PART IV	201
<hr/>	
8) Discussion and future perspectives	203
<hr/>	
APPENDICES	213
<hr/>	



CHAPTER 1

**General introduction and
outline of this thesis**



New imaging techniques in surgery are widely explored. A few examples of technological developments that have been successfully introduced in the operation room in the last decade are 3D printing and augmented reality (AR) for surgical planning. In addition, during surgery, the use of fluorescence guided surgery is increasing to intra-operatively detect tumor tissue^{1,2}. While the field of surgical oncology is evolving rapidly for adult patients, pediatric surgery has been lagging behind. Therefore, there is an urgent need to explore and implement new imaging technologies to optimize pediatric oncology surgery outcomes. This is of particular importance for two common childhood cancers: Wilms tumors and neuroblastoma, for which surgery has been proven especially challenging and prone to intraoperative complications^{3,4}.

PARTIAL NEPHRECTOMY IS A CHALLENGE IN THE TREATMENT OF WILMS TUMORS

A frequently performed procedure by pediatric oncologic surgeons is the resection of Wilms tumors. Wilms tumors are the most frequent occurring pediatric malignancies in the kidney. The overall survival rate of children with Wilms tumor lies around 90%⁵, yet approximately 5% of the cases present with bilateral disease, where both kidneys contain tumors. This group has an overall survival rate of roughly 80%⁶. In patients with bilateral disease, nephron sparing surgery (NSS) is the preferred treatment of choice. Operative morbidity, such as prolonged urinary leakage, infections and intestinal obstructions^{6,7} occur more frequently compared to patients with unilateral Wilms tumor. Also, nephron sparing surgery carries a higher rate of incomplete resection (up to 30%), leading to additional radiotherapy treatment and possibly more loss of renal function⁸. Compared to unilateral tumors, bilateral disease carries a higher risk for end-stage renal disease (12%). To reduce long-term kidney function loss and the occurrence of perioperative complications and to facilitate complete tumor resection, an improved personalized planning and surgical strategy is mandatory.

3D PRINTING AND AUGMENTED REALITY TECHNIQUES FOR THE OPERATIVE PLANNING OF WILMS TUMOR

To facilitate a personalized surgery planning, 3D printing and Virtual or augmented reality (AR) are upcoming tools to help inform and prepare surgeons for a difficult procedure by creating personalized tumor models⁹⁻¹². To prevent residual tumor

tissue in partial nephrectomies, we invested new imaging modalities to assist the surgical planning. In **chapter 2**, we explored the possibility to convert the data of existing preoperative imaging modalities (CT and/or MRI) into 3D-files. A panel of pediatric oncology surgeons in the Netherlands was then asked to evaluate the 3D visualization techniques and report back on the potential added value of their use prior to surgery for Wilms tumor cases eligible for partial nephrectomy.

SURGERY IS IMPORTANT IN THE TREATMENT OF HIGH-RISK NEUROBLASTOMA

1

Neuroblastoma accounts for 7-10% of all childhood cancers and it is the most common cancer diagnosed during infancy¹³. Neuroblastoma is derived from precursor cells of the sympathetic nervous system. About half of all neuroblastomas arise in the medulla of the adrenal gland, while the remaining originate in paraspinal sympathetic ganglia in the chest, abdomen, or in pelvic ganglia^{13,14}.

Neuroblastoma is a heterogeneous tumor with a variable clinical course that can be divided into low risk disease (stage 1,2, 4S) intermediate risk (stage 3) and high risk disease (stage 4)¹⁵. The long-term overall survival (OS) is good to excellent in low-risk disease (5-year OS >85%) but remains poor in patients with high-risk disease (5-year OS <50%)¹⁶. Of all children with neuroblastoma, around 60% are categorized as high-risk disease¹⁷. High-risk neuroblastoma is treated intensively with chemotherapy, surgery, high-dose chemotherapy, autologous stem-cell transplantation, radiotherapy and recently introduced immunotherapy¹⁸. In some patients, radio-active metaiodobenzylguanidine (MIBG) is added to the therapy. Because of this intensive treatment regimen, overall survival improved from 19% between 1990 and 1994 to 44% between 2010 and 2014¹⁷.

Surgery has an important place in treating high-risk neuroblastoma. Pre-operative chemotherapy is administered to decrease the tumor size in order to facilitate surgery. The surgical procedure is often referred to as 'debulking'. The ultimate goal of the surgeon is to remove all remaining tumor tissue. However, because of the encasement of vascular structures and the capacity of the tumor to invade into surrounding organs, surgery is almost never radical¹⁹. Therefore, the realistic aim of the surgeon is to remove as much neuroblastoma tissue as possible without causing permanent damage. The debulking strategy is further supported by the observation that removing more than 90% of the tumor does not improve the probability of survival^{20,21}. However, the optimal amount of tumor that should be removed remains unclear²².

After surgery, a pathologist specialized in pediatric tumors will score the resected tumor based on the Shimada classification²³ for further diagnostic and treatment stratification purposes. Distinction is made between neuroblastoma (immature), ganglioneuroblastoma (intermediate) and ganglioneuroma (mature) tumor tissue. All three tumor-types can be identified within the same patient (**figure 1**), illustrating the heterogeneity of neuroblastoma even within one tumor. During surgery, it is impossible for the surgeon to differentiate between these three pathological tumor stages. Of the three subtypes, neuroblastoma-tissue is considered to be most malignant, whereas ganglioneuroma is considered non-malignant. Therefore, it would be of importance if this differentiation could be made in real time during surgery. This approach would allow the surgeon to focus on removing the most malignant tissue and take less risk in case of non-malignant tumor tissue. Even more importantly, it is difficult for the surgeon to make the differentiation between normal and tumor tissue. As a result, surgery-related complications occur frequently, including hemorrhage, (unplanned) nephrectomy and chylous leakage as reviewed in **chapter 3**.

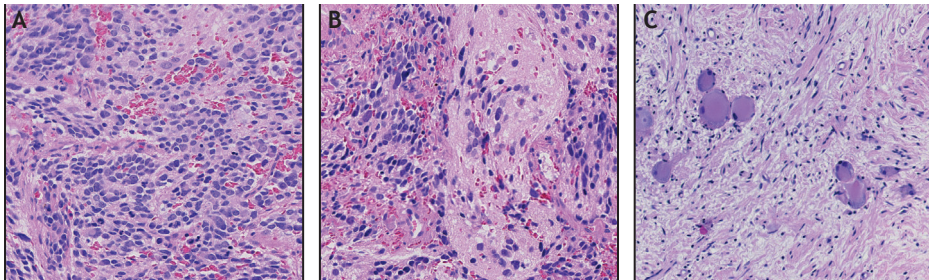


Figure 1. Hematoxylin and Eosin (HE) staining showing **a)** neuroblastoma, **b)** ganglioneuroblastoma and **c)** ganglioneuroma tissue from a patient diagnosed with high-risk neuroblastoma after chemotherapy treatment. Images were generated by the author of this thesis with the help of prof. dr. Ronald de Krijger from the pathology department of the Princess Máxima Center.

FLUORESCENCE GUIDED SURGERY IS A PROMISING TOOL IN CLINICAL CARE OF NEUROBLASTOMA

Fluorescence guided surgery (FGS) could be a powerful tool for limiting surgery-related complications in neuroblastoma. In the last decade, FGS has been introduced for surgical navigation, with clear clinical benefit in gliomas²⁴, and promising results for multiple solid tumors in ongoing phase III trials²⁵. A fluorescent agent is administered to visualize the tumor with high sensitivity and sufficient contrast to normal background tissue. Fluorescent agents often emit wavelengths in the near-infrared (NIR) region, between a 650 and 800nm wavelength, and can thereby penetrate deeper into the tissue, up to 10 mm, with less scattering and autofluorescence compared to visual white light (**figure 2a**)^{26,27}. The first tracers developed were not tumor specific and were labelling tumor cells based on the enhanced permeability and retention (EPR) effect. This entails that fluorescence particles or molecules tend to accumulate in tumors or pathological lymph nodes more easily than they do in normal tissues. Therefore, they reside longer in malignant tissue. In other words, the vasculature of tumor tissue is more permeable to these fluorophores than the vasculature of normal tissue. This approach uses the non-specific dyes such as indocyanogreen (ICG)^{2,28} and methylene blue (MB)^{29,30}. This way of tumor imaging has been around for almost a decade. However, identification of tumor-specific targets has opened up possibilities to fluorescently label tumor cells with greater specificity. For malignant glioma the use of 5-Aminolevulinic acid (5-ALA)^{31,32} has shown very promising results. Therefore, more recently, there has been a shift towards molecular fluorescence imaging using tumor-specific fluorescent tracers^{33,34}, such as antibodies that specifically bind to surface antigens. When conjugated to a NIR fluorophore, the imaging agent bound to the targeted cancer cells, will light up when excited by a NIR-light source, whereas normal tissue is expected to be significantly less fluorescent, once the unbound tracer has been cleared from the human body (**figure 2b**).

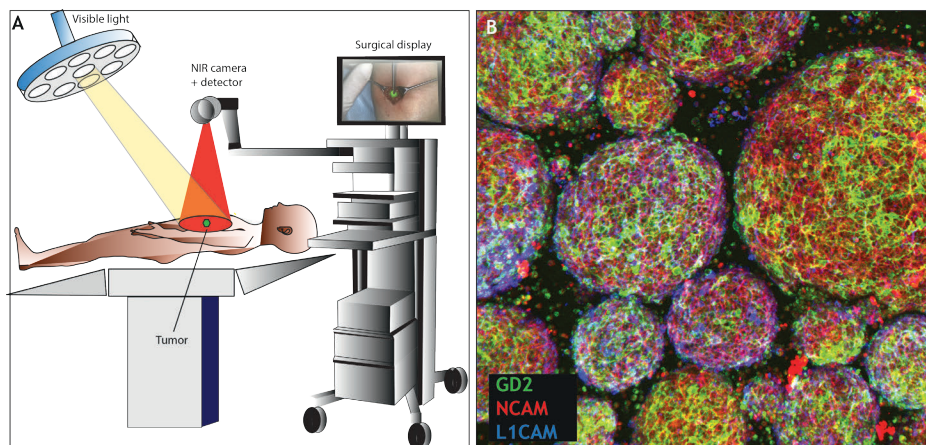


Figure 2. a) The mechanics of NIR fluorescence imaging. A NIR fluorescent contrast agents is administered intravenously. During surgery, the agents is visualized using a NIR fluorescence imaging system above the surgical field for open surgery. The system has adequate NIR excitation light, collection optics and filtration, a camera sensitive to NIR fluorescence emission light and a surgical display. An optimal imaging system includes simultaneous visible light illumination of the surgical field, which can be merged with NIR fluorescence images² **b)** In this image, neuroblastoma organoids can be appreciated, showing an example of specifically binding with fluorescence antibodies towards surface antigens, visualized by the SP8 microscope (40x objective).

PRECLINICAL RESEARCH FOR NEW FGS TARGETS IN NEUROBLASTOMA

Nowadays, an increasing number of fluorescent tracers are being developed, mostly for adult cancer types^{25,35}. To validate a new tracer, it requires both *in vitro* and *in vivo* studies. In **chapter 4**, we provide the first cancer-targeted fluorescent agent for FGS in pediatric oncology, by developing and preclinically evaluating a GD2-specific tracer consisting of the immunotherapeutic antibody dinutuximab-beta, used for neuroblastoma treatment, conjugated to near-infrared (NIR) fluorescent dye IRDye800CW. We demonstrated specific binding of anti-GD2-IRDye800CW to human neuroblastoma cells *in vitro* and *in vivo* using xenograft mouse models.

PATIENT-DERIVED ORGANOIDS: A POWERFUL PLATFORM FOR PERSONALIZED FGS TARGET IDENTIFICATION

In **chapter 4**, we demonstrate heterogeneity of the expression of GD2 between individual patients in each histological subtype of neuroblastoma. This could implicate that the use of anti-GD2-IRDye800CW will only work in a subset of patients. Therefore, we aim to predict the expression of other targets in post-chemotherapeutic neuroblastoma tissue. In the last decade, organoid technology has become a valuable *in vitro* tool to study human cancer in a patient-specific manner as it represents important characteristics of the original tumor specimen^{36,37}. In addition, imaging has proven to be a powerful complementary technology to characterize the cellular organization and tissue dynamics of these 3D structures^{38,39}. As microscopy has evolved to allow automated acquisition at multiple positions, imaging platforms can now be envisioned for evaluating (live) organoid imaging. Imaging of organoids can reveal ungoing biological processes of these 3D structures. In **chapter 5**, we describe the development of a detailed protocol for 3D imaging of organoids of various shape, size and origin, which may assist the scientific community to use different imaging techniques to visualize organoid systems derived from different organs and tumors.

As described in **chapter 4**, developing and testing a novel fluorescence tracer for surgery requires a variety of both *in vitro* and *in vivo* experiments. Furthermore, neuroblastoma is known to have a high inter- and intra-patient heterogeneity. To forestall the potential variety in expression of the fluorescence signal between patients and to replace, reduce and refine animal experiments while maintaining scientific accuracy, we developed a personalized evaluation strategy as described in **chapter 6**. By using a combination of an established and experimental neuroblastoma organoid model, we tested multiple alternative probes simultaneously^{40,41}. We aimed to create a comprehensive pipeline that can be used for testing and developing new suitable probes for fluorescence guided surgery in a more efficient way.

BRINGING TRANSLATIONAL SCIENCE TO THE CLINICAL CARE

The results generated in the studies of **chapter 4** provided evidence to write a detailed clinical study protocol for a NIR conjugated antibody that can be used for the first fluorescence guided surgery of children with neuroblastoma. Using anti-GD2-IRDye800CW, a phase I trial was designed in **chapter 7** to test the efficacy of

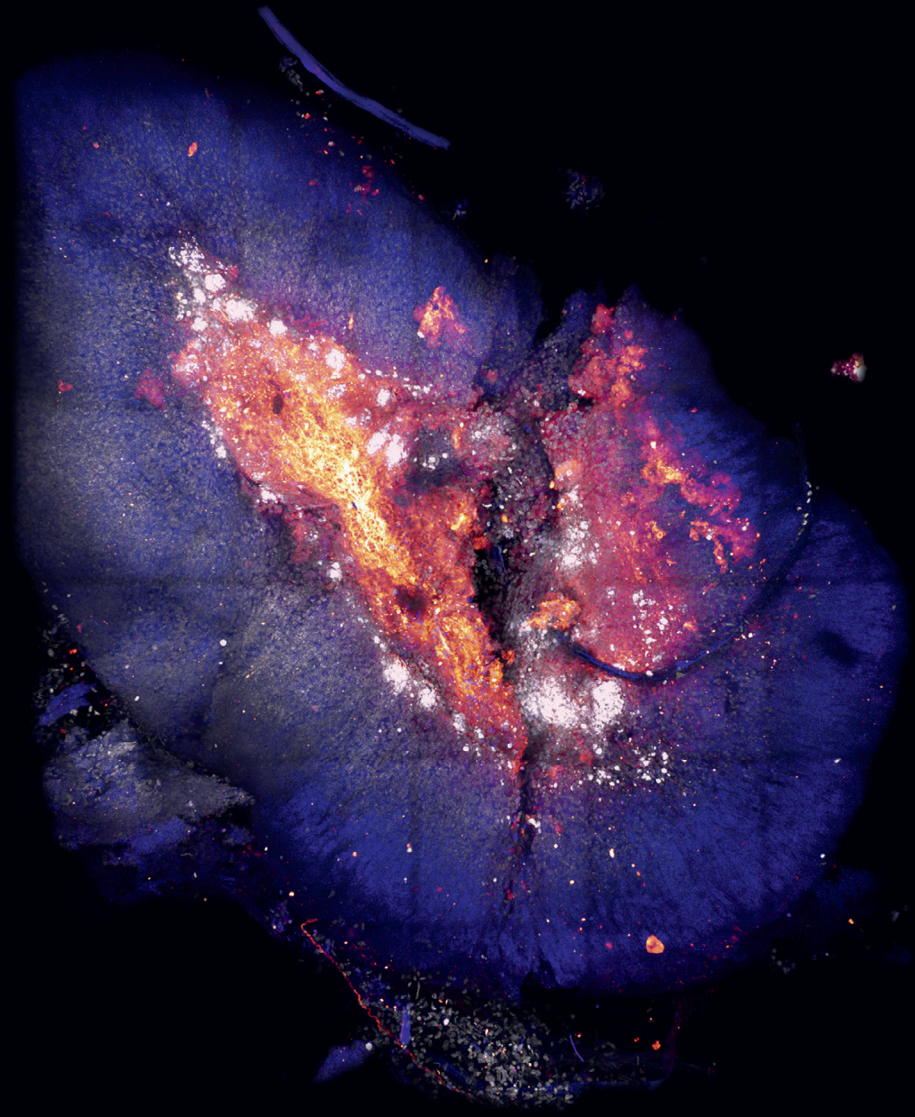
this newly antibody based fluorescent tracer as a first-in-child study. The protocol was written during the 2019 workshop on Methods in Clinical Cancer Research (MCCR) organised by the European Organisation of Research and Treatment of Cancer (EORTC), European Society for Medical Oncology (ESMO), and American Association for Cancer Research (AACR). The results of this thesis are summarized and put into perspective in **chapter 8**.

REFERENCES

- 1 Nagaya, T., Nakamura, Y.A., Choyke, P.L. & Kobayashi, H. Fluorescence-Guided Surgery. *Front Oncol* 7, 314, doi:10.3389/fonc.2017.00314 (2017).
- 2 Vahrmeijer, A.L., Hutteman, M., van der Vorst, J.R., van de Velde, C.J. & Frangioni, J.V. Image-guided cancer surgery using near-infrared fluorescence. *Nat Rev Clin Oncol* 10, 507-518, doi:10.1038/nrclinonc.2013.123 (2013).
- 3 Canete, A. et al. Surgical treatment for neuroblastoma: complications during 15 years' experience. *J Pediatr Surg* 33, 1526-1530, doi:10.1016/s0022-3468(98)90490-0 (1998).
- 4 Davidoff, A.M. & Fernandez-Pineda, I. Complications in the surgical management of children with malignant solid tumors. *Semin Pediatr Surg* 25, 395-403, doi:10.1053/j.sempedsurg.2016.10.003 (2016).
- 5 Dome, J.S. et al. Advances in Wilms Tumor Treatment and Biology: Progress Through International Collaboration. *J Clin Oncol* 33, 2999-3007, doi:10.1200/JCO.2015.62.1888 (2015).
- 6 Davidoff, A.M. et al. Overall Survival and Renal Function of Patients With Synchronous Bilateral Wilms Tumor Undergoing Surgery at a Single Institution. *Ann Surg* 262, 570-576, doi:10.1097/SLA.0000000000001451 (2015).
- 7 Davidoff, A.M. et al. The feasibility and outcome of nephron-sparing surgery for children with bilateral Wilms tumor. The St Jude Children's Research Hospital experience: 1999-2006. *Cancer* 112, 2060-2070, doi:10.1002/cncr.23406 (2008).
- 8 Wilde, J.C. et al. Nephron sparing surgery (NSS) for unilateral wilms tumor (UWT): the SIOP 2001 experience. *Pediatr Blood Cancer* 61, 2175-2179, doi:10.1002/pbc.25185 (2014).
- 9 Vannier, M.W. & Marsh, J.L. Three-dimensional imaging, surgical planning, and image-guided therapy. *Radiol Clin North Am* 34, 545-563 (1996).
- 10 Crossingham, J.L. et al. Interpreting three-dimensional structures from two-dimensional images: a web-based interactive 3D teaching model of surgical liver anatomy. *HPB (Oxford)* 11, 523-528, doi:10.1111/j.1477-2574.2009.00097.x (2009).
- 11 Cimerman, M. & Kristan, A. Preoperative planning in pelvic and acetabular surgery: the value of advanced computerised planning modules. *Injury* 38, 442-449, doi:10.1016/j.injury.2007.01.033 (2007).
- 12 Shin, J. & Truong, Q.A. Manufacturing Better Outcomes in Cardiovascular Intervention: 3D Printing in Clinical Practice Today. *Curr Treat Options Cardiovasc Med* 20, 95, doi:10.1007/s11936-018-0692-1 (2018).
- 13 Maris, J.M., Hogarty, M.D., Bagatell, R. & Cohn, S.L. Neuroblastoma. *Lancet* 369, 2106-2120, doi:10.1016/S0140-6736(07)60983-0 (2007).
- 14 Brodeur, G.M. Neuroblastoma: biological insights into a clinical enigma. *Nat Rev Cancer* 3, 203-216, doi:10.1038/nrc1014 (2003).
- 15 Brodeur, G.M. et al. Revisions of the international criteria for neuroblastoma diagnosis, staging, and response to treatment. *J Clin Oncol* 11, 1466-1477, doi:10.1200/JCO.1993.11.8.1466 (1993).
- 16 Cohn, S.L. et al. The International Neuroblastoma Risk Group (INRG) classification system: an INRG Task Force report. *J Clin Oncol* 27, 289-297, doi:10.1200/JCO.2008.16.6785 (2009).

- 17 Tas, M.L. *et al.* Neuroblastoma between 1990 and 2014 in the Netherlands: Increased incidence and improved survival of high-risk neuroblastoma. *Eur J Cancer* 124, 47-55, doi:10.1016/j.ejca.2019.09.025 (2020).
- 18 Yu, A.L. *et al.* Anti-GD2 antibody with GM-CSF, interleukin-2, and isotretinoin for neuroblastoma. *N Engl J Med* 363, 1324-1334, doi:10.1056/NEJMoa0911123 (2010).
- 19 Rich, B.S. *et al.* Resectability and operative morbidity after chemotherapy in neuroblastoma patients with encasement of major visceral arteries. *J Pediatr Surg* 46, 103-107, doi:10.1016/j.jpedsurg.2010.09.075 (2011).
- 20 Vollmer, K. *et al.* Radical Surgery Improves Survival in Patients with Stage 4 Neuroblastoma. *World J Surg* 42, 1877-1884, doi:10.1007/s00268-017-4340-9 (2018).
- 21 von Allmen, D. *et al.* Impact of Extent of Resection on Local Control and Survival in Patients From the COG A3973 Study With High-Risk Neuroblastoma. *J Clin Oncol* 35, 208-216, doi:10.1200/JCO.2016.67.2642 (2017).
- 22 von Schweinitz, D., Hero, B. & Berthold, F. The impact of surgical radicality on outcome in childhood neuroblastoma. *Eur J Pediatr Surg* 12, 402-409, doi:10.1055/s-2002-36952 (2002).
- 23 Shimada, H. *et al.* The International Neuroblastoma Pathology Classification (the Shimada system). *Cancer* 86, 364-372 (1999).
- 24 Hadjipanayis, C.G., Widhalm, G. & Stummer, W. What is the Surgical Benefit of Utilizing 5-Aminolevulinic Acid for Fluorescence-Guided Surgery of Malignant Gliomas? *Neurosurgery* 77, 663-673, doi:10.1227/NEU.0000000000000929 (2015).
- 25 Lauwerends, L.J. *et al.* Real-time fluorescence imaging in intraoperative decision making for cancer surgery. *Lancet Oncol*, doi:10.1016/S1470-2045(20)30600-8 (2021).
- 26 Gioux, S., Choi, H.S. & Frangioni, J.V. Image-guided surgery using invisible near-infrared light: fundamentals of clinical translation. *Mol Imaging* 9, 237-255 (2010).
- 27 Keereweer, S. *et al.* Optical image-guided cancer surgery: challenges and limitations. *Clin Cancer Res* 19, 3745-3754, doi:10.1158/1078-0432.CCR-12-3598 (2013).
- 28 van Manen, L. *et al.* A practical guide for the use of indocyanine green and methylene blue in fluorescence-guided abdominal surgery. *J Surg Oncol* 118, 283-300, doi:10.1002/jso.25105 (2018).
- 29 Giuliano, A.E., Kirgan, D.M., Guenther, J.M. & Morton, D.L. Lymphatic mapping and sentinel lymphadenectomy for breast cancer. *Ann Surg* 220, 391-398; discussion 398-401, doi:10.1097/00000658-199409000-00015 (1994).
- 30 Morton, D.L. *et al.* Sentinel-node biopsy or nodal observation in melanoma. *N Engl J Med* 355, 1307-1317, doi:10.1056/NEJMoa060992 (2006).
- 31 Schwake, M. *et al.* 5-ALA fluorescence-guided surgery in pediatric brain tumors-a systematic review. *Acta Neurochir (Wien)* 161, 1099-1108, doi:10.1007/s00701-019-03898-1 (2019).
- 32 Stummer, W. *et al.* Fluorescence-guided surgery with 5-aminolevulinic acid for resection of malignant glioma: a randomised controlled multicentre phase III trial. *Lancet Oncol* 7, 392-401, doi:10.1016/S1470-2045(06)70665-9 (2006).

- 33 Hernot, S., van Manen, L., Debie, P., Mieog, J.S.D. & Vahrmeijer, A.L. Latest developments in molecular tracers for fluorescence image-guided cancer surgery. *Lancet Oncol* 20, e354-e367, doi:10.1016/S1470-2045(19)30317-1 (2019).
- 34 Keereweer, S., Van Driel, P. B., Robinson, D. J. & Lowik, C.W. Shifting focus in optical image-guided cancer therapy. *Mol Imaging Biol* 16, 1-9, doi:10.1007/s11307-013-0688-x (2014).
- 35 Boonstra, M.C. et al. Preclinical evaluation of a novel CEA-targeting near-infrared fluorescent tracer delineating colorectal and pancreatic tumors. *Int J Cancer* 137, 1910-1920, doi:10.1002/ijc.29571 (2015).
- 36 Clevers, H. Modeling Development and Disease with Organoids. *Cell* 165, 1586-1597, doi:10.1016/j.cell.2016.05.082 (2016).
- 37 Tuveson, D. & Clevers, H. Cancer modeling meets human organoid technology. *Science* 364, 952-955, doi:10.1126/science.aaw6985 (2019).
- 38 Rios, A.C. & Clevers, H. Imaging organoids: a bright future ahead. *Nat Methods* 15, 24-26, doi:10.1038/nmeth.4537 (2018).
- 39 Serra, D. et al. Self-organization and symmetry breaking in intestinal organoid development. *Nature* 569, 66-72, doi:10.1038/s41586-019-1146-y (2019).
- 40 Bate-Eya, L.T. et al. Newly-derived neuroblastoma cell lines propagated in serum-free media recapitulate the genotype and phenotype of primary neuroblastoma tumours. *Eur J Cancer* 50, 628-637, doi:10.1016/j.ejca.2013.11.015 (2014).
- 41 Decaestecker, B. et al. TBX2 is a neuroblastoma core regulatory circuitry component enhancing MYCN/FOXM1 reactivation of DREAM targets. *Nat Commun* 9, 4866, doi:10.1038/s41467-018-06699-9 (2018).

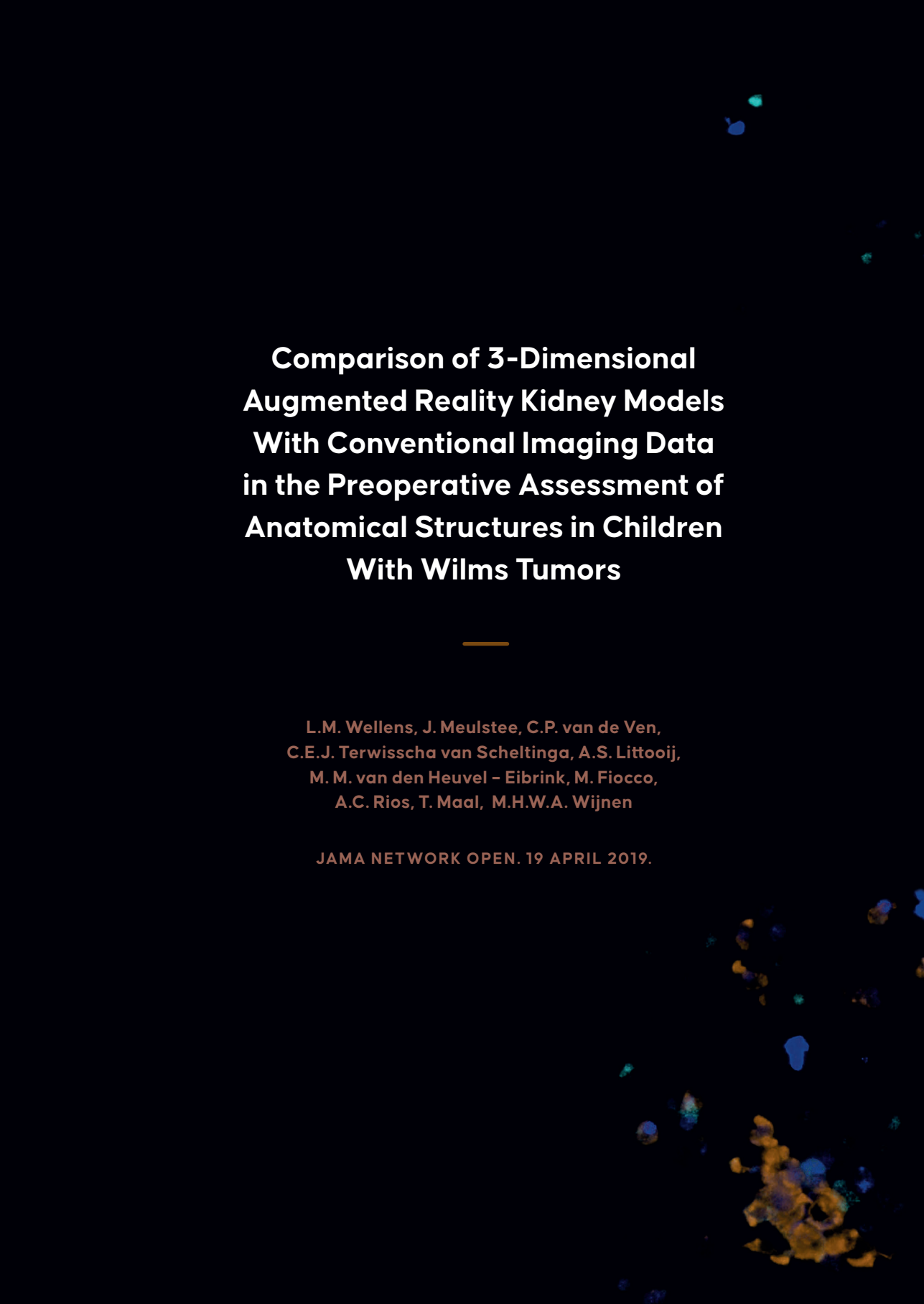


PART 1

Facing Complications
in Pediatric Surgery



CHAPTER 2



**Comparison of 3-Dimensional
Augmented Reality Kidney Models
With Conventional Imaging Data
in the Preoperative Assessment of
Anatomical Structures in Children
With Wilms Tumors**

L.M. Wellens, J. Meulstee, C.P. van de Ven,
C.E.J. Terwisscha van Scheltinga, A.S. Littooi,
M. M. van den Heuvel – Eibrink, M. Fiocco,
A.C. Rios, T. Maal, M.H.W.A. Wijnen

JAMA NETWORK OPEN. 19 APRIL 2019.

ABSTRACT

Importance: Nephron sparing surgery can be considered in well-defined cases of unilateral and bilateral Wilms tumors, but can be very challenging for the pediatric surgeon to perform.

Objective: To determine the value of personalized three-dimensional (3D) kidney models derived from conventional imaging (CI) data to enhance preoperative surgical planning.

Design: Kidney models were created with 3D-printing and augmented reality (AR) using the Microsoft HoloLens® for visualization.

Setting and Participants: The conventional imaging data of ten children with Wilms tumors were converted to 3D prints and AR holograms. A panel of pediatric oncology surgeons (n=7) assessed the quality of the different imaging modalities.

Main Outcome and Measure: The differences in the assessment of four anatomical structures (tumor, arteries, veins and urinary collecting structures) using questionnaires. A Likert scale was used to measure differences between the different imaging modalities.

Results: The test group of surgeons surveyed the conventional imaging, the 3D prints and the AR Holograms of the ten patients. Compared to CI, the 3D print and the AR models were evaluated superior for all anatomical structures: Tumor (median CI 4.01 [IQR 3.62 – 4.15] versus median 3D print 4.67 [IQR 4.15 – 4.71, p-value 0.008] and median AR 4.71 [IQR 4.26 – 4.75, p-value 0.002]), arteries (median CI 3.62 [IQR 3.43 – 3.93] versus 3D print median 4.54 [IQR 4.32 – 4.71, p-value 0.002] and AR median 4.83 [IQR 4.64 – 4.86, p-value <0.001]), veins (median CI 3.46 [IQR 3.39 – 3.63] versus 3D print median 4.50 [IQR 4.39 – 4.68, p-value <0.001] and AR median 4.83 [IQR 4.71 – 4.86 p-value <0.001]) and urinary collecting structures median (CI 2.76 [IQR 2.43 – 3.00] versus 3D print median 3.86 [IQR 3.64.32 – 4.39, p-value <0.001] and AR median 4.00 [IQR 4.3.93 – 4.58 p-value <0.001]). There were no differences in anatomical assessment found between the two 3D techniques; 3D print and AR.

Conclusions and Relevance: The 3D kidney models improved the anatomical understanding of the surgeons and can be of help in future pre-operative planning of nephron sparing surgery for Wilms tumors. It should be considered to embed these models as a supplementary visualisation in clinical care.

INTRODUCTION

Wilms tumors (WT) are the most frequently occurring pediatric malignancies in the kidney. The survival rate of children with WT is around 90%¹⁻³, yet approximately 5% of the cases present with bilateral disease, which itself reveals an overall survival rate of roughly 80%⁴.

In the presentation of bilateral disease, nephron sparing surgery (NSS) is the preferred/recommended treatment of choice. Compared to unilateral tumors, bilateral disease carries a higher risk for end-stage renal disease (12%) and secondary morbidity^{4,5}. The benefit of NSS in unilateral WT is debatable. The excellent survival of unilateral WT patients has motivated investigation into reducing treatment morbidity, whilst preserving survival, by considering NSS^{6,7}. To reduce the probability of long-term kidney function loss, the occurrence of perioperative complications and to facilitate complete tumor resection, a personalized planning and surgical strategy is essential.

Magnetic resonance imaging (MRI) and computed tomography (CT) are used for diagnosis and to differentiate between tumor and healthy renal tissue. Pediatric surgeons plan the surgery of Wilms tumors based on the two-dimensional (2D) interpretation of these conventional imaging techniques. The use of three-dimensional (3D) visualisations is hoped to further improve the understanding of the exact tumor location and assessment of relevant anatomic structures such as arteries, veins and urinary collection structures. Data of MRI and CT can be used, possibly fused and reconstructed into 3D visualizations⁸.

3D visualization is gradually gaining potential in many surgical disciplines and can be used to define the optimal surgical strategy⁹⁻¹². These new techniques can even further improve the assessment of the relevant anatomy and enhance preoperative surgical planning. 3D printing of organs and structures has proven value for multiple disciplines within the engineering field and clinical practice such as urology, neuro-, cardiac-, plastic-, and maxilla-facial surgery¹²⁻¹⁴. However, 3D printing is not the current standard of care. In addition, augmented reality (AR) is a technology which can visualize virtual 3D objects in the real world. The implementation of AR is promising as an operating assisting tool, its value currently being assessed in different medical specialties¹⁵.

In this study, we compared the use of different 3D visualization techniques, 3D printing and AR, for optimizing the surgical planning of nephron sparing surgery (NSS) for Wilms tumors. To the best of our knowledge, the added value of different 3D visualisation methods on conventional imaging in children with cancer has

never before been investigated. A panel of pediatric oncology surgeons in the Netherlands was asked to evaluate the 3D visualization techniques and report back on the potential added value of their use prior to surgery.

METHODS

POPULATION

Imaging data from 10 patients diagnosed with a Wilms tumor in the Princess Máxima Center between January 2016 and May 2017 were included in our study. Patients with metastases at diagnosis were excluded and three patients presenting with a bilateral Wilms tumors were selectively included. Seven others patients were selected based on best quality conventional imaging available. Data from conventional imaging, MRI and/or CT scans, were derived from these ten selected patients. In most patients MRI scanning was the preferred imaging technique for diagnosis considering optimal tumor assessment. A CT-scan was performed to clarify vascular anatomy when nephron sparing surgery was likely to be performed.

IMAGING METHODS

Contrast-enhanced MRI of the abdomen was performed on a 1.5-T system (Achieva; Philips Medical Systems, Best, the Netherlands). Coronal 3D T2-W imaging along with fat-suppressed T1-W imaging before and after gadolinium-contrast-medium administration was acquired¹⁶. CT-scans were performed with the 16-row MDCT (Brilliance 16P, Philips Medical Systems, OH, USA). All patients received 1.5 mL/kg contrast medium with a maximum of 120 mL scanned in arterial phase (injection rate of 2 mL/s with saline chaser) in accordance to standard protocol. Exposure settings were adjusted to patient size (range, 104-150 mAs and 80-90 kVp). Thin slice images were reconstructed with 0.90mm thickness and stored in a 512×512 data matrix.

3D SEGMENTATION

The MRI or CT scans from each patient were loaded as Digital Imaging and Communications in Medicine (DICOM) files and segmented by an IT expert of Materialise (Leuven, Belgium). After consulting the pediatric radiologist and a pediatric surgeon, the correct anatomical segmentations were generated based on the conventional imaging using 3D segmentation software (Mimics Innovation Suite, version 20).

Each anatomical structure (kidney parenchyma, tumor, arteries, veins, kidney urinary collecting structures) was segmented separately and given a different colour. After the full segmentation was completed, small windows were cut out of the parenchyma of the kidney, making it possible to get a full sight on the tumor and the border discriminated from the healthy tissue, intrarenal vasculature and urinary collecting structures. Segmentations were saved as a stereolithography file (.STL), suitable for 3D-printing and AR.

3D PRINTING

The 3D-models were printed using the Zcorp printing technology at Materialise. The Zcorp technology deposits a liquid binder onto thin layers of powder via the ink-jet printheads, which reacts with an agent in the powder, creating a solid, multicolour 3D-model.

AUGMENTED REALITY (AR)

The Microsoft HoloLens (Microsoft Corporation, Redmond, WA, USA) was used for AR visualization. The HoloLens is a head mounted display with a stereo see-through display and a wireless design. This provides a realistic 3D visual and stimulates the user to inspect holograms from different positions and view angles. The spatial impression enables doctors to analyze complex anatomical structures in an interactive way, enhancing their perspective of the surgical site¹⁷. Firstly, from the exported 3D-models, minor artefacts were repaired in MeshMixer 3D software (MeshMixer, San Rafael California, USA). The mesh density of every 3D model was optimized and consisted out of 2000 - 15000 triangles, depending on the size of the models. This guaranteed a clear visualization on the HoloLens without losing quality. Secondly, the Unity framework, (v5.6.5, Unity Technologies, San Francisco, California, USA) was used to create an application for the HoloLens to visualize the kidney, tumors and relevant anatomy in 3D. Voice instructions were implemented to rotate, adjust or manipulate the anatomical 3D objects and visualisation options were created to make structures transparent, to look inside the kidney, separate the tumor from the kidney and to zoom in on specific structures. Although each 3D model is different and unique to each patient's tumor and organ anatomy, the architecture and user interface of the application were similar across the sample group. Finally, the application was imported to the HoloLens. An example of the wilms tumor of a patient's case is provided online (**video 1**).

DATA ACQUISITION

A panel of 7 experts (6 pediatric oncologic surgeons in the Netherlands and 1 pediatric urologist with oncology experience) were asked to individually evaluate the MRI and/or CT scans prior to surgery for every patient. The years of expertise of the 7 surgeons varied from <1 year to 30 years. Scans were shown in 2D using The Horos Project DICOM viewer (version 2.4.1). Afterwards, the surgeons were asked to fill in a questionnaire regarding the quality of this conventional imaging on the visualisation of the anatomical structures in the kidney. This questionnaire consisted of questions assessing the anatomical understanding of the tumor, arteries, veins and urinary collecting structures, the decision making of the surgeons to perform nephron sparing surgery (NSS) or a nephrectomy and their pre-operative preparation. The questionnaires are enclosed in the Supplementary Material of this article (eAppendix 1).

Next, the 3D print of the corresponding patient was provided to the members of the panel. They were asked to fill in a second questionnaire with the same questions as for the conventional imaging techniques, but with supplementary questions about the added value of the 3D print in assessing the tumor, artery- and venous structures, and the urinary collecting structures.

Finally, the HoloLens was introduced to visualize the AR hologram of the corresponding patient and the same questions used to assess the 3D print were given in the 3rd questionnaire. All of the above took place in one session per expert of maximum three hours to score all three modalities for the 10 patients.

The cycle of questionnaires for conventional imaging, 3D print and AR was repeated for every patient, resulting in the opinions of the 7 experts on all 10 patients. The experts were asked to answer all questions of what level they agreed, based on a Likert-scale (1 = completely disagree, 5 = completely agree).

DATA ANALYSIS

Statistical analyses were performed using GraphPad prism (version 7). To compare scores on the MRI and/or CT scan, 3D print and AR hologram, the non-parametric grouped Wilcoxon matched pair signed rank test was used. The Mann Whitney U test was employed to compare the difference between questions about the four anatomical structures for the individual patients. A double sided p-value <0.025 (adjusted for multiple testing) was used to test for significant difference between the conventional imaging and the 3D visualizations.

ETHICAL APPROVAL

Medical Research Involving Human Subjects Act (WMO) did not apply to the above mentioned study and therefore we received official approval of this study by the medical research ethics committees of the University Medical Center Utrecht.

STANDARDS FOR QUALITY IMPROVEMENT REPORTING EXCELLENCE (SQUIRE)

This study follows the SQUIRE guidelines for quality improvement ¹⁸.

RESULTS

3D VISUALISATIONS

The kidney, Wilms tumor, arteries, veins and the urinary collecting structures were reconstructed as shown in **figure 1**. In one patient (patient 2), the urinary collecting structures was not reconstructed due to insufficient conventional imaging. The characteristics of the 10 patients are summarized in **table 1**.

For all four anatomical structures, the 3D print and the AR hologram received higher scores compared to the conventional imaging (**figure 2**). When comparing the four anatomical structures between the 3D print and the AR hologram, no difference was found.

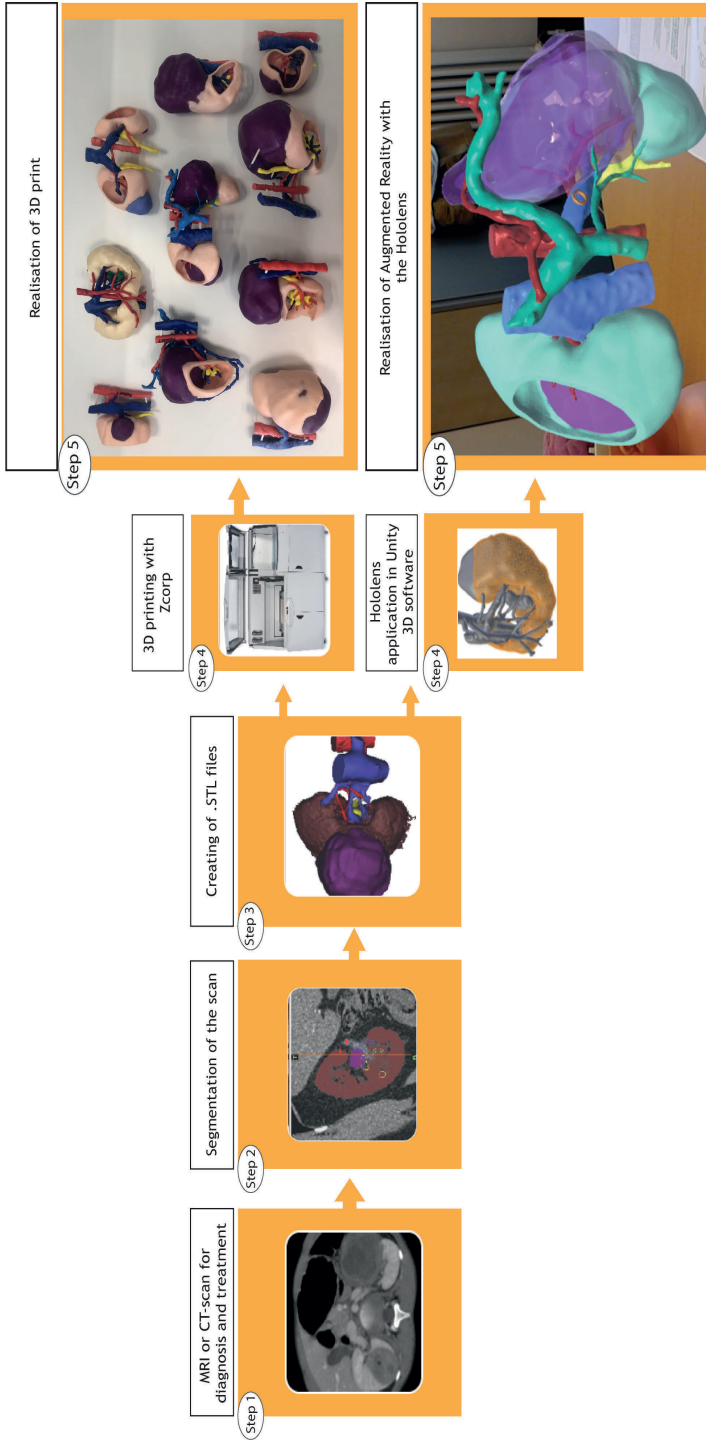


Figure 1. Workflow diagram depicting the construction process of 3D visualizations

This workflow shows the 3D visualization process used in this study: From the patient derived MRI and/or CT a segmentation was made leading to a corresponding 3D print and AR hologram.

ASSESSMENT OF THE TUMOR

Both 3D print and AR holograms led to better tumor assessment compared to conventional imaging (**figure 2**, median CI 4.01 [IQR 3.62 – 4.15] versus median 3D print 4.67 [IQR 4.15 – 4.71] and median AR 4.71 [IQR 4.26 – 4.75], p-value <0.01). There was no significant difference between conventional imaging and 3D printing or AR in individual cases.

ASSESSMENT OF THE ARTERIES

Both 3D print and AR holograms led to better assessment of the arteries compared to conventional imaging (**figure 2**, median CI 3.62 [IQR 3.43 – 3.93] versus 3D print median 4.54 [IQR 4.32 – 4.71] and AR median 4.83 [IQR 4.64 – 4.86], p-value <0.001). There was no significant difference between conventional imaging and 3D printing or AR in individual cases.

ASSESSMENT OF THE VENOUS STRUCTURES

Both 3D print and AR holograms led to better assessment of the venous structures compared to conventional imaging (**figure 2**, median CI 3.46 [IQR 3.39 – 3.63] versus 3D print median 4.50 [IQR 4.39 – 4.68] and AR median 4.83 [IQR 4.71 – 4.86], p-value <0.001). There was no significant difference between conventional imaging and 3D printing or AR in individual cases.

ASSESSMENT OF THE URINARY COLLECTING STRUCTURES

Both 3D print and AR holograms led to better assessment of the urinary collecting structures compared to conventional imaging (**figure 2**, median CI 2.76 [IQR 2.43 – 3.00] versus 3D print median 3.86 [IQR 3.64.32 – 4.39] and AR median 4.00 [IQR 4.3.93 – 4.58], p-value <0.001). There was no significant difference between conventional imaging and 3D printing or AR in individual cases.

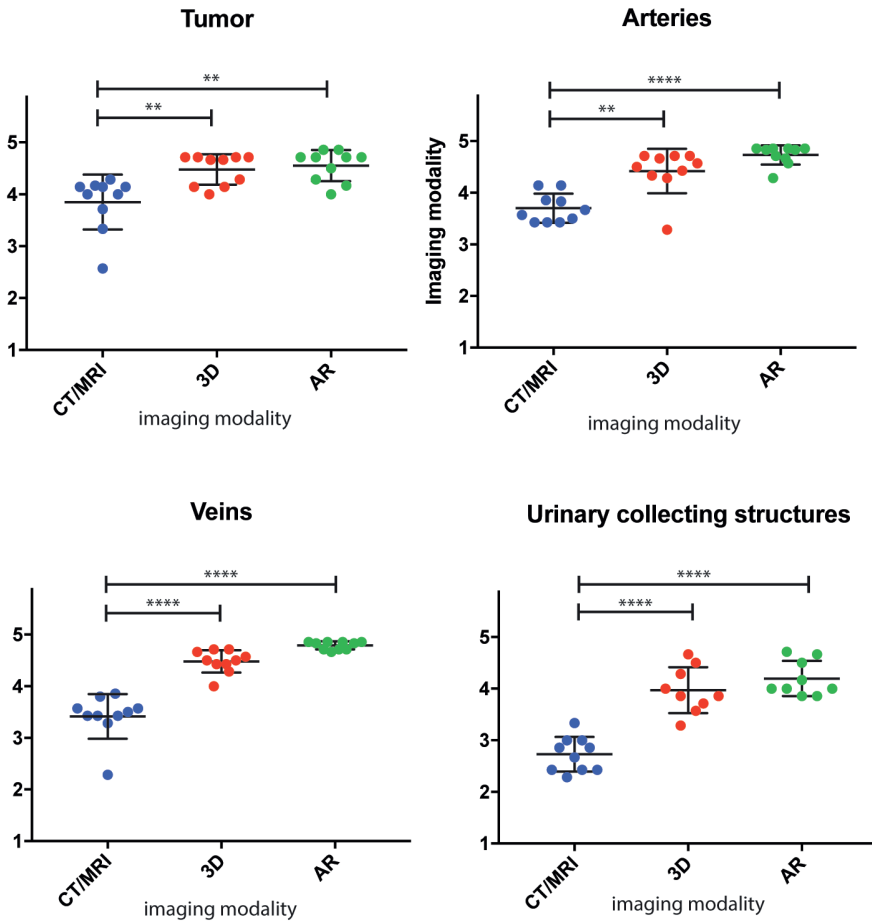


Figure 2. The outcome of the questionnaires of pediatric oncology surgeons on the conventional imaging, the 3D prints and the AR holograms visualized on the HoloLens.

Surgeons were asked to score the visibility of the four anatomical structures: tumor, arteries, veins and urinary collecting structures from 1 to 5 (1=completely disagree, 2=disagree, 3=neutral, 4=agree, 5=completely agree). Scores were asked for the conventional imaging (CI, meaning MRI and/or CT) and for the 3D visualizations (3D print and AR). **Figure 2.** shows the comparison of means of patient 1 to 10 for the three imaging modalities. The center lines indicate the medians of the score of the ten patients. The error bars indicate the interquartile ranges (IQR). P values less than 0.01 are marked with two asterisks (**) and p-values less than 0.001 are marked with four asterisks (****). **Table 2.** shows the statistical analyses of each anatomical structure. For baseline data the medians and interquartile ranges (IQR) are presented. Statistical testing was performed using Wilcoxon matched-pairs signed rank test. **CI** = conventional imaging (MRI and/or CT), **3D** = 3D print, **AR** = Augmented Reality, **IQR** = interquartile range.

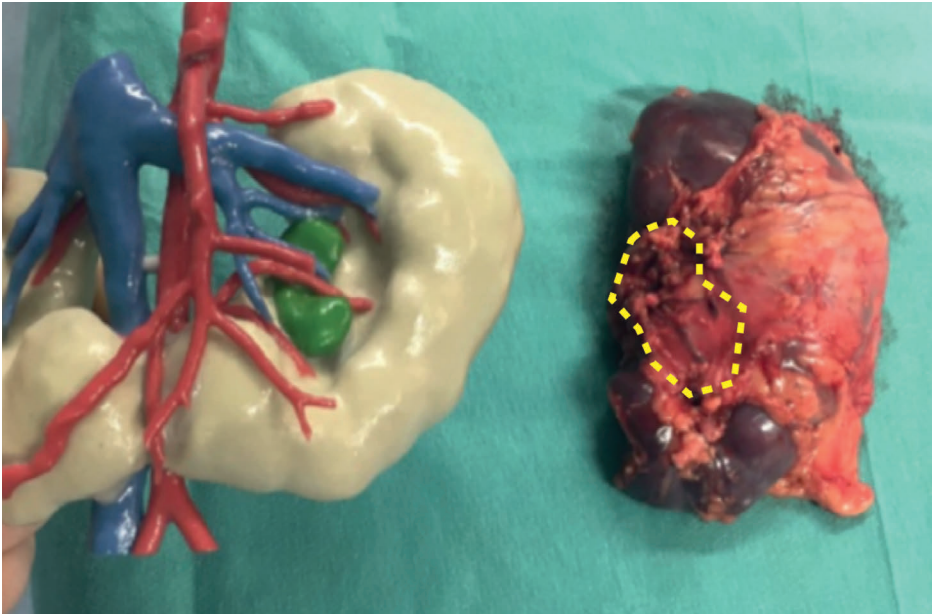


Figure 3. The use of a 3D-print during surgery

The Wilms tumour of one patient (patient 2) was printed prior to surgery. **Figure 3** shows the 3D print next to the corresponding kidney. The dotted line indicates the location of the tumor.

DISCUSSION

Preoperative imaging is paramount in achieving good results during oncological surgery. In nephron sparing surgery (NSS) for Wilms tumors, the risk of positive resection margins are high^{6,19}, therefore there is a necessity to improve the current procedure. As opposed to bilateral WT, NSS in unilateral WT is still debatable, but recently, surgeons are showing a higher interest in its use for unilateral WT^{6,7} in order to preserve long term renal function. However, it has been reported that the use of NSS leads to incomplete tumor resection in 30% of unilateral cases, resulting in reoperation and additional radiotherapy⁶. The novel 3D visualisation techniques presented here could be a useful assisting tool in planning NSS in unilateral and bilateral WT. In this study, we constructed personalized, high quality, physical and augmented reality 3D models of pediatric uni- and bi-lateral WT in children to create practice objects for preoperative planning.

We were the first to reconstruct MRI and/or CT scans of kidneys of 10 patients with Wilms tumors in both 3D print and AR. We have found a reported added value of both our 3D models regarding the pre-operative assessment by surgeons of the

four anatomical structures, respectively the tumor, the arteries, the veins and the urinary collecting structure. This data is consistent with prior studies using 3D prints in adults with renal cell carcinoma ^{20,21}.

Detailed understanding of the surgical anatomy of Wilms tumors and the surrounding anatomical renal structures in children can be a challenge based on standard 2D conventional imaging visualisations alone. The lack of ionizing radiation and the improved soft tissue contrast makes the MRI scan an attractive imaging method in children ²². However, when only MRI scans are performed, the challenge lies in the accurate detection of the vasculature in these often small children. This is particularly true with complex renal anatomy, which often is the case in children with Wilms tumors. This study indicates that new preoperative 3D imaging processing strategies help to increase the surgeons' knowledge on the kidney anatomy, thus assisting in improving the planning of tumor resection and optimizing the procedure of choice; nephron sparing surgery or nephrectomy. This could potentially improve radicality of tumor resection and spare healthy kidney tissue, thereby preserving long-term renal function.

Converting the existing conventional imaging data to 3D visualization contributes to overall anatomical understanding ²³. In this study, no differences were found between the type of 3D visualisations therefore the choice between 3D printing and AR reconstruction may be based on personal preference. Out of multiple 3D printing techniques, we used the Zcorp technology. The Zcorp technology is able to print accurate models while using different colours. A solid printed model can occlude relevant anatomy, such as blood vessel in the kidney or tumor. To overcome this, an opening window or transparent material can be used to provide a view inside the model ²⁴. Before the start of this study, we printed examples of kidneys with different techniques. We found the opening window in the solid Zcorp model to clarify the anatomy best. The cost for these multicoloured 3D printed models were 500 USD on average and had a manufacturing time of 4 – 5 days. In comparison, the production of an AR-reconstruction takes 1 – 2 hours and is, apart from the labor time, costless after initial hardware costs of 3000 to 5000 USD for the HoloLens. The relatively short lead time between chemotherapy and surgery can be an important advantage of the HoloLens. This might make AR reconstruction more feasible and preferable in certain cases. In addition, AR-hologram represent an adaptive and interactive technology compared to 3D print, in which every structure can be easily opened, switched to transparent, or moved away by giving a voice command.

The wireless design of the HoloLens and the use of voice commands for interaction, creates the possibility to use the HoloLens also during surgery ²⁵. The AR-visualisation can be consulted in the operation theatre to visualize the anatomy, pathology and 3D vascularisation. In future perspective, the holograms can be fused with the real anatomy of the patient creating a mixed reality setting, as previously described in neurosurgery ²⁶. However, more research on how to fuse the virtual holograms with the real non-rigid and deformable anatomy of especially young patients needs to be performed.

LIMITATIONS

There are still challenges for the clinical application of the proposed novel 3D visualization techniques. Conventional medical imaging techniques produce a large amount of information, but good interpretation of these data requires years of expertise. Diffusion weighed imaging in MRI already shows the increasing potential to discriminate tumor from normal tissue ¹⁶. To further objectify these data with scientific accuracy to convert them into 3D prints or AR holograms, more research on standardized algorithms needs to be performed. In addition, high quality conventional imaging (MRI or CT) is key for obtaining useful pre-operative 3D imaging. In this study, we had to exclude several cases based on insufficient imaging quality. There is a need for more research into standardizing the optimal imaging method (MRI, CT or CT-angiogram), slice thickness and timing for contrast enhancement, specifically in children of different ages. In the present study, the segmentation is performed manually in close collaboration between an information technology expert, pediatric radiologist and pediatric oncology surgeon. Standardizing this process may save valuable time for medical experts.

CONCLUSION

This study showed that 3D visualization has an added value for surgeons in the preoperative planning of children with Wilms tumor. Additional understanding of the anatomy using 3D technology was found for all four anatomical structures (tumor, the arteries, the veins and the urinary collecting structures). Future research should be aimed at improving the speed, accuracy and automation of the segmentation process for the 3D visualization and expanding its clinical use in pediatric oncological surgery.

ACKNOWLEDGEMENTS

This work has been funded by the KIKa foundation (Children Cancer-free). KiKa is an independent foundation with an independent board of advisors that took no

part in the design and conduct of the study. KIKA took no part in the collection, management, analysis, and interpretation of the data and in the preparation, review, or approval of the manuscript. KIKA took no part in the decision to submit the manuscript for publication.

First Author, Ms Wellens, had full access to all the data in the study and takes responsibility for the integrity of the data and the accuracy of the data analysis.

DATA STATEMENT

All data, including detailed questionnaire information and obtained answers, are in the paper or available upon request.

REFERENCES

- 1 Nakamura, L. & Ritchey, M. Current management of wilms' tumor. *Curr Urol Rep* 11, 58-65, doi:10.1007/s11934-009-0082-z (2010).
- 2 Dome, J.S. et al. Advances in Wilms Tumor Treatment and Biology: Progress Through International Collaboration. *J Clin Oncol* 33, 2999-3007, doi:10.1200/JCO.2015.62.1888 (2015).
- 3 Pritchard-Jones, K. et al. Treatment and outcome of Wilms' tumour patients: an analysis of all cases registered in the UKW3 trial. *Ann Oncol* 23, 2457-2463, doi:10.1093/annonc/mds025 (2012).
- 4 Davidoff, A.M. et al. Overall Survival and Renal Function of Patients With Synchronous Bilateral Wilms Tumor Undergoing Surgery at a Single Institution. *Ann Surg* 262, 570-576, doi:10.1097/SLA.0000000000001451 (2015).
- 5 Davidoff, A.M. et al. The feasibility and outcome of nephron-sparing surgery for children with bilateral Wilms tumor. The St Jude Children's Research Hospital experience: 1999-2006. *Cancer* 112, 2060-2070, doi:10.1002/cncr.23406 (2008).
- 6 Wilde, J.C. et al. Nephron sparing surgery (NSS) for unilateral wilms tumor (UWT): the SIOP 2001 experience. *Pediatr Blood Cancer* 61, 2175-2179, doi:10.1002/pbc.25185 (2014).
- 7 Interiano, R.B. et al. Renal function in survivors of nonsyndromic Wilms tumor treated with unilateral radical nephrectomy. *Cancer* 121, 2449-2456, doi:10.1002/cncr.29373 (2015).
- 8 Sato, M. et al. Three-dimensional multimodality fusion imaging as an educational and planning tool for deep-seated meningiomas. *Br J Neurosurg*, 1-7, doi:10.1080/02688697.2018.1485877 (2018).
- 9 Vannier, M.W. & Marsh, J.L. Three-dimensional imaging, surgical planning, and image-guided therapy. *Radiol Clin North Am* 34, 545-563 (1996).
- 10 Crossingham, J.L. et al. Interpreting three-dimensional structures from two-dimensional images: a web-based interactive 3D teaching model of surgical liver anatomy. *HPB (Oxford)* 11, 523-528, doi:10.1111/j.1477-2574.2009.00097.x (2009).
- 11 Cimerman, M. & Kristan, A. Preoperative planning in pelvic and acetabular surgery: the value of advanced computerised planning modules. *Injury* 38, 442-449, doi:10.1016/j.injury.2007.01.033 (2007).
- 12 Shin, J. & Truong, Q. A. Manufacturing Better Outcomes in Cardiovascular Intervention: 3D Printing in Clinical Practice Today. *Curr Treat Options Cardiovasc Med* 20, 95, doi:10.1007/s11936-018-0692-1 (2018).
- 13 Diment, L.E., Thompson, M.S. & Bergmann, J.H.M. Clinical efficacy and effectiveness of 3D printing: a systematic review. *BMJ Open* 7, e016891, doi:10.1136/bmjopen-2017-016891 (2017).
- 14 Yang, T. et al. Impact of 3D printing technology on the comprehension of surgical liver anatomy. *Surg Endosc*, doi:10.1007/s00464-018-6308-8 (2018).
- 15 van Oosterom, M.N., van der Poel, H.G., Navab, N., van de Velde, C.J.H. & van Leeuwen, F.W.B. Computer-assisted surgery: virtual- and augmented-reality displays for navigation during urological interventions. *Curr Opin Urol*, doi:10.1097/MOU.0000000000000478 (2017).

- 16 Littooj, A. S. *et al.* Apparent diffusion coefficient as it relates to histopathology findings in post-chemotherapy nephroblastoma: a feasibility study. *Pediatr Radiol* 47, 1608-1614, doi:10.1007/s00247-017-3931-9 (2017).
- 17 Nam, K. W., Park, J., Kim, I. Y. & Kim, K. G. Application of stereo-imaging technology to medical field. *Healthc Inform Res* 18, 158-163, doi:10.4258/hir.2012.18.3.158 (2012).
- 18 Ogrinc, G. *et al.* SQUIRE 2.0 (Standards for QUality Improvement Reporting Excellence): revised publication guidelines from a detailed consensus process. *BMJ Qual Saf* 25, 986-992, doi:10.1136/bmjqs-2015-004411 (2016).
- 19 Kieran, K. *et al.* Repeat nephron-sparing surgery for children with bilateral Wilms tumor. *J Pediatr Surg* 49, 149-153, doi:10.1016/j.jpedsurg.2013.09.048 (2014).
- 20 Wake, N., Bjurlin, M.A., Rostami, P., Chandarana, H. & Huang, W. C. Three-dimensional Printing and Augmented Reality: Enhanced Precision for Robotic Assisted Partial Nephrectomy. *Urology* 116, 227-228, doi:10.1016/j.urology.2017.12.038 (2018).
- 21 Maddox, M. M. *et al.* 3D-printed soft-tissue physical models of renal malignancies for individualized surgical simulation: a feasibility study. *J Robot Surg* 12, 27-33, doi:10.1007/s11701-017-0680-6 (2018).
- 22 Mathews, J. D. *et al.* Cancer risk in 680,000 people exposed to computed tomography scans in childhood or adolescence: data linkage study of 11 million Australians. *BMJ* 346, f2360, doi:10.1136/bmj.f2360 (2013).
- 23 Knoedler, M. *et al.* Individualized Physical 3-dimensional Kidney Tumor Models Constructed From 3-dimensional Printers Result in Improved Trainee Anatomic Understanding. *Urology* 85, 1257-1261, doi:10.1016/j.urology.2015.02.053 (2015).
- 24 Fan, G. *et al.* Three-Dimensional Physical Model-Assisted Planning and Navigation for Laparoscopic Partial Nephrectomy in Patients with Endophytic Renal Tumors. *Sci Rep* 8, 582, doi:10.1038/s41598-017-19056-5 (2018).
- 25 Incekara, F., Smits, M., Dirven, C. & Vincent, A. Clinical Feasibility of a Wearable Mixed-Reality Device in Neurosurgery. *World Neurosurg* 118, e422-e427, doi:10.1016/j.wneu.2018.06.208 (2018).
- 26 Meulstee, J.W. *et al.* Toward Holographic-Guided Surgery. *Surg Innov*, 1553350618799552, doi:10.1177/1553350618799552 (2018).

Table 1. Patient characteristics

Patient	Gender	Age (years)	Type of Wilms' tumour	Preoperative conventional imaging available
1	M	2	Unilateral	MRI
2	M	2	Bilateral	MRI and CT
3	F	3	Bilateral	MRI and CT
4	F	2	Unilateral	MRI
5	M	4	Bilateral	MRI and CT
6	F	3	Unilateral	MRI
7	F	5	Unilateral	MRI
8	F	5	Unilateral	MRI
9	F	7	Unilateral	MRI
10	F	4	Unilateral	MRI

MRI = magnetic resonance imaging, CT = Computer tomography.

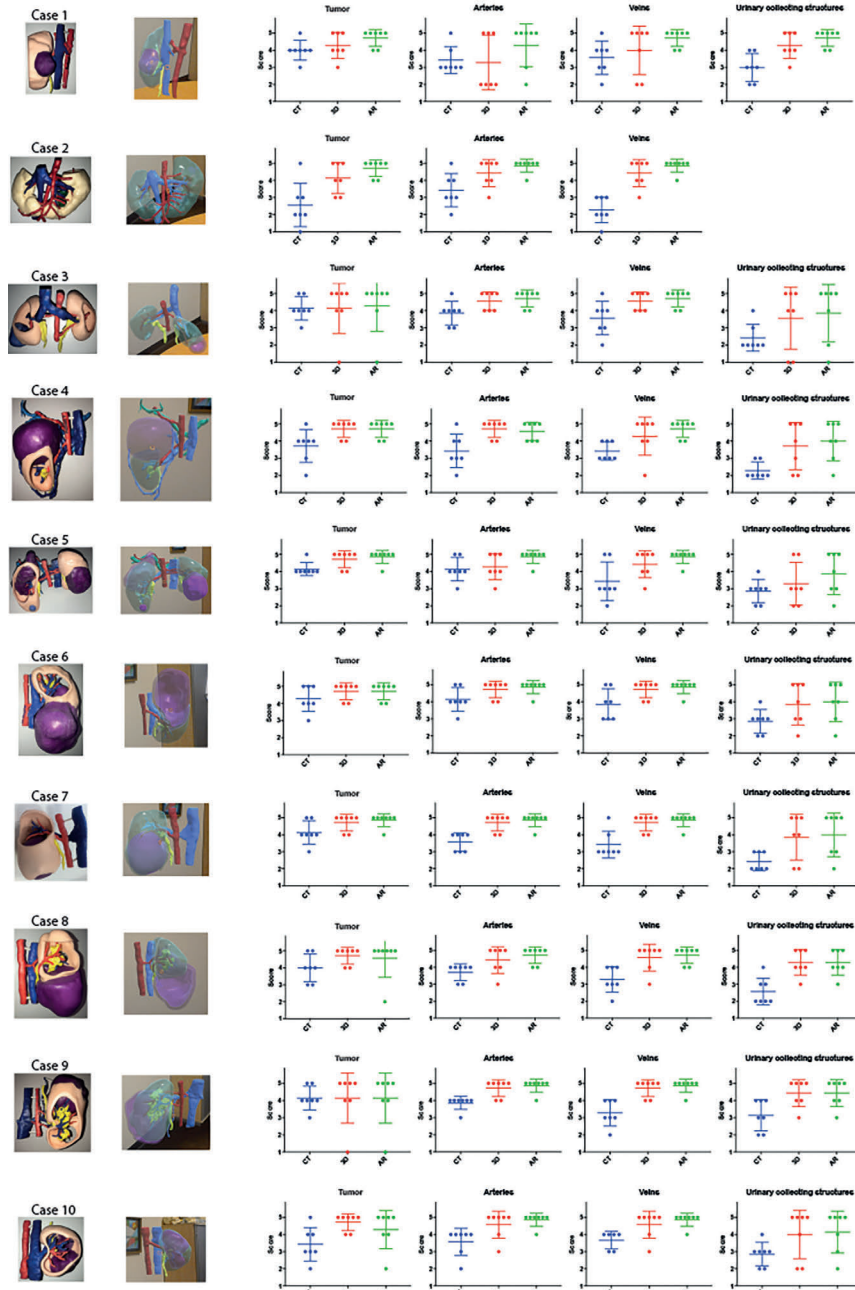
Table 2. Results of the survey amongst the pediatric surgeons

	Tumor			Arteries			Veins			Urinary Collecting Structures		
	CI	3D	AR	CI	3D	AR	CI	3D	AR	CI	3D	AR
IQR 25%	3,62	4,14	4,26	3,43	4,32	4,64	3,39	4,39	4,71	2,42	3,64	3,93
Median	4,07	4,67	4,71	3,62	4,54	4,83	3,46	4,5	4,83	2,76	3,86	4,00
IQR 75%	4,15	4,71	4,75	3,93	4,71	4,86	3,62	4,68	4,86	3,00	4,39	4,58
	0,008			0,002			<0,001			<0,001		
P-value	0.002			<0.001			<0.001			<0.001		

IQR = Inter Quartile Range, CI = conventional imaging, 3D = three-dimensional print, AR = Augmented Reality.

SUPPLEMENTARY DATA

Figure 1. The outcome of the questionnaires of pediatric oncologic surgeons on the conventional imaging, the 3D prints and the Augmented Reality holograms visualized on the HoloLens per case.





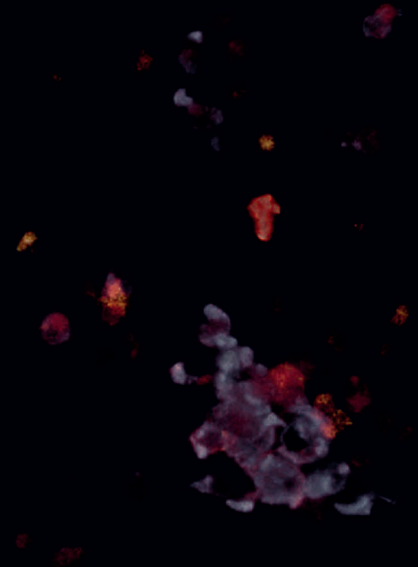
CHAPTER 3

Complications of Neuroblastoma Surgery: a Systematic Review

L.M. Wellens¹, M. Jans², G.A.M. Tytgat,
M.H.W.A. Wijnen, A.F.W. van der Steeg

* Shared first authorship

SUBMITTED



ABSTRACT

Background: Primary tumor resection in patients with neuroblastoma is associated with a high complication rate. The aim of this systematic review was to identify these complications in current literature, evaluate the quality of reporting and present a method for future reporting.

Patients and Methods: Embase and Pubmed databases were searched for literature on surgical complications in patients with neuroblastoma published between 1990 and 2019. Sixty-five studies met all inclusion criteria. Information on individual complications and their incidence was abstracted and the quality of each study was assessed.

Results: The median percentage of patients with complications was 17.5%. Validity and methodology were highly variable between included studies. Common definitions were not in use.

Conclusion: Complications in neuroblastoma surgery are common. However, uniform definitions are not in use, and current literature is subject to suboptimal methodology. A structured and standardized method of reporting on these complications is discussed.

INTRODUCTION

Neuroblastoma is the most frequent extracranial solid tumor in pediatric oncology, with a yearly incidence of 11 to 13 per million children under 15 years of age^{1,2}. Overall survival is good in low-risk disease, however high-risk patients still have a poor 5-year survival of less than 50%, despite intensive multimodal treatment². Surgical resection of the primary tumor is standard of care for most stages of disease. In medium and high-risk patients, the tumor often has an extensive growth pattern, encasing important vessels and invading organs. In these patients, surgery is usually preceded by chemotherapy to induce a reduction in tumor volume. The aim of the subsequent surgery is to remove as much tumor as possible while preserving adjacent structures and preventing additional damage. Since it has not been shown that complete removal of the tumor improves overall survival³⁻⁷, a 95% reduction of the primary tumor is deemed to be adequate surgery. This is however difficult to achieve when tumor tissue is encasing for example the aorta, inferior vena cava and the vascular pedicle of the kidney. As such, a 95% resection remains challenging and is unfortunately associated with a high probability of serious complications⁸⁻¹². Comprehensive insight into the nature of these adverse events is vital for improving surgical strategy and optimizing overall survival¹³. Structured methodology for reporting these complications is scarce and no commonly accepted definitions exist¹⁴. Therefore, the purpose of this systematic review was to (1) identify and summarize surgical complications currently reported in neuroblastoma literature; (2) evaluate the methodologies and quality of reporting; and (3) reflect on ideal uniform future reporting.

METHODS

SEARCH STRATEGY

This systematic review was conducted and reported according to the Preferred Reporting Items for Systematic Review (PRISMA) reporting standards¹⁵. In collaboration with an experienced clinical librarian, a comprehensive literature search was performed in PubMed and Embase from January 1, 1990 to October 1, 2019. For a detailed version of search terms in PubMed and Embase, please refer to **supplementary table 1**. Limitations were used to exclude articles written in another language than English, German or French.

ELIGIBILITY CRITERIA

Studies were eligible for inclusion if they met the following predefined criteria: (1) original report on original data; (2) study design other than case series/case report; (3) reporting on primary tumor excision exclusively for neuroblastoma and/or ganglioneuroblastoma; (4) surgical study population of at least 20 patients; (5) complications of surgery were reported and were related to the surgical excision of the primary tumor (i.e. the complications did not occur during primary tumor biopsy, chemotherapy or radiotherapy); (6) complications were specified, not just reported as only a number or percentage. Articles were excluded if they reported on neurosurgery for neuroblastoma invading the spinal canal (also referred to as 'dumbbell neuroblastoma'), if surgery was combined with intra-operative radiotherapy, or when they concerned ganglioneuroma. If separate articles from the same authors reported on overlapping population and complications, only the most comprehensive publication was included.

OUTCOME OF LITERATURE SEARCH

After completing the literature search and removal of duplicate records, two authors (LMW and MJ) independently screened all records based on title and abstract. The remaining eligible articles were then assessed based on full text. Disagreements were resolved by discussion until consensus. The final included articles were divided into two groups based on their design and reported complications: (A) Surgical complications were the primary outcome measure; (B) Surgical complications were an important secondary outcome measure. The flow chart and results of this literature search are presented in **supplementary figure 1**.

DATA EXTRACTION

Surgical complications were defined as any adverse event as a direct result of the primary tumor resection. For all articles the individually reported complications were collected and subsequently categorized according to the time of occurrence (intraoperative, postoperative <30 days, postoperative >30 days, timing unreported).

If provided by the original article, a specification of severity was noted per complication, as defined by short- or long-term clinical consequence, subsequent intervention or treatment, duration, extent, quantitative assessment or grade according to the validated Clavien-Dindo Classification of Surgical Complications^{16,17}.

To allow for identical representation of complication rate for all articles, nephrectomy was considered a complication in all cases. Hence, the number of kidney removals for completing tumor resection was added to the total number of complications. When provided, it was noted for every nephrectomy whether this was the result of completing the tumor resection or of an intra- or postoperative complication.

From each article, additional data was collected concerning years of inclusion, the total number of children with primary tumor resection, the total number of children with surgical complications, the total number of children with >1 surgical complication and the total number of complications.

To allow for unequivocal presentation, all individually reported complications were also categorized per organ system and type.

QUALITY ASSESSMENT OF INCLUDED STUDIES

A quality assessment of all included studies was performed to determine validity and assess methodology of reporting on surgical complications. Studies were evaluated based on the following four Evidence-Based Medicine Criteria described for observational studies¹⁸⁻²²: study group, follow up, outcome and risk estimation. All four criteria were screened for a clear definition (are the study group, follow-up, reported complications and the analyses of incidence well-defined?). In addition, it was evaluated if the study group was representative to report on surgical complications, if follow-up was complete, if a valid method of collecting data on complications was used, and if confounders were taken into account when outcome was interpreted. For a more detailed description of these criteria of validity, please refer to **table 1**.

Regarding the validity of the outcome, complications were considered well-defined if a specification of severity and a moment of occurrence were provided for the majority of reported complications. Moment of occurrence was regarded specified when the general distinction between intraoperative and postoperative occurrence was reported or a clear distinction between <30 days and >30 days post-operative was made.

STATISTICS

Statistical analysis was performed using Graph Pad Prism 8²³. The D'Agostino & Pearson test was used to test for normal distribution. Column statistics were calculated using the median and interquartile ranges when applicable.

Table 1. Criteria of validity

<p>STUDY GROUP</p> <p>Well-defined Children with (ganglio)neuroblastoma who underwent primary tumor resection</p> <p>Representative Complications are reported for the complete cohort who underwent primary tumor resection, not for a random sample of the patients</p>
<p>FOLLOW-UP</p> <p>Well-defined Follow-up is reported for all patients who underwent primary tumor resection</p> <p>Complete A minimal follow-up period is specified for all patients or the number of patients lost to follow-up is reported or oncological outcome of >95% of all patients is specified</p>
<p>OUTCOME</p> <p>Well-defined A specification of severity and the time of occurrence is provided for the majority of reported complications</p> <p>Valid detection method It is provided how the data on complications is collected</p>
<p>RISK ESTIMATION</p> <p>Well-defined The total number of individual children with one or more complications or the number of children with >1 complication is reported</p> <p>Adjustment for confounders The incidence of reported complications is compared to other literature and important prognostic factors or follow-up are taken into account when doing so</p>

RESULTS

STUDY CHARACTERISTICS

The search yielded 2266 unique articles, of which 65 matched the inclusion criteria, as presented in **supplementary figure 1**. Eleven of these articles reported surgical complications as the primary outcome measure and were added to group A^{9-11,24-3}. Fifty-four articles reported surgical complications as an important secondary outcome measure and were added to group B^{12,14,32-83}.

INCIDENCE OF COMPLICATIONS

Table 2 presents the data on surgical complications per study. The reported number of patients with a primary tumor resection ranged from 20 to 518 patients, with a median of 58 patients per study (IQR 42-105). Only thirty-four studies (7/11 in group A, 27/54 in group B) reported the total number of patients that had complications due to surgical resection. This provided a median percentage of 17.5% of surgical patients having complications (IQR: 9-27; minimum: 1%, maximum: 48%). Only seven studies (2/11 in group A, 5/54 in group B) provided the number of patients that experienced more than one complication^{24,30,34,49,72,73,78}. Hence, no additional analysis on incidence could be executed.

CHARACTERISTICS OF REPORTED COMPLICATIONS

Supplementary table 2 presents the reported complications per study, summarized per organ system and type. For the original description of the individual complications please refer to **supplementary table 3**. The most common intraoperative complication was kidney removal (reported in 32 studies), followed by vascular injury (22 studies) and hemorrhage (16 studies). As only a minority of studies provided reason for nephrectomy, no further definition can be given.

Twenty studies reported on intra- or postoperative hemorrhage. A quantitative assessment of the blood loss was given in only one study⁷³. Four of the 20 studies described a definition for major loss: $>40\text{cc/kg}^{45}$, >0.57 of total circulating blood volume⁷³, $>1\text{L}^{80}$ and $>10\%$ of total circulating blood volume⁸¹. Concerning chylous leakage, pleural effusion or ascites, only one study gave a quantitative assessment and duration of leakage²⁶. One other article described a definition for major leakage: $>400\text{ml/day}^{25}$.

Eleven studies reported on a total of 25 cases of mortality as a surgical complication. Time of occurrence was specified as intra- or postoperative for 8 cases in 5

studies^{9,12,39,41,81}. Cause of death was described for 11 cases in 6 studies^{9,12,39,41,59,70}. Most common cause was severe intra- or postoperative hemorrhage: 7 cases in 4 studies^{12,41,59,70}. Other reported causes hypoxic ischemic encephalopathy following rebound hypoglycaemia after massive transfusion¹², circulatory failure⁹, intestinal perforation followed by shock³⁹, and renal failure⁴¹.

Most common postoperative complication <30 days was either chylous leakage, pleural effusion or ascites (reported in 32 studies), followed by neurological (28 studies) and gastrointestinal complications (18 studies). Most common postoperative complications >30 days were renal complications (atrophy, failure; reported in 12 studies), followed by gastrointestinal complications (adhesions; 11 studies) and diarrhea (6 studies).

VALIDITY OF INCLUDED STUDIES

Data on the validity of all included studies is presented in **table 3**, according to the validity criteria reported in **table 1**. All studies reported on both a well-defined and representative study group, except for one study reporting complications for an unknown subset of the surgical population⁸¹. The length of follow-up of the surgical population was reported in 19 studies (5/11 in group A, 14/54 in group B). The follow-up was considered adequate and complete in 34 studies (5/11 in group A, 29/54 in group B). Regarding the validity of outcome, only 32 studies (7/11 in group A, 25/54 in group B) provided how data on surgical complications was collected. It was not possible to deduce time of occurrence of part of reported complications in 20 studies (2/11 in group A, 18/54 in group B). This mostly concerned hemorrhage, renal complications, gastrointestinal obstruction and mortality. Only 4 studies made a specific distinction between <30 days and >30 days occurrence of postoperative complications^{27,45,61,79}. Regarding severity of the complications, only 21 studies (6/11 group A, 15/54 group B) provided a specification of severity, including one [11] that used the Clavien-Dindo Classification. Thirty-four studies (7/11 in group A, 27/54 in group B) reported the total number of patients that had complications due to surgical resection, seven studies (2/11 in group A, 5/54 in group B) provided the number of patients that suffered more than one complication^{24,30,34,49,72,73,78}. Adjustment for confounders by comparing incidence of reported complications to other literature and taking important prognostic factors or follow-up into account when doing so, was done in 26 studies (6/11 in group A, 20/54 in group B).

Table 2. Characteristics and number of reported complications of included studies

Group	First author	Year of publication	Stage of disease of all included patients (staging system)	Reported number of patients with primary tumor resection	Reported number of patients with complications due to resection (%)	Reported number of patients with >1 complication due to resection (%)	Reported number of complications	Number of intra-operative complications	Number of post-operative complications <30 days	Number of post-operative complications >30 days	Number of post-operative complications, timing unreported	Number of any complications, timing unreported	
A	Barrette et al ²⁴	2006	I/II/III/IV/Vs (INSS)	45	7 (16)	1(2)	8	-	2	6	-	-	
	Canete et al ⁹	1998	I/II/III/IV/Vs (INSS)	78	NM	NM	38	19	18	1	-	-	
	Cantos et al ¹⁰	2006	IV (INSS)	51	NM	NM	82*	9*	24*	-	-	-	
	Chui et al ²⁵	2014	I/III/IV (INSS)	99	10 (10)	0	10	-	10	-	-	-	
	Qureshi et al ²⁶	2016	I/II/III/IV/Vs (INSS)	160	NM	NM	53	-	50	-	3	-	
	Qureshi et al ²⁷	2018	III/IV/Vs (INSS)	54	24 (44)	NM	29	11	18	-	-	-	
	Rees et al ²⁸	1998	III/IV (Evans)	77	19 (25)	0	19	-	-	19	-	-	
	Rich et al ¹¹	2011	II/III/IV (INSS)	207	NM	NM	71	6	15	5	41	4	
	Shamberger et al ²⁹	1998	III/IV (Evans)	349	52 (15)	0	52	52	-	-	-	-	
	Tanabe et al ³⁰	1996	II/III/IV (Evans)	45	13 (29)	1(2)	14	8	-	5	1	-	
	Yoneda et al ³¹	2016	I/II/III (INSS)	82	16 (20)	0	16	5	4	3	2	2	
	B	Adkins et al ³²	2004	II/III/IV (INSS)	399	131 (33)	NM	174	136	14	-	4	20
		Ahmed et al ³³	2018	III (INSS)	106	9 (9)	0	9	2	7	-	-	-
		Avanzini et al ³⁴	2017	III (INSS)	125	14 (11)	3 (2)	33	14	4	-	9	6
		Baker et al ³⁵	2010	III/IV/Vs (INSS)	234	NM	NM	NM	NNS	NNS	-	-	NNS
Ben Barak et al ³⁶		2017	I/III/IV (NM)	24	NM	NM	7	5	2	-	-	-	
Browne et al ³⁷		2006	III/IV (INSS)	30	10 (33)	NM	12	12	-	-	-	-	
Castel et al ³⁸		1999	I/II/III/IV/Vs (INSS)	95	10 (11)	0	10	3	4	-	1	2	

Table 2. Continued.

Group	First author	Year of publication	Stage of disease of all included patients (staging system)	Reported number of patients with primary tumor resection	Reported number of patients with complications due to resection (%)	Reported number of patients with >1 complication due to resection (%)	Reported number of complications	Number of intra-operative complications	Number of post-operative complications <30 days	Number of post-operative complications >30 days	Number of post-operative complications, timing unreported	Number of any complications, timing unreported
	Castel et al ³⁹	2002	IV (INSS)	71	NM	NM	8	5	2	-	1	-
	Castleberry et al ⁴⁰	1991	C (POG)	45	NM	NM	10	6	2	-	-	2
	Cecchetto et al ⁴¹	2005	NM	518	47 (9)	NM	71	22	33	1	2	13
	De Bernardi et al ⁴²	2009	IV/IVs (INSS)	92	NM	NM	11	-	4	-	4	3
	De Couet et al ⁴³	1995	C/D/Ds (POG)	81	12 (15)	0	12	9	3	-	-	-
	Du et al ⁴⁴	2014	IV (INSS)	41	19 (46)	NM	35	27	8	-	-	-
	Fahy et al ⁴⁵	2019	III/IV (INSS)	58	NM	NM	23	23	-	-	-	-
	Fischer et al ⁴⁶	2017	I/III/III (INSS)	179	40 (22)	NM	50	NNS	NNS	-	NNS	NNS
	Fraga et al ⁴⁷	2010	I/II/III/IV/IVs (INSS)	43 (10 GN)	11 (24)	0	11	-	11	-	-	-
	Fumino et al ⁴⁸	2015	I/II/III (INSS)	30	2 (7)	0	2	1	1	-	-	-
	Haase et al ⁴⁹	1991	II/III/IV (Evans)	52	18 (35)	1 (2)	38	23	9	2	-	4
	Haberle et al ⁵⁰	2002	I/II/III/IV/IVs (INSS)	104	NM	NM	43	5	36	1	-	1
	Hase et al ⁵¹	2002	I/II/III/IVa/IVb (Evans)	20	NM	NM	5	4	1	-	-	-
	Hishiki et al ⁵²	2018	II/III/IV (INSS)	47	NM	NM	11	8	3	-	-	-
	Hsu et al ⁵³	2006	III/IV (INSS)	45	NM	NM	8	5	1	2	-	-
	Iehara et al ⁵⁴	2013	I/II/III (INSS)	233	NM	NM	29	1	9	5	11	3
	Iehara et al ⁵⁵	2019	I/II/III/IVs (INSS)	38	NM	NM	45	3	1	1	-	40
	Ikedo et al ⁵⁶	1998	I/II/III/IV/IVs (INSS)	50	9 (18)	0	9	1	4	4	-	-

Table 2. Continued.

Group	First author	Year of publication	Stage of disease of all included patients (staging system)	Reported number of patients with primary tumor resection	Reported number of patients with complications due to resection (%)	Reported number of patients with >1 complication due to resection (%)	Reported number of complications	Number of intra-operative complications	Number of post-operative complications <30 days	Number of post-operative complications >30 days	Number of post-operative complications, timing unreported	Number of any complications, timing unreported
	Irtan et al ⁵⁷	2015	I/L2/M/Ms (INRGSS)	39 (6 GN)	5 (13)	0	5	-	4	1	-	-
	Irtan et al ⁵⁸	2015	L2/M/Ms (INRGSS)	39	NM	NM	18	12	4	2	-	-
	Kiely et al ¹²	2007	I/II/III/IV (INSS)	255	NM	NM	NM	3	NNS	6	-	-
	Kohler et al ⁵⁹	2013	II/III (INSS)	130	NM	NM	36	18	13	-	-	5
	Kubota et al ⁶⁰	2010	I/II/III/IV/IVs (INSS)	83	5 (6)	0	5	3	1	1	-	-
	La Quaglia et al ⁶¹	2004	IV (INSS)	103	NM	NM	15	7	4	4	-	-
	Leclair et al ⁶²	2008	I/II/III/IV/IVs (INSS)	45	NM	NM	4	-	4	-	-	-
	Li et al ⁶³	2012	I/II/III/IV/IVs (INSS)	77	NM	NM	11	8	3	-	-	-
	Malek et al ⁶⁴	2010	I/II/III/IV (NM)	36	NM	NM	8	-	7	1	-	-
	Martinez et al ⁶⁵	1992	IVs (Evans)	24	4 (17)	0	4	-	2	2	-	-
	Nishio et al ⁶⁶	2006	I/II/III/IV/IVs (Evans)	51	NM	NM	16	-	3	2	11	-
	Olgun et al ⁶⁷	2003	I/III/IV/IVs (INSS)	57	2 (4)	0	2	-	2	-	-	-
	Parikh et al ⁶⁸	2012	I/II/III/IV (INSS)	24	NM	NM	5	-	5	-	-	-
	Phelps et al ⁶⁹	2019	I/II/III/IV (INSS)	86 (5 GN)	NM	NM	19	14	5	-	-	-
	Rubie et al ⁷⁰	1997	I/II/III (INSS)	211	15 (7)	NM	26	13	8	-	-	5
	Rubie et al ⁷¹	2011	II/III (INSS)	102	6 (6)	0	6	2	4	-	-	-
	Salim et al ⁷²	2011	I/II/III/IV/IVs (INSS)	53	13 (25)	1 (2)	14	6	8	-	-	-
	Shamberger et al ⁷⁵	1991	III/IV (Evans)	42	9 (21)	1 (2)	10	5	1	-	1	3

Table 2. Continued.

Group	First author	Year of publication	Stage of disease of all included patients (staging system)	Reported number of patients with primary tumor resection	Reported number of patients with complications due to resection (%)	Reported number of patients with >1 complication due to resection (%)	Reported number of complications	Number of intra-operative complications	Number of post-operative complications <30 days	Number of post-operative complications >30 days	Number of post-operative complications, timing unreported	Number of any complications, timing unreported
	Simon et al ¹⁴	2008	I/II/III (INSS)	366	70 (19)	NM	82	19	29	-	4	30
	Simon et al ⁷⁴	2013	IV (INSS)	237	NM	NM	75	44	17	-	14	-
	Tajiri et al ⁷⁵	2012	I/II/III/IV/IVs (INSS)	82	5 (6)	0	5	-	1	4	-	-
	Tanaka et al ⁷⁶	2016	I/II/III/IV/IVs (INSS)	20	2 (1)	0	2	-	-	-	-	2
	Tokiwa et al ⁷⁷	2003	I/II/III/IV/IVs (Evans)	47	NM	NM	15	-	10	5	-	-
	Varan et al ⁷⁸	2015	II/III/IV (INSS)	23	5 (22)	2 (9)	8	7	-	-	1	-
	Vollmer et al ⁷⁹	2018	IV (INSS)	40	19 (48)	NM	40	30	10	-	-	-
	Von Allmen et al ⁸⁰	2005	III/IV (INSS)	70	22 (31)	NM	24	10	11	2	1	-
	Von Allmen et al ⁸¹	2017	II/III/IV/IVs (INSS)	110	NM	NM	40	28	-	-	4	8
	Yao et al ⁸²	2018	I/II (INSS)	39	NM	NM	6	6	-	-	-	-
	Yao et al ⁸³	2019	I/II/IVs (INSS)	34	NM	NM	3	1	2	-	-	-

Group A: surgical complications were reported as the primary outcome measure.

Group B: surgical complications were reported as an important secondary outcome measure.

*not all complications are specified.

INSS International Neuroblastoma Staging System; NM Not Mentioned; NNS Number Not Specified; POG Pediatric Oncology Group; INRGSS International Neuroblastoma Risk Group Staging System; GN Ganglioneuroma.

Table 3. Validity of the included studies

Group	Author	Year	Study group		Follow-up		Outcome		Risk estimation	
			Well defined	Representative	Well defined	Complete	Well defined	Valid detection method	Well defined	Adjustment confounders
A	Barrette et al ²⁴	2006	+	+	+	+	+	+	+	+
	Canete et al ⁹	1998	+	+	-	+	-	+	-	+
	Cantos et al ¹⁰	2006	+	+	+	-	-	+	-	-
	Chui et al ²⁵	2014	+	+	+	+	+	+	+	-
	Qureshi et al ²⁶	2016	+	+	+	-	+	-	+	-
	Qureshi et al ²⁷	2018	+	+	+	+	-	-	+	+
	Rees et al ²⁸	1998	+	+	-	+	+	+	+	+
	Rich et al ¹¹	2011	+	+	-	-	-	+	-	+
	Shamberger et al ²⁹	1998	+	+	-	-	-	+	+	+
	Tanabe et al ³⁰	1996	+	+	-	-	+	-	+	-
	Yoneda et al ³¹	2016	+	+	-	-	-	-	+	-
	No. of studies (total 11)			11	11	5	5	5	7	8
B	Adkins et al ³²	2004	+	+	-	-	-	-	+	+
	Ahmed et al ³³	2018	+	+	-	-	-	+	+	+
	Avanzini et al ³⁴	2017	+	+	-	-	-	-	+	+
	Baker et al ³⁵	2010	+	+	-	+	-	-	-	-
	Ben Barak et al ³⁶	2017	+	+	-	+	+	+	-	-
	Browne et al ³⁷	2006	+	+	+	+	-	-	+	+
	Castel et al ³⁸	1999	+	+	-	-	-	-	+	-
	Castel et al ³⁹	2002	+	+	-	-	-	+	-	-
	Castleberry et al ⁴⁰	1991	+	+	-	-	-	-	-	-
	Cecchetto et al ⁴¹	2005	+	+	+	-	-	+	+	-
	De Bernardi et al ⁴²	2009	+	+	-	+	-	-	-	-
	De Cou et al ⁴³	1995	+	+	-	-	-	+	+	+
	Du et al ⁴⁴	2014	+	+	-	-	-	+	+	-
	Fahy et al ⁴⁵	2019	+	+	+	+	-	+	-	+

Table 3. Continued.

Group	Author	Year	Study group		Follow-up		Outcome		Risk estimation	
			Well defined	Representative	Well defined	Complete	Well defined	Valid detection method	Well defined	Adjustment confounders
	Fischer et al ⁴⁶	2017	+	+	-	-	-	-	+	+
	Fraga et al ⁴⁷	2010	+	+	+	-	+	-	+	+
	Fumino et al ⁴⁸	2015	+	+	+	+	-	+	+	-
	Haase et al ⁴⁹	1991	+	+	-	+	-	-	+	+
	Haberle et al ⁵⁰	2002	+	+	+	+	-	+	-	+
	Hase et al ⁵¹	2002	+	+	-	+	+	-	-	-
	Hishiki et al ⁵²	2018	+	+	-	+	-	-	-	-
	Hsu et al ⁵³	2006	+	+	+	+	-	+	-	+
	lehara et al ⁵⁴	2013	+	+	-	-	-	-	-	-
	lehara et al ⁵⁵	2019	+	+	-	-	-	-	-	+
	Ikeda et al ⁵⁶	1998	+	+	-	+	+	+	+	+
	Irtan et al ⁵⁷	2015	+	+	+	-	+	-	+	-
	Irtan et al ⁵⁸	2015	+	+	-	-	+	-	-	-
	Kiely et al ¹²	2007	+	+	-	-	+	-	-	-
	Kohler et al ⁵⁹	2013	+	+	-	-	-	-	-	-
	Kubota et al ⁶⁰	2010	+	+	-	+	-	-	+	-
	La Quaglia et al ⁶¹	2004	+	+	-	+	+	+	-	-
	Leclair et al ⁶²	2008	+	+	+	+	+	-	-	-
	Li et al ⁶³	2012	+	+	-	+	+	+	-	-
	Malek et al ⁶⁴	2010	+	+	-	-	-	+	-	+
	Martinez et al ⁶⁵	1992	+	+	-	+	+	+	+	-
	Nishio et al ⁶⁶	2006	+	+	-	+	-	-	+	+
	Olgun et al ⁶⁷	2003	+	+	-	+	-	-	+	-
	Parikh et al ⁶⁸	2012	+	+	-	+	+	-	-	-
	Phelps et al ⁶⁹	2019	+	+	-	-	-	+	-	+
	Rubie et al ⁷⁰	1997	+	+	-	+	-	-	+	+
	Rubie et al ⁷¹	2011	+	+	-	+	-	-	+	-
	Salim et al ⁷²	2011	+	+	-	-	+	+	+	-

Table 3. Continued.

Group	Author	Year	Study group		Follow-up		Outcome		Risk estimation	
			Well defined	Representative	Well defined	Complete	Well defined	Valid detection method	Well defined	Adjustment confounders
	Shamberger et al ⁷³	1991	+	+	-	-	-	+	+	-
	Simon et al ¹⁴	2008	+	+	-	-	-	+	+	+
	Simon et al ⁷⁴	2013	+	+	-	-	-	+	-	-
	Tajiri et al ⁷⁵	2012	+	+	-	-	-	-	+	-
	Tanaka et al ⁷⁶	2016	+	+	+	+	-	-	+	-
	Tokiwa et al ⁷⁷	2003	+	+	+	+	+	+	+	-
	Varan et al ⁷⁸	2015	+	+	+	+	-	+	+	+
	Vollmer et al ⁷⁹	2018	+	+	-	+	-	+	+	-
	Von Allmen et al ⁸⁰	2005	+	+	-	+	-	-	+	+
	Von Allmen et al ⁸¹	2017	+	-	-	-	-	+	-	-
	Yao et al ⁸²	2018	+	+	+	+	-	-	-	-
	Yao et al ⁸³	2019	+	+	+	+	+	+	-	-
	No. of studies (total 54)		54	53	14	29	15	25	29	20

Group A: surgical complications were reported as the primary outcome measure.

Group B: surgical complications were reported as an important secondary outcome measure.

DISCUSSION

In this systematic review, literature concerning frequency and characteristics of surgical complications in patients with neuroblastoma is summarized. In addition, we evaluated the quality of reporting on these complications to gain understanding of the validity of the current reports.

Primary tumor resection is an important part of treatment in patients with neuroblastoma, however, is often related to serious morbidity and mortality. We found a median percentage of 17.5% of surgical patients who suffered complications. However, structured reporting of complications was scarce. The total number of patients with complications was reported in only half of the studies and a minority

of 7 studies provided the number of patients with more than one complication. These factors made it impossible to perform any analysis other than providing a descriptive summary.

Certain factors also need to be taken into account when interpreting the validity of the reported number of complications.

There is debate in literature and clinical practice whether some adverse events linked to resection should be considered as complications for example sequelae such as scoliosis, Horner syndrome and adrenal insufficiency after bilateral adrenal resection. We feel that the primary aim of resection is to remove the tumor while causing no harm to adjacent structures, and thus all sequelae should be considered as complications. A similar debate exists for kidney removal. Although nephrectomy performed for the completion of tumor excision is now considered a surgical complication and therefore avoided in most institutions, this was not the case in earlier days⁶¹. We found that the majority of the included studies did not consider unplanned kidney removal to be a complication, nor provided a statement on reason for nephrectomy. When analyzing all kidney removal over time the number seemed to decrease slightly, however not significantly. A general consensus on whether these specific adverse events are to be considered surgical complications is vital for a reliable interpretation of the risks of neuroblastoma surgery.

As reflected in the performed quality assessment of the included studies, we found a high variability in methodology, and completeness of data was often not guaranteed. Incomplete information on follow-up and not providing the method of collecting data on complications provided additional opportunity for missing data and underreporting. Some studies collected the complications from national registries, even though this method is at risk of representing incomplete data as opposed to analysis of the clinical records^{84,85}.

For the appropriate interpretation of reports on surgical complications, the use of uniform definitions and a description of severity and impact is fundamental^{86,87}. In the included studies, hemorrhage and chylous leakage were among the most frequently reported complications, however no uniform definition was found for reporting on either and most studies did not provide their own definition. Information on time of occurrence for hemorrhage, renal events, gastrointestinal obstruction and mortality was often missing, making them completely uninterpretable. Cause of death was provided in only the minority of mortality cases. Accurate description of the clinical consequence of the complications using the validated Clavien-Dindo Classification of surgical complications was done in only one study¹¹.

These described gaps in methodology impede uniform interpretation and reliable comparison of the quality of reporting between studies. This then hinders proper estimation of the difficulties encountered in neuroblastoma surgery and obstructs insight in points of improvement of surgical strategy. In order to learn from past experiences and optimize surgical strategies, openness with regard to this sensitive topic is essential and necessary.

FUTURE REPORTING

To improve future reporting on surgical complications, several issues are of importance: the method of data collection on complications should be provided; the total number of patients that suffered complications as well as the total number that suffered more than one complication should be reported; follow-up should be specified and complete. Furthermore, definitions of specific complications should be provided.

Recently a joint initiative by the SIOPEN (SIOP Europe International Neuroblastoma Study Groep), COG (Children's Oncology Group) and GPOH (German Association of Pediatric Oncology and Haematology) was published concerning systematic reporting of neuroblastoma surgery by the use of an International Neuroblastoma Surgical Report Form (INSRF) [88]. This publication proposes a standard form to be completed after every surgery in neuroblastoma patients and includes a registration form for complications in the first 30 days. **Table 4** shows the complication form of the INSRF. The form uses the Clavien-Dindo Classification of Surgical Complications^{16,17} and thus the subsequent intervention or treatment and clinical consequence of any complication are uniformly reported.

We feel that with regard to specific complications, additional aspects to accurately describe severity should also be added to the Clavien-Dindo grade, such as a quantitative assessment (e.g. hemorrhage, chylous leakage), the duration (e.g. diarrhea, gastrointestinal obstruction), the extent (e.g. ischemia) and the cause (mortality). In addition, we find it is important to report on long term complications and sequelae as well.

ACKNOWLEDGEMENTS

We would like to thank dr. Lucas Matthijssens and his group for their kind permission to reprint the complication form of the INSRF.

Table 4. The International Neuroblastoma Surgical Report Form

POSTOPERATIVE COMPLICATIONS up till Postoperative Day 30	CLAVIEN-DINDO CLASSIFICATION (see next page)	SPECIFY
Postoperative bleeding: <input type="checkbox"/> NO / <input type="checkbox"/> YES, specify cause:	<input type="checkbox"/> I <input type="checkbox"/> II <input type="checkbox"/> III-a <input type="checkbox"/> III-b <input type="checkbox"/> IV-a <input type="checkbox"/> IV-b <input type="checkbox"/> V	
Hypovolemia requiring inotropic support: <input type="checkbox"/> NO / <input type="checkbox"/> YES	<input type="checkbox"/> I <input type="checkbox"/> II <input type="checkbox"/> III-a <input type="checkbox"/> III-b <input type="checkbox"/> IV-a <input type="checkbox"/> IV-b <input type="checkbox"/> V	
Fluid overload requiring diuretics +/- O2: <input type="checkbox"/> NO / <input type="checkbox"/> YES	<input type="checkbox"/> I <input type="checkbox"/> II <input type="checkbox"/> III-a <input type="checkbox"/> III-b <input type="checkbox"/> IV-a <input type="checkbox"/> IV-b <input type="checkbox"/> V	
Systemic inflammatory response syndrome (SIRS) requiring intensive care > 72h: <input type="checkbox"/> NO / <input type="checkbox"/> YES	<input type="checkbox"/> I <input type="checkbox"/> II <input type="checkbox"/> III-a <input type="checkbox"/> III-b <input type="checkbox"/> IV-a <input type="checkbox"/> IV-b <input type="checkbox"/> V	
Stroke: <input type="checkbox"/> NO / <input type="checkbox"/> YES	<input type="checkbox"/> I <input type="checkbox"/> II <input type="checkbox"/> III-a <input type="checkbox"/> III-b <input type="checkbox"/> IV-a <input type="checkbox"/> IV-b <input type="checkbox"/> V	
Vascular spinal cord injury: <input type="checkbox"/> NO / <input type="checkbox"/> YES	<input type="checkbox"/> I <input type="checkbox"/> II <input type="checkbox"/> III-a <input type="checkbox"/> III-b <input type="checkbox"/> IV-a <input type="checkbox"/> IV-b <input type="checkbox"/> V	
Renal atrophy (ischemia): <input type="checkbox"/> Right / <input type="checkbox"/> Left <input type="checkbox"/> NO <input type="checkbox"/> YES, specify: <input type="checkbox"/> Partial ischemia <input type="checkbox"/> Total ischemia	<input type="checkbox"/> I <input type="checkbox"/> II <input type="checkbox"/> III-a <input type="checkbox"/> III-b <input type="checkbox"/> IV-a <input type="checkbox"/> IV-b <input type="checkbox"/> V	Diagnosis: <input type="checkbox"/> US <input type="checkbox"/> CT <input type="checkbox"/> Nuclear scan
Renal dysfunction: <input type="checkbox"/> NO / <input type="checkbox"/> YES, specify:	<input type="checkbox"/> I <input type="checkbox"/> II <input type="checkbox"/> III-a <input type="checkbox"/> III-b <input type="checkbox"/> IV-a <input type="checkbox"/> IV-b <input type="checkbox"/> V	
Bladder dysfunction: <input type="checkbox"/> NO / <input type="checkbox"/> YES, specify:	<input type="checkbox"/> I <input type="checkbox"/> II <input type="checkbox"/> III-a <input type="checkbox"/> III-b <input type="checkbox"/> IV-a <input type="checkbox"/> IV-b <input type="checkbox"/> V	
Hepatic dysfunction: <input type="checkbox"/> NO / <input type="checkbox"/> YES, specify:	<input type="checkbox"/> I <input type="checkbox"/> II <input type="checkbox"/> III-a <input type="checkbox"/> III-b <input type="checkbox"/> IV-a <input type="checkbox"/> IV-b <input type="checkbox"/> V	
Pulmonary dysfunction: <input type="checkbox"/> NO / <input type="checkbox"/> YES, specify:	<input type="checkbox"/> I <input type="checkbox"/> II <input type="checkbox"/> III-a <input type="checkbox"/> III-b <input type="checkbox"/> IV-a <input type="checkbox"/> IV-b <input type="checkbox"/> V	
Postop stenosis of vascular structures: <input type="checkbox"/> NO / <input type="checkbox"/> YES:	<input type="checkbox"/> I <input type="checkbox"/> II <input type="checkbox"/> III-a <input type="checkbox"/> III-b <input type="checkbox"/> IV-a <input type="checkbox"/> IV-b <input type="checkbox"/> V	
Infection: <input type="checkbox"/> NO <input type="checkbox"/> YES: <input type="checkbox"/> Fever >48h postop eci, AB administ <input type="checkbox"/> Pneumonia <input type="checkbox"/> Urinary tract <input type="checkbox"/> Wound <input type="checkbox"/> Intravenous access line <input type="checkbox"/> Other, please specify:	<input type="checkbox"/> I <input type="checkbox"/> II <input type="checkbox"/> III-a <input type="checkbox"/> III-b <input type="checkbox"/> IV-a <input type="checkbox"/> IV-b <input type="checkbox"/> V	Specify on postop day...
Adrenal insufficiency: <input type="checkbox"/> NO / <input type="checkbox"/> YES, specify	<input type="checkbox"/> I <input type="checkbox"/> II <input type="checkbox"/> III-a <input type="checkbox"/> III-b <input type="checkbox"/> IV-a <input type="checkbox"/> IV-b <input type="checkbox"/> V	
Intestinal obstruction > 7 days <input type="checkbox"/> NO <input type="checkbox"/> YES, specify: <input type="checkbox"/> Paralytic Ileus <input type="checkbox"/> Mechanical Obstruction	<input type="checkbox"/> I <input type="checkbox"/> II <input type="checkbox"/> III-a <input type="checkbox"/> III-b <input type="checkbox"/> IV-a <input type="checkbox"/> IV-b <input type="checkbox"/> V	
Wound dehiscence <input type="checkbox"/> NO <input type="checkbox"/> YES, specify location & postop day	<input type="checkbox"/> I <input type="checkbox"/> II <input type="checkbox"/> III-a <input type="checkbox"/> III-b <input type="checkbox"/> IV-a <input type="checkbox"/> IV-b <input type="checkbox"/> V	
Chylous leak – Chest: <input type="checkbox"/> NO / <input type="checkbox"/> YES	<input type="checkbox"/> I <input type="checkbox"/> II <input type="checkbox"/> III-a <input type="checkbox"/> III-b <input type="checkbox"/> IV-a <input type="checkbox"/> IV-b <input type="checkbox"/> V	
Chylous leak – Abdomen: <input type="checkbox"/> NO / <input type="checkbox"/> YES	<input type="checkbox"/> I <input type="checkbox"/> II <input type="checkbox"/> III-a <input type="checkbox"/> III-b <input type="checkbox"/> IV-a <input type="checkbox"/> IV-b <input type="checkbox"/> V	
Unplanned ICU admission: <input type="checkbox"/> NO <input type="checkbox"/> YES, specify	<input type="checkbox"/> I <input type="checkbox"/> II <input type="checkbox"/> III-a <input type="checkbox"/> III-b <input type="checkbox"/> IV-a <input type="checkbox"/> IV-b <input type="checkbox"/> V	Postop day: Cause: Treatment:
Unplanned return to operating theater <input type="checkbox"/> NO <input type="checkbox"/> YES, specify	<input type="checkbox"/> I <input type="checkbox"/> II <input type="checkbox"/> III-a <input type="checkbox"/> III-b <input type="checkbox"/> IV-a <input type="checkbox"/> IV-b <input type="checkbox"/> V	Postop day: Cause: Treatment::
Diarrhea 30 days postop (without infectious cause) <input type="checkbox"/> NO <input type="checkbox"/> YES	<input type="checkbox"/> I <input type="checkbox"/> II <input type="checkbox"/> III-a <input type="checkbox"/> III-b <input type="checkbox"/> IV-a <input type="checkbox"/> IV-b <input type="checkbox"/> V	
Motor Nerve dysfunction: <input type="checkbox"/> NO <input type="checkbox"/> YES, please specify cause:	<input type="checkbox"/> I <input type="checkbox"/> II <input type="checkbox"/> III-a <input type="checkbox"/> III-b <input type="checkbox"/> IV-a <input type="checkbox"/> IV-b <input type="checkbox"/> V	Nerve(s) affected:
Sensory Nerve dysfunction: <input type="checkbox"/> NO <input type="checkbox"/> YES, please specify cause:	<input type="checkbox"/> I <input type="checkbox"/> II <input type="checkbox"/> III-a <input type="checkbox"/> III-b <input type="checkbox"/> IV-a <input type="checkbox"/> IV-b <input type="checkbox"/> V	Nerve(s) affected:
Postoperative death <input type="checkbox"/> NO <input type="checkbox"/> YES, specify cause: <input type="checkbox"/> Bleeding <input type="checkbox"/> Other: specify: <input type="checkbox"/> Unknown cause	<input type="checkbox"/> V	When? postop day Autopsy performed?: Findings

Was there an unscheduled DELAY of postoperative chemotherapy regimen? NO / YES → Delay in number of days:

Was this delay of postoperative chemotherapy due to surgery? NO / YES → Cause:

REFERENCES

- 1 Maris JM. Recent Advances in Neuroblastoma. *N Engl J Med* 2010;362:2202-11. <https://doi.org/10.1056/NEJMra0804577>.
- 2 Tas ML, Reedijk AMJ, Karim-Kos HE, Kremer LCM, van de Ven CP, Dierselhuis MP, et al. Neuroblastoma between 1990 and 2014 in the Netherlands: Increased incidence and improved survival of high-risk neuroblastoma. *Eur J Cancer* 2020;124:47-55. <https://doi.org/10.1016/j.ejca.2019.09.025>.
- 3 Ryan AL, Akinkuotu A, Pierro A, Morgenstern DA, Irwin MS. The Role of Surgery in High-risk Neuroblastoma. *J Pediatr Hematol Oncol* 2020;42:1-7. <https://doi.org/10.1097/MPH.0000000000001607>.
- 4 Yang X, Chen J, Wang N, Liu Z, Li F, Zhou J, et al. Impact of extent of resection on survival in high-risk neuroblastoma: A systematic review and meta-analysis. *J Pediatr Surg* 2019;54:1487-94. <https://doi.org/10.1016/j.jpedsurg.2018.08.046>.
- 5 Mullassery D, Farrelly P, Losty PD. Does Aggressive Surgical Resection Improve Survival in Advanced Stage 3 and 4 Neuroblastoma? A Systematic Review and Meta-analysis. *Pediatr Hematol Oncol* 2014;31:703-16. <https://doi.org/10.3109/08880018.2014.947009>.
- 6 La Quaglia MP. State of the art in oncology: high risk neuroblastoma, alveolar rhabdomyosarcoma, desmoplastic small round cell tumor, and POST-TEXT 3 and 4 hepatoblastoma. *J Pediatr Surg* 2014;49:233-40. <https://doi.org/10.1016/j.jpedsurg.2013.11.029>.
- 7 Zwaveling S, Tytgat GAM, van der Zee DC, Wijnen MHWA, Heij HA. Is complete surgical resection of stage 4 neuroblastoma a prerequisite for optimal survival or may >95 % tumour resection suffice? *Pediatr Surg Int* 2012;28:953-9. <https://doi.org/10.1007/s00383-012-3109-3>.
- 8 Jans M, Wijnen M, Van De Ven C, Van Baren R, Tytgat G, Zwaveling S. Analysis of surgery for neuroblastoma in the Netherlands. Abstract O-155, SIOP ABSTRACTS. *Pediatr Blood Cancer* 2016;63:S5-321. <https://doi.org/http://dx.doi.org/10.1002/pbc.26233>.
- 9 Canete A, Jovani C, Lopez A, Costa E, Segarra V, Fernandez JM, et al. Surgical treatment for neuroblastoma: complications during 15 years' experience. *J Pediatr Surg* 1998;33:1526-30.
- 10 Cantos MF, Gerstle JT, Irwin MS, Pappo A, Farley S, Cheang T, et al. Surgical challenges associated with intensive treatment protocols for high-risk neuroblastoma. *J Pediatr Surg* 2006;41:960-5. <https://doi.org/10.1016/j.jpedsurg.2006.01.059>.
- 11 Rich BS, McEvoy MP, Kelly NE, Oh E, Abramson SJ, Price AP, et al. Resectability and operative morbidity after chemotherapy in neuroblastoma patients with encasement of major visceral arteries. *J Pediatr Surg* 2011;46:103-7. <https://doi.org/10.1016/j.jpedsurg.2010.09.075>.
- 12 Kiely E. A technique for excision of abdominal and pelvic neuroblastomas. *Ann R Coll Surg Engl* 2007;89:342-8. <https://doi.org/10.1308/003588407X179071>.

- 13 Davidoff AM, Fernandez-Pineda I. Complications in the surgical management of children with malignant solid tumors. *Semin Pediatr Surg* 2016;25:395–403. <https://doi.org/10.1053/j.sempedsurg.2016.10.003>.
- 14 Simon T, Hero B, Benz-Bohm G, Von Schweinitz D, Berthold F. Review of image defined risk factors in localized neuroblastoma patients: Results of the GPOH NB97 trial. *Pediatr Blood Cancer* 2008. <https://doi.org/10.1002/pbc.21343>.
- 15 Liberati A, Altman DG, Tetzlaff J, Mulrow C, Gotzsche PC, Ioannidis JPA, et al. The PRISMA statement for reporting systematic reviews and meta-analyses of studies that evaluate healthcare interventions: explanation and elaboration. *BMJ* 2009;339:b2700–b2700. <https://doi.org/10.1136/bmj.b2700>.
- 16 Dindo D, Demartines N, Clavien PA. Classification of surgical complications: A new proposal with evaluation in a cohort of 6336 patients and results of a survey. *Ann Surg* 2004;240:205–13. <https://doi.org/10.1097/01.sla.0000133083.54934.ae>.
- 17 Clavien PA, Barkun J, De Oliveira ML, Vauthey JN, Dindo D, Schulick RD, et al. The Clavien-Dindo classification of surgical complications: Five-year experience. *Ann Surg* 2009;250:187–96. <https://doi.org/10.1097/SLA.0b013e3181b13ca2>.
- 18 Laupacis A, Wells G, Richardson WS, Tugwell P. Users' Guides to the Medical Literature: V. How to Use an Article About Prognosis. *JAMA J Am Med Assoc* 1994;272:234–7. <https://doi.org/10.1001/jama.1994.03520030076032>.
- 19 Grimes DA, Schulz KF. Cohort studies: Marching towards outcomes. *Lancet* 2002;359:341–5. [https://doi.org/10.1016/S0140-6736\(02\)07500-1](https://doi.org/10.1016/S0140-6736(02)07500-1).
- 20 Kremer LCM, van der Pal HJH, Offringa M, van Dalen EC, Voute PA. Frequency and risk factors of subclinical cardiotoxicity after anthracycline therapy in children: A systematic review. *Ann Oncol* 2002;13:819–29. <https://doi.org/10.1093/annonc/mdf167>.
- 21 Van Dalen EC, Van Der Pal HJH, Bakker PJM, Caron HN, Kremer LCM. Cumulative incidence and risk factors of mitoxantrone-induced cardiotoxicity in children: A systematic review. *Eur J Cancer* 2004;40:643–52. <https://doi.org/10.1016/j.ejca.2003.12.006>.
- 22 Van der Pal HJH, van Dalen EC, Kremer LCM, Bakker PJM, van Leeuwen FE. Risk of morbidity and mortality from cardiovascular disease following radiotherapy for childhood cancer: A systematic review. *Cancer Treat Rev* 2005;31:173–85. <https://doi.org/10.1016/j.ctrv.2005.03.008>.
- 23 Graph Pad Software Inc., La Jolla, CA, USA.
- 24 Barrette S, Bernstein ML, Leclerc JM, Champagne MA, Samson Y, Brossurad J, et al. Treatment complications in children diagnosed with neuroblastoma during a screening program. *J Clin Oncol* 2006;24:1542–5. <https://doi.org/10.1200/JCO.2005.04.4602>.
- 25 Chui C-H. Mesenteric lymphatic ligation in the prevention of chylous fistulae in abdominal neuroblastoma surgery. *Pediatr Surg Int* 2014;30:1009–12. <https://doi.org/10.1007/s00383-014-3581-z>.
- 26 Qureshi SS, Rent EG, Bhagat M, Dsouza P, Kembhavi S, Vora T, et al. Chyle leak following surgery for abdominal neuroblastoma. *J Pediatr Surg* 2016;51:1557–60. <https://doi.org/10.1016/j.jpedsurg.2015.11.002>.

- 27 Qureshi SS, Bhagat M, Harris C, Chinnaswamy G, Vora T, Kembhavi S, et al. Outcomes and complications of surgery in patients with intermediate-risk neuroblastoma: experience from an Indian tertiary Cancer Centre. *Pediatr Surg Int* 2018;34:435–42. <https://doi.org/10.1007/s00383-018-4241-5>.
- 28 Rees H, Markley MA, Kiely EM, Pierro A, Pritchard J. Diarrhea after resection of advanced abdominal neuroblastoma: A common management problem. *Surgery* 1998;123:568–72. <https://doi.org/10.1067/msy.1998.88092>.
- 29 Shamberger RC, Smith EI, Joshi V V, Rao P V, Hayes FA, Bowman LC, et al. The risk of nephrectomy during local control in abdominal neuroblastoma. *J Pediatr Surg* 1998;33:161–4.
- 30 Tanabe M, Ohnuma N, Iwai J, Yoshida H, Takahashi H. Renal impairment after surgical resection of neuroblastoma. *J Pediatr Surg* 1996;31:1252–5. [https://doi.org/10.1016/S0022-3468\(96\)90244-4](https://doi.org/10.1016/S0022-3468(96)90244-4).
- 31 Yoneda A, Nishikawa M, Uehara S, Oue T, Usui N, Inoue M, et al. Can Image-Defined Risk Factors Predict Surgical Complications in Localized Neuroblastoma? *Eur J Pediatr Surg* 2015;26:117–22. <https://doi.org/10.1055/s-0035-1566100>.
- 32 Adkins ES, Sawin R, Gerbing RB, London WB, Matthay KK, Haase GM. Efficacy of complete resection for high-risk neuroblastoma: a Children's Cancer Group study. *J Pediatr Surg* 2004;39:931–6. <https://doi.org/10.1016/j.jpedsurg.2004.02.041>.
- 33 Ahmed G, Fawzy M, Elmenawi S, Elzomor H, Yosif Y, Elkinaai N, et al. Role of surgery in localized initially unresectable neuroblastoma. *J Pediatr Urol* 2018;14:231–6. <https://doi.org/10.1016/j.jpuro.2018.03.008>.
- 34 Avanzini S, Pio L, Erminio G, Granata C, Holmes K, Gambart M, et al. Image-defined risk factors in unresectable neuroblastoma: SIOPEN study on incidence, chemotherapy-induced variation, and impact on surgical outcomes. *Pediatr Blood Cancer* 2017. <https://doi.org/10.1002/pcb.26605>.
- 35 Baker DL, Schmidt ML, Cohn SL, Maris JM, London WB, Buxton A, et al. Outcome after Reduced Chemotherapy for Intermediate-Risk Neuroblastoma. *N Engl J Med* 2010;363:1313–23. <https://doi.org/10.1056/NEJMoa1001527>.
- 36 Ben Barak A, Golan H, Waldman D, Arkovitz MS. Surgical Treatment of Neuroblastoma. *Isr Med Assoc J* 2017;19:691–5. <https://doi.org/10.24110/0031-403X-2020-99-4-93-102>.
- 37 Browne M, Kletzel M, Cohn SL, Seshadri R, Reynolds M. Excellent local tumor control regardless of extent of surgical resection after treatment on the Chicago Pilot II protocol for neuroblastoma. *J Pediatr Surg* 2006;41:271–6. <https://doi.org/10.1016/j.jpedsurg.2005.10.050>.
- 38 Castel V, Garcia-Miguel, P, Cañete, A, Melero C, Navajas A, Ruiz-Jiménez, JI, et al. Prospective evaluation of the International Neuroblastoma Staging System (INSS) and the International Neuroblastoma Response Criteria (INRC) in a multicentre setting. *Eur J Cancer* 1999;35:606–11. [https://doi.org/10.1016/S0959-8049\(98\)00395-5](https://doi.org/10.1016/S0959-8049(98)00395-5).
- 39 Castel V, Tovar JA, Costa E, Cuadros J, Ruiz A, Rollan V, et al. The role of surgery in stage IV neuroblastoma. *J Pediatr Surg* 2002;37:1574–8.

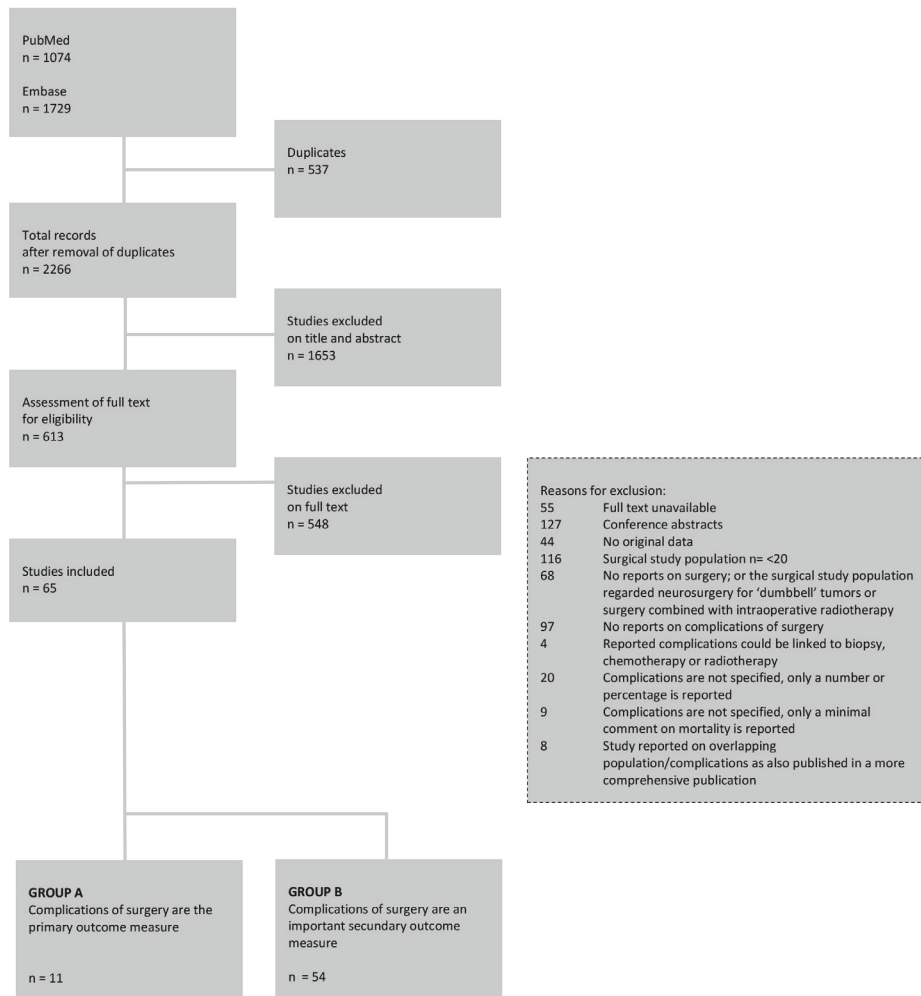
- 40 Castleberry RP, Kun LE, Shuster JJ, Altshuler G, Smith IE, Nitschke R, et al. Radiotherapy improves the outlook for patients older than 1 year with Pediatric Oncology Group stage C neuroblastoma. *J Clin Oncol* 1991;9:789–95. <https://doi.org/10.1200/jco.1991.9.5.789>.
- 41 Cecchetto G, Mosseri V, De Bernardi B, Helardot P, Monclair T, Costa E, et al. Surgical risk factors in primary surgery for localized neuroblastoma: The LNESG1 study of the European International Society of Pediatric Oncology Neuroblastoma Group. *J Clin Oncol* 2005. <https://doi.org/10.1200/JCO.2005.02.4661>.
- 42 De Bernardi B, Gerrard M, Boni L, Rubi  H, Ca ete A, Cataldo AD, et al. Excellent outcome with reduced treatment for infants with disseminated neuroblastoma without MYCN gene amplification. *J Clin Oncol* 2009;27:1034–40. <https://doi.org/10.1200/JCO.2008.17.5877>.
- 43 DeCou JM, Bowman LC, Rao BN, Santana VM, Furman WL, Luo X, et al. Infants with metastatic neuroblastoma have improved survival with resection of the primary tumor. *J Pediatr Surg* 1995;30:937–41. [https://doi.org/10.1016/0022-3468\(95\)90316-X](https://doi.org/10.1016/0022-3468(95)90316-X).
- 44 Du L, Liu L, Zhang C, Cai W, Wu Y, Wang J, et al. Role of surgery in the treatment of patients with high-risk neuroblastoma who have a poor response to induction chemotherapy. *J Pediatr Surg* 2014;49:528–33. <https://doi.org/10.1016/j.jpedsurg.2013.11.061>.
- 45 Fahy AS, Roberts A, Nasr A, Irwin MS, Gerstle JT. Long term outcomes after concurrent ipsilateral nephrectomy versus kidney-sparing surgery for high-risk, intraabdominal neuroblastoma. *J Pediatr Surg* 2019;54:1632–7. <https://doi.org/10.1016/j.jpedsurg.2018.06.031>.
- 46 Fischer J, Pohl A, Volland R, Hero B, Dubbers M, Cernaianu G, et al. Complete surgical resection improves outcome in INRG high-risk patients with localized neuroblastoma older than 18 months. *BMC Cancer* 2017;17:520. <https://doi.org/10.1186/s12885-017-3493-0>.
- 47 Fraga JC, Aydogdu B, Aufieri R, Silva GVM, Schopf L, Takamatu E, et al. Surgical treatment for pediatric mediastinal neurogenic tumors. *Ann Thorac Surg* 2010;90:413–8. <https://doi.org/10.1016/j.athoracsur.2010.04.086>.
- 48 Fumino S, Kimura K, Iehara T, Nishimura M, Nakamura S, Souzaki R, et al. Validity of image-defined risk factors in localized neuroblastoma: A report from two centers in Western Japan 2015. <https://doi.org/10.1016/j.jpedsurg.2015.08.039>.
- 49 Haase GM, O’Leary MC, Ramsay NK, Romansky SG, Stram DO, Seeger RC, et al. Aggressive surgery combined with intensive chemotherapy improves survival in poor-risk neuroblastoma. *J Pediatr Surg* 1991;26:1114–9.
- 50 H berle B, Hero B, Berthold F, Von Schweinitz D. Characteristics and outcome of thoracic neuroblastoma. *Eur J Pediatr Surg* 2002;12:145–50. <https://doi.org/10.1055/s-2002-32721>.
- 51 Hase T, Ohta S, Tani T, Mizukuro T, Mekata E, Naitoh H, et al. Outcome of infants with neuroblastoma detected by mass screening and surgically treated in Shiga Prefecture, Japan: what is the role of surgery? *Pediatr Surg Int* 2002;18:289–94. <https://doi.org/10.1007/s003830100701>.
- 52 Hishiki T, Matsumoto K, Ohira M, Kamijo T, Shichino H, Kuroda T, et al. Results of a phase II trial for high-risk neuroblastoma treatment protocol JN-H-07: a report from the Japan Childhood Cancer Group Neuroblastoma Committee (JNBSG). *Int J Clin Oncol* 2018;23:965–73. <https://doi.org/10.1007/s10147-018-1281-8>.

- 53 Hsu W-M, Jen Y-M, Lee H, Kuo M-L, Tsao P-N, Chen C-N, et al. The influence of biologic factors on the surgical decision in advanced neuroblastoma. *Ann Surg Oncol* 2006;13:238-44. <https://doi.org/10.1245/ASO.2006.10.012>.
- 54 lehara T, Hamazaki M, Tajiri T, Kawano Y, Kaneko M, Ikeda H, et al. Successful treatment of infants with localized neuroblastoma based on their MYCN status. *Int J Clin Oncol* 2013;18:389-95. <https://doi.org/10.1007/s10147-012-0391-y>.
- 55 lehara T, Yoneda A, Yokota I, Takahashi H, Teramukai S, Kamiyjo T, et al. Results of a prospective clinical trial JN-L-10 using image-defined risk factors to inform surgical decisions for children with low-risk neuroblastoma disease: A report from the Japan Children's Cancer Group Neuroblastoma Committee. *Pediatr Blood Cancer* 2019;66:e27914. <https://doi.org/10.1002/psc.27914>.
- 56 Ikeda H, Suzuki N, Takahashi A, Kuroiwa M, Nagashima K, Tsuchida Y, et al. Surgical treatment of neuroblastomas in infants under 12 months of age. *J Pediatr Surg* 1998;33:1246-50. [https://doi.org/10.1016/S0022-3468\(98\)90160-9](https://doi.org/10.1016/S0022-3468(98)90160-9).
- 57 Irtan S, Brisse HJ, Minard-Colin V, Schleiermacher G, Canale S, Sarnacki S. Minimally invasive surgery of neuroblastic tumors in children: Indications depend on anatomical location and image-defined risk factors. *Pediatr Blood Cancer* 2015;62:257-61. <https://doi.org/10.1002/psc.25248>.
- 58 Irtan S, Brisse HJ, Minard-Colin V, Schleiermacher G, Galmiche-Rolland L, Le Cossec C, et al. Image-defined risk factor assessment of neurogenic tumors after neoadjuvant chemotherapy is useful for predicting intra-operative risk factors and the completeness of resection. *Pediatr Blood Cancer* 2015;62:1543-9. <https://doi.org/10.1002/psc.25511>.
- 59 Kohler JA, Rubie H, Castel V, Beiske K, Holmes K, Gambini C, et al. Treatment of children over the age of one year with unresectable localised neuroblastoma without MYCN amplification: Results of the SIOPEN study. *Eur J Cancer* 2013. <https://doi.org/10.1016/j.ejca.2013.07.002>.
- 60 Kubota M, Okuyama N, Hirayama Y, Asami K, Ogawa A, Watanabe A. Mortality and morbidity of patients with neuroblastoma who survived for more than 10 years after treatment--Niigata Tumor Board Study. *J Pediatr Surg* 2010;45:673-7. <https://doi.org/10.1016/j.jpedsurg.2009.09.002>.
- 61 La Quaglia MP, Kushner BH, Su W, Heller G, Kramer K, Abramson S, et al. The impact of gross total resection on local control and survival in high-risk neuroblastoma. *J Pediatr Surg* 2004;39:412-7.
- 62 Leclair M-D, de Lagausie P, Becmeur F, Varlet F, Thomas C, Valla J-S, et al. Laparoscopic resection of abdominal neuroblastoma. *Ann Surg Oncol* 2008;15:117-24. <https://doi.org/10.1245/s10434-007-9499-0>.
- 63 Li K, Dong K, Gao J, Yao W, Xiao X, Zheng S. Neuroblastoma management in Chinese children. *J Invest Surg* 2012;25:86-92. <https://doi.org/10.3109/08941939.2011.605203>.
- 64 Malek MM, Mollen KP, Kane TD, Shah SR, Irwin C. Thoracic neuroblastoma: a retrospective review of our institutional experience with comparison of the thoracoscopic and open approaches to resection. *J Pediatr Surg* 2010;45:1622-6. <https://doi.org/10.1016/j.jpedsurg.2010.03.018>.
- 65 Martinez DA, King DR, Ginn-Pease ME, Haase GM, Wiener ES. Resection of the primary tumor is appropriate for children with stage IV-S neuroblastoma: an analysis of 37 patients. *J Pediatr Surg* 1992;27:1011-6.

- 66 Nishio N, Mimaya JI, Nara T, Takashima Y, Horikoshi Y, Urushihara N, et al. Results for 79 patients with neuroblastoma detected through mass screening at 6 months of age in a single institute. *Pediatr Int* 2006;48:531-5. <https://doi.org/http://dx.doi.org/10.1111/j.1442-200X.2006.02284.x>.
- 67 Olgun N, Kansoy S, Aksoylar S, Cetingul N, Vergin C, Oniz H, et al. Experience of the Izmir Pediatric Oncology Group on neuroblastoma: IPOG-NBL-92 protocol. *Pediatr Hematol Oncol* 2003;20:211-8. <https://doi.org/10.1080/08880010390158838>.
- 68 Parikh D, Short M, Eshmayw M, Brown R. Surgical outcome analysis of paediatric thoracic and cervical neuroblastoma. *Eur J Cardiothorac Surg* 2012;41:630-4. <https://doi.org/10.1093/ejcts/ezr005>.
- 69 Phelps HM, Ndolo JM, Van Arendonk KJ, Chen H, Dietrich HL, Watson KD, et al. Association between image-defined risk factors and neuroblastoma outcomes. *J Pediatr Surg* 2019;54:1184-91. <https://doi.org/10.1016/j.jpedsurg.2019.02.040>.
- 70 Rubie H, Hartmann O, Michon J, Frappaz D, Coze C, Chastagner P, et al. N-Myc gene amplification is a major prognostic factor in localized neuroblastoma: Results of the French NBL 90 study. *J Clin Oncol* 1997;15:1171-82. <https://doi.org/10.1200/JCO.1997.15.3.1171>.
- 71 Rubie H, De Bernardi B, Gerrard M, Canete A, Ladenstein R, Couturier J, et al. Excellent outcome with reduced treatment in infants with nonmetastatic and unresectable neuroblastoma without MYCN amplification: Results of the prospective INES 99.1. *J Clin Oncol* 2011;29:449-55. <https://doi.org/10.1200/JCO.2010.29.5196>.
- 72 Salim A, Mullassery D, Pizer B, McDowell HP, Losty PD. Neuroblastoma: a 20-year experience in a UK regional centre. *Pediatr Blood Cancer* 2011;57:1254-60. <https://doi.org/10.1002/pbc.23149>.
- 73 Shamberger RC, Allarde-Segundo A, Kozakewich HP, Grier HE. Surgical management of stage III and IV neuroblastoma: resection before or after chemotherapy? *J Pediatr Surg* 1991;26:1113-8.
- 74 Simon T, Haberle B, Hero B, Von Schweinitz D, Berthold F. Role of surgery in the treatment of patients with stage 4 neuroblastoma age 18 months or older at diagnosis. *J Clin Oncol* 2013;31:752-8. <https://doi.org/10.1200/JCO.2012.45.9339>.
- 75 Tajiri T, Souzaki R, Kinoshita Y, Koga Y, Suminoe A, Hara T, et al. Implications of surgical intervention in the treatment of neuroblastomas: 20-year experience of a single institution. *Surg Today* 2012;42:220-4. <https://doi.org/10.1007/s00595-011-0053-0>.
- 76 Tanaka Y, Kawashima H, Mori M, Fujiogi M, Suzuki K, Amano H, et al. Contraindications and image-defined risk factors in laparoscopic resection of abdominal neuroblastoma. *Pediatr Surg Int* 2016;32:845-50. <https://doi.org/10.1007/s00383-016-3932-z>.
- 77 Tokiwa K, Fumino S, Ono S, Iwai N. Results of retroperitoneal lymphadenectomy in the treatment of abdominal neuroblastoma. *Arch Surg* 2003;138:711-5. <https://doi.org/10.1001/archsurg.138.7.711>.
- 78 Varan A, Kesik V, Senocak M, Kale G, Akyüz C, Büyükpamukçu M. The efficacy of delayed surgery in children with high-risk neuroblastoma. *J Cancer Res Ther* 2015;11:268. <https://doi.org/10.4103/0973-1482.151852>.

- 79 Vollmer K, Gfroerer S, Theilen TM, Bochennek K, Klingebiel T, Rolle U, et al. Radical Surgery Improves Survival in Patients with Stage 4 Neuroblastoma. *World J Surg* 2018;42:1877-84. <https://doi.org/10.1007/s00268-017-4340-9>.
- 80 Von Allmen D, Grupp S, Diller L, Marcus K, Ecklund K, Meyer J, et al. Aggressive surgical therapy and radiotherapy for patients with high-risk neuroblastoma treated with rapid sequence tandem transplant. *J Pediatr Surg* 2005;40:936-41; discussion 941. <https://doi.org/10.1016/j.jpedsurg.2005.03.008>.
- 81 Von Allmen D, Davidoff AM, London WB, Van Ryn C, Haas-Kogan DA, Kreissman SG, et al. Impact of extent of resection on local control and survival in patients from the COG A3973 study with high-risk neuroblastoma. *J Clin Oncol* 2017;35:208-16. <https://doi.org/10.1200/JCO.2016.67.2642>.
- 82 Yao W, Dong K, Li K, Zheng S, Xiao X. Comparison of long-term prognosis of laparoscopic and open adrenalectomy for local adrenal neuroblastoma in children. *Pediatr Surg Int* 2018;34:851-6. <https://doi.org/10.1007/s00383-018-4294-5>.
- 83 Yao W, Li K, Dong K-R, Zheng S, Xiao X-M. Long-term prognosis of low-risk neuroblastoma treated by surgery alone: an experience from a single institution of China. *World J Pediatr* 2019;15:148-52. <https://doi.org/10.1007/s12519-018-0205-z>.
- 84 Veen EJ, Janssen-Heijnen MLG, Bosma E, De Jongh MAC, Roukema JA. The accuracy of complications documented in a prospective complication registry. *J Surg Res* , 2012 173: 54-59. <http://dx.doi.org/10.1016/j.jss.2010.08.042>
- 85 Van Poll D, Wilde J, van de Ven K, Asimakidou M, Heij H, Wijnen M. Higher incidence of surgery-related complications in Wilms tumor nephrectomy from clinical records analysis compared with central database registration. *Pediatr Blood Cancer*, 2019 66(2):e27502. doi:10.1002/pbc.27502.
- 86 Veen EJ, Steenbruggen J, Roukema JA. Classifying surgical complications: a critical appraisal. *Arch Surg* , 2005 140: 1078-1083. doi: 10.1001/archsurg.140.11.1078.
- 87 Bosma E, Veen EJ, De Jongh MAC, Roukema JA. Variable impact of complications in general surgery: A prospective cohort study. *Can J Surg* , 2012 55: 163-170. doi: 10.1503/cjs.027810.
- 88 Matthyssens LE, Nuchtern JG, Van de Ven CP, Gabra HOS, Bjornland K, Irtan S, et al. A novel standard for systematic reporting of neuroblastoma surgery: the International Neuroblastoma Surgical Report Form (INSRF). *Ann Surg*, 2020 Jul 7. doi: 10.1097/SLA.0000000000003947.

Supplementary figure 1. Flowchart of included studies



Supplementary table 1. Literature search performed in PubMed and Embase

Database	Search strategy
PubMed	((Neuroblastoma[Mesh] OR Ganglioneuroblastoma[Mesh] OR neuroblastoma*[tiab] OR ganglioneuroblastoma*[tiab]) AND (surgery [Subheading] OR surgery[tiab] OR surgical[tiab] OR resection*[tiab] OR excision*[tiab]) AND (Child[Mesh] OR Infant[Mesh] OR Newborn[Mesh] OR Adolescent[Mesh] OR Pediatric[Mesh] OR child*[tiab] OR infan*[tiab] OR newborn*[tiab] OR neonat*[tiab] OR baby[tiab] OR babies[tiab] OR pediatr*[tiab] OR paediatr*[tiab] OR adoles*[tiab] OR teen*[tiab] OR puber*[tiab] OR prepubert*[tiab] OR boy*[tiab] OR girl*[tiab]) AND (Postoperative Complications[Mesh] OR Intraoperative Complications[Mesh] OR complications[Subheading] OR Mortality[Mesh] OR Morbidity[Mesh] OR mortality[Subheading] OR morbidity [Subheading] OR complication*[tiab] OR mortality[tiab] OR morbidity[tiab] OR sequelae[tiab]))
Embase	('neuroblastoma'/exp OR neuroblastoma* OR ganglioneuroblastoma*:ti,ab,kw) AND ('surgery' OR 'surgery'/lnk OR surgical OR resection* OR excision*:ti,ab,kw) AND ('child' OR 'infant' OR 'newborn' OR 'adolescent' OR 'pediatric' OR 'paediatric' OR child* OR infan* OR newborn* OR neonat* OR baby OR babies OR pediatr* OR paediatr* OR adoles* OR teen* OR puber* OR boy* OR girl*:ti,ab,kw) AND ('complication'/exp OR 'complication'/lnk OR 'mortality'/exp OR 'morbidity'/exp OR complication* OR mortality OR morbidity OR sequelae:ti,ab,kw)

Supplementary table 2. Individual complications reported as categories, including definition and severity.

Group A: surgical complications were reported as the primary outcome measure, Group B: surgical complications were reported as an important secondary outcome measure. CD Clavien-Dindo grade; TCBV complete Circulating Blood Volume; ICU Intensive Care Unit admission; TPN Total Parenteral Nutrition; NM Not Mentioned.

Group	First author	Year of publication	Intraoperative complications	Postoperative complications <30 days	Postoperative complications >30 days	Postoperative complications Timing unreported	Any complications unreported
A	Barrette et al ²⁴	2006	-	1 Neurological 1 Gastrointestinal	4 Renal (complete atrophy) 2 Gastro-intestinal (1 return to OR, 1 persistent vegetative state)	-	-
	Canete et al ⁹	1998	2 Hemorrhage (severe) 1 Vascular injury 3 Organ injury 1 Organ removal (partial) 1 Kidney removal 1 Other complication	6 Neurological 3 Gastro-intestinal 1 Urological 5 Chylous leakage, pleural effusion or ascites 1 Wound complication 1 Abscess complication 1 Death (cause: unexplained circulatory failure)	1 Gastro-intestinal	-	-
	Cantos et al ¹⁰	2006	5 Vascular injury (primary repair) 3 Organ injury (primary repair) 1 Circulatory complication	4 Hemorrhage (4 transfusion, 1 return to OR) 9 Infectious 1 Gastrointestinal 1 Diarrhea 5 Chylous leakage, pleural effusion or ascites 3 Wound complication	-	-	-
	Chui et al ²⁵	2014	-	10 Chylous leakage, pleural effusion or ascites (significant; >400ml/day; 10 diet, 10 tube drainage, 2 return to OR)	-	-	-

Supplementary table 2. Continued.

Group	First author	Year of publication	Intraoperative complications	Postoperative complications <30 days	Postoperative complications >30 days	Postoperative complications Timing unreported	Any complications unreported
	Qureshi et al ²⁶	2016	-	5 Infectious 4 Neurological 2 Renal 32 Chylous leakage, pleural effusion or ascites (conservative, median measure of leakage 100 ml (30–800 ml), 10 pt leakage over two wk) 7 Wound complication (1 Return to OR)	-	3 Gastro-intestinal	-
	Qureshi et al ²⁷	2018	5 Hemorrhage (excessive) 4 Vascular injury (primary repair) 1 Kidney removal (cause: tumor resection) 1 Other structure injury	7 Neurological 1 Renal 3 Gastrointestinal 6 Chylous leakage, pleural effusion or ascites (conservative) 1 Wound complication	-	-	-
	Rees et al ²⁸	1998	-	23 Diarrhea (5 transient, 19 persistent)	19 Diarrhea (persistent)	-	-
	Rich et al ¹¹	2011	5 Kidney removal (CD I; 5 tumor resection) 1 Vascular injury (CD IIIb, reconstruction)	2 Ischemic (CD IIIb, bowel resection; CD IVb, infarction of the stomach/spleen/liver/pancreas/duodenum, residual pancreatic insufficiency and diabetes mellitus) 11 Renal (4 CD I; 1 IIIa, stent; 6 IIIb, 1 exploration, 4 stent, 1 kidney removal) 1 Gastrointestinal (CD IIIb, pyloromyotomy) 1 Abscess complication (CD IIIa, drain)	5 Gastro-intestinal (4 CD IIIb, 3 lysis, 1 ileal resection, 1 bowel resection)	41 Renal (1 CD IIIb, vascular repair; 40 CD I)	1 Gastro-intestinal (CD IIIb, bowel resection) 1 Ischemic (CD IIIb, splenectomy, small distal pancreatectomy, repair of gastric wall) 2 Renal (CD I)
	Sham-berger et al ²⁹	1998	52 Kidney removal (cause: 15 complication, 37 tumor resection)	-	-	-	-

Supplementary table 2. Continued.

Group	First author	Year of publication	Intraoperative complications	Postoperative complications <30 days	Postoperative complications >30 days	Postoperative complications Timing unreported	Any complications unreported
	Tanabe et al ³⁰	1996	1 Vascular injury (no persistent effect) 7 Kidney removal	-	5 Renal	1 Renal (resolved after pharmacological intervention)	-
	Yoneda et al ³¹	2016	4 Vascular injury 1 Kidney removal (cause: tumor resection)	2 Organ failure (hepatic) 2 Chylous leakage, pleural effusion or ascites	3 Renal	2 Gastro-intestinal	2 Unknown
	B Adkins et al ³²	2004	26 Hemorrhage ('major') 34 Organ injury 76 Organ removal	1 Hemorrhage ('major') 8 Pulmonary 5 Wound complication	-	4 Gastro-intestinal	20 Unknown
	Ahmed et al ³³	2018	2 Kidney removal (cause: tumor resection)	1 Neurological 2 Pulmonary 3 Gastrointestinal 1 Chylous leakage, pleural effusion or ascites	-	-	-
	Avanzini et al ³⁴	2017	14 Kidney removal (cause: tumor resection)	1 Neurological 1 Gastrointestinal 2 Chylous leakage, pleural effusion or ascites	-	5 Renal 1 Gastro-intestinal 2 Ischemic 1 Other	5 Hemorrhage ('serious') 1 Death
	Baker et al ³⁵	2010	4% Vascular injury 2% Nerve injury (resection) Organ injury (n=NIM) 6% Organ removal 1% Kidney removal	2% Wound complication	-	-	14% Hemorrhage ('major') 4 Death 7% Unknown
	Ben Barak et al ³⁶	2017	5 Vascular injury (4 primary repair)	1 Vascular (return to OR) 1 Wound complication	-	-	-
	Browne et al ³⁷	2006	3 Hemorrhage ('major') 2 Organ removal (complete) 6 Kidney removal 1 Other structure injury	-	-	-	-

Supplementary table 2. Continued.

Group	First author	Year of publication	Intraoperative complications	Postoperative complications <30 days	Postoperative complications >30 days	Postoperative complications Timing unreported	Any complications unreported
	Castel et al ³⁸	1999	2 Kidney removal 1 Other	1 Vascular 2 Neurological 1 Infectious	-	1 Gastro-intestinal	2 Hemorrhage
	Castel et al ³⁹	2002	5 Kidney removal (cause: tumor resection)	1 Chylous leakage, pleural effusion or ascites 1 Abscess complication	-	1 Death (cause: intestinal perforation followed by shock and death)	-
	Castleberry et al ⁴⁰	1991	1 Hemorrhage 5 Kidney removal (cause: tumor resection)	1 Renal complication 1 Gastrointestinal	-	-	2 Unknown
	Cecchetto et al ⁴¹	2005	2 Vascular injury 2 Organ injury 2 Organ removal (1 partial, 1 complete) 13 Kidney removal (1 partial; cause: 2 complication, 10 tumor resection) 1 Other structure injury 2 Other structure removal	4 Infectious 10 Neurological 2 Pulmonary 9 Renal 1 Diarrhea 5 Chylous leakage, pleural effusion or ascites 1 Respiratory 1 Death (cause: bleeding and multiple organ failure)	1 Renal	1 Death (cause: renal failure) 1 Other	10 Hemorrhage ('serious') 1 Gastro-intestinal 2 Unknown
	De Bernardi et al ⁴²	2009	-	2 Neurological 1 Infectious 1 Wound complication	-	2 Renal 2 Gastro-intestinal	3 Hemorrhage
	De Cou et al ⁴³	1995	9 Kidney removal (cause: tumor resection)	2 Neurological 1 Wound complication	-	-	-
	Du et al ⁴⁴	2014	9 Hemorrhage ('major') 12 Vascular injury 5 Organ injury 1 Organ removal	1 Hemorrhage ('major') 2 Gastrointestinal 5 Unknown	-	-	-

Supplementary table 2. Continued.

Group	First author	Year of publication	Intraoperative complications	Postoperative complications <30 days	Postoperative complications >30 days	Postoperative complications >30 days	Postoperative complications Timing unreported	Any complications unreported	Any complications Timing unreported
Fahy et al ⁴⁵	2019	2 Hemorrhage ('major', >40cc/kg) 14 Vascular or other structure injury 6 Kidney removal (cause: tumor resection) 1 Other	-	-	-	-	-	-	-
Fischer et al ⁴⁶	2017	2.8% Hemorrhage ('major') Vascular injury (n=NM) Nerve injury (n=NM) 4.4% Organ injury	5.6% Neurological Infectious (n=NM)	-	1 Gastro-intestinal	2 Death	-	-	-
Fraga et al ⁴⁷	2010	-	6 Neurological (1 return to OR) 2 Chylous leakage, pleural effusion or ascites (2 diet, 2 drainage) 2 Pulmonary (1 re-intervention, 1 conservative) 1 Abscess complication (antibiotics + return to OR)	-	-	-	-	-	-
Fumino et al ⁴⁸	2015	1 Vascular injury	1 Renal	-	-	-	-	-	-
Haase et al ⁴⁹	1991	3 Vascular injury (2 primary repair) 1 Organ ischemia (partial) 1 Organ removal (complete, permanent pharmacological treatment) 18 Kidney removal	2 Infectious 1 Gastrointestinal 1 Urological 1 Chylous leakage, pleural effusion or ascites 2 Wound complication 1 Abscess complication 1 Respiratory	2 Gastro-intestinal	-	2 Hemorrhage 1 Gastro-intestinal 1 Urological	-	-	-
Haberle et al ⁵⁰	2002	5 Other structure removal	19 Neurological 13 Pulmonary 4 Chylous leakage, pleural effusion or ascites	1 Scoliosis	-	1 Hemorrhage (resuscitation)	-	-	-

Supplementary table 2. Continued.

Group	First author	Year of publication	Intraoperative complications	Postoperative complications <30 days	Postoperative complications >30 days	Postoperative complications Timing unreported	Any complications unreported	Timing
	Hase et al ⁵¹	2002	4 Kidney removal (cause: tumor resection)	1 Gastrointestinal (manual re-intervention)	-	-	-	-
	Hishiki et al ⁵²	2018	8 Kidney removal	2 Chylous leakage, pleural effusion or ascites 1 Wound complication	-	-	-	-
	Hsu et al ⁵³	2006	5 Kidney removal (cause: tumor resection)	1 Chylous leakage, pleural effusion or ascites	2 Gastro-intestinal	-	-	-
	lehara et al ⁵⁴	2013	1 Kidney removal (cause: complication)	1 Hemorrhage 3 Neurological complication 1 Gastrointestinal 1 Urological complication 1 Chylous leakage, pleural effusion or ascites 2 Abscess complication	5 Renal (complete atrophy) 1 Gastro-intestinal	8 Gastro-intestinal 3 Renal	3 Renal	-
	lehara et al ⁵⁵	2019	3 Vascular injury	1 Chylous leakage, pleural effusion or ascites	1 Renal	-	40 Hemorrhage	-
	Ikedo et al ⁵⁶	1998	1 Nerve injury (return to OR)	2 Neurological 1 Chylous leakage, pleural effusion or ascites (TPN) 1 Gastrointestinal (return to OR)	2 Renal 2 Gastro-intestinal (1 conservative, 1 return to OR)	-	-	-
	Irtan et al ⁵⁷	2015	-	1 Neurological 3 Chylous leakage, pleural effusion or ascites (2 conservative, 1 re-intervention)	1 Renal (return to OR)	-	-	-

Supplementary table 2. Continued.

Group	First author	Year of publication	Intraoperative complications	Postoperative complications <30 days	Postoperative complications >30 days	Postoperative complications Timing unreported	Any complications unreported
Irtan et al ⁵⁸		2015	3 Vascular injury (1 no consequence, 1 organ failure, 1 delayed resection) 2 Nerve injury 6 Kidney removal (cause: tumor resection) 1 Other structure injury (reconstruction)	4 Neurological	1 Diarrhea (persistent) 1 Organ failure (persistent)	-	-
Kiely et al ¹²		2007	3 Vascular injury (primary repair)	30% Diarrhea 3 Chylous leakage, pleural effusion or ascites (1 return to OR) 2 Death (cause: 1 severe brain damage after rebound hypoglycaemia after massive postoperative transfusion, 1 postoperative rupture of aorta and splenic artery)	1 Renal (complete) 5 Gastro-intestinal (return to OR) Diarrhea (persistent, n=NIM)	-	-
Kohler et al ⁵⁹		2013	18 Kidney removal	3 Neurological 2 Ischemic (1 return to OR) 5 Renal (transient) 1 Gastrointestinal 2 Chylous leakage, pleural effusion or ascites	-	-	4 Hemorrhage (severe) 1 Death (cause: bleeding complications)
Kubota et al ⁶⁰		2010	4 Kidney removal (2 complication; 1 kidney transplant)	1 Urological	1 Neurological	-	-
La Quaglia et al ⁶¹		2004	2 Vascular injury (primary repair) with hemorrhage (excessive) 5 Kidney removal	1 Hemorrhage (excessive; drainage) 2 Respiratory (ICU) 1 Abscess complication	1 Gastro-intestinal 2 Diarrhea (transient) 1 Ischemic	-	-

Supplementary table 2. Continued.

Group	First author	Year of publication	Intraoperative complications	Postoperative complications <30 days	Postoperative complications >30 days	Postoperative complications Timing unreported	Any complications unreported	Timing
	Leclair et al ⁶²	2008	-	1 Renal (loss of kidney) 1 Gastrointestinal (return to OR) 1 Urological	-	-	-	-
	Li et al ⁶³	2012	8 Vascular injury (2 direct repair, 6 return to OR for organ removal)	1 Wound complication (drainage) 2 Chylous leakage, pleural effusion or ascites (1 conservative, 1 return to OR) 1 Gastrointestinal	-	-	-	-
	Malek et al ⁶⁴	2010	-	4 Neurological 2 Pulmonary 1 Chylous leakage, pleural effusion or ascites	1 Scoliosis	-	-	-
	Martinez et al ⁶⁵	1992	-	2 Wound complication (local care)	2 Gastro-intestinal (2 return to OR)	-	-	-
	Nishio et al ⁶⁶	2006	-	2 Neurological 1 Chylous leakage, pleural effusion or ascites	2 Renal	1 Gastro-intestinal	-	-
	Olgun et al ⁶⁷	2003	-	1 Neurological 1 Other	-	-	-	-
	Parikh et al ⁶⁸	2012	-	3 Neurological 2 Chylous leakage, pleural effusion or ascites (conservative)	-	-	-	-
	Phelps et al ⁶⁹	2019	10 Vascular injury 1 Lymphatic vessel injury 3 Organ removal	1 Hemorrhage (return to OR) 1 Renal (return to OR, loss of kidney) 2 Respiratory or circulatory 1 Unknown (return to OR)	-	-	-	-
	Rubie et al ⁷⁰	1997	2 Hemorrhage (major) 1 Kidney removal (cause: tumor resection)	4 Neurological 1 Ischemic 3 Chylous leakage, pleural effusion or ascites	-	-	5 Death (cause: 4 bleeding during or immediately after procedure, 1 unknown cause)	-

Supplementary table 2. Continued.

Group	First author	Year of publication	Intraoperative complications	Postoperative complications <30 days	Postoperative complications >30 days	Postoperative complications >30 days	Postoperative complications Timing unreported	Any complications unreported	Timing
	Rubie et al ⁷¹	2011	1 Kidney removal 1 Other structure removal	1 Neurological (transient) 2 Chylous leakage, pleural effusion or ascites 1 Respiratory (ICU)	-	-	-	-	-
	Salim et al ⁷²	2011	1 Hemorrhage ('massive'; primary repair/transfusion) 1 Nerve injury 4 Kidney removal (cause: tumor resection, 1 renal insufficiency)	6 Neurological 1 Renal (after nephrectomy) 1 Wound complication (return to OR)	-	-	-	-	-
	Shamberger et al ⁷³	1991	5 Hemorrhage ('excessive', 0.57, 1.3, 2.0, and 3.0 times estimated TCBV) 2 Nerve injury 10 Kidney removal 7 Other	1 Chylous leakage, pleural effusion or ascites	-	1 Other	3 Renal		
	Simon et al ⁷⁴	2008	2 Nerve injury 10 Kidney removal 7 Other	18 Neurological 9 Gastrointestinal 2 Chylous leakage, pleural effusion or ascites	-	4 Renal	14 Hemorrhage 2 Respiratory or circulatory complication 3 Death 11 Unknown		
	Simon et al ⁷⁴	2013	26 Hemorrhage ('relevant') 18 Kidney removal	17 Infectious	-	14 Gastro-intestinal	-		
	Tajiri et al ⁷⁵	2012	-	1 Hemorrhage	3 Renal 1 Gastro-intestinal	-	-		
	Tanaka et al ⁷⁶	2016	-	-	-	-	2 Renal		
	Tokiwa et al ⁷⁷	2003	-	1 Gastrointestinal (return to OR) 7 Diarrhea (6 transient, 1 prolonged) 1 Chylous leakage, pleural effusion or ascites (conservative) 1 Wound complication	3 Renal 1 Gastro-intestinal 1 Diarrhea (prolonged)	-	-		

Supplementary table 2. Continued.

Group	First author	Year of publication	Intraoperative complications	Postoperative complications <30 days	Postoperative complications >30 days	Postoperative complications <30 days	Postoperative complications >30 days	Any complications unreported	Timing
	Varan et al ⁷⁸	2015	4 Vascular injury 1 Lymphatic vessel injury 1 Organ injury 1 Kidney removal	-	-	1 Gastro-intestinal	-	-	-
	Vollmer et al ⁷⁹	2018	7 Vascular injury 7 Nerve injury 7 Organ injury 6 Organ removal (partial) 3 Other structure removal	2 Neurological 4 Renal 4 Gastrointestinal	-	-	-	-	-
	Von Allmen et al ⁸⁰	2005	6 Hemorrhage ('significant', >1L; 1 reconstruction, 1 return to OR) 1 Nerve injury 3 Kidney removal	1 Infectious 8 Diarrhea (transient) 2 Chylous leakage, pleural effusion or ascites	2 Diarrhea (transient)	1 Gastro-intestinal	-	-	
	Von Allmen et al ⁸¹	2017	14 Hemorrhage ('major', >10% TCBV); 13 transfusion 4 Vascular injury 3 Organ injury 7 Organ removal	-	-	1 Gastro-intestinal 2 Death 1 Unknown	3 Pulmonary 5 Unknown	-	
	Yao et al ⁸²	2018	5 Hemorrhage (transfusion) 1 Other structure injury	-	-	-	-	-	-
	Yao et al ⁸³	2019	1 Lymphatic vessel injury (primary repair)	1 Neurological (transient) 1 Chylous leakage, pleural effusion or ascites (return to OR)	-	-	-	-	-

Supplementary table 3. Individual complications as reported by the included studies, including definition and severity when provided

Group	First author	Year of publication	Intraoperative complications	Postoperative complications <30 days	Postoperative complications >30 days	Postoperative complications Timing unreported	Any complications Timing unreported
A	Barrette et al ²⁴	2006	-	1 Horner syndrome, 1 intussusception	4 renal atrophy (2 renal artery thrombosis, 1 renal ischemia), 2 intestinal adhesions (1 return to OR, 1 causing volvulus progressed to hypovolemic shock, enoxic encephalopathy and finally persistent vegetative state)	-	-
	Canete et al ⁶	1998	1 segmentectomy, 3 adjacent organ lesion, 1 great vessel injury, 2 severe hemorrhage, 11 nephrectomy (reason not reported), 1 tumor rupture	5 pleural effusion, 5 Horner syndrome, 1 deglutatory paresia, 2 paralytic ileus, 1 mechanical ileus, 1 hematuria, 1 intra-abdominal abscess, 1 seroma, 1 death (lethal arrhythmia direct postoperative)	1 intestinal obstruction	-	-
	Cantos et al ¹⁰	2006	1 liver perforation and repair, 1 gastric perforation and repair, 1 spleen perforation and repair, 3 venous injury and repair, 2 arterial injury and repair, 1 hypertension	3 pleural effusion, 1 vomiting/ bowel obstruction, 1 diarrhea, 4 postoperative hemorrhage (4 transfusion, 1 ligation), 3 wound complication, 8 infection, 2 chyle leak, 1 sepsis	-	-	-
	Chui et al ²⁵	2014	-	10 significant chylous fistula (defined as >400 ml/day; all received abdominal tube drainage, total parenteral nutrition, MCT or non-fat diet or nil orally, 2 received exploratory laparotomy and repair of chylous fistulae	-	-	-

Supplementary table 3. Continued.

Group	First author	Year of publication	Intraoperative complications	Postoperative complications <30 days	Postoperative complications >30 days	Postoperative complications Timing unreported	Any complications Timing unreported
	Qureshi et al ²⁶	2016	-	32 chyle leak (conservative management, median measure of leakage 100 ml (30–800 ml), 10 pt leakage over two wks), 1 wound dehiscence (exploration), 6 wound infection, 5 fever, 1 acute renal failure, 1 renal infarct, 1 nerve entrapment, 3 neurological lesions	-	3 intestinal obstruction	-
	Qureshi et al ²⁷	2018	5 excessive blood loss, 4 vascular injuries needing minor repair, 1 ureteric injury, 1 nephrectomy (tumor resection)	3 neuropraxia pharyngeal plexus, 6 chylous leak (conservative management), 4 neurological, 1 wound infection, 1 acute renal failure, 3 gastrointestinal obstruction	-	-	-
	Rees et al ²⁸	1998	-	11 mild diarrhea (less than 3 loose stools per day), 7 moderate diarrhea (3 to 5 loose stools per day), 5 severe diarrhea (more than 5 loose stools per day and/or urgency, incontinence, or nocturnal diarrhea)	19 persistent diarrhea	-	-

Supplementary table 3. Continued.

Group	First author	Year of publication	Intraoperative complications	Postoperative complications <30 days	Postoperative complications >30 days	Postoperative complications Timing unreported	Any complications Timing unreported
	Rich et al ¹¹	2011	5 nephrectomy (CD I; 5 tumor resection), 1 undefined aortic complication (CD IIIb, graft placement)	10 hydronephrosis (4 CD I; 1 IIIa, stent; 5 IIIb, 4 stent), 1 retroperitoneal abscess (CD IIIa, drain), 1 gastroparesis (CD IIIb, pyloromyotomy), 1 bowel infarction (CD IIIb, bowel resection), 1 portal and splenic vein thrombosis (CD IVb, infarction of the stomach/spleen/liver/pancreas/duodenum, residual pancreatic insufficiency and diabetes mellitus), 1 infarcted kidney (CD IIIb, nephrectomy)	5 small bowel adhesions (4 CD IIIb, 4 lysis, 1 ileal resection, 1 bowel resection)	1 renal artery aneurysm (CD IIIb, renal artery repair), 22 renal polar atrophy (CD I), 15 complete renal atrophy (CD I), 2 nonfunctioning kidney (CD I), 1 decreased renal function (CD I)	1 bowel perforation (CD IIIb, bowel resection), 1 splenic infarct and gastric perforation (CD IIIb, splenectomy, small distal pancreatectomy, repair of gastric wall), 2 partial kidney infarction (CD I)
	Shamberger et al ²⁹	1998	52 nephrectomy (37 tumor resection, 15 complication)	-	-	-	-
	Tanabe et al ³⁰	1996	1 injury renal artery (no persistent effect), 7 nephrectomy (reason not reported)	-	2 kidney atrophy, 3 vanishing kidney	1 renal infarction (resolved by administration of lipoprostaglandin)	-
	Yoneda et al ³¹	2016	2 injury of the renal artery, 2 injury major artery, 1 nephrectomy (tumor resection)	2 elevated liver enzymes > 500 IU/L, 2 ascites	3 renal atrophy	2 intestinal obstruction	2 other complications
B	Adkins et al ³²	2004	34 renal injury, 76 normal organs removed with tumor, 26 major hemorrhage	8 pulmonary complications, 1 major hemorrhage, 5 wound complications	-	4 bowel obstruction	20 other complications
	Ahmed et al ³³	2018	2 nephrectomy (tumor resection)	3 intestinal obstruction, 2 lung collaps, 1 Horner syndrome, 1 chylous effusion	-	-	-

Supplementary table 3. Continued.

Group	First author	Year of publication	Intraoperative complications	Postoperative complications <30 days	Postoperative complications >30 days	Postoperative complications Timing unreported	Any complications Timing unreported
	Avanzini et al ³⁴	2017	14 nephrectomy (11 tumor resection, 3 reason not reported)	2 chylous effusion, 1 Horner syndrome, 1 intussusception	-	1 aponeurotomy of left leg due to transitory ischemia, 2 renal insufficiency, 3 renal ischemic complication, 1 small bowel obstruction, 1 ischemic liver damage, 1 right lower limb string pain	5 serious bleeding, 1 death (cause and timing not reported)
	Baker et al ³⁵	2010	6% Loss of a normal organ during surgery, 4% renal injury, 4% vascular injury, 3% pulmonary injury, 2% nerve resection, 1% nephrectomy	2% wound complications	-	-	14% major hemorrhage, 7% other complications, 4 deaths (cause and timing not reported)
	Ben Barak et al ³⁶	2017	1 iliac artery injury, 4 minor injuries to aorta or vena cava (primary repair)	1 partial renal artery thrombosis (stent placement) with normal renal function, 1 cellulitis of the surgical wound	-	-	-
	Browne et al ³⁷	2006	1 bilateral adrenalectomy, 1 bile duct injury, 1 splenectomy, 3 major hemorrhage, 6 nephrectomy (reason not reported)	2 Horner syndrome, 1 sepsis, 1 renal artery thrombosis	-	1 intestinal obstruction	2 bleeding
	Castelet al ³⁸	1999	1 tumour rupture, 2 nephrectomy (reason not reported)	1 subhepatic collection, 1 pleural effusion	-	1 death (intestinal perforation followed by shock and death)	-
	Castelet al ³⁹	2002	5 nephrectomy (tumor resection)	-	-	-	-

Supplementary table 3. Continued.

Group	First author	Year of publication	Intraoperative complications	Postoperative complications <30 days	Postoperative complications >30 days	Postoperative complications Timing unreported	Any complications Timing unreported
	Castleberry et al ⁴⁰	1991	1 operative hemorrhage, 5 nephrectomy (tumor resection)	1 acute renal failure, 1 intussusception	-	-	2 unknown
	Cecchetto et al ⁴¹	2005	2 parietal/pleural resections, 1 tracheal injury, 2 renal artery injury, 1 partial pancreatectomy, 1 injury duodenum, 1 intestinal perforation, 12 nephrectomy (10 tumor resection, 2 complication), 1 heminephrectomy (reason not reported), 1 splenectomy	6 Horner syndrome, 7 renal insufficiency, 1 diaphragmatic paresis, 2 pneumothorax, 2 chylothorax, 1 pleural effusion, 2 sepsis, 1 paresis n. medianus, 1 respiratory distress, 1 muscle weakness, 2 renal ischemia, 1 ascites, 2 pneumonia, 1 sciatic paresis, 1 lymphorrhea, 1 watery diarrhea, 1 death (bleeding and multiple organ failure)	1 renal atrophy	1 tracheotomy, 1 death (1 renal failure)	1 other, 1 not described, 10 serious bleeding, 1 intestinal perforation
	De Bernardi et al ⁴²	2009	-	1 sepsis, 1 delayed wound healing, 2 Horner syndrome	-	2 renal insufficiency, 2 intestinal obstruction	3 peri-operative hemorrhage
	De Couet et al ⁴³	1995	9 nephrectomy (tumor resection)	1 lower extremity paresis, 1 Horner syndrome, 1 severe staphylococcal wound infection	-	-	-
	Du et al ⁴⁴	2014	5 renal injury (often caused by a vascular injury during dissection), 9 major intra-operative hemorrhage, 1 normal organs removed with tumor, 12 damage to major blood vessel	5 immediate postoperative complication, 1 major post-operative hemorrhage, 2 small bowel obstruction	-	-	-

Supplementary table 3. Continued.

Group	First author	Year of publication	Intraoperative complications	Postoperative complications <30 days	Postoperative complications >30 days	Postoperative complications unreported	Any complications Timing unreported
	Fahy et al ⁴⁵	2019	6 nephrectomy (tumor resection), 2 major hemorrhage (defined as >40cc/kg), 1 renal artery vasospasm, 14 traumatic vascular or ureter injuries	-	-	-	-
	Fischer et al ⁴⁶	2017	4.4% organ injury, 2.8% major bleeding/vessel injury, other vessel injury, nerve injury	5.6% Horner syndrome, infection	-	ileus	2 death (cause and timing not reported)
	Fraga et al ⁴⁷	2010	-	5 Horner syndrome, 2 chylothorax (chest tube drainage and diet with medium-chain lipids), 2 pneumothorax (aspiration of the chest tube; spontaneous absorption), 1 empyema (improvement after antibiotic therapy and pleural cleaning through pleuroscope), 1 left diaphragmatic and left vocal cord paralysis (diaphragmatic plication)	-	-	-
	Fumino et al ⁴⁸	2015	1 renal artery injury	1 renal atrophy	-	-	-
	Haase et al ⁴⁹	1991	18 nephrectomy (tumor resection), 3 vascular injury (1 renal repair, 1 iliac repair, 1 splenic laceration followed by partial splenic infarction), 1 bilateral adrenalectomy requiring permanent steroid replacement	2 wound, 2 infection (1 subhepatic abscess), 1 cholecystitis, 1 prolonged intubation, 1 chylothorax, 1 intussusception, 1 nephrostomy drainage	2 adhesions	-	2 hemorrhage, 1 colon perforation, 1 bladder repair

Supplementary table 3. Continued.

Group	First author	Year of publication	Intraoperative complications	Postoperative complications <30 days	Postoperative complications >30 days	Postoperative complications Timing unreported	Any complications Timing unreported
	Haberle et al ⁵⁰	2002	4 costal resections, 1 en bloc resection of oesophagus/vagus/n. phrenicus	14 Horner syndrome, 13 pulmonary complications, 4 chylothorax, 4 other neurological disorders, 1 secondary paraplegia	1 scoliosis after costal resection	-	1 resuscitation after hemorrhagic shock
	Hase et al ⁵¹	2002	4 nephrectomy (tumor resection)	1 ileo-ileal intussusception causing postoperative intestinal obstruction (manual reduction)	-	-	-
	Hishiki et al ⁵²	2018	8 nephrectomy (reason not reported)	2 chylous ascites, 1 wound infection	-	-	-
	Hsu et al ⁵³	2006	5 nephrectomy (tumor resection)	1 chylothorax	2 adhesion ileus	-	-
	lehar et al ⁵⁴	2013	1 nephrectomy (complication)	1 pulmonary effusion, 3 Horner syndrome, 1 dysuria, 1 hemorrhage, 2 abscess, 1 invagination	5 vanishing kidney	8 mechanical ileus, 2 renal hypertension, 1 hydronephrosis	3 kidney infarction
	lehar et al ⁵⁵	2019	3 vascular injury	1 pleural effusion/ascites	1 renal atrophy	-	40 Bleeding I/II/III/IV (no definition given): 36/2/1/1
	Ikeda et al ⁵⁶	1998	1 phrenic nerve injury (plication of diaphragm)	2 Horner syndrome, 1 chylous ascites (TPN), 1 intussusception/invagination (laparotomy)	1 renal atrophy, 2 postoperative adhesions (1 conservative, 1 emergency laparotomy for strangulations), 1 renal failure after nephrectomy	-	-
	Irtan et al ⁵⁷	2015	-	3 chylothorax (2 conservative, 1 re-intervention), 1 Horner syndrome	1 renal atrophy (followed by nephrectomy to control hypertension)	-	-

Supplementary table 3. Continued.

Group	First author	Year of publication	Intraoperative complications	Postoperative complications <30 days	Postoperative complications >30 days	Postoperative complications Timing unreported	Any complications Timing unreported
	Irtan et al ⁶⁸	2015	6 nephrectomy (tumor resection), 1 phrenic nerve injury, 1 IVC injury (no clinical consequence), 1 Roux-en-Y hepaticojejunostomy after main bile duct section, 1 section of the celiac trunk (biliary cirrhosis), 1 sciatic notch branch injury, 1 aortic injury (second resection necessary)	4 Horner syndrome	1 chronic diarrhea (3 yrs post-surgery), 1 biliary cirrhosis (linked to section of celiac trunk)	-	-
	Kiely et al ¹²	2007	3 aortic injuries with formal patch repair	30% of postoperative diarrhea in those who had undergone clearance of coeliac and superior mesenteric arteries, 3 persisting lymphatic leakage (peritoneo-venous shunt insertion), 2 death (1 severe brain damage after rebound hypoglycaemia after massive postoperative trans-fusion, 1 postoperative rupture of aorta and splenic artery)	1 late loss of kidney due to renal vein thrombosis, 5 adhesions (operative division), 7% Diarrhea (persistent)	-	-
	Kohler et al ⁶⁹	2013	18 nephrectomy (reason not reported)	2 serous effusion, 5 transient renal insufficiency, 1 Horner syndrome, 1 leg weakness and pain, 1 leg ischemia requiring fasciotomy, 1 transient ischaemic liver damage, 1 neuropathic bladder, 1 intussusception	1 retrograde ejaculation	-	4 severe haemorrhage, 1 death (bleeding complications, timing not reported)
	Kubota et al ⁶⁰	2010	1 bilateral kidney loss due to complication (followed by kidney transplant), 2 unilateral kidney loss	1 impaired development of extremity	-	-	-

Supplementary table 3. Continued.

Group	First author	Year of publication	Intraoperative complications	Postoperative complications <30 days	Postoperative complications >30 days	Postoperative complications Timing unreported	Any complications Timing unreported
	LaQuaglia et al ⁶¹	2004	5 nephrectomy (reason not reported), 1 caval injury with primary repair (excessive hemorrhage), 1 aortic injury with primary repair (excessive hemorrhage)	2 more than 7 days of mechanical ventilation, 1 excessive hemorrhage (stopped spontaneously after chest tube placement), 1 pelvic and subphrenic abscesses	1 bowel obstruction, 2 prolonged diarrhea (eventually asymptomatic), 1 cecal necrosis secondary to venous thrombosis	-	-
	Leclair et al ⁶²	2008	-	1 bowel obstruction (surgery) due to bowel loop pinched in trocar orifice, 1 persistent renal ischemia with complete loss of kidney function, 1 urinary retention, 1 wound abscess (drainage)	-	-	-
	Li et al ⁶³	2012	6 renal vessel injury (nephrectomy due to refractory hypertension), 2 superior mesenteric artery injury (angiography)	2 chyloperitoneum (1 conservative, 1 neoplasty of lymphatic trunk), 1 intussusception	-	-	-
	Malek et al ⁶⁴	2010	-	4 Horner syndrome, 1 chylothorax, 2 severe atelectasis	1 scoliosis	-	-
	Martinez et al ⁶⁵	1992	-	2 wound infection (local care)	2 bowel adhesions (1 adhesiolysis, 1 intestinal resection)	-	-
	Nishio et al ⁶⁶	2006	-	1 phrenic nerve palsy, 1 Horner syndrome, 1 chylothorax	2 atrophic kidney	1 ileus	-
	Olgun et al ⁶⁷	2003	-	1 Horner syndrome, 1 transient blindness due to hypoxic encephalopathy	-	-	-
	Parikh et al ⁶⁸	2012	-	3 Horner syndrome, 2 chylothorax (conservative management)	-	-	-

Supplementary table 3. Continued.

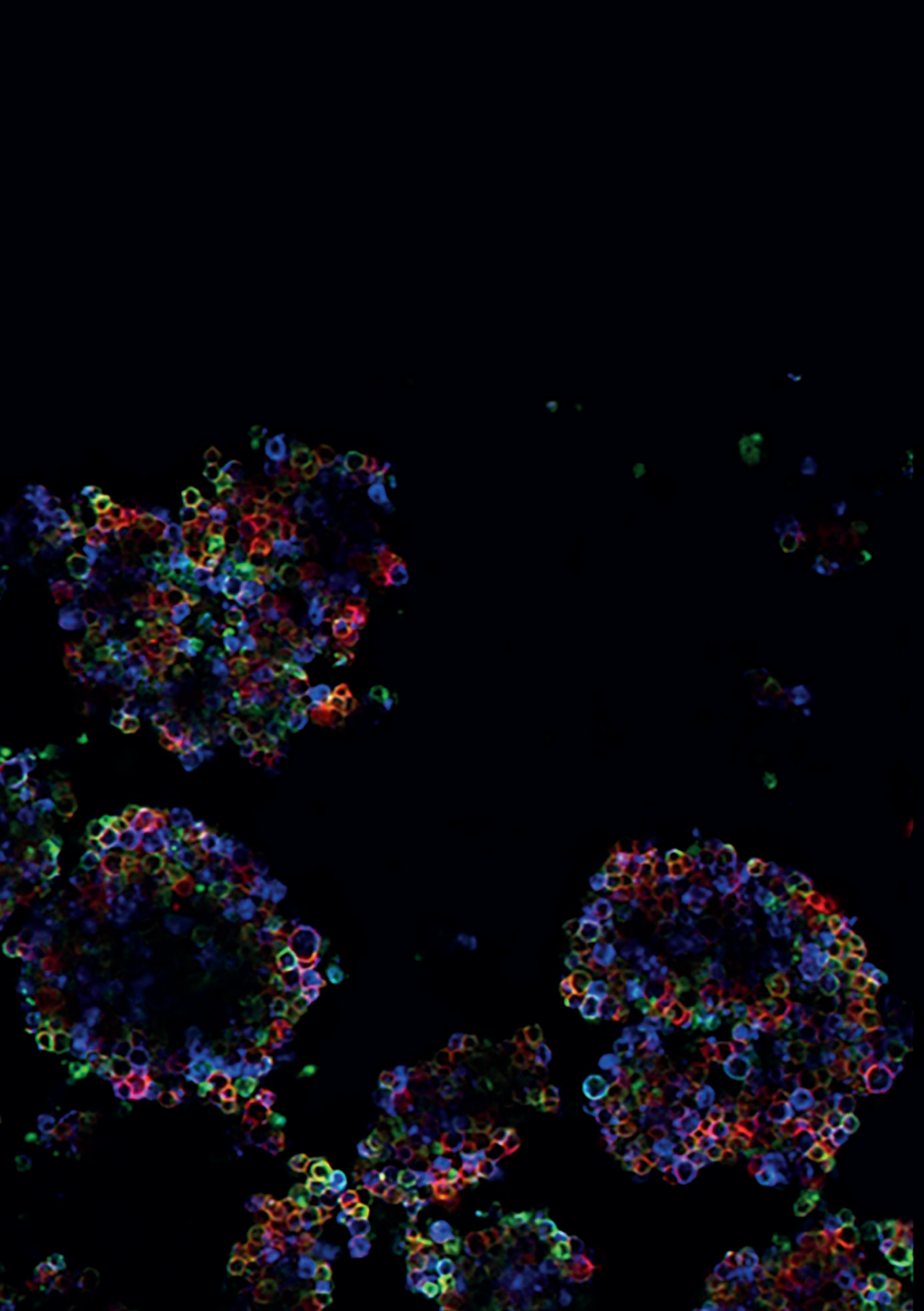
Group	First author	Year of publication	Intraoperative complications	Postoperative complications <30 days	Postoperative complications >30 days	Postoperative complications Timing unreported	Any complications Timing unreported
	Phelps et al ⁶⁹	2019	1 thoracic duct injury, 1 superior mesenteric artery injury, 3 inferior vena cava injury, 3 renal vein injury, 1 aortic injury, 2 unspecified vessel injury, 3 adjacent organ resections (not specified)	1 return to OR for chest tube (reason not reported), 1 return to OR for bleeding, 2 cardio-pulmonary complication, 1 kidney infarction (return OR nephrectomy)	-	-	-
	Rubie et al ⁷⁰	1997	11 nephrectomy (tumor resection), 2 major bleeding during excision	3 prolonged chylous effusion, 3 swallowing abnormalities, 1 phrenic palsy, 1 renal ischemic symptoms	-	-	5 death (4 bleeding during or immediately after procedure, 1 unknown cause)
	Rubie et al ⁷¹	2011	1 nephrectomy (reason not reported), 1 common bile duct resection	2 chylous effusion, 1 transient partial diaphragm palsy, 1 respiratory distress (ICU)	-	-	-
	Salim et al ⁷²	2011	4 nephrectomy (tumor resection; 1 renal insufficiency), 1 massive intraoperative hemorrhage after damage to renal vein and vena cava (vascular repair, 5L transfusion), 1 injury to sympathetic nerve supply to lower limb	5 Horner syndrome, 1 phrenic nerve palsy, 1 renal insufficiency after nephrectomy, 1 minor wound dehiscence (return to OR)	-	-	-
	Shamberger et al ⁷³	1991	5 excessive blood loss (0.57, 1.3, 2.0, and 3.0 times estimated TBV)	1 chylothorax	-	1 colocolic fistula	3 renal infarction

Supplementary table 3. Continued.

Group	First author	Year of publication	Intraoperative complications	Postoperative complications <30 days	Postoperative complications >30 days	Postoperative complications Timing unreported	Any complications Timing unreported
	Simon et al ¹⁴	2008	10 nephrectomy (reason not reported), 2 nerve lesion, 7 tumor perforation (not specified)	2 ascites, 9 postoperative ileus, 18 Horner syndrome	-	4 renal impairment	3 death (cause and timing not reported), 14 bleeding, 2 cardiac arrest, 11 other
	Simon et al ¹⁴	2013	18 nephrectomy (reason not reported), 26 relevant bleeding	17 postoperative local or systemic infections	-	14 intestinal obstruction	-
	Tajiri et al ¹⁵	2012	-	1 postoperative bleeding	3 renal atrophy, 1 adhesive intestinal obstruction	-	-
	Tanaka et al ¹⁶	2016	-	-	-	-	2 partial kidney infarction
	Tokiwa et al ¹⁷	2003	-	1 chylous ascites (conservative), 1 wound infection, 7 diarrhea (6 transient, 1 prolonged), 1 intussusception (return to OR)	1 diarrhea (prolonged), 3 renal atrophy, 1 adhesions (return to OR)	-	-
	Varan et al ¹⁸	2015	1 nephrectomy (reason not reported), 1 spermatic vein injury, 1 cysterna chyli injury, 1 renal artery injury, 2 renal vein injury, 1 colonic injury	-	-	1 ileus (volvulus)	-
	Vollmer et al ¹⁹	2018	7 kidney injury, 7 renal vessel injury, 2 segmental bowel resection, 4 partial liver resection, 3 loss of gallbladder, 7 nerve injury	4 renal failure, 4 ileus (< 30 days), 2 neurogenic bladder dysfunction	-	-	-

Supplementary table 3. Continued.

Group	First author	Year of publication	Intraoperative complications	Postoperative complications <30 days	Postoperative complications >30 days	Postoperative complications Timing unreported	Any complications Timing unreported
	Von Allmen et al ⁸⁰	2005	3 nephrectomy (reason not reported), 6 significant bleeding (>1L), 1 aortic interposition graft, 1 re-exploring retroperitoneal hematoma, 1 L5 nerve root injury	8 transient postoperative diarrhea, 2 ascites, 1 pseudomonas urinary tract infection	2 persistent diarrhea (resolved)	1 bowel obstruction	-
	Von Allmen et al ⁸¹	2017	7 normal organs removed with tumor, 14 major intraoperative hemorrhage (>10% EBV; 13 transfusion administered), 3 renal injury, 4 vascular injury	-	-	2 death (cause and timing not reported), 1 bowel obstruction, 1 surgery required	3 pulmonary complications, 5 other complications
	Yao et al ⁸²	2018	1 diaphragm rupture, 5 blood transfusions	-	-	-	-
	Yao et al ⁸⁵	2019	1 thoracic duct leak (direct repair)	1 vocal cord paralysis (temporary), 1 pleural effusion (return to OR)	-	-	-

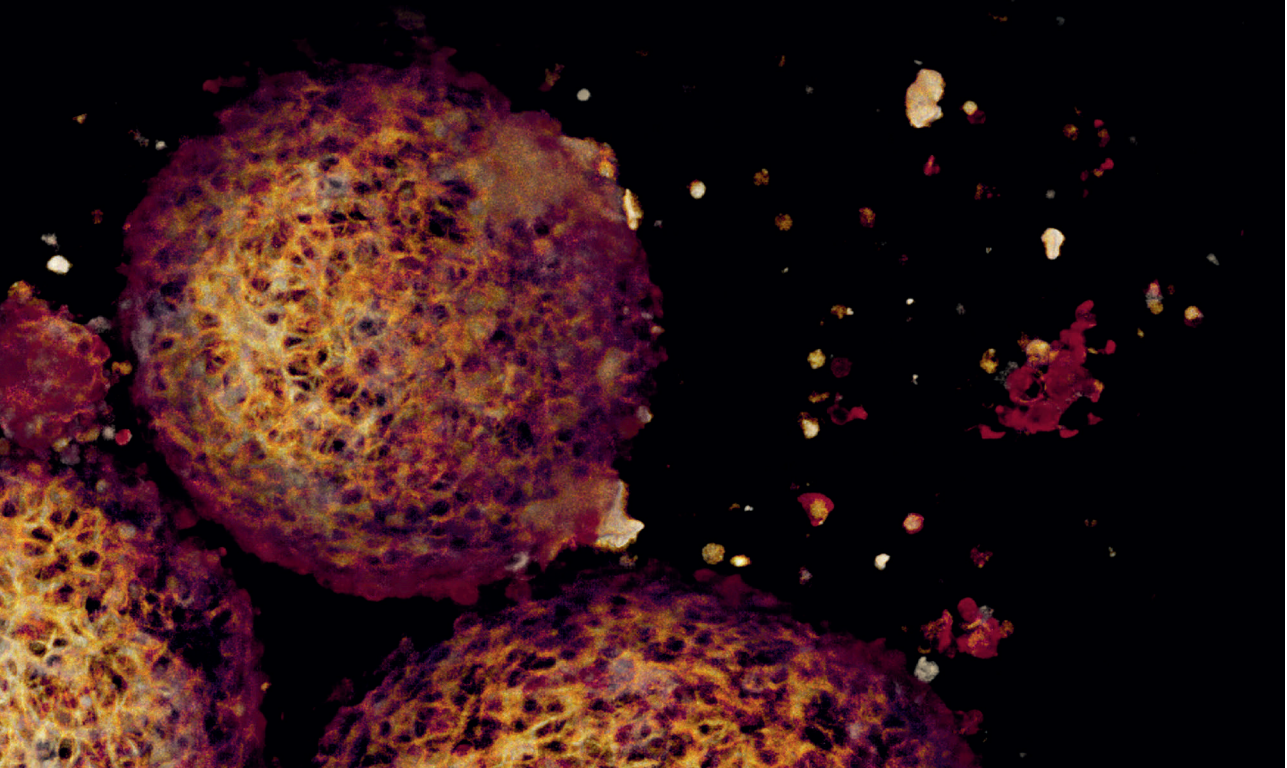



A microscopic image of cells, likely stained with fluorescent dyes, showing various colors (red, green, blue) against a dark background. A large white circle is overlaid on the center of the image, containing the text.

PART 2

Translational Science for
Image-guided Surgery

CHAPTER 4





Anti-GD2-IRDye800CW as a targeted probe for fluorescence- guided surgery in neuroblastoma

L.M. Wellens, M.M. Deken, C.F.M. Sier,
H.R. Johnson, F. de la Jara Ortiz,
S.S. Bhairosingh, R.D. Houvast, W.M. Kholosy,
V. M. Baart, A.M.M.J. Pieters, R.R. de Krijger,
J.J. Molenaar, E.J. Wehrens, J.F. Dekkers,
M.H.W.A. Wijnen, A.L. Vahrmeijer, A.C. Rios

SCIENTIFIC REPORTS - NATURE, 19 OCTOBER 2020

ABSTRACT

Neuroblastoma resection represents a major challenge in pediatric surgery, because of the high risk of complications. Fluorescence-guided surgery (FGS) could lower this risk by facilitating discrimination of tumor from normal tissue and is gaining momentum in adult oncology. Here, we provide the first molecular-targeted fluorescent agent for FGS in pediatric oncology, by developing and preclinically evaluating a GD2-specific tracer consisting of the immunotherapeutic antibody dinutuximab-beta, recently approved for neuroblastoma treatment, conjugated to near-infrared (NIR) fluorescent dye IRDye800CW.

We demonstrated specific binding of anti-GD2-IRDye800CW to human neuroblastoma cells *in vitro* and *in vivo* using xenograft mouse models. Furthermore, we defined an optimal dose of 1 nmol, an imaging time window of 4 days after administration and show that neoadjuvant treatment with anti-GD2 immunotherapy does not interfere with fluorescence imaging. Importantly, as we observed universal, yet heterogenous expression of GD2 on neuroblastoma tissue of a wide range of patients, we implemented a xenograft model of patient-derived neuroblastoma organoids with differential GD2 expression and show that even low GD2 expressing tumors still provide an adequate real-time fluorescence signal.

Hence, the imaging advancement presented in this study offers an opportunity for improving surgery and potentially survival of a broad group of children with neuroblastoma.

INTRODUCTION

Neuroblastoma (NB) is the most common extracranial solid tumor occurring in children¹. Over 75% of patients are categorized as high-risk with a poor overall 5-year survival of less than 50%, despite intensive treatment with high-dose chemotherapy followed by surgery, autologous stem cell transplantation, radiotherapy and immunotherapy^{2,3}. Resection of high-risk NB is associated with a risk for serious surgical complications, since the tumor often encases major blood vessels leading to severe hemorrhage and/or unplanned organ damage⁴. Discriminating cancerous tissue from healthy tissue is challenging, but of great importance to achieve optimal tumor resection, while preserving healthy tissue, which can thereby increase survival^{5,6}. Fluorescence-guided surgery (FGS) is a novel intra-operative imaging technique that empowers surgeons to visualize tumor tissue in real time using exogenous fluorescent agents. Most of the FDA-approved FGS probes are targeted against generic tumor markers⁷, with fluorescent 5-aminolevulinic acid (5-ALA) widely used for FGS on pediatric brain tumors⁸. However, recently, there has been a shift in this field towards the development of targeted probes that specifically bind surface markers on cancerous cells for molecular imaging⁹. Although the first cancer-targeted fluorescent agents have been evaluated in clinical trials for adults¹⁰, no specific probes have been developed so far for pediatric patients. GD2 is a disialoganglioside present on peripheral nerves and known to be overexpressed on most tumors from neuroectodermal origin, including NB^{11,12}. GD2 represents a clinically relevant target, as patients with remnant NB are currently successfully treated with anti-GD2 immunotherapy after surgery^{13,14}. Here, we conjugated this clinical grade antibody to the near-infrared (NIR) fluorophore IRDye800CW to explore its potential as a FGS probe for NB in preclinical settings.

RESULTS

ANTI-GD2-IRDYE800CW SPECIFICALLY LABELS KCNR CELLS IN VITRO

Specific binding of anti-GD2-IRDye800CW was evaluated on the widely used patient-derived NB cell line; SMS-KCNR (KCNR)¹⁵ using an established evaluation pipeline¹⁶ that includes flow cytometry *in vitro* and fluorescence molecular imaging *in vivo* (**figure 1a**). Specific binding of anti-GD2-IRDye800CW to NB cells was observed by flow cytometry, with > 95% of cells staining positive, while a negative control colorectal cancer cell line HT-29 showed no staining, similar to unstained cells (**figure 1b**). In addition, control anti-CD52-IRDye800CW, specific

for CD52 (CAMPATH-1) present on the surface of mature lymphocytes, did not label KCNR cells (**figure 1c**). Overall, this demonstrates specific binding of anti-GD2-IRDye800CW to GD2 expressing KCNR cells *in vitro*.

EFFECTIVE KCNR-DERIVED TUMOR DETECTION IN VIVO AND IDENTIFICATION OF OPTIMAL DOSE AND IMAGING TIME WINDOW

We next addressed the *in vivo* potential of our probe in a subcutaneous xenograft mouse model. Fluorescence images were generated at multiple days after intravenous administration of 3 different doses of anti-GD2-IRDye800CW. Tumors were visualised with a clinical imaging device that is commonly used for FGS in patients and a preclinical system used for *in vivo* small animal imaging for fluorescence quantification (**figure 1d and supplementary figure S1**). Fluorescence quantification showed a higher tumor-to-background ratio (TBR) for subcutaneous tumors of mice receiving a dose of 1 nmol and 0.3 nmol anti-GD2-IRDye800CW compared to 3 nmol (**figure 1e**), with a mean fluorescence intensity (MFI) of the tumor significantly higher for 1nmol dose compared to 0.3 nmol (**figure 1f**). Based on the TBR and MFI curves, we defined an optimal time window for imaging 4 days after administration of 1 nmol anti-GD2-IRDye800CW, with a TBR of 5.2 (SEM \pm 1.3) and MFI of 0.28 (SEM \pm 0.1), comparable to preclinical TBR and MFI values previously reported for FGS agents successfully used in adult oncology¹⁶⁻¹⁸. Mice receiving the control antibody anti-CD52-IRDye800CW had a significantly lower TBR and MFI, compared to the 1nmol dose (**figure 1e and f, supplementary figure S1**), further demonstrating specific binding of anti-GD2-IRDye800CW to GD2 within tumors. No difference in fluorescence signal was found between tumors of different size (**supplementary figure S2 and supplementary table S1**).

ORTHOTOPIC TUMOR ENGRAFTMENT DEMONSTRATES FEASIBILITY FOR FLUORESCENCE-GUIDED SURGERY

To investigate our tracer in a more clinical setting, we implemented an orthotopic model with KCNR cells transplanted in the adrenal gland, the most common location for NB¹⁹. Following the optimized conditions determined in the subcutaneous model, mice were intravenously injected with 1 nmol anti-GD2-IRDye800CW and the tumors were resected 4 days post injection guided by the Quest camera (**figure 2a-d, supplementary video S1**). In this surgical set-up, we defined a TBR of 6.1 (SEM \pm 2.2), similar to the subcutaneous model (**figure 2e**) and detected no remaining fluorescent tissue after surgery (**supplementary video S1**).

After harvesting the tumors, histology confirmed that NB cells on hematoxylin and eosin (H&E) staining overlapped with fluorescence of anti-GD2 (**figure 2f-h**), whereas, importantly, healthy adrenal from non-transplanted control mice gland remained negative for anti-GD2-IRDye800CW (**figure 2i-k**).

By quantifying the biodistribution, fluorescence in non-tumor tissue was only seen in the femur, as well as in the liver at day 1, which importantly was significantly lower compared to tumor tissue and further diminished by day 4 (**figure 3a and b**), confirming the mostly hepatic clearance of anti-GD2-IRDye800CW. Overall, these data show that anti-GD2-IRDye800CW is a suitable probe for fluorescence tumor detection *in vivo*.

UPFRONT DINUTUXIMAB-BETA IMMUNOTHERAPY DOES NOT INTERFERE WITH TUMOR DETECTION

Currently, clinical trials are being initiated with neoadjuvant anti-GD2 immunotherapy prior to surgery in high-risk NB²⁰. Therefore, we investigated whether this neoadjuvant immunotherapy would not interfere with the use of anti-GD2-IRDye800CW for FGS. *In vitro* we showed that 24 hours after incubation with a human anti-GD2-FITC antibody (**figure. 4a**), KCNR cells could effectively be stained a second time with a human anti-GD2 coupled to a different fluorophore; Phycoerythrin (PE) (**figure 4b-c**). This indicates that GD2 is not lost from the cell surface after antibody binding and that upfront anti-GD2 treatment should not interfere with membranous GD2 fluorescent imaging. To confirm this *in vivo*, mice with orthotopic induced tumors were pre-treated with a clinically derived dose of 1 nmol anti-GD2 for 2 cycles with 4 days in between, before receiving 1 nmol anti-GD2-IRDye800CW. In this model, the fluorescence signal in mice pre-treated with anti-GD2 dinutuximab-beta was sufficient for intraoperative fluorescence imaging and tumor resection (**figure 4d-g**) and TBR's (7.0 SEM \pm 3.4) were comparable to those without pre-treatment (6.1 SEM \pm 2.2) (**figure 4h**). This demonstrates that the use of neoadjuvant anti-GD2 immunotherapy is unlikely to diminish the fluorescence signal and that anti-GD2-IRDye800CW can be used for FGS in high-risk NB patients regardless of their order of treatment.

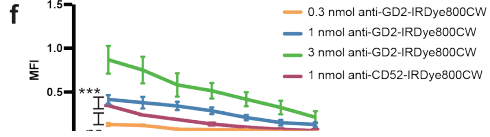
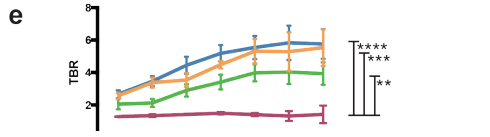
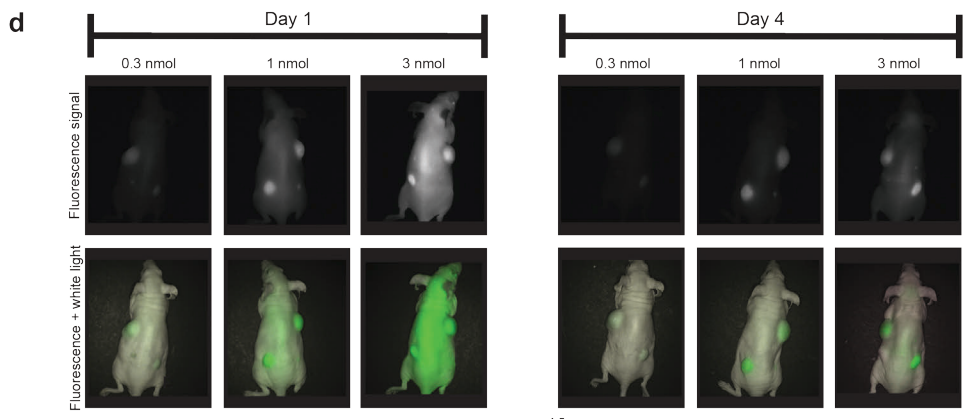
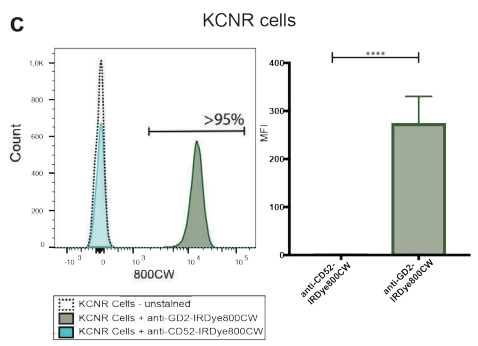
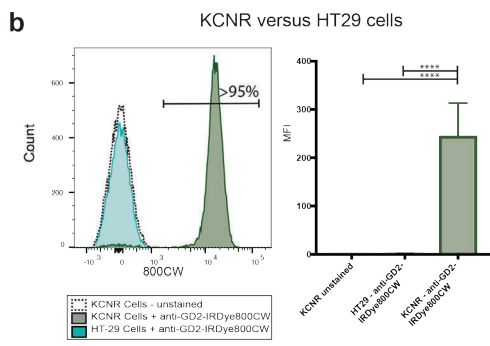
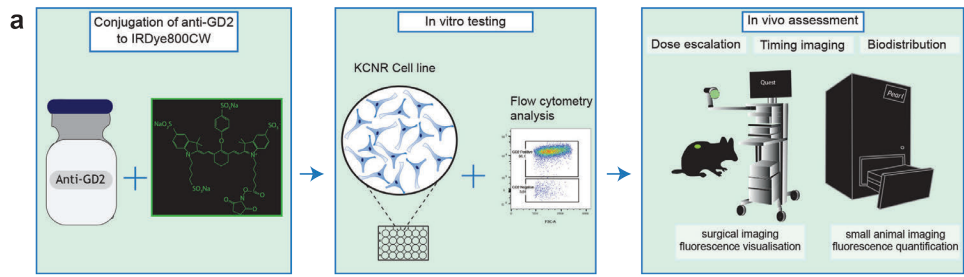


Figure 1. Dose escalating study in subcutaneous KCNR-derived tumor model reveals 1 nmol as the optimal dose and efficient real-time visualization of NB after 4 days.

a) Schematic overview of the preclinical evaluation pipeline. Anti-GD2 chimeric monoclonal antibody was conjugated to IRDye800CW (left panel) and evaluated *in vitro* on the NB KCNR cell line by flow cytometry (middle panel). *In vivo* validation was performed in NB cell line derived xenograft mouse models using the Pearl Trilogy Small Animal imaging system and Quest Spectrum imaging system (right panel). **b)** Representative histogram (left panel) and accumulative data (right panel) of anti-GD2-IRDye800CW staining by flow cytometry on KCNR and HT-29 cells, compared to unstained cells. **c)** Representative histogram (left panel) and accumulative data (right panel) of anti-GD2-IRDye800CW staining on KCNR cells compared to CD52-IRDye-800CW staining. b, c) n=3 independent experimental repeats. Graphs depict mean + SEM, ****p<0.0001. **d)** Representative images using the surgical imaging device of mice bearing subcutaneous human KCNR-derived tumors, acquired 1 day (left panel) and 4 days (right panel) after administration of 3 ascending doses of anti-GD2-IRDye800CW. **e)** Tumor-to-background ratio (TBR) for 7 consecutive days of mice receiving different doses of anti-GD2-IRDye800CW and or 1 nmol anti-CD52-IRDye800W as a negative control. Mean ± SEM. ****p < 0.0001; ***p = 0.0006 and **p = 0.0018 for comparison of 1, 0.5, and 3 nmol dose anti-GD2-IRDye800CW respectively to 1nmol dose anti-CD52-IRDye800W. **f)** The mean fluorescence intensity (MFI) for all concentrations in arbitrary units. Mean ± SEM. ****p<0.0001 for comparison of 1nmol dose anti-GD2-IRDye800CW to 0.3 nmol dose and non-significant (ns) for comparison 0.3 nmol anti-GD2-IRDye800CW to control 1 nmol anti-CD52-IRDye800CW (p=0.08). d-f) n=2 independent experiments with 3 to 4 mice per group.

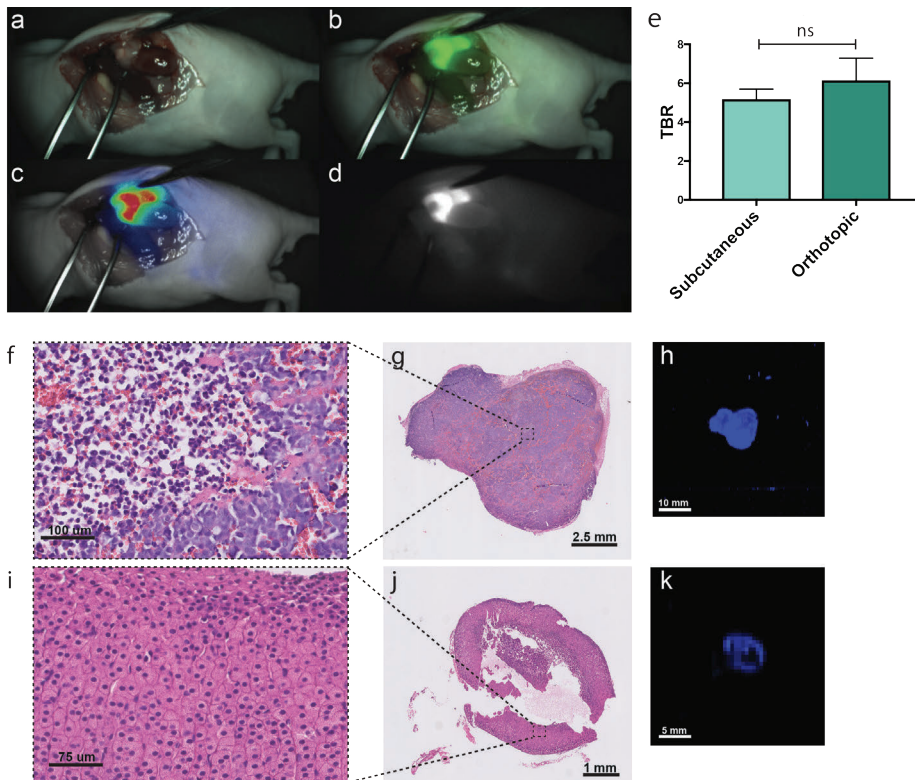


Figure 2. Orthotopic KCNR-derived tumor model confirms clinical potential of anti-GD2-IRDye-800CW for FGS.

a-d) Representative images of FGS of an orthotopic KCNR-derived tumor 4 days post-injection using the Quest Artemis imaging system as a real time-navigator. **a)** shows the white light view of the surgeon **b)** the overlay with the fluorescence signal in green, **c)** the overlay of the heatmap and **d)** the fluorescence signal. **e)** TBR obtained with the Pearl imaging system and compared to TBR from the subcutaneous model. Mean + SEM, non-significant (ns) $p=0.264$. **f - h)** Representative H&E images of a tumor section imaged at 40x magnification. **(f)** depicts an enlargement from **(g)**. Scalebar 100 μm. **h)** Representative 2D image of the same section imaged in the Odyssey Clx for fluorescence intensity. **i - k)** Similar representative images as in f - h) for the adrenal gland of a control mouse not engrafted with KCNR cells. Scalebar 75 μm. $n=2$ independent experiments with $n=5$ mice per group.

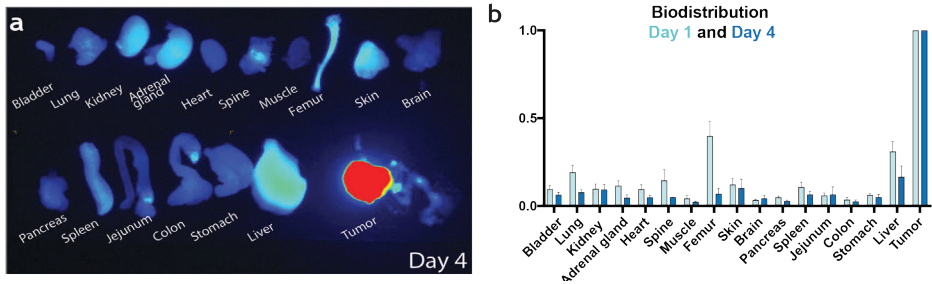


Figure 3. Biodistribution demonstrates the mostly hepatic clearance of anti-GD2-IRDye800CW.
a) Representative images at day 4 for the biodistribution of anti-GD2-IRDye800CW in multiple organs of orthotopic tumor-bearing mice receiving a 1nmol dose imaged with the Pearl imaging system. **b)** accumulative data at day 1 and 4. Mean MFI normalized to tumor + SEM. n=2 independent experiments with n=3-4 mice.

TISSUE MICROARRAY OF DIFFERENT PATHOLOGICAL STAGES REVEALS CONSISTENT, YET HETEROGENOUS GD2 EXPRESSION IN HIGH-RISK NB PATIENTS

To further investigate the extent of patients that can potentially benefit from anti-GD2-IRDye800CW guided surgery, we defined the expression of GD2 on a tissue microarray (TMA) consisting of tumor samples from 28 high-risk NB patients treated with chemotherapy (**supplementary table 3**). This demonstrated consistent expression of GD2 across multiple pathological tumor stages; neuroblastoma (**figure 5a**), ganglioneuroblastoma (**figure 5b**) and ganglioneuroma (**figure 5c**) after chemotherapy, in line with previous literature^{12,21}. Importantly, no signal was detected in control peripheral nerve tissue (**figure 5d**). However, even when belonging to the same tumor category, heterogeneity between individual patients could be observed and in each subtype we could identify samples with high, intermediate, or low GD2 expression (**figure 5a-c**).

PATIENT-DERIVED ORGANOID LINES DEMONSTRATE ADEQUATE TUMOR DETECTION ACROSS DIFFERENTIAL GD2 EXPRESSION LEVELS

In the last decade, organoid technology has become a valuable *in vitro* tool to study human cancer in a patient-specific manner²². Since the above results show that GD2 is not uniformly highly expressed in NB patients, we made use of three patient-derived neuroblastoma organoid lines; TIC772²³, NB67 and NB39 (**supplementary table 2** and unpublished data) that reflect the high, intermediate and low GD2 expression levels observed in patients, as shown by confocal imaging (**figure 6a**) and flow cytometry (**figure 6b**). Upon subcutaneous transplantation *in vivo*, tumors derived from each line showed detectable real time fluorescence with

differential MFI as observed *in vitro* (figure 6c and d) but, importantly, no difference in TBR compared to KCNR-derived tumors (figure 6e). This indicates that even in patients with low GD2 expressing tumors, fluorescence obtained with anti-GD2-IRDye800CW will be sufficient for FGS.

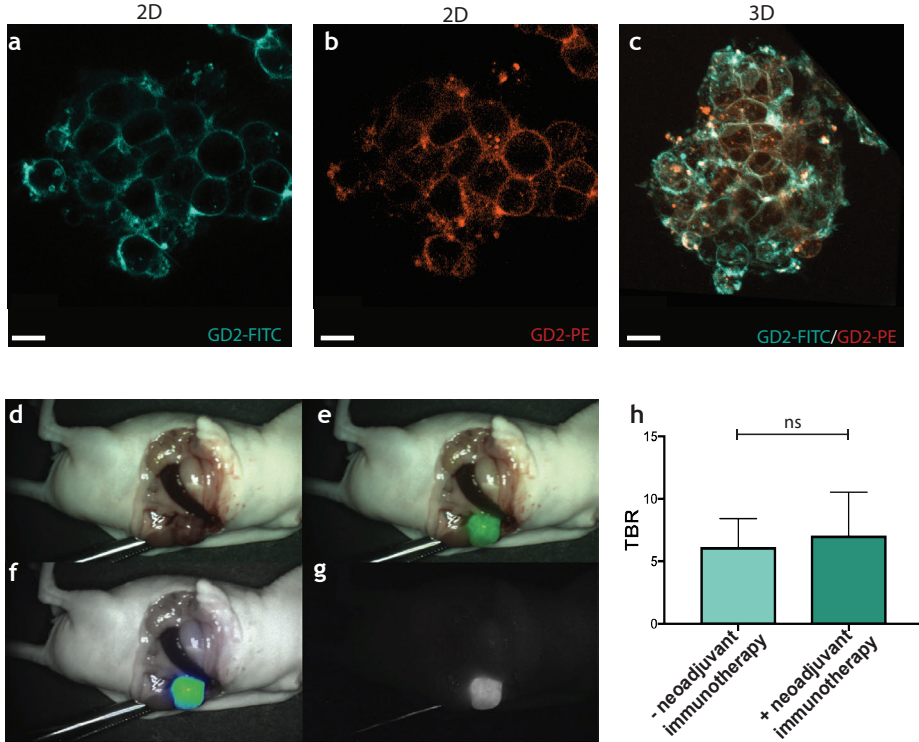


Figure 4. Anti-GD2 dinutuximab-beta treatment does not interfere with anti-GD2-IRDye800CW fluorescence.

a – c) Representative confocal images of KCNR cell 3D spheroids after incubation with anti-GD2-FITC (in cyan) (a), followed by anti-GD2-PE (in red) (b), or an overlay of both channels in 3D (c). n=3 independent experiments. Scalebars 10 μ m. **d – g)** Representative images of FGS in orthotopic NB tumor-bearing mice receiving upfront anti-GD2 immunotherapy, using the Quest Artemis imaging system as a real time-navigator. **d)** shows the white light view of the surgeon, **e)** the overlay with the fluorescence signal in green, **f)** the overlay of the heatmap and **g)** the fluorescence signal. **h)** TBR measured from images recorded using the Pearl imaging system in mice receiving upfront anti-GD2 immunotherapy compared to mice without anti-GD2 upfront treatment, non-significant (ns) p=0.503 D-H) n=2 independent experiments with n=5 mice per group.

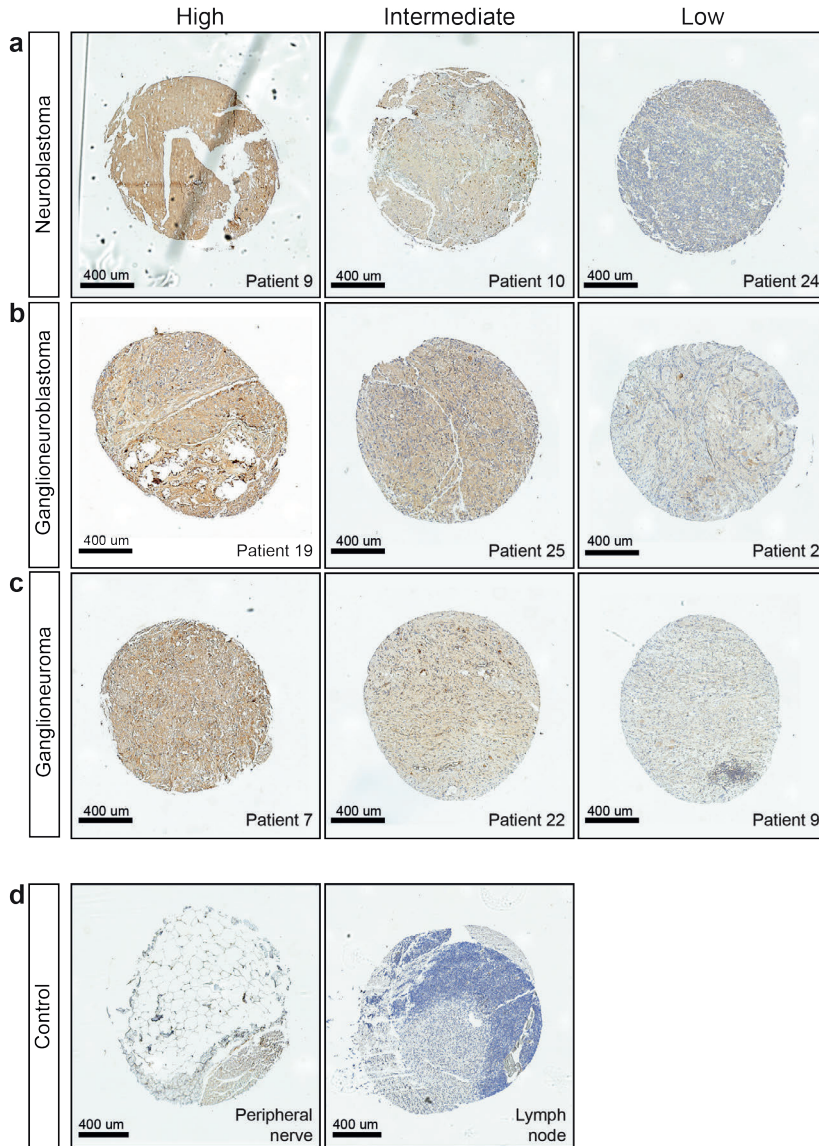


Figure 5. Tissue microarray of different stages of NB shows a heterogeneous expression of anti-GD2 between patients.

a-d) Representative images of anti-GD2 Immunohistochemical staining on a tissue microarray (TMA) containing tissue of 27 patients in duplicate and 1 patient in singular. **(a)** Three representative images of differential labelling for neuroblastoma tissues on high, intermediate and low labelling for GD2. **(b)** Three representative images of differential labelling for ganglioneuroblastoma tissues and **(c)** Three representative images for ganglioneuroma tissues. **(d)** Two control stainings on peripheral nerve tissue (left) and lymph node tissue (right) for anti-GD2. Scalebars 400 μ m.

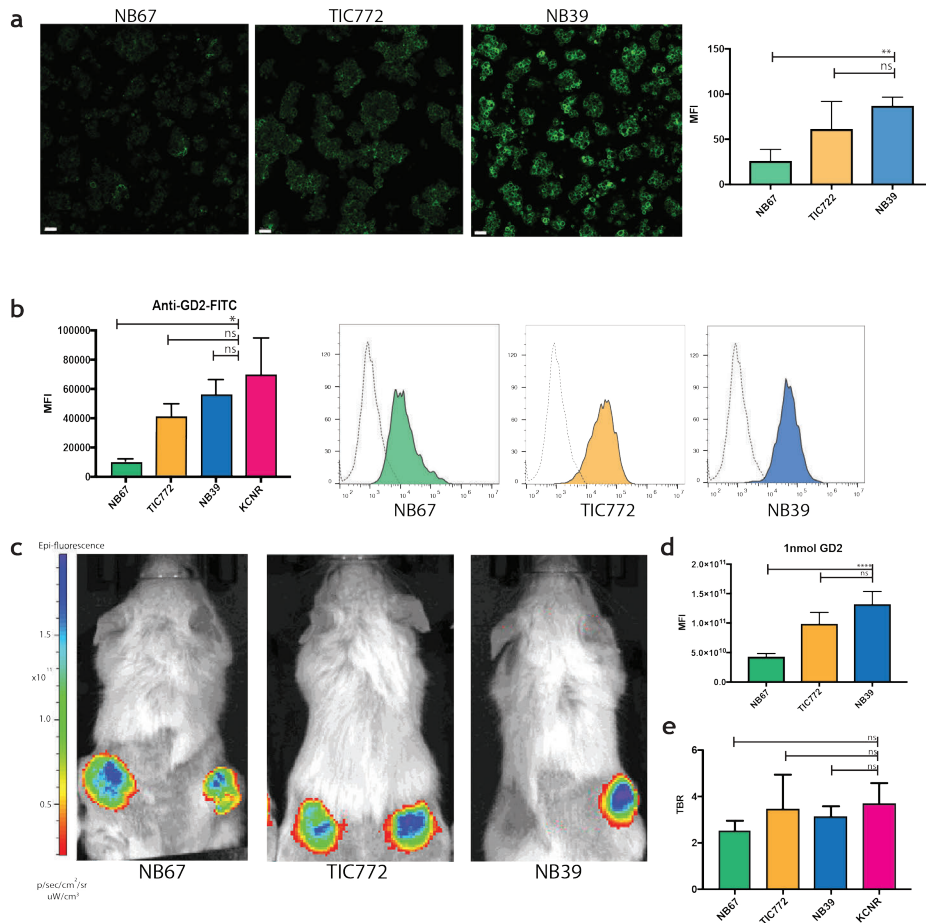


Figure 6. Patient-derived organoid lines representing heterogeneous GD-2 expression demonstrate adequate fluorescent signal in case of low GD2 expression.

a) Representative confocal images of the three different patient-derived NB organoid lines NB67, TIC772 and NB39 showing anti-GD2 staining at different intensities. Scale bars 30 μm . Graphs (right panel) depict mean intensities + SEM, ** $p=0.0028$ for comparison of NB67 and NB39 and non-significant (ns) ($p=0.2365$) for comparison TIC772 and NB39. **b)** Accumulative data (left panel) and representative histograms (right panel) of anti-GD2-IRDye800CW staining analysed by flow cytometry. MFI + SEM * $p=0.05$ for comparison of NB67 and KCNR, and non-significant (ns) for comparison TIC772 to KCNR ($p=0.3429$) and NB39 to KCNR ($p=0.4857$). **c)** Representative *in vivo* images from patient-derived organoid xenograft models. **d)** The mean fluorescence intensity (MFI) for all concentrations in arbitrary units. Mean \pm SEM. **** $p<0.001$ for comparison of 1nmol dose anti-GD2-IRDye800CW of NB67 to NB39 and non-significant (ns) for comparison of NB67 to NB39 $p=0.06$ **e)** TBR at day 4 of mice receiving anti-GD2-IRDye800CW. The TBR's of all organoid lines were non-significant (ns) when compared to the TBR of the KCNR cell line ($p=0.07$ for comparing KCNR to NB67, $p=0.257$ when comparing KCNR to NB39 and $p>0.999$ when comparing TIC772 to KCNR).

DISCUSSION

By showing the feasibility of intraoperative fluorescence imaging of NB with anti-GD2-IRDye800CW, our preclinical study presents the first suitable molecular-targeted candidate for FGS to guide tumor resection in children. Although FGS with tumor surface antigen specific probes is increasingly implemented in adult oncology^{10,24}, its application in pediatric oncology is still scarce. To the best of our knowledge, we here for the first time show that xenograft tumors derived from pediatric tumor cell lines or patient-derived organoids can be detected effectively *in vivo* using a real time intraoperative imaging system and thereby provide the first step towards closing this translational gap. Importantly, by using a clinical approved antibody combined with a NIR fluorescent probe, we are on a fast track for getting this tumor-specific tracer in a first in-child clinical trial.

Before testing efficacy in phase II/III clinical trials, phase I clinical trials will be required to determine the safety of anti-GD2-IRDye800CW. However, the immunotherapeutic antibody dinutuximab-beta, one component of our probe, has already been FDA approved. Based on our optimal dose of 1nmol (0.15mg) in mice, we expect an effective dose of 0.9 mg/kg (22mg/m²) in children²⁵, close to the dose of 20mg/m² that has been reported to have minimal toxicity in children²⁶. In addition, the second part of our probe, the near-infrared dye 800CW has shown to be non-immunogenic in previous preclinical studies²⁷ and has been safely administrated in multiple clinical trials^{28,29}. One important limitation of our preclinical evaluation is that we cannot evaluate binding to GD2 potentially expressed on healthy tissue, because dinutuximab-beta is not cross-reactive with mouse GD2. However, other clinical studies have shown that GD2 expression is restricted to neurons, skin melanocytes, and peripheral sensory nerve fibers³⁰ with expected intensity signals not-detectable compared to NB. In line with this, we did not obtain positive GD2 staining on control peripheral nerve tissue in our TMA. Although safety levels of the conjugated probe still need to be carefully evaluated, these results are highly promising towards the outcome of such evaluations.

Timely progress into clinical trials might benefit children suffering from high-risk NB in multiple ways. Due to the localization of most NB tumors, their encasement in important vasculature and the surgeon's challenge to discern tumor from healthy tissue, resection is almost never complete^{31,32}. While standard of care, this also complicates understanding the long-term patient benefit of tumor resection. Indeed, although some studies report that gross total resection improves overall survival^{6,33} or event-free survival³⁴, others claim no obvious survival benefit³⁵. Bias in determining the extent to which tumor resection was complete might contribute to this discrepancy. This is now based on the subjective impression of

the surgeon, which is known to have a poor correlation with the results of post-operative imaging³⁴. Introduction of FGS for NB resection, will provide an additional modality to quantify tumor cells or tissue remaining, based on fluorescence signal. The extent of resection can thereby be more accurately determined, which opens up new possibilities to reliably assess the effect of surgery on overall survival. In addition, a more accurate quantification of remaining tumor tissue, will help guide decision making on post-surgery course of treatment, and potential benefit of dinutuximab-beta immunotherapy in particular. Most importantly, by providing a precise surgery tool to resect tumoral tissue with higher confidence, chances of relapse due to remaining tumor might decrease. At the same time, damage to surrounding healthy organs and vasculature can be prevented, thereby lowering the risk of surgical complications that is still high in NB patients undergoing surgery³⁶.

Considering the overexpression of GD2 on neuroblastoma cells¹², we expect our GD2 specific tracer to be of clinical value for the majority of NB patients, which was confirmed by our TMA results showing GD2 expression on NB tissue in the majority of patients, across tumor subtypes and after chemotherapy treatment. Importantly, although we observed heterogeneous expression of GD2, with some patients only expressing intermediate or even low expression levels, experiments with patient-derived organoid lines reflecting these expression levels, showed that TBRs of subsequent xenografted tumors were still sufficiently high to discriminate tumor from healthy tissue, even for low expressing organoid lines. Finally, anti-GD2 is increasingly used for immunotherapy in high-risk NB³⁷. Currently, after surgery, but ongoing trials will assess the advantage of neoadjuvant treatment^{38,39}. Therefore, we also confirmed that anti-GD2-IRDye800CW can still detect NB tissue after upfront anti-GD2 treatment, further validating the wide range of patients that could potentially benefit from anti-GD2-IRDye800CW guided surgery.

In conclusion, we here present a first pediatric cancer specific tracer with potential for the vast majority of high-risk NB patients to guide tumor resection with greater accuracy, thereby lowering the risk of surgical complications and reducing the incidence of relapse. In addition, we envision the comprehensive preclinical evaluation pipeline presented, using both patient derived cell line and organoid xenograft models and encompassing multiple imaging technologies, to be highly applicable for the development of other targeted probes.

METHODS

ANTIBODY CONJUGATION

Chimeric monoclonal antibody Dinutuximab-beta (Qarziba, USA) was conjugated to the NIR fluorophore IRDye800CW, (LI-COR Biosciences, Nebraska, USA), as previously described¹⁸. A degree of labelling (DoL) between 1.0 and 1.5 was considered successful. As a control, the antibody alemtuzumab directed against CD52 present on the surface of mature lymphocytes, was also conjugated to IRDye800CW.

HUMAN CANCER CELL LINES

After evaluation of different neuroblastoma cell lines for GD2 expression, the neuroblastoma cell line SMS-KCNR (KCNR)¹⁵ was selected based on GD2 expression and *in vitro* and *in vivo* growth rate. The human colon colorectal cancer cell line HT-29 was used as a negative control. KCNR line was cultured in Dulbecco's modified Eagle's medium (DMEM)-GlumaMAX containing low glucose, 10% Fetal Bovine Serum (FBS), 1%ml NEAA, 100 IU/ml penicillin and 100ug/ml streptomycin. HT-29 cells were cultured in RPMI-1640 medium (Life technologies, Gibco) with 10% FBS and 100 IU/ml penicillin. Both lines were cultured in a humidified incubator at 37° C and 5% CO₂ and free of *Mycoplasma* species.

PATIENT-DERIVED NEUROBLASTOMA ORGANIDS

Patient-derived neuroblastoma organoids^{19,23} (Kholosy et al, submitted) were grown in Dulbecco's modified Eagle's medium (DMEM)-GlumaMAX containing low glucose with addition of 20% Ham's F-12 Nutrient Mixture, B-27 Supplement minus vitamin A, N-2 supplement, 100 IU/ml penicillin, 100ug/ml streptomycin, 20ng/mL epidermal growth factor (EGF), 40ng/ml fibroblast growth factor-basic (FGF-2), 200 ng/ml insulin-like growth factor (IGF-1), 10ng/ml platelet-derived growth factor AA (PDGF-AA) and 10 ng/ml platelet-derived growth factor BB (PDGF-BB).

FLOW CYTOMETRY

KCNR and HT-29 were grown to 90% confluence and detached with TrypleLE. Organoids were processed into single cells using 200 ul accutase. Cells were adjusted to 0.5 x 10⁶ viable cells per tube in FACS buffer and incubated with 200 ml phosphate buffer solution (PBS) and 2 ml anti-GD2-IRDye800CW, or anti-CD52-800CW, as a negative control. Organoids were incubated with 2 ul anti-GD2-FITC (mouse 14g2a, Biolegend). After incubation, cells were washed three times in ice-

cold PBS and resuspended in 500 ml PBS containing propidium iodine (PI) to stain dead cells. Samples were acquired on a LSRII flow cytometer (BD Biosciences, Singapore) and analysis was performed using FlowJo software (TreeStar, Ashland, Oregon, United States, version 10.6.2).

3D CONFOCAL IMAGING

KCNR cells were transferred to a 96 well sensoplate microplate (Greiner BIO-ONE) 24 hours prior to imaging, allowing the cells to form 3D spheroids, due to the low adherence conditions, and incubated with anti-GD2-FITC (mouse 14g2a, Biolegend, 1/200) overnight at 4°C. The following day, the cells were washed 3 times with medium before incubation with anti-GD2-PE (mouse 14g2a, Biolegend, 1/200) for 15 minutes on ice.

Patient-derived organoids were incubated directly after culture for 30 minutes with anti-GD2-FITC on ice before imaging. Imaging was performed on a confocal microscope using a 25X 0.8 NA objective (SP8 Leica microscope, LSM880 Zeiss microscope). 3D rendering was performed using Imaris (Bitplane).

ETHICS

All human organoid samples were obtained from the biobank of the Princess Máxima Center (PMCLAB2019.037). Authorizations were obtained from the medical ethical committee of UMC Utrecht (METC UMCU) to ensure compliance with the Dutch Medical Research Involving Human Subjects Act, and informed consent was obtained from all donors. All animal experiments were approved by the Animal Welfare Committee of either the LUMC or the Princess Máxima Center and carried out in compliance with both local and international regulations.

GENERATION OF NEUROBLASTOMA XENOGRAFT MODELS

Mice. Six-week-old athymic nude female mice (CD1-Foxn1^{nu}, Charles River Laboratories) were used for xenografting of KCNR cells and NSG-mice (bred in house) for organoid xenograft models.

Subcutaneous xenograft models. On average, 1.0×10^6 KCNR cells or 1.0×10^6 single cells from patient-derived organoids were injected subcutaneously at 2 - 4 dorsal sites in 50ul 50% medium/50% BME. Throughout the injection of tumor cells and imaging procedures, animals were anesthetized with 2.5% isoflurane for induction of anesthesia and 2% isoflurane for maintenance with a flow of 0.5 L/min.

Orthotopic xenograft model. Mice were injected with 1:1:2 Hypnorm/Dormicum/PBS for analgesia. After 30 min, mice were anesthetized with 3% isoflurane and positioned with the left flank facing upward. After opening the skin and incision of the retroperitoneum, 1.0×10^6 KCNR cells were injected in 10ml medium in the left adrenal gland using a 0.5 – 10 ml syringe. Tumor growth was followed up by palpation of the back three times per week. When tumors were approximately 8 x 8 mm, mice were injected with anti-GD2-IRDye800CW and imaging performed. In experiments investigating the effect of neoadjuvant dinutuximab-beta treatment, mice were pretreated with 1nmol in 50 μ l PBS 3 weeks after engraftment, followed by a second dose 4 days later. 8 days after the first dose, 1 nmol of anti-GD2-IRDye800CW was administered for subsequent imaging.

IN VIVO IMAGING OF FGS PROBES

Mice bearing subcutaneous tumors starting from a size of 8 x 8 mm were intravenously injected in the tail vein with 0.3 nmol, 1 nmol or 3 nmol anti-GD2-IRDye800CW in 50 μ l PBS. Fluorescence signal was measured using both the Pearl Trilogy Small Animal imaging system (LI-COR Biosciences, Lincoln, Nebraska, U.S.A) and the Quest Artemis imaging system (Quest Medical Imaging, Middenmeer, The Netherlands). When the mice had multiple tumors, a size of 5 x 5 mm was considered the lower threshold to be included for analysis. Mice bearing organoid-derived subcutaneous tumors, were imaged by the IVIS Spectrum In Vivo Imaging System (Perkin Elmer, Waltham, MA, U.S.A.). Control mice were injected with antibody CD52-IRDye800CW (1 nmol). For orthotopic KCNR and patient derived organoid xenograft models, mice were injected with the optimal dose of 1nmol anti-GD2-IRDye800CW.

TBR CALCULATION AND MEASUREMENT OF BIODISTRIBUTION

Regions of interest were drawn based on the visible tumor to measure the mean fluorescence intensity (MFI) on the Pearl and the IVIS. Imaging data from the Pearl, Quest and IVIS were analysed using respectively Pearl Cam Software, ImageJ (W. Rasband, Bethesda, Maryland, U.S.A.) and Living Image Software (Perkin Elmer, Waltham, MA, U.S.A., version 4.7.3.). Tumor-to-background ratios (TBRs) were calculated by dividing the mean fluorescence intensity (MFI) of the tumor by the adjacent abdominal background signal in donut shape surrounding the tumor. Biodistribution of anti-GD2-IRDye800CW was determined by measurement at 24 and 96 hours after administration of MFI from multiple organs in mice bearing subcutaneous tumors and injected with 1 nmol anti-GD2-IRDye800CW.

GENERATION OF PATIENT TISSUE MICROARRAY

A tissue micro array (TMA) was created using paraffin-embedded tissue blocks of patients diagnosed with high-risk neuroblastoma, who underwent surgical resection after chemotherapy treatment between 2014 and 2017 at the Princess Máxima Center, Utrecht, The Netherlands. Three different TMA blocks were created containing the three different histological subtypes found in the 28 different patients according to the International Neuroblastoma Pathology Classification (INPC); neuroblastoma (n=18), ganglioneuroblastoma (n=20) and ganglioneuroma (n=20)²¹. Samples were obtained during debulking surgery, formalin fixed, confirmed to represent neuroblastoma tissue by a professor in pediatric oncology pathology and histologically scored as neuroblastoma, ganglioneuroblastoma or ganglioneuroma. Samples were placed on the TMA in duplicate. Control samples of healthy tissue from peripheral nerves (n=2) and lymphoid tissue (n=2) were added. The TMA was subsequently stained with anti-GD2 (mouse 14g2a, Biolegend, 1/50).

HISTOLOGICAL ANALYSIS

After euthanizing the mice, tumors were surgically removed and fixed in formalin. Tumors were sectioned and scanned on the Odyssey Clx (LI-COR Biosciences, Lincoln, NE, USA). A solid state laser diode tuned at 785nm was used for optimal excitation of the fluorophore IRDye800CW and light was collected in the 800 nm channel for evaluation of the fluorescence location. Slides of subsequent sections were stained with haematoxylin-eosin.

STATISTICAL ANALYSES

Statistical analysis was performed using Graphpad Prism software (version 7, GraphPad Software Inc, La Jolla, CA, USA). The Area Under the Curve (AUC) was calculated for the different dose groups and comparison of means were performed with the unpaired t-test. All other comparisons of means were performed with the Mann Whitney U test.

DATA AVAILABILITY STATEMENT

All data is included in either the main manuscript or Supplementary Information.

REFERENCES

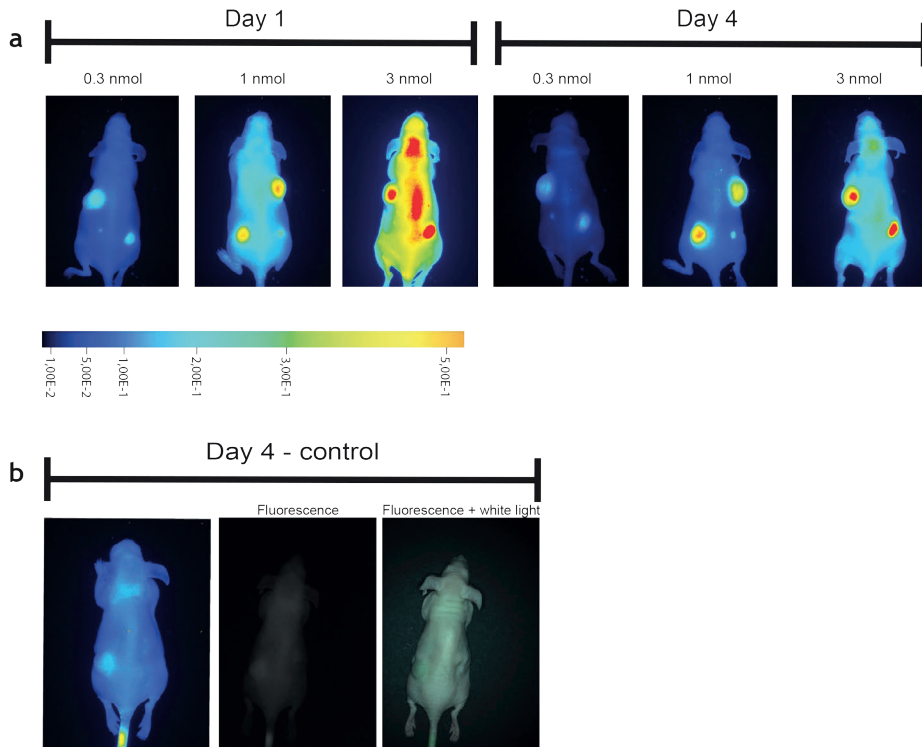
- 1 Maris, J.M. Recent advances in neuroblastoma. *N Engl J Med* 362, 2202-2211, doi:10.1056/NEJMr0804577 (2010).
- 2 Gatta, G. et al. Childhood cancer survival in Europe 1999-2007: results of EUROCare-5--a population-based study. *Lancet Oncol* 15, 35-47, doi:10.1016/S1470-2045(13)70548-5 (2014).
- 3 Tas, M.L. et al. Neuroblastoma between 1990 and 2014 in the Netherlands: Increased incidence and improved survival of high-risk neuroblastoma. *Eur J Cancer* 124, 47-55, doi:10.1016/j.ejca.2019.09.025 (2020).
- 4 Jans M., W.M., Van De Ven C., Van Baren R., Tytgat G., Zwaveling S. . *Analysis of Surgery for Neuroblastoma in The Netherlands* (Catalogue No. S5-S321 (abstr O-155), SIOP 2016 Scientific Programme+Index).
- 5 Irwin, M.S. & Park, J.R. Neuroblastoma: paradigm for precision medicine. *Pediatr Clin North Am* 62, 225-256, doi:10.1016/j.pcl.2014.09.015 (2015).
- 6 Vollmer, K. et al. Radical Surgery Improves Survival in Patients with Stage 4 Neuroblastoma. *World J Surg* 42, 1877-1884, doi:10.1007/s00268-017-4340-9 (2018).
- 7 van Manen, L. et al. A practical guide for the use of indocyanine green and methylene blue in fluorescence-guided abdominal surgery. *J Surg Oncol* 118, 283-300, doi:10.1002/jso.25105 (2018).
- 8 Schwake, M. et al. 5-ALA fluorescence-guided surgery in pediatric brain tumors-a systematic review. *Acta Neurochir (Wien)* 161, 1099-1108, doi:10.1007/s00701-019-03898-1 (2019).
- 9 Debie, P., Devoogdt, N. & Hernot, S. Targeted Nanobody-Based Molecular Tracers for Nuclear Imaging and Image-Guided Surgery. *Antibodies (Basel)* 8, doi:10.3390/antib8010012 (2019).
- 10 Hernot, S., van Manen, L., Debie, P., Mieog, J.S.D. & Vahrmeijer, A.L. Latest developments in molecular tracers for fluorescence image-guided cancer surgery. *Lancet Oncol* 20, e354-e367, doi:10.1016/S1470-2045(19)30317-1 (2019).
- 11 Mujoo, K., Cheresh, D.A., Yang, H. M. & Reisfeld, R.A. Disialoganglioside GD2 on human neuroblastoma cells: target antigen for monoclonal antibody-mediated cytotoxicity and suppression of tumor growth. *Cancer Res* 47, 1098-1104 (1987).
- 12 Terzic, T. et al. Expression of Disialoganglioside (GD2) in Neuroblastic Tumors: A Prognostic Value for Patients Treated With Anti-GD2 Immunotherapy. *Pediatr Dev Pathol* 21, 355-362, doi:10.1177/1093526617723972 (2018).
- 13 Yu, A.L. et al. Anti-GD2 antibody with GM-CSF, interleukin-2, and isotretinoin for neuroblastoma. *N Engl J Med* 363, 1324-1334, doi:10.1056/NEJMoa0911123 (2010).
- 14 Ladenstein, R. et al. Investigation of the Role of Dinutuximab Beta-Based Immunotherapy in the SIOPEN High-Risk Neuroblastoma 1 Trial (HR-NBL1). *Cancers (Basel)* 12, doi:10.3390/cancers12020309 (2020).
- 15 Reynolds, C.P. et al. Characterization of human neuroblastoma cell lines established before and after therapy. *J Natl Cancer Inst* 76, 375-387 (1986).
- 16 Boonstra, M.C. et al. Preclinical evaluation of a novel CEA-targeting near-infrared fluorescent tracer delineating colorectal and pancreatic tumors. *Int J Cancer* 137, 1910-1920, doi:10.1002/ijc.29571 (2015).

- 17 Boogerd, L.S. F. *et al.* Fluorescence-guided tumor detection with a novel anti-EpCAM targeted antibody fragment: Preclinical validation. *Surg Oncol* 28, 1-8, doi:10.1016/j.suronc.2018.10.004 (2019).
- 18 Boonstra, M.C. *et al.* Preclinical uPAR-targeted multimodal imaging of locoregional oral cancer. *Oral Oncol* 66, 1-8, doi:10.1016/j.oraloncology.2016.12.026 (2017).
- 19 Decaestecker, B. *et al.* TBX2 is a neuroblastoma core regulatory circuitry component enhancing MYCN/FOXM1 reactivation of DREAM targets. *Nat Commun* 9, 4866, doi:10.1038/s41467-018-06699-9 (2018).
- 20 Furman, W.L. *et al.* A Phase II Trial of Hu14.18K322A in Combination with Induction Chemotherapy in Children with Newly Diagnosed High-Risk Neuroblastoma. *Clin Cancer Res* 25, 6320-6328, doi:10.1158/1078-0432.CCR-19-1452 (2019).
- 21 Shimada, H. *et al.* The International Neuroblastoma Pathology Classification (the Shimada system). *Cancer* 86, 364-372 (1999).
- 22 Tuveson, D. & Clevers, H. Cancer modeling meets human organoid technology. *Science* 364, 952-955, doi:10.1126/science.aaw6985 (2019).
- 23 Bate-Eya, L.T. *et al.* Newly-derived neuroblastoma cell lines propagated in serum-free media recapitulate the genotype and phenotype of primary neuroblastoma tumours. *Eur J Cancer* 50, 628-637, doi:10.1016/j.ejca.2013.11.015 (2014).
- 24 Vahrmeijer, A.L., Hutteman, M., van der Vorst, J.R., van de Velde, C. J. & Frangioni, J. V. Image-guided cancer surgery using near-infrared fluorescence. *Nat Rev Clin Oncol* 10, 507-518, doi:10.1038/nrclinonc.2013.123 (2013).
- 25 Reagan-Shaw, S., Nihal, M. & Ahmad, N. Dose translation from animal to human studies revisited. *FASEB J* 22, 659-661, doi:10.1096/fj.07-9574LSF (2008).
- 26 Yu, A.L. *et al.* Phase I trial of a human-mouse chimeric anti-disialoganglioside monoclonal antibody ch14.18 in patients with refractory neuroblastoma and osteosarcoma. *J Clin Oncol* 16, 2169-2180, doi:10.1200/JCO.1998.16.6.2169 (1998).
- 27 Marshall, M.V., Draney, D., Sevick-Muraca, E.M. & Olive, D.M. Single-dose intravenous toxicity study of IRDye 800CW in Sprague-Dawley rats. *Mol Imaging Biol* 12, 583-594, doi:10.1007/s11307-010-0317-x (2010).
- 28 Lamberts, L.E. *et al.* Tumor-Specific Uptake of Fluorescent Bevacizumab-IRDye800CW Microdosing in Patients with Primary Breast Cancer: A Phase I Feasibility Study. *Clin Cancer Res* 23, 2730-2741, doi:10.1158/1078-0432.CCR-16-0437 (2017).
- 29 Gao, R.W. *et al.* Safety of panitumumab-IRDye800CW and cetuximab-IRDye800CW for fluorescence-guided surgical navigation in head and neck cancers. *Theranostics* 8, 2488-2495, doi:10.7150/thno.24487 (2018).
- 30 Svennerholm, L. *et al.* Gangliosides and allied glycosphingolipids in human peripheral nerve and spinal cord. *Biochim Biophys Acta* 1214, 115-123, doi:10.1016/0005-2760(94)90034-5 (1994).
- 31 Cecchetto, G. *et al.* Surgical risk factors in primary surgery for localized neuroblastoma: the LNESG1 study of the European International Society of Pediatric Oncology Neuroblastoma Group. *J Clin Oncol* 23, 8483-8489, doi:10.1200/JCO.2005.02.4661 (2005).
- 32 Fischer, J. *et al.* Complete surgical resection improves outcome in INRG high-risk patients with localized neuroblastoma older than 18 months. *BMC Cancer* 17, 520, doi:10.1186/s12885-017-3493-0 (2017).

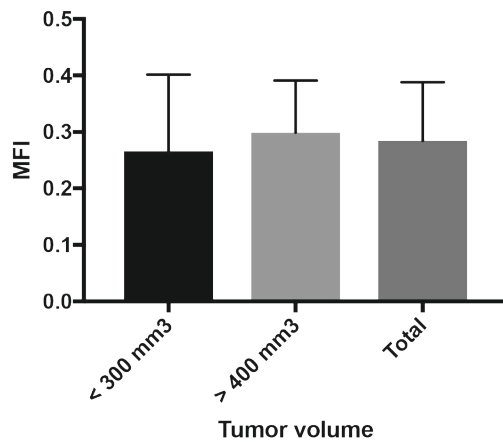
- 33 La Quaglia, M.P. *et al.* The impact of gross total resection on local control and survival in high-risk neuroblastoma. *J Pediatr Surg* 39, 412-417; discussion 412-417, doi:10.1016/j.jpedsurg.2003.11.028 (2004).
- 34 von Allmen, D. *et al.* Impact of Extent of Resection on Local Control and Survival in Patients From the COG A3973 Study With High-Risk Neuroblastoma. *J Clin Oncol* 35, 208-216, doi:10.1200/JCO.2016.67.2642 (2017).
- 35 von Schweinitz, D., Hero, B. & Berthold, F. The impact of surgical radicality on outcome in childhood neuroblastoma. *Eur J Pediatr Surg* 12, 402-409, doi:10.1055/s-2002-36952 (2002).
- 36 Rich, B.S. *et al.* Resectability and operative morbidity after chemotherapy in neuroblastoma patients with encasement of major visceral arteries. *J Pediatr Surg* 46, 103-107, doi:10.1016/j.jpedsurg.2010.09.075 (2011).
- 37 Park, J.A. & Cheung, N. V. Targets and Antibody Formats for Immunotherapy of Neuroblastoma. *J Clin Oncol*, JCO1901410, doi:10.1200/JCO.19.01410 (2020).
- 38 Mody, R. *et al.* Irinotecan-temozolomide with temsirolimus or dinutuximab in children with refractory or relapsed neuroblastoma (COG ANBL1221): an open-label, randomised, phase 2 trial. *Lancet Oncol* 18, 946-957, doi:10.1016/S1470-2045(17)30355-8 (2017).
- 39 Mody, R. *et al.* Irinotecan, Temozolomide, and Dinutuximab With GM-CSF in Children With Refractory or Relapsed Neuroblastoma: A Report From the Children's Oncology Group. *J Clin Oncol*, JCO2000203, doi:10.1200/JCO.20.00203 (2020).

SUPPLEMENTARY DATA

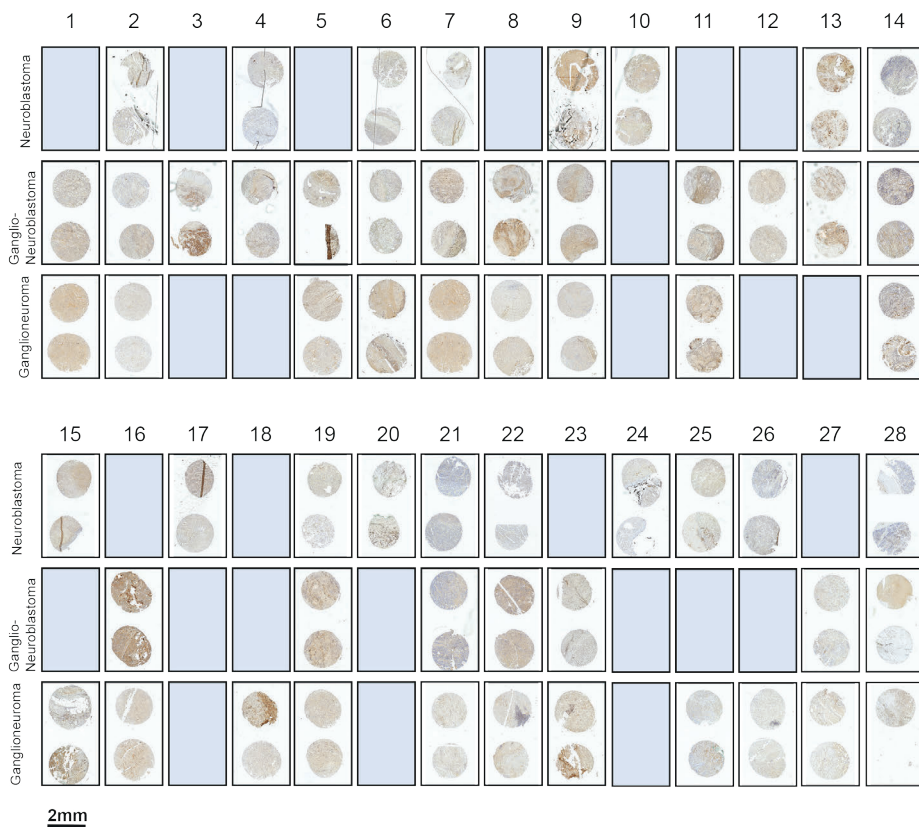
Supplementary Figure 1



Supplementary Figure 2



Supplementary Figure 3



Supplementary table 1

Subcutaneous tumors (Pearl)

mouse	tumor size (lxh)	tumor size (mm ³)	MFI tumor	MFI background	TBR
R-72	11x9	445,5	0,242	0,0584	4,14383562
R-72	6x8	144	0,304	0,0541	5,61922366
LL-73	10x9	405	0,214	0,0471	4,54352442
LL-73	8x7	196	0,115	0,0298	3,8590604
LL - 64	10x9	405	0,419	0,0526	7,96577947
LL - 64	10x11	550	0,321	0,0629	5,10333863
O	8x8	256	0,378	0,075	5,04

Supplementary table 2

Organoid line	Age at diagnosis (months)	INSS stage	Type of Tissue	Location	PA	MYCN amplified	Mutations	Culturing conditions
NB 39	24	4	Biopsy relapse	Lymph node	Poorly differentiated NB	Yes	Unknown	Organoid Medium
NB 67	29	4	Biopsy primary tumor	Adrenal gland	Poorly differentiated NB	Yes	ALK	Organoid Medium
TIC 772	36	4	Biopsy primary tumor	Adrenal gland	Poorly differentiated NB	No	No	TIC Medium

Supplementary table 3

Patient	neuroblastoma	ganglioneuroblastoma	ganglioneuroma
1	-	x	x
2	x	x	x
3	-	x	-
4	x	x	-
5	-	x	x
6	x	x	x
7	x	x	x
8	-	x	x
9	x	x	x
10	-	x	x
11	-	x	-
12	x	x	-
13	x	x	-
14	x	-	x
15	-	x	x
16	x	-	-
17	-	-	x
18	x	x	x
19	x	-	-
20	x	x	x
21	x	x	x
22	-	x	x
23	x	-	-
24	x	-	x
25	x	-	x
26	-	x	x
27	x	x	x
28	x	x	x
29	x	x	-
30	x	x	-
31	-	-	x

A microscopic image of biological tissue, possibly a cross-section of a plant stem or a similar structure, stained with blue and orange dyes. The blue staining highlights the cell walls and vascular bundles, while the orange staining highlights the cytoplasm and other cellular components. The tissue is arranged in a circular pattern, with a central pith and an outer cortex. The overall appearance is that of a complex, interconnected network of cells and fibers.

CHAPTER 5



High-resolution 3D imaging of fixed and cleared organoids

J.F. Dekkers, L.M. Wellens*, M. Alieva*,
H.C.R. Ariese, P.R. Jamieson, A.M. Vonk,
G.D. Amatngalim, H. Hu, K.C. Oost,
H.J.G. Snippert, J.M. Beekman, E.J. Wehrens,
J.E. Visvader, H. Clevers and A.C. Rios

*Shared second authorship

NATURE PROTOCOLS, JUNE 2019.

ABSTRACT

In vitro 3D organoid systems have revolutionized the modeling of organ development and diseases in a dish. Fluorescence microscopy has contributed to the characterization of the cellular composition of organoids and demonstrated organoids' phenotypic resemblance to their original tissues. Here, we provide a detailed protocol for performing high-resolution 3D imaging of entire organoids harboring fluorescence reporters and upon immunolabeling. This method is applicable to a wide range of organoids of differing origins and of various sizes and shapes. We have successfully used it on human airway, colon, kidney, liver and breast tumor organoids, as well as on mouse mammary gland organoids. It includes a simple clearing method utilizing a homemade fructose-glycerol clearing agent that captures 3D organoids in full and enables marker quantification on a cell-by-cell basis. Sample preparation has been optimized for 3D imaging by confocal, super-resolution confocal, multiphoton and light-sheet microscopy. From organoid harvest to image analysis, the protocol takes 3d.

The development of advanced culture methods has enabled the scientific research community to culture 'organs in a dish'¹. These organoid systems self-organize into 3D structures and recapitulate phenotypic and functional traits of the original biological specimens. Organoid models have become instrumental in unraveling fundamental biological questions², modeling diseases such as cancer³, and developing personalized treatment strategies⁴⁻⁷. Since the generation of the first intestinal organoid model⁸, protocols have been extended to a wide range of healthy and cancerous tissues derived from organs such as prostate⁹, brain¹⁰, liver^{11,12}, stomach¹³, breast^{14,15}, endometrium¹⁶, salivary gland¹⁷ and taste bud¹⁸.

The development of organoids has coincided with the rise of novel volume imaging methods that can characterize the architecture of whole-mount tissues in 3D¹⁹⁻²²; these represent a powerful imaging approach for probing the cellular complexity modeled with organoids²³. Compared to traditional tissue-sectioning 2D imaging, 3D imaging is superior in visualizing the complexity of biological specimens. The superior qualities of 3D imaging are essential to understanding cellular composition, cell shape, cell-fate decisions and cell-cell interactions of intact biological samples. Non-invasive optical sectioning microscopic methods such as confocal or multiphoton laser scanning microscopy and, more recently, light-sheet fluorescence microscopy (LSFM), now make it possible to visualize fine cellular details as well as overall tissue architecture within a single biological sample.

With the development of an increasing number of organoid systems and applications, 3D characterization of intact organoids at a single-cell level is highly valuable for demonstrating that they reflect their *in vivo* counterparts and for analysing mechanisms underlying cell lineage decisions and differentiation.

Here, we provide a detailed protocol for high resolution 3D imaging of entire organoids. This method is applicable to a wide range of organoids of differing origins and of various sizes, shapes and cellular content. We have recently used this method to reveal the morphology and cellular composition of newly developed organoid systems derived from various tissues, including airways²⁴, kidney²⁵, liver¹¹ and human breast cancer organoids¹⁵. Together with a multicolor fluorescent lineage-tracing strategy, this methodology has been used to reveal the bipotency of basal cells in mouse mammary organoids¹⁴. A graphical overview of the protocol is provided in Figure 1a. In short, organoids are recovered from their 3D matrix, fixed and immunolabeled, optically cleared, and then 3D rendered with visualization software after imaging. The advantages of this method include the following:

- This protocol is widely applicable to a broad range of organoids, which vary in size, origin and morphology (Figure 1b).

- This method allows imaging of entire immunolabeled organoids in 3D (Figure 1c).
- Maintenance of native fluorescence is important for imaging organoids containing fluorescent reporter genes. This method allows for imaging of cultures that express reporter fluorophores such as the confetti locus proteins (Figure 1d). Immunolabeling and fluorescent reporter visualization can be combined.
- This protocol includes a simple and non-toxic optical clearing step that allows imaging of complete (large) organoids with minimal light scattering.
- The protocol describes sample preparation for confocal, super-resolution confocal, multiphoton and light-sheet technology for faster imaging (Supplementary Video 1 and Figure 2).

Samples can be stored long term (for at least 6 months) with minimal loss of fluorescence.

COMPARISON WITH OTHER METHODS

Other sample preparation methods have been developed for 3D imaging of intact biological samples (immunolabeling and optical clearing)²⁶. However, clearing methodologies, including DISCO^{27,28}, CUBIC^{29–31} and CLARITY^{32,33}, are often laborious protocols (requiring a few weeks of sample preparation with several steps and buffers) that were developed for very large tissues or organs. By contrast, this protocol (3 d) is designed and optimized for the handling of small and fragile organoid structures. Moreover, in contrast to other clearing methods, we provide a single-step non-toxic clearing agent that is both easy to make and safe to handle on a daily basis. As compared with 2D imaging techniques, the combination of (i) overnight incubation of antibodies for proper penetration to provide uniform staining throughout the organoid, (ii) an optical clearing step, (iii) microscopy scanning in the x, y and z directions (usually with multiple tiles) to capture complete organoids and (iv) processing of large 3D datasets require investment of more time. In addition, although the procedure can be performed with commonly used laboratory reagents and equipment (a basic confocal microscope is sufficient), expensive licenses are required for optimal 3D rendering software, such as Imaris. However, free options such as Fiji can be explored.

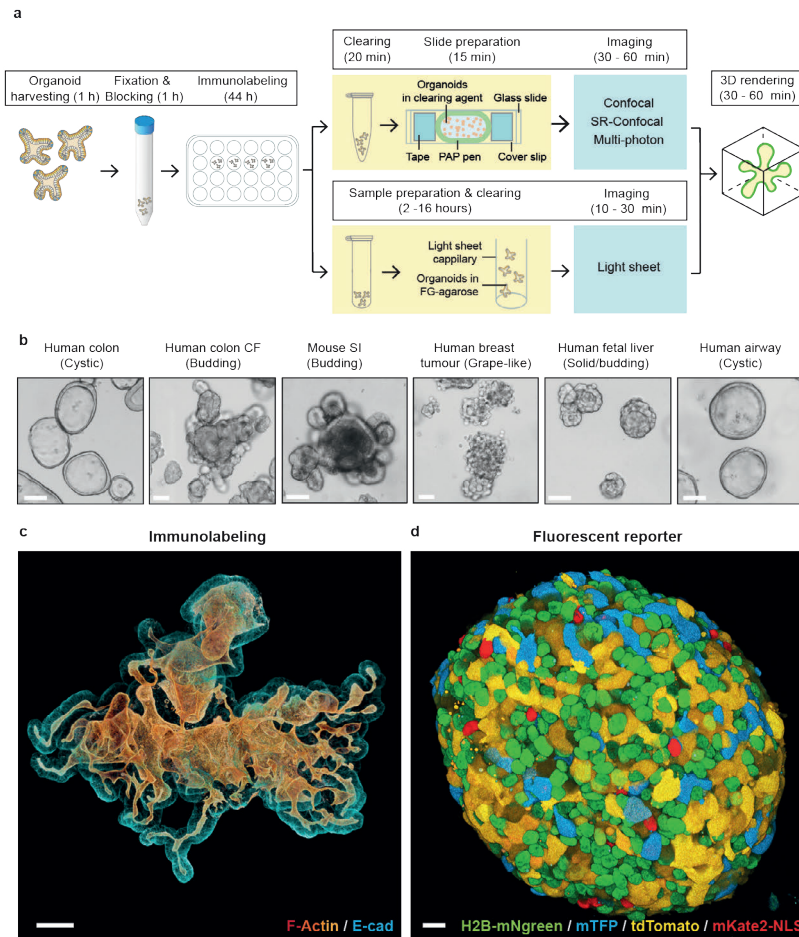


Figure 1. a) Schematic overview of the procedure. Organoids are recovered from their 3D matrix, and fixation and blocking are performed before immunolabeling with antibodies. An optical clearing step using a homemade fructose-glycerol (FG) clearing agent is performed to equalize the refractive index of the organoids and to reduce light scattering during imaging. Organoids can be imaged using single-photon confocal, super resolution (SR)-confocal, multiphoton or light-sheet microscopy. 3D rendering of images is performed using Imaris imaging software. **b)** Bright-field imaging of organoids of different origins representing the variation in organoid size and morphology between different organoid types that can be imaged in 3D using this sample preparation protocol. It includes human colon, human colon derived from a patient with cystic fibrosis (CF), mouse small intestine (SI), human breast tumor, human fetal liver and human airway organoids. Scale bars, 50 μm . **c)** Whole-mount 3D confocal image of a human colonic organoid immunolabeled for F-actin (red-yellow) and E-cadherin (E-cad; blue) (fructose-glycerol clearing; 25 \times oil objective). Scale bar, 40 μm . **d)** Whole-mount 3D confocal image of a human breast tumor organoid that expresses a confetti construct containing the fluorescent proteins H2B-mNeon green (H2B-mNgreen; green), mTFP (blue), tdTomato (yellow) and mKate2-NLS (red) (fructose-glycerol clearing; 40 \times oil objective). Scale bar, 10 μm . c and d were rendered in Imaris using the 'blend 3D' mode.

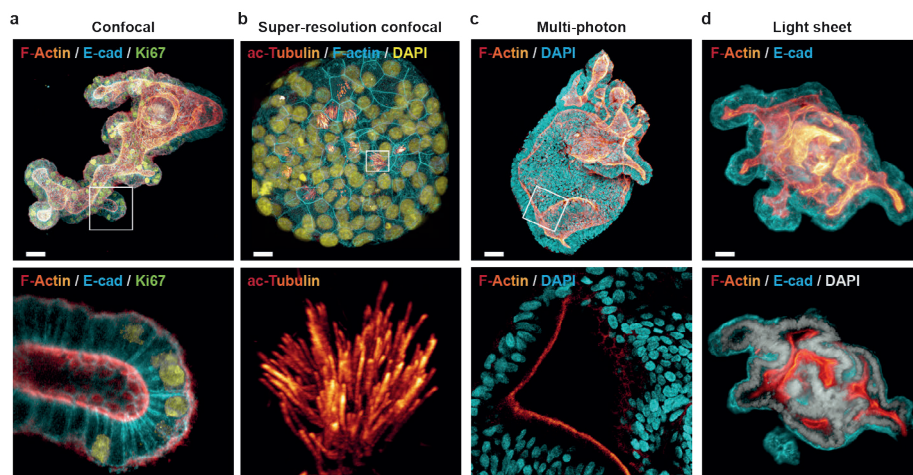


Figure 2 a) Whole-mount 3D confocal image (top) and enlarged optical section (bottom) of a human colonic organoid immunolabeled for F-actin (red-yellow), E-cadherin (E-cad; blue) and Ki67 (yellow) (fructose-glycerol clearing; 25 \times oil objective). Scale bars, 20 μ m (top) and 5 μ m (bottom). **b)** The Airyscan Fast module was used to obtain a confocal 3D whole-mount image (top) and enlarged area (bottom) of a human airway organoid immunolabeled with acetylated-tubulin (ac-Tubulin; red-yellow), F-actin (blue) and DAPI (yellow) (40 \times water objective). Scale bars, 15 μ m (top) and 2 μ m (bottom). **c)** Multiphoton 3D whole-mount image (top) and enlarged optical section (bottom) of a human colonic organoid labeled for F-actin (red-yellow) and DAPI (blue) (no clearing; 32 \times water objective). Scale bars, 50 μ m (top) and 10 μ m (bottom). **d)** Light-sheet 3D whole-mount image (top) and optical section (bottom) of a human colonic organoid immunolabeled for F-actin (red-yellow), E-cadherin (E-cad; blue) and DAPI (white) (fructose-glycerol clearing; 20 \times objective). Scale bars, 15 μ m. a-c) were rendered in Imaris using the transparent 3D mode (MIP mode), and d) was rendered in Imaris using the blend 3D mode.

EXPERIMENTAL DESIGN

Organoid harvesting (Steps 1–6)

Organoid cultures are often propagated *in vitro* by using matrices that mimic the *in vivo* extracellular environment and support their 3D structure. For most efficient antibody penetration during immunolabeling, the organoids are first extracted from Matrigel in a manner that maintains morphology. Efficient removal is influenced by the type of matrix, the number and size of organoids per drop and the time in culture after passaging and requires optimization for different culture conditions. We have determined that for the types of organoids imaged here, which were grown in basement membrane extract (BME) or Matrigel, typically a 30- to 60-min step in ice-cold recovery solution is sufficient to dissolve matrices without damaging organoids.

Fixation (Steps 7–9)

Tissue fixation is a critical step in preserving tissue architecture and protein antigenicity, as well as minimizing autofluorescence. A 45-min fixation step with 4% (wt/vol) paraformaldehyde (PFA) at 4 °C is suitable for immunostaining a wide range of organoids (various sizes, shapes and origins). In general, longer fixation times (up to 4 h) are better suited to preserving fluorescence of reporters expressed in organoids, such as the confetti reporter proteins (H2B-mNeongreen, mTFP, tdTomato and mKate2-NLS, which were adapted from Snippert et al.³⁴; **figure 1d**). For cystic organoids, we sometimes observe collapsing structures during fixation. For these particular cases, alternative fixative methods, including formalin or PFA-glutaraldehyde (2% (vol/vol)) can be used; these help preserve fragile tissue architecture. However, these two methodologies can impair fluorescent reporter detection and increase background autofluorescence.

Immunolabeling (Steps 12–23)

Organoids may consist of a polarized epithelial monolayer, in which the apical membrane lines a central lumen, or may present as more solid multilayered epithelial structures, which is the case for most tumor-originated cultures (**figure 1b**). Organoids can reach large sizes, and appropriate antibody incubation times are important for proper penetration. It is important to wash the samples extensively to avoid background or loss of signal.

Clearing (Step 24)

High scattering of thick tissues can be a hurdle for the optical imaging of 3D structures because of the mismatching of refractive indices between different cellular components. Over the past few years, there have been significant advances in overcoming this scattering through tissue-clearing techniques (e.g., the DISCO^{27,28}, CUBIC^{29–31} and CLARITY^{32,33} protocols). However, these clearing methodologies may be too harsh for fragile tissues such as organoids. We provide a simple, non-toxic optical clearing step that facilitates imaging of complete organoids, thereby limiting the decline in fluorescence in the z direction (**figure 3a**). It is applicable to either immunolabeled organoids (**figure 1c**) or fluorescent reporter detection (**figure 1d**) and is suitable for most light microscopy technologies (**figure 2**). By comparing different clearing reagents, we observed that both commercially available FocusClear and our homemade fructose-glycerol clearing agent were able to efficiently clear the tissue and thus limit the decrease in fluorescence intensity in the z direction (**figure 3b**). However, immersion of organoids in FocusClear led to an overall fluorescence quenching and loss of signal intensity (**figure 3c**).

Optical clearing is important to obtaining a cellular resolution suitable for performing automated cellular segmentation and quantification algorithms. Importantly, immunolabeled organoids can be stored long term (up to 6 months) in the fructose–glycerol-based clearing solution at -20°C . In addition, the clearing step is reversible, and new antibodies can be added to initial stainings with no loss of resolution or brightness.

However, once mounted, slides can be stored at 4°C for at least 1 week and at -20°C for at least 6 months following fructose–glycerol-based clearing. For light-sheet imaging, a modified clearing solution containing low-melting-point (LMP) agarose is used to hold the sample.

Slide preparation and Storage (step 24)

In contrast to imaging monolayers of adherent cells, mounting of 3D organoids requires a refined method for slide preparation. We use double-sided sticky tape to lift the coverslip, thereby maintaining 3D organoid morphology (and fixing the coverslip to the slide). The viscous clearing agent we use in our protocol is optimal for keeping organoids in place during slide preparation and while imaging. It is advised that organoids be imaged directly after mounting for optimal detection. However, once mounted, slides can be stored at 4°C for at least 1 week and at -20°C for at least 6 months following fructose–glycerol-based clearing. For light-sheet imaging, a modified clearing solution containing low-melting-point (LMP) agarose is used to hold the sample.

Microscopy (Step 25)

Imaging and visualization modalities applicable to complex structures include single-photon confocal, multiphoton and LSM. Each system has specific features and applications based on compromises between the imaging speed, resolution and convenience of use. Confocal (single-photon) microscopy provides high-quality imaging with high single-cell resolution but with an accompanying rapid decrease in intensity with increasing depth, whereas multiphoton microscopy enables deep imaging into tissues. Optical clearing is not advised for cystic organoids containing large lumens (see ‘Troubleshooting’ section for Step 24A(iii)). For these types of organoids, we advise multiphoton imaging without clearing. To support this, we show that multiphoton imaging is superior to singlephoton imaging of organoids that were not optically cleared (**figure 3d–f**). Furthermore, multiphoton excitation provides higher 3D resolution of large organoids, as fluorophores are excited in only one focal plane (**figure 3d**). To illustrate this, we performed nuclear segmentation of the same organoid imaged using single-photon and multiphoton microscopy (**figure 3d**). Although the two imaging methods gave similar nuclear resolution on the surface of the organoid, multiphoton microscopy performed better at deeper

layers (**figure 3d-f**). As both techniques use point-by-point scanning along the entire sample, imaging is relatively time consuming and may lead to bleaching of fluorophores (photobleaching)³⁵. Yet we rarely observed loss of intensity due to photobleaching. By contrast, LSM provides fast optical sectioning with minimal photobleaching of large tissue samples. However, it requires the imaging specimen to be completely cleared, and obstacles such as air bubbles can cause shadows along the illumination path³⁶. In addition, the resolution obtained with light-sheet imaging remains suboptimal, as compared with confocal and multiphoton microscopy, for obtaining subcellular resolution (**figure 2d**).

MATERIALS

Biological materials

- Organoids of human or murine origin. We have successfully used mouse small intestinal organoids, human colonic organoids, human breast tumor organoids, human fetal liver organoids, human airway organoids and murine mammary gland organoids. Mammary gland organoids can be derived from 6- to 10-week-old wild-type FVB/N female mice (obtained from the Walter and Eliza Hall Institute (WEHI) Animal Facility). ! CAUTION Use of animals or human material for research purposes requires approval from institutional and national regulatory bodies. Do not proceed without appropriate approval and, for materials derived from human tissues, informed consent from all subjects. All our animal experiments conformed to regulatory standards and were approved by the Walter and Eliza Hall Institute (WEHI) Animal Ethics Committee. All human organoid samples were obtained from biobanks through Hubrecht Organoid Technology (HUB, www.hub4organoids.nl). Authorizations were obtained from the medical ethical committee of UMC Utrecht (METC UMCU) at the request of HUB in order to ensure compliance with the Dutch Medical Research Involving Human Subjects Act, and informed consent was obtained from donors when appropriate.

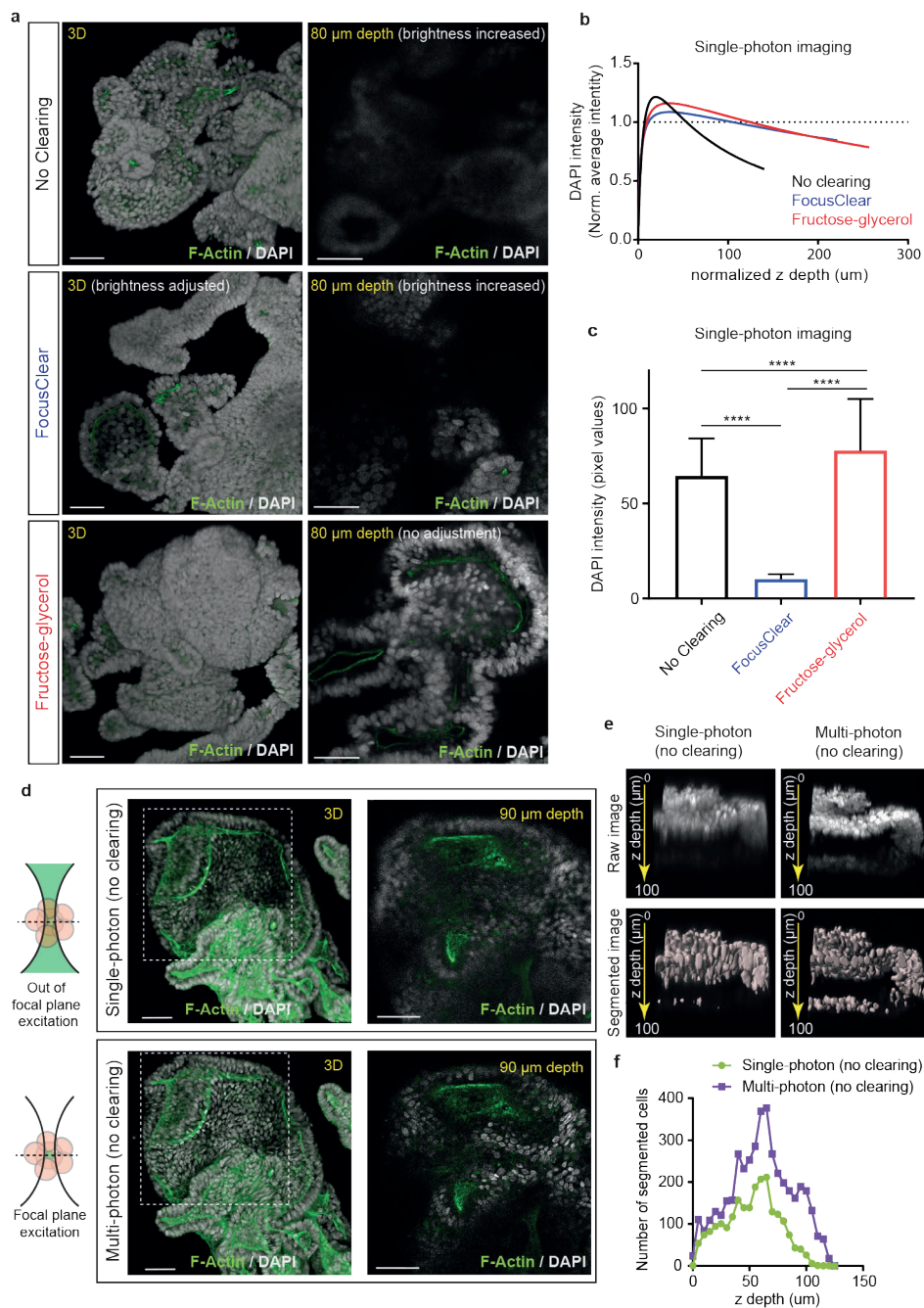


Figure 3 a-e) Human colonic organoids were stained with F-actin (green) and DAPI (gray) and imaged with single-photon (**a-c**) or both single-photon and multiphoton (**d,e**) microscopy. **a)** Representative images of human colonic organoids imaged without clearing, or cleared with FocusClear or fructose-glycerol (25 \times water objective). (Left) 3D reconstruction of the organoid. (Right) cross-section of the organoid at an 80- μ m depth. Note that, for the 'No clearing' and 'FocusClear' conditions, the brightness of the image was increased as compared to that of the 'Fructose-glycerol' condition to visualize the organoid. Scale bars, 50 μ m. **b)** Non-linear regression fit analyzed in GraphPad Prism 6 between DAPI intensity and z depth for different clearing methods. For each imaged organoid, the DAPI intensity was normalized to the average intensity of all the organoids. Values represent intensities of individual cells detected by DAPI segmentation and analyzed by the v.8.2.1 Imaris software. **c)** Bar graph plotted in GraphPad Prism 6 showing average DAPI intensity with different clearing methods. Data depicted as mean \pm s.d. Values are intensities of >4,000 individual cells detected by DAPI segmentation. ****P < 0.0001, Kruskal-Wallis test with two-sided Dunn's multiple comparison post hoc testing. **d)** Representative images of the same colonic organoid imaged with single-photon (top) or multiphoton (bottom) microscopy (no clearing; 20 \times dry objective). (Left) 3D reconstruction of the organoid. (Right) Cross-section of the organoid at a 90- μ m depth; images correspond to the dashed boxes in the images on the left. Scale bars, 50 μ m. **e)** Representative raw images (top) and DAPI-segmented images (bottom) of the same cystic fibrosis organoid imaged with single-photon or multiphoton microscopy. Loss of resolution in z is delimited by the decrease in the number of cells that can be detected. Image segmentation was achieved using local contrast of the nuclear staining intensity with the Imaris software. Touching objects were split on the basis of a minimal distance of 4 μ m. Finally, surfaces with a voxel size >10 were selected. **f)** Histogram plotted in GraphPad Prism 6 showing the number of segmented cells per z cross-section of the same organoid imaged with single-photon or multiphoton microscopy. Images in **a** and **d** were rendered in Imaris using the transparent 3D mode (MIP mode).

REAGENTS

- Paraformaldehyde (PFA) powder (Sigma-Aldrich, cat. no. P6148-500g) ! CAUTION PFA is hazardous. Manipulate in a fume hood. Avoid direct contact with skin. Wear rubber gloves and protective eye goggles.
- Sodium hydroxide (NaOH) pellets (10 M stock solution; Merck Millipore, cat. no. 567530)
- ! CAUTION NaOH is corrosive. Wear rubber gloves and protective eye goggles.
- Hydrochloric acid (HCl; 10 M stock solution; Ajax FineChem, cat. no. 256.2.5L-PL)! CAUTION HCl is corrosive. Manipulate in a fume hood. Wear rubber gloves and protective eye goggles.
- BSA (Sigma-Aldrich, cat. no. A3059)
- Tween 20 (Sigma-Aldrich, cat. no. P7949)
- Triton X100 (Sigma-Aldrich, cat. no. T8532)! CAUTION Triton X100 is hazardous. Avoid contact with skin and eyes.
- PBS (Dulbecco's phosphate-buffered saline, 1Å~; Gibco, cat. no. 14190144)
- Fructose (Sigma-Aldrich, cat. no. F0127)
- Glycerol (Ajax FineChem, cat. no. 242-500ml)
- Cell recovery solution (Corning, cat. no. 354253)
- FocusClear (CelExplorer, cat. no. FC-101)
- UltraPure low-melting-point (LMP) Agarose (Thermo Fisher, cat. no. 16520050)
- Primary antibodies, user specific (see Table 1 for details of antibodies that we used successfully in human and mouse organoid tissues)
- Secondary antibodies: unconjugated primary antibodies are labeled with species-specific secondary antibodies containing the desired fluorophore (e.g., Donkey Anti-Mouse IgG (H+L) Highly Cross-Adsorbed Alexa Fluor 488, Life Technologies, cat. no. A-21202)
- DAPI (stock solution, 1 mg/ml, 1:500 dilution; Thermo Fisher, cat. no. D9542)
- Alexa Fluor 647 phalloidin (1:100 dilution, for staining F-actin; Thermo Fisher, cat. no. A22287)
- SDS (sodium dodecyl sulfate; Sigma-Aldrich, cat. no. L6026)

EQUIPMENT

Organoid harvesting

Conical tubes (15 ml; Greiner BioOne, cat. no. 5618-8271)

Immunostaining

- Conical tubes (15 ml; Greiner BioOne, cat. no. 5618-8271)
- 2-ml Safe-lock centrifuge tubes (Eppendorf, cat. no. EPO030 120.094)
- Suspension cell culture plates (24-well; Greiner Bio-One, cat. no. 662102)

- Horizontal shaker (VWR, cat. no. 444-2900)
- Magnetic stirrer (IKA, cat. no. 0005019700)

Slide preparation for confocal and multiphoton microscopy

- 1.5-ml Safe-lock centrifuge tubes (Eppendorf, cat. no. EP0030 120.094)
- Dissection stereomicroscope (Leica, model no. M205 FA)
- Cover glass, no. 1.5 (24 x 60 mm; VWR, cat. no. 630-2108)
- Cover glass, no. 1.5 (48 x 60 mm; ProSciTech, cat. no. G425-4860)
- Microscope slides (Superfrost, ground edge, 90°, 26 x 76 mm; Menzel Gläser; Thermo Fisher, cat. no. AA00008032E00MNT10)
- Ace O-rings (fluoroelastomer with tetrafluoroethylene additives (FETFE), 23.5 mm, wall size 1.78 mm; Sigma-Aldrich, cat. no. Z504785)
- Graduated transfer pipettes (small bulb; Samco, cat. no. 222-15)
- Double-sided sticky tape (12.7 mm x 6.35 m; Scotch 3M)
- PAP pen (DAKO, cat. no. S2002) c CRITICAL Pens from different brands vary in their capacity to prevent the fructose-glycerol clearing agent from spreading out over the coverslip. Sample preparation for light-sheet microscopy
- Capillary (size ~1.5 mm; Carl Zeiss Microscopy, cat. no. 701908) with associated plunger (Carl Zeiss Microscopy, cat. no. 701998) Microscopy platforms and objectives
- Confocal microscopes (Zeiss, model no. LSM 880 (25x, numerical aperture (NA) 0.8, multi immersion; 32Å~ NA 0.85, water immersion; and 40x NA 1.3, oil immersion; working distance: 570 μm, 1.1 mm and 210 μm, respectively)
- Multiphoton microscope (Zeiss, model no. LSM 880 (32x, NA 0.85, water immersion, working distance: 1,100 μm)
- Light-sheet microscope: Zeiss Light Sheet . (illumination objective: 10x, NA 0.2; detection objective: 20Å~, clearing immersion, NA 1.0, $n = 1.45 \pm 0.03$, working distance: 5.6 mm)
- Image processing
- Dell Precision workstation (64-bit, Windows 8, 512 GB RAM, AMD Radeon R9 200 series graphics card)

Software

- Imaris v.8.2.1 for 3D and 3D stereo visualization and segmentation of confocal and multiphoton data (Bitplane, <http://www.bitplane.com/imaris>)
- Arivis tiling and 3D reconstruction software for light-sheet datasets (Vision 4D, <https://www.arivis.com/>)
- ZEN Black software (the link for downloading the software is available upon request through the Zeiss website (<https://www.zeiss.com/microscopy/int/products/microscope-software/zen.html>))
- GraphPad Prism 6 (<https://www.graphpad.com/scientific-software/prism/>)

REAGENT SETUP

PFA (4% (wt/vol))

To prepare 4% (wt/vol) PFA, heat 500 ml of PBS to 60 °C in a microwave. Add 20 g of PFA and dissolve on a stirrer. Add a few drops of 10 M NaOH. Cool on ice and adjust the pH to 7.4 by adding a few drops of 10 M HCl (store at -20 °C for up to 2 months).

PBT (0.1% (vol/vol))

To prepare 0.1% (vol/vol) PBS-Tween (PBT), add 1 ml of Tween 20 to 1,000 ml of PBS (store at 4 °C for up to 4 weeks).

ORGANOID WASHING BUFFER

To prepare organoid washing buffer (OWB), add 1 ml of Triton X-100 and 2 g of BSA to 1 liter of PBS (store at 4 °C for up to 2 weeks).

FRUCTOSE-GLYCEROL CLEARING SOLUTION

Fructose-glycerol clearing solution is 60% (vol/vol) glycerol and 2.5 M fructose. To prepare 660 ml of this solution, mix 330 ml of glycerol, 70 ml of dH₂O and 297.2 g of fructose on a magnetic stirrer. Refractive index = 1.4688 at room temperature (RT: 19-23 °C). Store at 4 °C in dark for up to 1 month.

PBS-BSA (1% (WT/VOL))

To prepare 1% (wt/vol) PBS-BSA, dissolve 1 g of BSA in 100 ml of PBS (store at 4 °C for up to 2 weeks)

LIGHT-SHEET EMBEDDING SOLUTION

To prepare light-sheet embedding solution, dissolve 0.4 g of LMP agarose in 10 ml of water using a microwave and let it cool to 40 °C on a heat block with a magnetic stirrer. Add 10 ml of fructose-glycerol clearing solution (40 °C) and mix on a heat block with a magnetic stirrer until the solution is clear; keep at 40 °C until use. **!CRITICAL!** Prepare the solution fresh every time.

PROCEDURE

Organoid recovery from 3D matrix

Timing 1-1.5 h

This section describes recovery of organoid cultures grown in drops of BME or Matrigel from a 24-well plate. We recommend using organoids with a size ranging from 100 to 500 μm and to use one confluent culture well per staining. Depending on the organoid size and origin, the well should ideally contain 50–200 organoids for confocal or multiphoton imaging and 100–200 organoids for light-sheet imaging

1. Remove the culture medium from the wells and wash with 1 ml of PBS without disrupting the 3D matrix.
2. Put the plate on ice, add 1 ml of ice-cold cell recovery solution to each well and incubate on a horizontal shaker at 4 °C (60 r.p.m.) for 30–60 min. After incubation, the 3D drops should be dissolved.
3. Precoat the inside and outside of a 1-ml tip with protein by dipping the full length of the tip in 1% (wt/vol) PBS-BSA and resuspending 1 ml of 1% (wt/vol) PBS-BSA two times. This will prevent the organoids from sticking to the tip. After coating the tip, gently resuspend the contents of the well five to ten times.
4. Transfer the organoids to a 15-ml tube pre-coated with 1% (wt/vol) PBS-BSA. Pool organoids from different wells but with the same identity in the same tube.
5. Rinse out the culture well with 1 ml of ice-cold 1% (wt/vol) PBS-BSA to collect all organoids.
6. Fill up to 10 ml with cold PBS and spin down at 70g for 3 min at 4 °C. Remove the supernatant. The pellet should be tight without a visible layer of 3D matrix.

CRITICAL STEP

Organoid recovery from the 3D matrix is essential for optimal immunolabeling. Remaining 3D matrix can hamper proper antibody penetration of the organoid structure or lead to high background staining due to a specific binding of antibodies to the matrices.

FIXATION AND BLOCKING

Timing 1 h

7. Gently resuspend the pellet of organoids in 1 ml of PFA, using a 1-ml tip pre-coated with 1% (wt/vol) PBS-BSA as described in Step 3.
8. Incubate at 4 °C for 45 min (halfway through the incubation period, gently resuspend the organoids, using a 1-ml tip pre-coated with 1% (wt/vol) PBS-BSA). During fixation, a minimal change in morphology is observed for most mono- or multilayered organoids. However, fixation can cause spherical, monolayered organoids that contain large fluid-filled lumens to ‘collapse’. This has been

observed for human intestinal samples and may depend on the donor and the quality of the culture medium.

9. Fill the tube up to 10 ml with cold (4 °C) PBT, gently mix by swirling the tube, incubate for 10 min at 4 °C and spin down at 70g for 5 min at 4 °C. From this step onward, precoating of tips is not needed.

PAUSE POINT

Organoids can be stored in PBT at 4 °C for 2 d or over the weekend, but, ideally, one should continue with the next steps as soon as possible

10. For blocking the organoids, resuspend the pellet in cold (4 °C) OWB and transfer the appropriate amount of organoids per staining to a low-adherence/ suspension 24-well plate (use at least 200 µl per well).

CRITICAL STEP

Compared to blocking and immunolabeling in tubes or Eppendorf tubes, the 24-well format allows gentle movement of organoids for optimal antibody penetration and washings, and allows organoid visualization at any moment during the procedure using microscopy.

11. Incubate at 4 °C for 15 min.

IMMUNOLABELING

Timing 44 h

12. Add 200 µl of OWB to one of the empty wells and use this as a reference well.
13. Make sure that the organoids are settled at the bottom of each well; then tilt the plate to 45° and remove the OWB, leaving the organoids in 200 µl of OWB (use the reference well to estimate 200 µl).
14. Add 200 µl of OWB with primary antibodies (2× concentration) to each well and incubate overnight at 4 °C with mild rocking/shaking (60 r.p.m. on a horizontal shaker).
15. Add 1 ml of OWB per well.
16. Wait for 3 min until all organoids are settled at the bottom of each well.
17. Remove 1 ml of OWB, leaving 200 µl in each well.
18. Add 1 ml of OWB per well and incubate for 2 h with mild rocking/shaking.
19. Repeat Steps 16–18 two more times.

20. Wait for 3 min, until all organoids are settled at the bottom of each well.
21. Remove 1 ml of OWB, leaving 200 μ l in each well.
22. Add 200 μ l of OWB with secondary antibodies (2 \times concentration) per well and incubate overnight at 4 $^{\circ}$ C with mild rocking/shaking.
23. Repeat Steps 15–19. Transfer the organoids of each well to a 1.5-ml (confocal or multiphoton imaging) or 2-ml (light-sheet imaging) Eppendorf tube and let the organoids settle at the bottom or spin down (70g, 4 $^{\circ}$ C, 2 min).

CRITICAL STEP

Reagent changes and organoid transfers can cause sample loss during fixation and immunolabeling. A loss of \approx 10–20% of the initial number of organoids in the culture well (Step 1) is expected. We advise reading ‘Troubleshooting’ section for Steps 1, 10 and 20 to ensure a minimal loss of sample.

PAUSE POINT

At any point between Steps 12 and 23, the organoids can be stored in OWB (with or without antibodies) at 4 $^{\circ}$ C for 2 d or over the weekend without rocking, but, ideally, one should continue with the next steps as soon as possible.

SAMPLE PREPARATION FOR IMAGING

24. Continue with confocal or multiphoton sample preparation (option A) or with light-sheet sample preparation (option B).

(A) SAMPLE PREPARATION FOR SINGLE-PHOTON CONFOCAL OR MULTIPHOTON IMAGING

Timing 35 min

- (i) *Clearing.* Remove as much of the OWB as possible without touching the organoids.
- (ii) Add fructose–glycerol clearing solution (minimum of 50 μ l at RT) using a 200- μ l tip with the end cut off and resuspend gently. Prevent bubble formation.

The fructose–glycerol clearing solution has high viscosity. It is therefore difficult to handle small volumes. Make sure to use the fructose–glycerol clearing solution at RT and pipette slowly and carefully.

- (iii) Incubate at RT for 20 min. Clearing causes organoid shrinkage. This does not change the general morphology of most mono- and multilayered organoids, but it can alter the spherical shape of mono-layered organoids with large lumens.

PAUSE POINT

At this stage, the sample can be stored at 4 °C (for at least 1 week) or -20 °C (for at least 6 months).

- (iv) *Slide preparation for imaging.* Draw a 1 × 2-cm rectangle in the middle of a slide, using a PAP pen.
- (v) Place a 1-cm-long piece of sticky tape at both sides of the rectangle. Use 1, 2 or 3 layers, depending on the organoid size.
- (vi) Cut off the end of a 200- μ l tip and use it to place the organoids in the middle of the rectangle. Use 20 μ l per layer of tape.
- (vii) Place a coverslip on top. Place the left side of the coverslip on the left stack of sticky tape and then slowly lower the right side of the coverslip until it touches the right stack of sticky tape; then let go of the coverslip.
- (viii) Wait for 1 min to allow the fluid to spread out.
- (ix) Gently apply pressure to both sides of the coverslip to firmly attach it to the double-sided sticky tape. The slide is now ready for imaging.

PAUSE POINT

At this stage, the sample can be stored at 4 °C (for at least 1 week) or -20 °C (for at least 6 months).

(B) SAMPLE PREPARATION FOR LIGHT-SHEET MICROSCOPY

Timing 2–16 h

- (i) Remove most of the OWB and place the Eppendorf tube on a heat block at 40 °C.
- (ii) Before the pellet dries out, resuspend the pellet in 300 μ l of light-sheet embedding solution and put back at 40 °C.
- (iii) While the Eppendorf tube is at 40 °C, use a light-sheet glass capillary to aspirate the mix and let it solidify at 4 °C.
- (iv) Place the capillary containing the sample in the light-sheet chamber and fill the chamber with fructose-glycerol clearing solution.
- (v) Push down the agarose-based clearing solution (light-sheet embedding solution) of the capillary to expose the sample for imaging.

CRITICAL STEP

The quality of light-sheet images is severely affected by the presence of air bubbles or other small objects in the light path, so work cleanly and prevent bubble formation. In addition, allow the sample to settle in the imaging chamber for a couple of hours to overnight at RT before imaging.

25. Proceed with single-photon or multiphoton (option A) or light-sheet (option B) imaging.

(A) SINGLE-PHOTON AND MULTIPHOTON IMAGING

Timing 1–2 h

- (i) Use a confocal microscope to image the slide, using a multi-immersion 25× or oil immersion 40× objective for single-photon imaging or a 32× water immersion objective for multiphoton imaging. The acquisition mode settings we use most commonly are as follows: scan mode = frame, frame size = 1,024 × 1,024, line step = 2, bidirectional scanning, speed = 7, averaging number = 1, bit depth = 12 and bidirectional scanning. Activate the z-stack mode and define the lower and upper limits. For imaging large organoids or multiple organoids together, activate the tile scan and indicate the borders of the organoids. Of note, other confocal microscopes can be used for similar results (we have tested the protocol with the Leica SP8 and Olympus FV 3000). For tile scan acquisition, stitch the imaging using the ZEN Black software (Imaris, Fiji or ImageJ software can also be used).
- (ii) For tile scan acquisition, stitch the imaging using the ZEN Black software (Imaris, Fiji or ImageJ software can also be used).
- (iii) Use the 3D view tab in the Imaris imaging software to optimize brightness, contrast and 3D-rendering properties for the best representation of the imaging. After corrections, the RGB images can be exported as TIFF files.

(B) LIGHT-SHEET IMAGING

Timing 40–90 min

- (i) Use a light-sheet microscope to image the samples in the light-sheet embedding solution, using a 20× detection objective (clearing immersion NA = 1.0). The acquisition mode settings we most commonly use are as follows: scan mode = frame, frame size = 1,024 × 1,024, averaging number = 1, bit depth = 8.

Activate the z-stack mode (define lower and upper limits) and multi-view mode ($\times 4$). Set the light-sheet thickness to $\sim 6 \mu\text{m}$ and use dual illumination.

- (ii) Use the 3D view tab in the Arivis imaging software to optimize brightness, contrast and 3D-rendering properties for the best representation of the imaging. After corrections, the RGB images can be exported as TIFF files (>300 d.p.i. is recommended).

TIMING

- Steps 1–6, organoid recovery from 3D matrix: 1–1.5 h
- Steps 7–11, fixation and blocking: 1 h
- Steps 12–23, immunolabeling: 44 h
- Step 24A(i–iii), sample preparation, clearing: 20 min
- Step 24A(iv–ix), slide preparation for imaging: 15 min
- Step 24B, sample preparation for light-sheet microscopy: 2–16 h
- Step 25A, imaging and image processing for single-photon and multiphoton imaging: 1–2 h
- Step 25B, imaging and image processing for light-sheet imaging: 40–90 min

ANTICIPATED RESULTS

Imaging organoids in 3D opens new opportunities to visualize morphology, cell type composition and intracellular processes in detail in their 3D culture environment. This technique is simple and probably applicable to most organoid systems derived from different host species or organs.

The power of 3D imaging, as compared to 2D imaging, is demonstrated by images of a mouse mammary gland organoid generated using recently published methods¹⁴. These organoids contain a central layer of columnar-shaped K8+/K18+ luminal cells and an outer layer of elongated K5+ basal cells (**figure 4a**), which is similar to their morphology *in vivo*²². It is difficult to appreciate this morphology on a 2D section of the same organoid (**figure 4a**, middle panel). Another example using human liver organoid culture methods¹¹ shows that 3D imaging is superior to 2D imaging for viewing the network of MRP2+ canaliculi that facilitate the collection of bile fluid (**figure 4b**). These methods thus allow visualization of essential structural features of organoid specimens.

In addition to visualization of whole-mount organoids at cellular resolution, we combined organoid 3D imaging with the Airyscan Fast imaging module of the Zeiss LSM 880 confocal microscope to enable high-resolution imaging (120 nm of lateral and 350 nm of axial resolution, as compared with 250 and 800 nm for conventional

confocal microscopy). For example, in a human airway organoid, the different stages of development of acetylated-tubulin+ cilia can be seen at high resolution (**figure 2b**). This opens possibilities for studying intracellular processes, such as cytoskeleton remodeling or vesicle transport, in different types of organoids.

With the optical clearing step described above, organoids can be imaged with enhanced fluorescence intensity and increasing z-depth penetration as compared with those of a commercially available reagent, FocusClear, and uncleared sample (**figure 3a-c**). The resolution obtained allows cellular segmentation algorithms to quantify the number of cells and presence of different cell markers in different cellular subtypes in whole organoids. We present an example of an organoid containing 140 cells, in which 3 cells are highly positive for the Ki67 cell cycle marker (**figure 4c**).

In summary, the 3D imaging technique we describe here is simple, is reproducible and can provide volumetric data for immunolabeled organoids, as well as for organoids expressing fluorescent reporters, within 3d. The protocol has been successfully applied to a broad range of organoids, including those of mouse or human origin, as well as healthy versus disease models. The sample preparation is versatile, and the samples can be imaged using confocal, multiphoton and light-sheet fluorescent microscopes to obtain cellular to subcellular resolution of intact organoids.

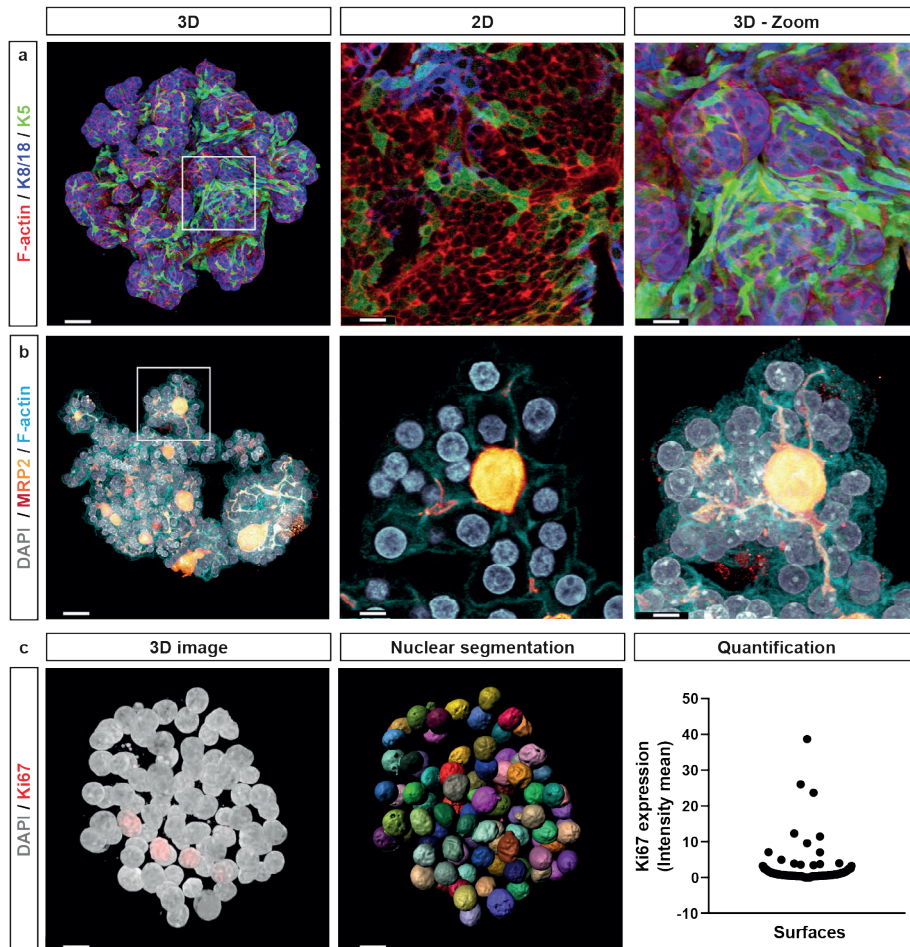


Figure 4 a,b) Confocal images representing whole-mount 3D images (left), 2D optical sections (middle) and 3D areas of an enlarged section (right) of an organoid derived from a single basal cell of the mouse mammary gland **(a)** labeled for K8/18 (blue), K5 (green) and F-actin (red) (fructose-glycerol clearing; 25 \times oil objective) or a human fetal liver organoid **(b)** labeled for DAPI (gray), MRP2 (yellow-red) and F-actin (blue) (fructose-glycerol clearing; 40 \times oil objective). The images illustrate the advantage of 3D imaging as compared with 2D sectioning to appreciate the morphology of elongated mammary basal cells that surround luminal cells **(a, white square)** or the network of MRP2-positive canaliculi **(b, white square)**. Scale bars, 55 μm (**a, left**), 40 μm (**a, middle and right**), 25 μm (**b, left**), and 8 μm (**b, middle and right**). **c)** Confocal 3D whole-mount image of a human fetal liver organoid labeled with DAPI and Ki67 (left) and a segmented image on the DAPI channel generated using Imaris (middle). Scale bars, 15 μm . (Right) Graph plotted in GraphPad Prism 6 representing the Ki67 mean intensity in all the cells (DAPI-segmented) of the entire organoid (140 cells).

REFERENCES

1. Sato, T. & Clevers, H. SnapShot: growing organoids from stem cells. *Cell* 161, 1700–1700.e1 (2015).
2. Clevers, H. Modeling development and disease with organoids. *Cell* 165, 1586–1597 (2016).
3. Drost, J. & Clevers, H. Organoids in cancer research. *Nat. Rev. Cancer* 18, 407–418 (2018).
4. Bartfeld, S. & Clevers, H. Stem cell-derived organoids and their application for medical research and patient treatment. *J. Mol. Med.* 95, 729–738 (2017).
5. Broutier, L. et al. Human primary liver cancer-derived organoid cultures for disease modeling and drug screening. *Nat. Med.* 23, 1424–1435 (2017).
6. Dekkers, J.F. et al. Characterizing responses to CFTR-modulating drugs using rectal organoids derived from subjects with cystic fibrosis. *Sci. Transl. Med.* 8, 344ra384 (2016).
7. Dekkers, J.F. et al. A functional CFTR assay using primary cystic fibrosis intestinal organoids. *Nat. Med.* 19, 939–945 (2013).
8. Sato, T. et al. Single Lgr5 stem cells build crypt-villus structures in vitro without a mesenchymal niche. *Nature* 459, 262–265 (2009).
9. Karthaus, W.R. et al. Identification of multipotent luminal progenitor cells in human prostate organoid cultures. *Cell* 159, 163–175 (2014).
10. Lancaster, M.A. et al. Cerebral organoids model human brain development and microcephaly. *Nature* 501, 373–379 (2013).
11. Hu, H. et al. Long-term expansion of functional mouse and human hepatocytes as 3D organoids. *Cell* 175, 1591–1606.e19 (2018).
12. Huch, M. et al. Long-term culture of genome-stable bipotent stem cells from adult human liver. *Cell* 160, 299–312 (2015).
13. Nanki, K. et al. Divergent routes toward Wnt and R-spondin niche independency during human gastric carcinogenesis. *Cell* 174, 856–869.e17 (2018).
14. Jamieson, P.R. et al. Derivation of a robust mouse mammary organoid system for studying tissue dynamics. *Development* 144, 1065–1071 (2017).
15. Sachs, N. et al. A living biobank of breast cancer organoids captures disease heterogeneity. *Cell* 172, 373–386. e10 (2018).
16. Turco, M.Y. et al. Long-term, hormone-responsive organoid cultures of human endometrium in a chemically defined medium. *Nat. Cell Biol.* 19, 568–577 (2017).
17. Maimets, M. et al. Long-term in vitro expansion of salivary gland stem cells driven by Wnt signals. *Stem Cell Rep.* 6, 150–162 (2016).
18. Ren, W. et al. Single Lgr5- or Lgr6-expressing taste stem/progenitor cells generate taste bud cells ex vivo. *Proc. Natl. Acad. Sci. USA* 111, 16401–16406 (2014).
19. Richardson, D.S. & Lichtman, J.W. Clarifying tissue clearing. *Cell* 162, 246–257 (2015).
20. Richardson, D.S. & Lichtman, J.W. SnapShot: tissue clearing. *Cell* 171, 496–496.e1 (2017).
21. Rios, A.C. et al. Essential role for a novel population of binucleated mammary epithelial cells in lactation. *Nat. Commun.* 7, 11400 (2016).
22. Rios, A.C., Fu, N.Y., Lindeman, G.J. & Visvader, J.E. In situ identification of bipotent stem cells in the mammary gland. *Nature* 506, 322–327 (2014).

23. Rios, A.C. & Clevers, H. Imaging organoids: a bright future ahead. *Nat. Methods* 15, 24–26 (2018).
24. Sachs, N. et al. Long-term expanding human airway organoids for disease modeling. *EMBO J.* 38, e100300 (2019).
25. Schutgens, F. et al. Tubuloids derived from human adult kidney and urine for personalized disease modelling. *Nat. Biotechnol.* 37, 303–313 (2019).
26. Eisenstein, M. Transparent tissues bring cells into focus for microscopy. *Nature* 564, 147–149 (2018).
27. Erturk, A. et al. Three-dimensional imaging of solvent-cleared organs using 3DISCO. *Nat. Protoc.* 7, 1983–1995 (2012).
28. Renier, N. et al. iDISCO: a simple, rapid method to immunolabel large tissue samples for volume imaging. *Cell* 159, 896–910 (2014).
29. Kubota, S.I. et al. Whole-body profiling of cancer metastasis with single-cell resolution. *Cell Rep.* 20, 236–250 (2017).
30. Murakami, T.C. et al. A three-dimensional single-cell-resolution whole-brain atlas using CUBIC-X expansion microscopy and tissue clearing. *Nat. Neurosci.* 21, 625–637 (2018).
31. Susaki, E.A. et al. Whole-brain imaging with single-cell resolution using chemical cocktails and computational analysis. *Cell* 157, 726–739 (2014).
32. Chung, K. et al. Structural and molecular interrogation of intact biological systems. *Nature* 497, 332–337 (2013).
33. Tomer, R., Ye, L., Hsueh, B. & Deisseroth, K. Advanced CLARITY for rapid and high-resolution imaging of intact tissues. *Nat. Protoc.* 9, 1682–1697 (2014).
34. Snippert, H.J. et al. Intestinal crypt homeostasis results from neutral competition between symmetrically dividing Lgr5 stem cells. *Cell* 143, 134–144 (2010).
35. Stelzer, E.H. Light-sheet fluorescence microscopy for quantitative biology. *Nat. Methods* 12, 23–26 (2015).
36. Huisken, J., Swoger, J., Del Bene, F., Wittbrodt, J. & Stelzer, E.H. Optical sectioning deep inside live embryos by selective plane illumination microscopy. *Science* 305, 1007–1009 (2004).



CHAPTER 6



Tumor organoids and 3D imaging offer a patient-specific screening tool for FGS probes

L.M. Wellens, B. Jeremiase, F. de la Jara Ortiz,
G. Llibre, H. Johnson, W.M. Kholosy, P. van Sluis,
R. Volckmann, R. Versteeg, J. Koster,
E.J. Wehrens, M. Alieva, J.J. Molenaar,
J.F. Dekkers, M.H.W.A. Wijnen, A.C. Rios.

MANUSCRIPT IN PREPARATION

ABSTRACT

Fluorescence-guided surgery (FGS) with tumor-specific tracers can discriminate tumor from normal tissue, thereby promoting complete tumor resection with minimal surgical complications. Yet, predictive platforms to develop tracers in a patient-specific manner are lacking. In this study, we combined tumor organoid technology with 3D imaging to assess suitability of various FGS tracers simultaneously. We included a probe against the disialoganglioside GD2, which has been shown to efficiently visualise neuroblastoma tissue in a preclinical setting. However, because not all neuroblastoma tumors express GD2 we searched for novel tracers in literature and by RNA profiling and identified surface markers NCAM and L1CAM as FGS candidate-probes. Both surface markers have been described to be overexpressed in different tumor types as well as neuroblastoma. By using live confocal microscopy on different patient-derived neuroblastoma organoids, a strategy was created to test multiple (new) FGS tracers in a fast, high-throughput way for their potential in surgery. We found tracers for NCAM and L1CAM to be of additional value to complement the use of anti-GD2 as a FGS tracer. The designed organoid platform captures patient-specific tumor characteristics, including tumor heterogeneity, by showing different levels of expression in between patients. We also provide evidence that patient-specific expression levels are maintained *in vivo*. Thus, we provide proof of principle for using an imaging-based neuroblastoma organoid platform to screen for known and novel FGS tracers in a patient-specific manner with the potential to develop personalized marker selection for FGS.

INTRODUCTION

Fluorescence-guided surgery (FGS) with tumor-specific agents provides a powerful means to discriminate tumor from healthy tissue, thereby promoting complete tumor resection. In the last decade, multiple specific and non-specific fluorescence tracers have been developed and tested in phase I-III trials¹⁻⁵, with specific molecular tracers showing most promising results^{6,7}. Yet, predictive platforms to develop tracers that can be used in a patient-specific manner are lacking. Developing and testing novel fluorescence tracers for surgery requires a comprehensive pipeline containing both *in vitro* and *in vivo* experiments. Although animal studies are necessary to validate a single FGS tracer, they do not allow for rapid and high throughput testing of various FGS probes. Furthermore, cancer presents with inter and intra-heterogeneity in patients, complicating the choice of fluorescence agents that will enable visualization of the entire tumor of all patients of a certain cancer type. With the increasing arsenal of molecular fluorescent tracers that have been developed, we currently lack a strategy to simultaneously test multiple new tracers quickly for efficacy and specificity for real-time fluorescent labelling of cancer cells during surgery.

Recently, we showed that the disialoganglioside GD2 is a promising candidate to specifically light up neuroblastoma tissue in a preclinical setting⁸. Neuroblastoma is the most common extracranial solid tumor occurring in children⁹. Surgical resection is standard of care in patients with high-risk neuroblastoma¹⁰, but is associated with serious surgical complications^{11,12}. Therefore, there is an urgent need for new strategies to optimize neuroblastoma surgery. Unfortunately, neuroblastoma is a heterogeneous disease, and GD2 is not expressed in all patients at the same level¹³. Therefore, additional neuroblastoma specific probes should be used as an alternative, or to complement the use of anti-GD2 when GD2 expression is low.

In the last decade, *in vitro* 3D organoid cultures have revolutionized the modelling of organ development and diseases in a dish¹⁴. These organoids self-organize into 3D structures that recapitulate characteristics of the original biological specimen. Organoid models have become instrumental in cancer modelling^{15,16} and developing personalized treatment strategies¹⁷⁻²⁰. Since the generation of the first intestinal organoid model²¹, protocols have been extended to a wide range of healthy and cancerous tissues derived from organs such as prostate²², brain²³, liver^{24,25}, stomach²⁶, breast^{27,28}, kidney²⁹, endometrium³⁰, salivary gland³¹ and taste bud³². This rise in organoid (or tumor organoid) models has coincided with advances in 3D imaging technologies that, compared to 2D imaging, are superior in visualizing the cellular complexity modelled by organoids^{33,34}. Therefore, 3D imaging can be used to study the specificity and discriminative potential of

fluorescent probes in organoid models and provide comparative quantification to select the most promising candidates for *in vivo* validation.

Here, we took such a combined organoid and 3D imaging approach, to establish a pipeline for testing the efficacy and specificity of suitable probes for FGS in neuroblastoma. To develop additional fluorescent tracers for neuroblastoma, we made use of recently established tumor-initiated cell (TIC) lines³⁵, as well as organoids, derived from tumor tissue of neuroblastoma patients undergoing treatment at the Princess Máxima Center for pediatric oncology in the Netherlands³⁶. To test multiple tracers simultaneously, we present a personalized high-throughput evaluation strategy using an organoid platform in combination with 3D imaging technology. We were able to accurately quantify fluorescence of the investigated probes and show their tumor-specific labeling *in vitro*, thereby identifying both NCAM and L1CAM to have potential to act as targeted probe for FGS in neuroblastoma.

RESULTS

LITERATURE REVIEW COMBINED WITH RNA ANALYSIS REVEALS POTENTIAL CANDIDATE TARGETS FOR FGS IN NEUROBLASTOMA

To identify new targets for FGS in neuroblastoma, we reviewed recent literature^{37,38} and compiled a list of cell surface proteins highly expressed in neuroblastoma. In addition, through literature, we assessed their expression in other cancer subtypes to provide a sense of their potential pan-tumor utility. Next to our previous published marker GD2, we selected surface targets that are currently researched for drug development, either preclinically, or in Phase I/II/III trials for diagnostic or treatment purposes (**table 1**).

Targets selected from literature were cross-referenced to a microarray data base of the Amsterdam Medical Center oncogenomics research group, containing 133 neuroblastoma samples⁶⁶, 120 of which were primary samples derived from tumor biopsies, and 13 consisted of debulking samples. Importantly, 8 of the 13 debulking samples could be correlated to their corresponding primary biopsy sample, included in the n = 133 primary biopsy data set. These matched samples were key for proper validation, as neuroblastoma resection surgery is typically performed after initial chemotherapy treatment. When comparing the RNA affymetrix data with normal tissue⁶⁷ RNA-affymetrix data (n = 504 samples across 77 healthy organs of different donors), this revealed overexpression of NCAM (CD56), Norepinephrine

reporter (NET1 or SLC6A2), Glypican 2 (GPC2) and L1 cell adhesion molecule (L1CAM or CD171) pre- and post- chemotherapy (**figure 1a, supplementary figure 1**) in neuroblastoma compared to healthy tissue. Since GD2 is a ganglioside⁶⁸, RNA could not be traced by RNA profiling. Therefore, we screened for the presence of the RNA of enzyme beta-1,4 N-acetylgalactosaminyltransferase 1 (B4GALNT1) that catalyzes precursor GM3 into GD2 instead⁶⁹.

Table 1. Literature search for neuroblastoma probes

Neuroblastoma-expressed surface proteins	Gene	Other tumors expressing this target	Clinical use
GD-2 receptor (GD2) ¹³	B4GALNT1	Melanoma ³⁹	Yes, FDA approved immunotherapeutic target ⁴⁰
Norepinephrine transporter (NET1) ⁴¹	SL6CA2		Yes, GMP approved nuclear therapy target (MIBG).
L1CAM (CD171) ⁴²	L1CAM	Ovarian ⁴³ , Renal ⁴⁴ , colorectal ⁴⁵ , gastrointestinal ⁴⁶ , breast ⁴⁷ , melanoma ⁴⁸	Yes, phase I trial target ⁴²
NCAM (CD56) ^{49 50}	NCAM		Yes, a Phase I-II study to a chemotherapeutic agent ⁵¹ .
Glypican 2 (GPC2) ⁵²	GPC2	Testis ⁵³ , Glioma ⁵⁴ [ref]	No, proposed Phase I drug screening target ⁵²
Prominin-1 (CD133) ⁵⁵	PROM1	Colorectal cancer ⁵⁶ , hepatocellular carcinoma ⁵⁷ , glioma ⁵⁸	Preclinically validated ⁵⁹
Granulocyte colony-stimulating factor receptor (G-CSF-R or CD114) ⁶⁰	CSF3R	Ovarian ⁶¹ , Bladder ⁶² and squamous cell cancers ⁶³	Yes, used to ensure bone marrow recovery after chemotherapy ⁶⁰ , although G-CSF might also stimulates cell proliferation and increase chemoresistance ⁶⁴
Human natural killer-1 (HNK-1 or CD57)	B3GAT1	Melanoma ⁶⁵	

The RNA expression of NCAM, NET1 and GPC2 appeared higher in primary neuroblastoma material compared to neuroblastoma after chemotherapy. In contrast, the expression of B4GALNT1 and L1CAM was higher (**figure 1a**) in the chemotherapy-treated debulking tumor. The expression of CD133, CD114 and CD57 remained relatively low, pre and post chemotherapy (**supplementary figure 1**). Based on these RNA expression levels, we prioritized the targets NCAM, L1CAM, GPC2, NET1 identified through literature for further evaluation and continued testing of GD2.

A PATIENT-DERIVED ORGANOID SCREENING PLATFORM REVEALS INTER- AND INTRATUMOR HETEROGENEITY IN LABELING FOR SEVERAL FGS PROBES

To test whether the identified neuroblastoma over-expressed cell surface receptors could serve as potential targets for FGS, they were evaluated in a pre-clinical pipeline, encompassing patient-derived neuroblastoma organoids, 3D imaging, and *in vivo* imaging in xenograft models (**figure 1b**). Importantly, 3D-imaging was performed in a live setting, to reflect a surgical real-time situation.

First, we performed 3D imaging on neuroblastoma organoids derived from 7 high-risk patients (**supplementary table 1**) using confocal microscopy (**figure 1c**) by simultaneously staining with a mix of different antibodies (**supplementary table 2**) conjugated to different fluorophores. This revealed a positive membranous staining pattern for NCAM, similar to GD2. In addition, L1CAM displayed positive membranous staining as well. In contrast, NET1 showed no positive staining and while we detected fluorescence for GPC2, it did not reveal the expected membranous staining pattern. Based on these results, we selected NCAM and L1CAM for further evaluation additional to GD2.

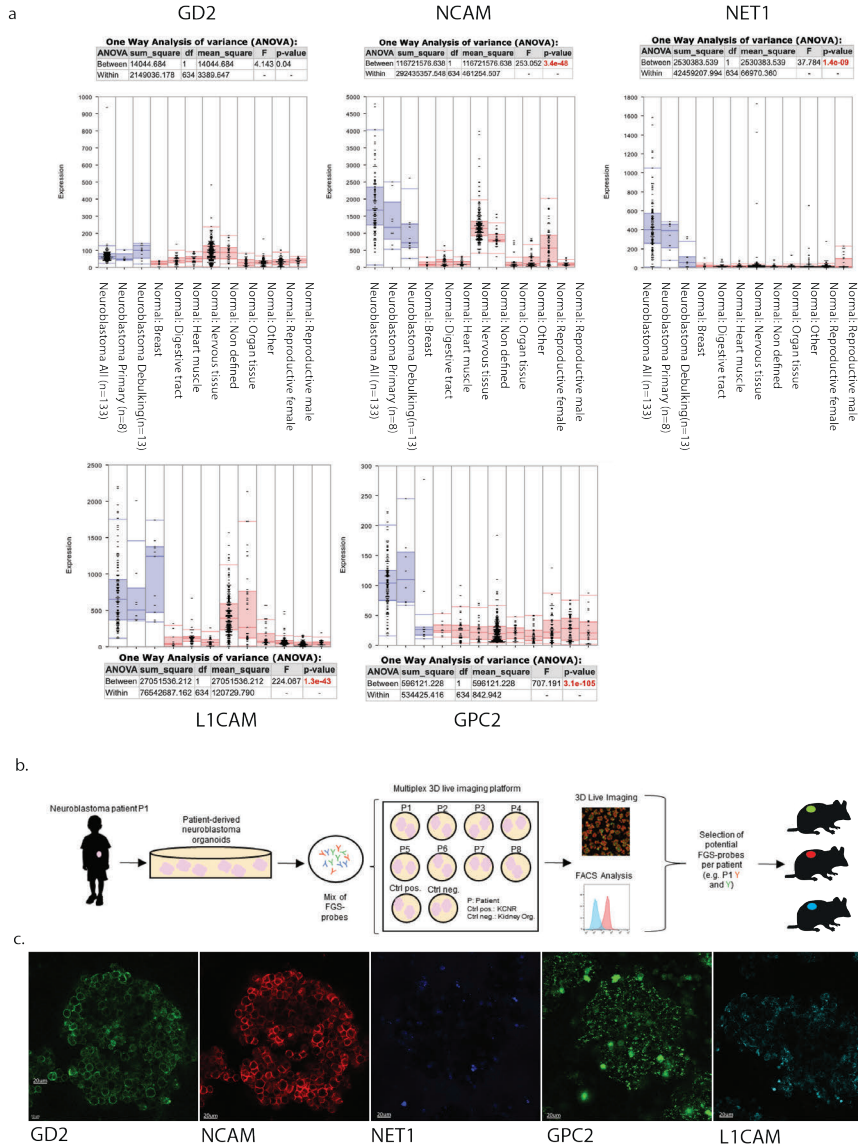


Figure 1. RNA expression and 3D imaging data identify NCAM and L1CAM as potential neuroblastoma-specific targets for FGS.

a) RNA expression analysis by microarray visualized by the R2 platform (R2.amc.nl) shows the expression of GD2, NCAM, NET1, GPC2 and L1CAM in neuroblastoma tissue compared to various normal tissue. b) Schematic representing the comprehensive pipeline used to evaluate the tumor organoid and 3D imaging platform as a screening tool for novel FGS tracers. c) 3D imaging of a neuroblastoma organoid line shows membranous staining for GD2, NCAM and L1CAM, whereas NET1 and GPC2 remain negative for a membranous staining.

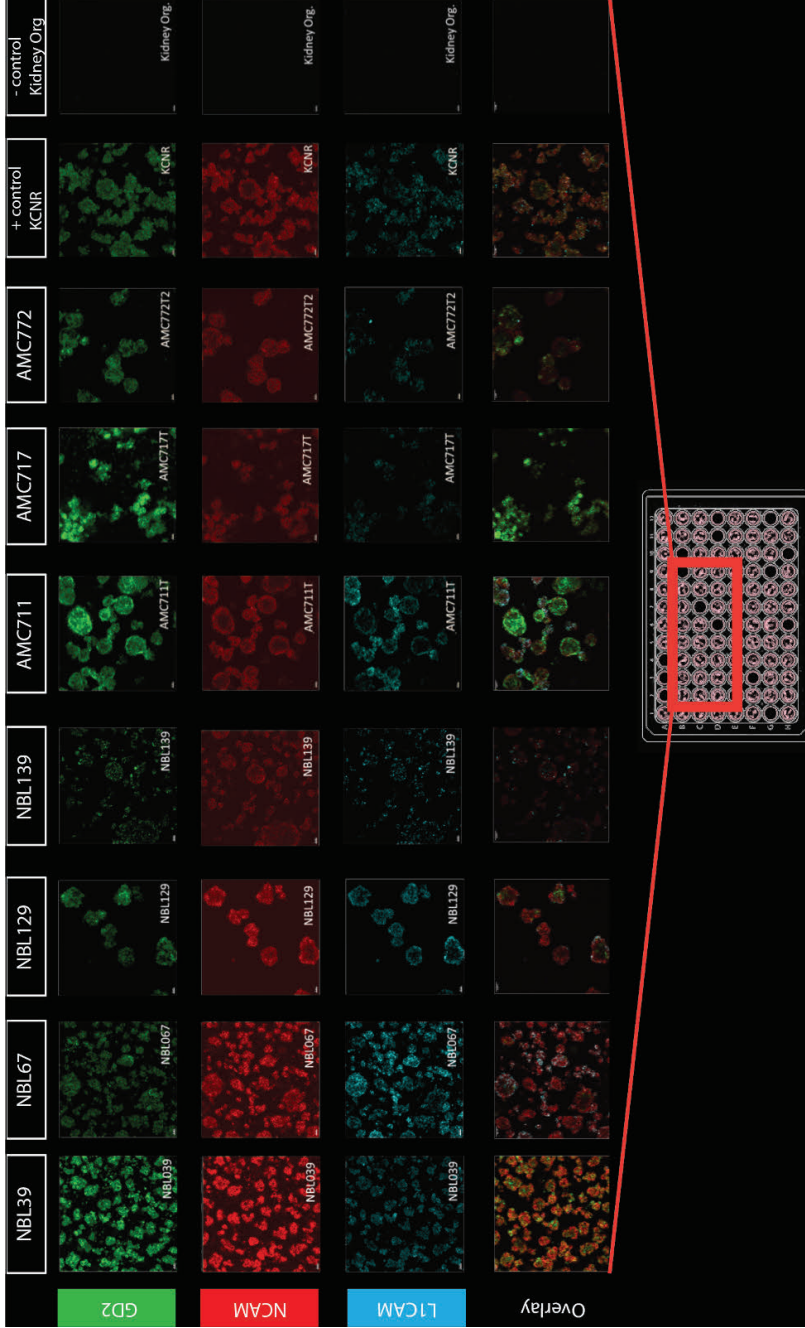


Figure 2. Representative image of all neuroblastoma lines showing variable expression of GD2, NCAM and L1CAM.

Seven patient-derived neuroblastoma organoid lines, the neuroblastoma cell line KCNR and healthy control kidney organoids were compared for fluorescence staining of anti-GD2-FITC, anti-NCAM-555 and anti-L1CAM-APC. One representative of $n = 3$ experiments.

Specific binding of our selected panel of probes (anti-GD2-FITC, anti-NCAM-555 and anti-L1CAM-APC) was evaluated on multiple patient-derived neuroblastoma organoids (**table 2**) by 3D confocal imaging and flow cytometry. For this, all organoid lines were imaged simultaneously using a standardized set-up that included SMS-KCNR cell line as a positive control, and healthy kidney organoids, as a healthy tissue control. We choose to use the kidney organoids as a healthy control, since in surgery, the kidney is close to the neuroblastoma and therefore a high fluorescence uptake is unwanted. Using this set-up, differences in fluorescence intensity between organoid lines were visualized (**figure 2**) and quantified across 3 independent experiments (**figure 3a**). Organoid lines NBL39 and AMC717 showed a relatively high fluorescence signal for GD2, comparable to KCNR cell lines and in line with our previous results⁸ (**figure 3a**). Meanwhile, other lines showed an intermediate to low fluorescence signal. NCAM displayed an intermediate to high fluorescence level across all organoid lines, whereas L1CAM staining intensity seemed low for most lines, especially NBL139 (**figure 3a**). Importantly, GD2 and NCAM did not label healthy kidney organoids, where L1CAM was seen positive in one experiment out of three. This indicates that L1CAM is also expressed in healthy kidney tissue, as described in literature⁷⁰. Remarkably, line NBL67 showed a low visible staining for GD2, while having a relatively high fluorescence intensity for NCAM and L1CAM (**figure 2 and figure 3a**). This could indicate that these tracers might be helpful for FGS in patients where GD2 expression is low.

3D IMAGING IS A POWERFUL TOOL FOR QUANTIFICATION OF FLUORESCENCE INTENSITY

Next to 3D confocal imaging, we also performed flow cytometry analysis on the organoids stained with the fluorescence-conjugated antibodies, and similarly quantified mean fluorescence intensity. This again revealed heterogeneity in expression levels between the different organoid lines (**figure 3b**). When directly comparing fluorescence intensity of 3D imaging quantification with the fluorescence intensity of flow cytometry quantification, both datasets show almost a similar trend in expression patterns between the different neuroblastoma organoid lines (**figure 3a and b**). Indeed, a significant correlation between 3D imaging and flow cytometry data is observed for GD2 ($p < 0.05$), NCAM ($p < 0.01$) and L1CAM ($p < 0.05$) (**figure 3c**). These results show that quantification of fluorescence with 3D imaging is similar to flow cytometry, demonstrating successful validation of our 3D imaging read-out.

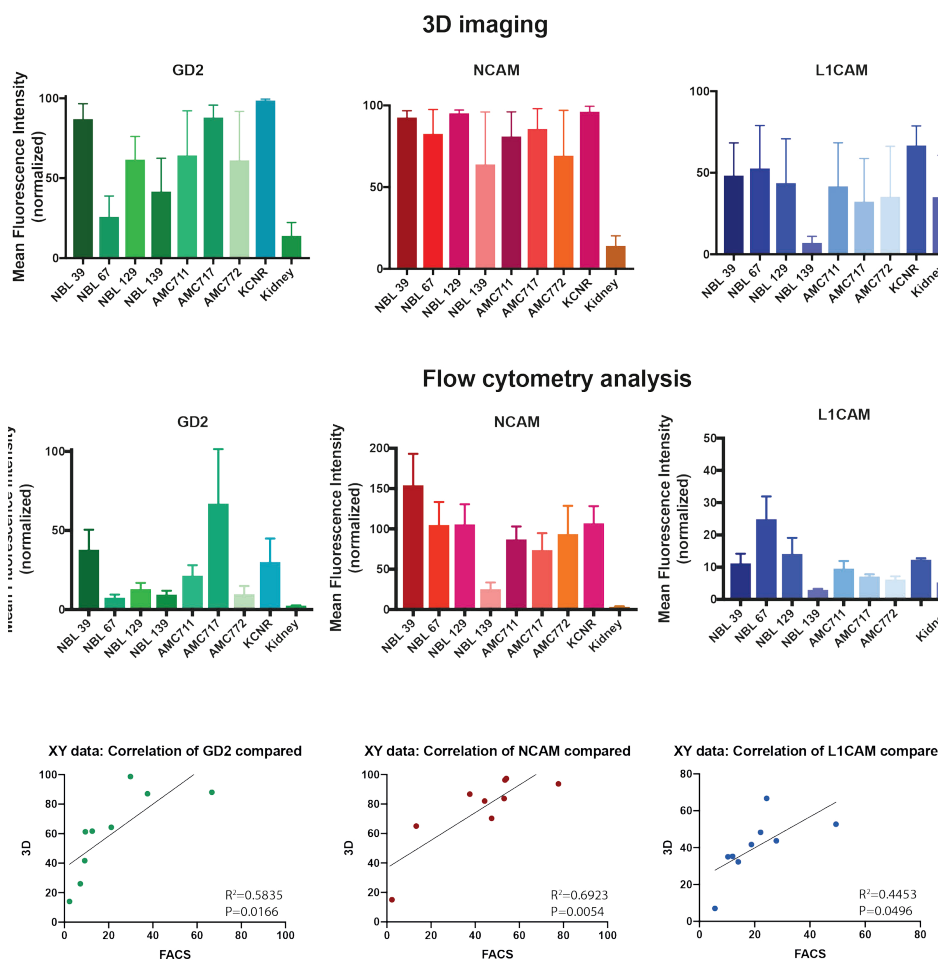


Figure 3. Quantification of fluorescence shows a variability between different organoid lines

Quantification of fluorescence for different patient-derived neuroblastoma organoids obtained through **a)** 3D imaging, or **b)** flow cytometry analysis for the antibodies used in Figure 2. **c)** the fluorescence of the two modalities compared by Pearson correlation. Mean \pm SEM of $n = 3$ independent experiments.

In vivo and in vitro imaging of GD2 shows a similar trend in fluorescence intensity

To be able to validate the *in vitro* results, we established a xenograft model for *in vivo* imaging by transplanting different organoid lines and measuring the growth curves of resulting tumors. This revealed tumor growth starting between 2 and 8 weeks (**figure 4a**) in 58% up to 100% of mice transplanted with the different organoid lines. A dose escalation study performed for anti-GD2-IRDye800CW, as previously described⁸ showed differences in *real time* fluorescence intensity amongst the various organoids, but all adequate for per-operative imaging. With the xenograft tumor models established (**figure 4a**), the other tracers should be tested for their *in vivo* efficiency and dose escalation as well on the IVIS. However, when comparing the fluorescence signal of the *in vivo* experiments with the fluorescence signal of anti-GD2 on three organoid lines (NB39, NB67 and NB 139) *in vitro*, we found a strong ($R^2=0.99$) and significant ($p=0.0358$) correlation between *in vitro* and *in vivo* results. This indicates that our *in vitro* imaging results for the new NCAM and L1CAM tracers (**figure 3a**) are likely to translate *in vivo*, further demonstrating their potential as an effective fluorescent probe for FGS.

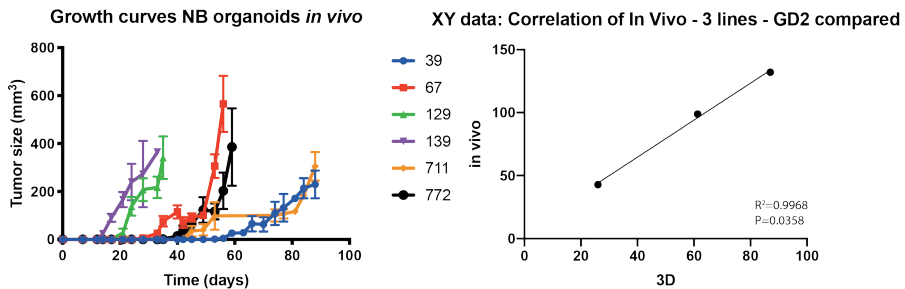


Figure 4. The *in vivo* fluorescence of GD2 can be correlated to the *in vitro* fluorescence signal measured on the organoids.

- a)** After injecting 6 different organoid lines in NGS-mice, all lines grew out to tumors within 1 - 12 weeks.
- b)** The *in vivo* fluorescence of anti-GD2-IRDye800 on the IVIS is correlated to the *in vitro* fluorescence measured on the organoids by the SP8 ($R^2=0.9968$, $p=0.0358$).

DISCUSSION

With the use of organoid technology, here we designed a patient-specific tumor platform to test for tracers that can be used for FGS. We found the tracers of NCAM and L1CAM to be of additional value to complement GD2 as a tracer for FGS in neuroblastoma. Since not all neuroblastoma patient express GD2 to the same extent, these novel candidate probes could be of particular interest to complement the use of GD2 or could be an alternative option in case of low GD2 expression⁸. Indeed, for some patient-derived organoid lines this was shown, while binding of our GD2-specific tracer is low, fluorescence for anti-NCAM and L1CAM is high. This shows that patient heterogeneity is adequately captured, a key asset of our platform as it can be exploited towards an optimal personalized FGS strategy.

We furthermore show that 3D imaging of organoids is a good screening tool to test for efficiency of FGS tracers *in vitro*. 3D imaging has an advantage above conventional flow cytometry when searching for FGS probes, since 3D imaging can provide volumetric data for immunolabeled organoids as a whole. By immunolabeling live organoids, imaging techniques such as confocal, multiphoton and light-sheet fluorescent microscopy can be used to obtain cellular to subcellular resolution and provide in depth information of the exact location of the fluorescent binding of the specific antibodies. Multiple fluorophores can be imaged simultaneously and therefore the overall fluorescence of the organoids with different antibodies can be shown at a glance³³. This means that the heterogeneity of multiple fluorescence probes can be easier compared on the same organoid compared to flow cytometry. Furthermore, the organoids do not have to be made into single cells and can even be kept in culture after imaging to be used for additional experiments. Most, importantly, by staining organoids *live* and in a 3D composition, the organoid remains intact as a whole and therefore this represents the closest comparison to a real-time surgical setting for fluorescence staining. Therefore, the use of the organoid platform is a good qualitative assay to simultaneously test multiple fluorescence probes in a high throughput way with 3D imaging and has the potential to predict the efficiency of probes for FGS.

The potential of our organoid and 3D imaging platform for predicting FGS probe efficacy is further supported by our observation that 3D imaging of organoids *in vitro* could give a comparable fluorescence to *in vivo* experiments. When we compare our findings of the 3D imaging with anti-GD2 with the results from our previous publication⁸, the heterogenous fluorescence intensity between lines is translated between *in vitro* and *in vivo* experiments. This would mean that the 3D imaging of organoids performed *in vitro* accurately predicts the fluorescence intensity measured on the *real time In Vivo NIR imaging systems*, that up till today

is still extensively performed on experimental animals when new probes need to be tested. Of course, the results above need to be generated for additional probes, before this conclusion can be drawn in general, but these preliminary results are promising. If the results from this study will be supported by data from the newly identified NCAM and L1CAM probes, *in vivo* studies for efficacy might potentially be omitted in the near future. Also, given the results from previous *in vivo* studies where all fluorescent conjugated antibodies have an optimal time window of 3-5 days after administration^{71,72}, it could be chosen to omit an optimal time window study when antibodies have a similar half-time and chemical characteristic. However, toxicity studies and biodistribution will still need to be assessed *in vivo* for now.

In conclusion, we established the organoid technology and 3D imaging platform to test for FGS candidate probes for a broad range of neuroblastoma tumors. However, with a high number of organoid biobanks nowadays available to model multiple cancer subtypes¹⁵, the platform could easily be adapted to expand its application and discover probes for other tumor types. Next to potentially replacing animal- and material use in time-consuming *in vivo* studies, the organoid platform has the important future perspective of incorporating a personalized FGS strategy. For neuroblastoma, we show that candidate fluorescence probes can be tested on organoids derived from biopsies a few months prior to debulking surgery, to find the optimal candidate for a personalized FGS approach. Furthermore, our comparative results with multiple probes in parallel, show that a combination of probes should be tested to arrive at the most optimal strategy.

METHODS

RNA ANALYSIS OF NEUROBLASTOMA TUMOR SAMPLES IN COMPARISON TO HEALTHY TISSUE

A biobank containing 120 samples of primary neuroblastoma biopsies for which RNA was profiled by Affymetrix microarray as previously described⁶⁶. Additionally, samples of the corresponding debulking samples, stored at -80 degrees, were HE stained and scored by a pathologist. Debulking samples containing >50% neuroblastoma tissue was selected for RNA analysis, bringing the total number of paired samples at 8, with 5 extra debulking samples not containing a corresponding primary sample. RNA was extracted from tumours with TRIzol (Invitrogen, Carlsbad, CA) following the manufacturer's protocols. RNA quality was determined using the RNA 6000 Nano assay on the Agilent 2100 Bioanalyzer (Agilent Technologies). Fragmentation of cRNA, hybridisation to hg-u133 plus 2.0, microarrays and scanning were carried out according to the manufacturer's protocol (Affymetrix Inc., Santa

Barbara, CA). The mRNA gene expression data were normalised with the MAS5.0 algorithm within the GCOS programme of Affymetrix. All data were analysed using the R2 genomic analysis and visualisation platform (<http://r2.amc.nl>).

ETHICAL APPROVAL FOR THE USE OF HUMAN MATERIAL

Authorizations for the organoids were obtained by the medical ethical committee of UMC Utrecht (METC UMCU) at request of the HUB in order to ensure compliance with the Dutch medical research involving human subjects' act and informed consent was obtained from donors where appropriate. Authorization for the neuroblastoma samples used for rna profiling were obtained by the medical ethical committee of the Amsterdam University Medical Center, and informed consent was also obtained from the parents of donors.

Origin and culture of organoids and cell lines

Patient-derived neuroblastoma organoids were cultured as described previously^{35,36} (Kholosy et al, submitted). Briefly, organoids were grown in Dulbecco's modified Eagle's medium (DMEM)-GlumaMAX containing low glucose with addition of 20% Ham's F-12 Nutrient Mixture, B-27 Supplement minus vitamin A, N-2 supplement, 100 IU/ml penicillin, 100ug/ml streptomycin, 20ng/mL epidermal growth factor (EGF), 40ng/ml fibroblast growth factor-basic (FGF-2), 200 ng/ml insulin-like growth factor (IGF-1), 10ng/ml platelet-derived growth factor AA (PDGF-AA) and 10 ng/ml platelet-derived growth factor BB (PDGF-BB).

SMS-KCNR cell line was cultured in Dulbecco's modified Eagle's medium (DMEM)-GlumaMAX containing low glucose, 10% Fetal Bovine Serum (FBS), 1%ml NEAA, 100 IU/ml penicillin and 100ug/ml streptomycin. All organoids and cell lines were cultured in a humidified incubator at 37° C and 5% CO₂ and free of *Mycoplasma* species.

Kidney organoids were a kind gift from the *Jarno Drost group* and used as healthy control.

3D IMAGING

Patient-derived (tumor) organoids were incubated for 30 minutes on ice before imaging (**Supplementary table 2**). *In vitro* imaging was performed on a confocal microscope using a 25X multi immersion (Zeiss NA, Zeiss microscope). *In vivo* imaging was performed using the IVIS spectrum In Vivo Imaging System, (Perkin Elmer). 3D rendering and quantification of the mean fluorescence was performed using Imaris (Bitplane).

FLOW CYTOMETRY

Organoids were processed into single cells using 200 μ l accutase and 10 times pipetted up-and-down in a 15ml tube. Cells were adjusted to 0.5×10^6 viable cells per tube in flow cytometry buffer and incubated with 200 μ l phosphate buffer solution (PBS) and 2 ml anti-GD2-FITC, 2 ml anti-NCAM-555 and 4 ml anti-L1CAM-AF647, and 2 ml anti-CD52-800CW, as a negative control. After incubation, cells were washed three times in ice-cold PBS and resuspended in 500 μ l PBS containing propidium iodide (PI) to stain dead cells. Samples were acquired on a LSRII flow cytometer (BD Biosciences, Singapore) and analysis and quantification of the mean fluorescence was performed using FlowJo software (TreeStar, Ashland, Oregon, United States, version 10.6.2).

Animal Experiments

Six-week-old athymic nude female mice (CD1-Foxn1^{nu}, Charles River Laboratories) were used for xenografting of the organoids and ethical approval was obtained from the Animal Welfare Committee from the Utrecht University. On average 1.0×10^6 single cells from patient-derived organoids were injected subcutaneously at 1 dorsal site in 50 μ l solution (50% Basal Medium Eagle (BME) and 50% medium) and 1 dorsal site in a medium only solution. Throughout the injection of organoids and imaging procedures, animals were anesthetized with 2.5% isoflurane for induction of anesthesia and 2% isoflurane for maintenance with a flow of 0.5 L/min.

STATISTICAL ANALYSIS

Statistical analyses of the RNA profiling by the R2 platform were performed using one way ANOVA on the R2.amc.nl platform. All other analysis were performed using Graphpad, Prism. Pearson correlation was used for paired comparison between the three different imaging modalities (Flow cytometry, 3D imaging and *In Vivo* imaging). The graphs of the growth curves of the *in vivo* experiments were generated in Prism.

REFERENCES

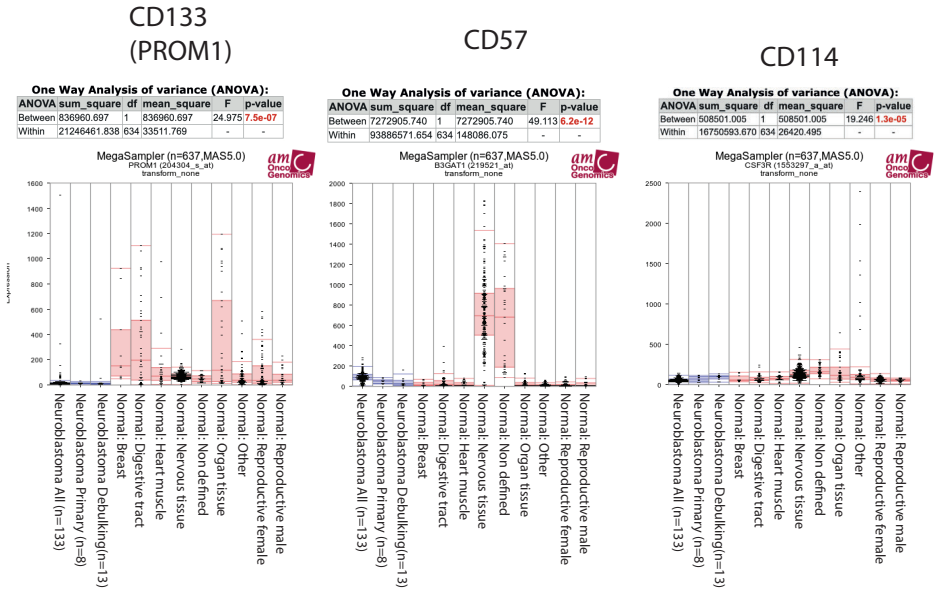
- 1 Lamberts, L.E. et al. Tumor-Specific Uptake of Fluorescent Bevacizumab-IRDye800CW Microdosing in Patients with Primary Breast Cancer: A Phase I Feasibility Study. *Clin Cancer Res* 23, 2730-2741, doi:10.1158/1078-0432.CCR-16-0437 (2017).
- 2 Hoogstins, C.E. et al. In Search for Optimal Targets for Intraoperative Fluorescence Imaging of Peritoneal Metastasis From Colorectal Cancer. *Biomark Cancer* 9, 1179299X17728254, doi:10.1177/1179299X17728254 (2017).
- 3 Stummer, W. et al. Fluorescence-guided surgery with 5-aminolevulinic acid for resection of malignant glioma: a randomised controlled multicentre phase III trial. *Lancet Oncol* 7, 392-401, doi:10.1016/S1470-2045(06)70665-9 (2006).
- 4 van der Vorst, J.R. et al. Intraoperative near-infrared fluorescence imaging of parathyroid adenomas with use of low-dose methylene blue. *Head Neck* 36, 853-858, doi:10.1002/hed.23384 (2014).
- 5 van der Vorst, J.R. et al. Near-infrared fluorescence-guided resection of colorectal liver metastases. *Cancer* 119, 3411-3418, doi:10.1002/cncr.28203 (2013).
- 6 Hernot, S., van Manen, L., Debie, P., Mieog, J.S.D. & Vahrmeijer, A.L. Latest developments in molecular tracers for fluorescence image-guided cancer surgery. *Lancet Oncol* 20, e354-e367, doi:10.1016/S1470-2045(19)30317-1 (2019).
- 7 Keereweer, S., Van Driel, P. B., Robinson, D. J. & Lowik, C.W. Shifting focus in optical image-guided cancer therapy. *Mol Imaging Biol* 16, 1-9, doi:10.1007/s11307-013-0688-x (2014).
- 8 Wellens, L.M. et al. Anti-GD2-IRDye800CW as a targeted probe for fluorescence-guided surgery in neuroblastoma. *Sci Rep* 10, 17667, doi:10.1038/s41598-020-74464-4 (2020).
- 9 Maris, J.M. Recent advances in neuroblastoma. *N Engl J Med* 362, 2202-2211, doi:10.1056/NEJMra0804577 (2010).
- 10 Irwin, M.S. & Park, J.R. Neuroblastoma: paradigm for precision medicine. *Pediatr Clin North Am* 62, 225-256, doi:10.1016/j.pcl.2014.09.015 (2015).
- 11 Rich, B.S., McEvoy, M.P., LaQuaglia, M.P. & Wolden, S.L. Local control, survival, and operative morbidity and mortality after re-resection, and intraoperative radiation therapy for recurrent or persistent primary high-risk neuroblastoma. *J Pediatr Surg* 46, 97-102, doi:10.1016/j.jpedsurg.2010.09.068 (2011).
- 12 von Allmen, D. et al. Impact of Extent of Resection on Local Control and Survival in Patients From the COG A3973 Study With High-Risk Neuroblastoma. *J Clin Oncol* 35, 208-216, doi:10.1200/JCO.2016.67.2642 (2017).
- 13 Terzic, T. et al. Expression of Disialoganglioside (GD2) in Neuroblastic Tumors: A Prognostic Value for Patients Treated With Anti-GD2 Immunotherapy. *Pediatr Dev Pathol* 21, 355-362, doi:10.1177/1093526617723972 (2018).
- 14 Sato, T. & Clevers, H. SnapShot: Growing Organoids from Stem Cells. *Cell* 161, 1700-1700 e1701, doi:10.1016/j.cell.2015.06.028 (2015).
- 15 Clevers, H. Modeling Development and Disease with Organoids. *Cell* 165, 1586-1597, doi:10.1016/j.cell.2016.05.082 (2016).
- 16 Drost, J. & Clevers, H. Organoids in cancer research. *Nat Rev Cancer* 18, 407-418, doi:10.1038/s41568-018-0007-6 (2018).

- 17 Dekkers, J.F. et al. Characterizing responses to CFTR-modulating drugs using rectal organoids derived from subjects with cystic fibrosis. *Sci Transl Med* 8, 344ra384, doi:10.1126/scitranslmed.aad8278 (2016).
- 18 Dekkers, J.F. et al. A functional CFTR assay using primary cystic fibrosis intestinal organoids. *Nat Med* 19, 939–945, doi:10.1038/nm.3201 (2013).
- 19 Broutier, L. et al. Human primary liver cancer-derived organoid cultures for disease modeling and drug screening. *Nat Med* 23, 1424–1435, doi:10.1038/nm.4438 (2017).
- 20 Bartfeld, S. & Clevers, H. Stem cell-derived organoids and their application for medical research and patient treatment. *J Mol Med (Berl)* 95, 729–738, doi:10.1007/s00109-017-1531-7 (2017).
- 21 Sato, T. et al. Single Lgr5 stem cells build crypt-villus structures in vitro without a mesenchymal niche. *Nature* 459, 262–265, doi:10.1038/nature07935 (2009).
- 22 Karthaus, W.R. et al. Identification of multipotent luminal progenitor cells in human prostate organoid cultures. *Cell* 159, 163–175, doi:10.1016/j.cell.2014.08.017 (2014).
- 23 Lancaster, M.A. et al. Cerebral organoids model human brain development and microcephaly. *Nature* 501, 373–379, doi:10.1038/nature12517 (2013).
- 24 Hu, H. et al. Long-Term Expansion of Functional Mouse and Human Hepatocytes as 3D Organoids. *Cell* 175, 1591–1606 e1519, doi:10.1016/j.cell.2018.11.013 (2018).
- 25 Huch, M. et al. Long-term culture of genome-stable bipotent stem cells from adult human liver. *Cell* 160, 299–312, doi:10.1016/j.cell.2014.11.050 (2015).
- 26 Nanki, K. et al. Divergent Routes toward Wnt and R-spondin Niche Independence during Human Gastric Carcinogenesis. *Cell* 174, 856–869 e817, doi:10.1016/j.cell.2018.07.027 (2018).
- 27 Jamieson, P.R. et al. Derivation of a robust mouse mammary organoid system for studying tissue dynamics. *Development* 144, 1065–1071, doi:10.1242/dev.145045 (2017).
- 28 Sachs, N. et al. A Living Biobank of Breast Cancer Organoids Captures Disease Heterogeneity. *Cell* 172, 373–386 e310, doi:10.1016/j.cell.2017.11.010 (2018).
- 29 Schutgens, F. et al. Tubuloids derived from human adult kidney and urine for personalized disease modeling. *Nat Biotechnol* 37, 303–313, doi:10.1038/s41587-019-0048-8 (2019).
- 30 Turco, M.Y. et al. Long-term, hormone-responsive organoid cultures of human endometrium in a chemically defined medium. *Nat Cell Biol* 19, 568–577, doi:10.1038/ncb3516 (2017).
- 31 Maimets, M. et al. Long-Term In Vitro Expansion of Salivary Gland Stem Cells Driven by Wnt Signals. *Stem Cell Reports* 6, 150–162, doi:10.1016/j.stemcr.2015.11.009 (2016).
- 32 Ren, W. et al. Single Lgr5- or Lgr6-expressing taste stem/progenitor cells generate taste bud cells ex vivo. *Proc Natl Acad Sci U S A* 111, 16401–16406, doi:10.1073/pnas.1409064111 (2014).
- 33 Dekkers, J.F. et al. High-resolution 3D imaging of fixed and cleared organoids. *Nat Protoc* 14, 1756–1771, doi:10.1038/s41596-019-0160-8 (2019).
- 34 Rios, A.C. et al. Essential role for a novel population of binucleated mammary epithelial cells in lactation. *Nat Commun* 7, 11400, doi:10.1038/ncomms11400 (2016).
- 35 Bate-Eya, L.T. et al. Newly-derived neuroblastoma cell lines propagated in serum-free media recapitulate the genotype and phenotype of primary neuroblastoma tumours. *Eur J Cancer* 50, 628–637, doi:10.1016/j.ejca.2013.11.015 (2014).

- 36 Decaestecker, B. et al. TBX2 is a neuroblastoma core regulatory circuitry component enhancing MYCN/FOXM1 reactivation of DREAM targets. *Nat Commun* 9, 4866, doi:10.1038/s41467-018-06699-9 (2018).
- 37 Orentas, R.J. et al. Identification of cell surface proteins as potential immunotherapy targets in 12 pediatric cancers. *Front Oncol* 2, 194, doi:10.3389/fonc.2012.00194 (2012).
- 38 Kholodenko, I.V., Kalinovskiy, D.V., Doronin, I.I., Deyev, S.M. & Kholodenko, R. V. Neuroblastoma Origin and Therapeutic Targets for Immunotherapy. *J Immunol Res* 2018, 7394268, doi:10.1155/2018/7394268 (2018).
- 39 Suzuki, M. & Cheung, N.K. Disialoganglioside GD2 as a therapeutic target for human diseases. *Expert Opin Ther Targets* 19, 349-362, doi:10.1517/14728222.2014.986459 (2015).
- 40 Yu, A.L. et al. Anti-GD2 antibody with GM-CSF, interleukin-2, and isotretinoin for neuroblastoma. *N Engl J Med* 363, 1324-1334, doi:10.1056/NEJMoa0911123 (2010).
- 41 Pandit-Taskar, N. & Modak, S. Norepinephrine Transporter as a Target for Imaging and Therapy. *J Nucl Med* 58, 39S-53S, doi:10.2967/jnumed.116.186833 (2017).
- 42 Kunkele, A. et al. Preclinical Assessment of CD171-Directed CAR T-cell Adoptive Therapy for Childhood Neuroblastoma: CE7 Epitope Target Safety and Product Manufacturing Feasibility. *Clin Cancer Res* 23, 466-477, doi:10.1158/1078-0432.CCR-16-0354 (2017).
- 43 Zecchini, S. et al. The differential role of L1 in ovarian carcinoma and normal ovarian surface epithelium. *Cancer Res* 68, 1110-1118, doi:10.1158/0008-5472.CAN-07-2897 (2008).
- 44 Meli, M.L. et al. Anti-neuroblastoma antibody chCE7 binds to an isoform of L1-CAM present in renal carcinoma cells. *Int J Cancer* 83, 401-408, doi:10.1002/(sici)1097-0215(19991029)83:3<401::aid-ijc17>3.0.co;2-a (1999).
- 45 Kajiwara, Y. et al. Expression of L1 cell adhesion molecule and morphologic features at the invasive front of colorectal cancer. *Am J Clin Pathol* 136, 138-144, doi:10.1309/AJCP63NRBNGCTXVF (2011).
- 46 Kaifi, J.T. et al. L1 (CD171) is highly expressed in gastrointestinal stromal tumors. *Mod Pathol* 19, 399-406, doi:10.1038/modpathol.3800547 (2006).
- 47 Shtutman, M., Levina, E., Ohouo, P., Baig, M. & Roninson, I.B. Cell adhesion molecule L1 disrupts E-cadherin-containing adherens junctions and increases scattering and motility of MCF7 breast carcinoma cells. *Cancer Res* 66, 11370-11380, doi:10.1158/0008-5472.CAN-06-2106 (2006).
- 48 Fogel, M. et al. L1 adhesion molecule (CD 171) in development and progression of human malignant melanoma. *Cancer Lett* 189, 237-247, doi:10.1016/s0304-3835(02)00513-x (2003).
- 49 Bourne, S.P. et al. A monoclonal antibody (ERIC-1), raised against retinoblastoma, that recognizes the neural cell adhesion molecule (NCAM) expressed on brain and tumours arising from the neuroectoderm. *J Neurooncol* 10, 111-119, doi:10.1007/BF00146871 (1991).
- 50 Markovsky, E. et al. Targeting NCAM-expressing neuroblastoma with polymeric precision nanomedicine. *J Control Release* 249, 162-172, doi:10.1016/j.jconrel.2017.01.044 (2017).

- 51 Socinski, M.A. *et al.* Phase 1/2 Study of the CD56-Targeting Antibody-Drug Conjugate Lorvotuzumab Mertansine (IMGN901) in Combination With Carboplatin/Etoposide in Small-Cell Lung Cancer Patients With Extensive-Stage Disease. *Clin Lung Cancer* 18, 68-76 e62, doi:10.1016/j.clcc.2016.09.002 (2017).
- 52 Bosse, K.R. *et al.* Identification of GPC2 as an Oncoprotein and Candidate Immunotherapeutic Target in High-Risk Neuroblastoma. *Cancer Cell* 32, 295-309 e212, doi:10.1016/j.ccell.2017.08.003 (2017).
- 53 Kim, M.S. *et al.* A draft map of the human proteome. *Nature* 509, 575-581, doi:10.1038/nature13302 (2014).
- 54 Oh, S. *et al.* Integrated pharmacoproteogenomics defines two subgroups in isocitrate dehydrogenase wild-type glioblastoma with prognostic and therapeutic opportunities. *Nat Commun* 11, 3288, doi:10.1038/s41467-020-17139-y (2020).
- 55 Tong, Q.S. *et al.* Expression and clinical significance of stem cell marker CD133 in human neuroblastoma. *World J Pediatr* 4, 58-62, doi:10.1007/s12519-008-0012-z (2008).
- 56 Yu, X. *et al.* CD133, Stem Cells, and Cancer Stem Cells: Myth or Reality? *Curr Colorectal Cancer Rep* 7, 253-259, doi:10.1007/s11888-011-0106-1 (2011).
- 57 Chen, Y.L. *et al.* The effects of the location of cancer stem cell marker CD133 on the prognosis of hepatocellular carcinoma patients. *BMC Cancer* 17, 474, doi:10.1186/s12885-017-3460-9 (2017).
- 58 Zeppernick, F. *et al.* Stem cell marker CD133 affects clinical outcome in glioma patients. *Clin Cancer Res* 14, 123-129, doi:10.1158/1078-0432.CCR-07-0932 (2008).
- 59 Kobayashi, H. & Choyke, P.L. Near-Infrared Photoimmunotherapy of Cancer. *Acc Chem Res* 52, 2332-2339, doi:10.1021/acs.accounts.9b00273 (2019).
- 60 Zage, P.E., Whittle, S.B. & Shohet, J.M. CD114: A New Member of the Neural Crest-Derived Cancer Stem Cell Marker Family. *J Cell Biochem* 118, 221-231, doi:10.1002/jcb.25656 (2017).
- 61 Savarese, T.M. *et al.* Coexpression of granulocyte colony stimulating factor and its receptor in primary ovarian carcinomas. *Cancer Lett* 162, 105-115, doi:10.1016/s0304-3835(00)00623-6 (2001).
- 62 Chakraborty, A. & Guha, S. Granulocyte colony-stimulating factor/granulocyte colony-stimulating factor receptor biological axis promotes survival and growth of bladder cancer cells. *Urology* 69, 1210-1215, doi:10.1016/j.urology.2007.02.035 (2007).
- 63 Hirai, K. *et al.* Expression of granulocyte colony-stimulating factor and its receptor in epithelial skin tumors. *J Dermatol Sci* 25, 179-188, doi:10.1016/s0923-1811(00)00131-6 (2001).
- 64 Russell, H. & Shohet, J.M. Pediatric oncology: G-CSF counteracts chemotherapy toxicity in neuroblastoma. *Nat Rev Clin Oncol* 8, 6-8, doi:10.1038/nrclinonc.2010.195 (2011).
- 65 Thies, A. *et al.* The developmentally regulated neural crest-associated glycotope HNK-1 predicts metastasis in cutaneous malignant melanoma. *J Pathol* 203, 933-939, doi:10.1002/path.1595 (2004).
- 66 van Nes, J. *et al.* A NOTCH3 transcriptional module induces cell motility in neuroblastoma. *Clin Cancer Res* 19, 3485-3494, doi:10.1158/1078-0432.CCR-12-3021 (2013).
- 67 Roth, R.B. *et al.* Gene expression analyses reveal molecular relationships among 20 regions of the human CNS. *Neurogenetics* 7, 67-80, doi:10.1007/s10048-006-0032-6 (2006).
- 68 Kolter, T. Ganglioside biochemistry. *ISRN Biochem* 2012, 506160, doi:10.5402/2012/506160 (2012).

- 69 Yoshida, H. *et al.* B4GALNT1 induces angiogenesis, anchorage independence growth and motility, and promotes tumorigenesis in melanoma by induction of ganglioside GM2/GD2. *Sci Rep* 10, 1199, doi:10.1038/s41598-019-57130-2 (2020).
- 70 Debiec, H., Christensen, E. I. & Ronco, P. M. The cell adhesion molecule L1 is developmentally regulated in the renal epithelium and is involved in kidney branching morphogenesis. *J Cell Biol* 143, 2067-2079, doi:10.1083/jcb.143.7.2067 (1998).
- 71 Boonstra, M.C. *et al.* Preclinical evaluation of a novel CEA-targeting near-infrared fluorescent tracer delineating colorectal and pancreatic tumors. *Int J Cancer* 137, 1910-1920, doi:10.1002/ijc.29571 (2015).
- 72 Terwisscha van Scheltinga, A.G. *et al.* Intraoperative near-infrared fluorescence tumor imaging with vascular endothelial growth factor and human epidermal growth factor receptor 2 targeting antibodies. *J Nucl Med* 52, 1778-1785, doi:10.2967/jnumed.111.092833 (2011).



Supplementary figure 1.

RNA expression analysis by microarray visualized by the R2 platform (R2.amc.nl) shows the expression of CD133, CD57 and CD114, in neuroblastoma tissue (primary and debulking) compared to various normal tissue

CHAPTER 6



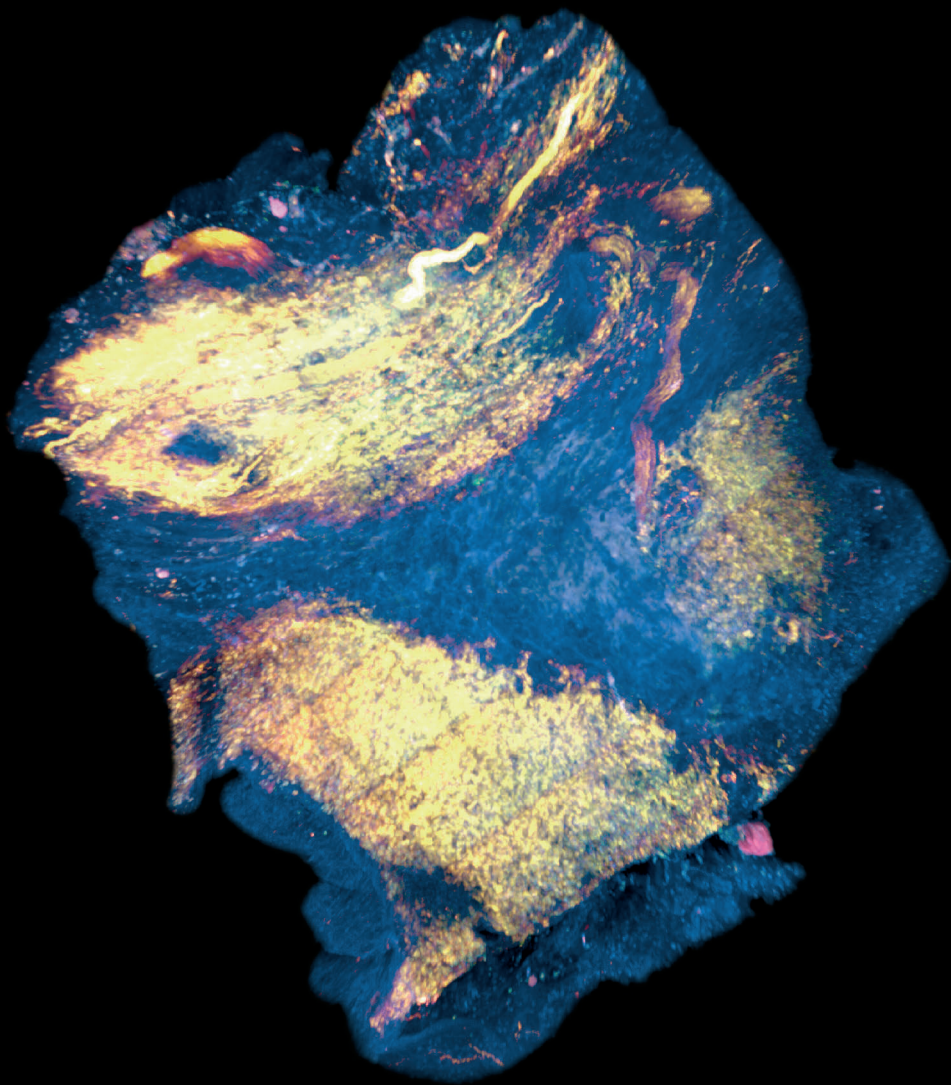
Supplementary figure 2.

Supplementary table 1.

Org-anoid line	Age at diagnosis (months)	INSS stage	Type of Tissue	Location	PA	MYCN amplified	Mutations	Culturing conditions
NB 39	24	4	Biopsy relapse	Lymph node	Poorly differentiated NB	Yes	Un-known	Organoid Medium
NB 67	29	4	Biopsy primary tumor	Adrenal gland	Poorly differentiated	Yes	ALK	Organoid Medium
NB 129	21	4	Biopsy Relapse	Pleura	Un-differentiated	Yes	ALK, loss of 1P	Organoid Medium
NB 139	5	4	Biopsy Relapse	Adrenal gland	Poorly differentiated	No	No	TIC Medium
TIC 711	15	4	Biopsy primary tumor	Abdominal side chain		Yes	No	TIC Medium
TIC 717	18	4	Biopsy primary tumor	Adrenal gland		Yes	No	TIC Medium
TIC 772	36	4	Biopsy primary tumor	Adrenal gland	Poorly differentiated	No	No	TIC Medium

Supplementary table 2.

Antibody or nanobody	Antibody specifics
Anti-GD2	Mouse, monoclonal, BD Pharmingen, CAT # 554272
Anti-NET1	Rabbit, polyclonal, Sigma-Aldrich Cat# HPA004057
Anti-L1CAM	Mouse, monoclonal, Sigma-Aldrich Cat#L 4543
Anti-NCAM	Llama, nanobody VHH, FSH-10B10, QVQ.
Anti-GPC2	Mouse, monoclonal antibody, R&D Systems, MAB2304



PART 3

Bridging the Gap between
Translational Science and
Surgery in Pediatric
Oncology



CHAPTER 7

A Phase 1 first-in-human imaging study of anti-GD2-IRDye800CW in patients with High-Risk Neuroblastoma

Coordinating Center: Princess Máxima Center

Principal Investigator:

Prof. dr. M.H.W.A. Wijnen
Heidelberglaan 25
3584 CS Utrecht
+31 88 972 7272
m.h.wijnen-4@prinsesmaximacentrum.nl

Co-Investigators:

DrS.L.M. Wellens
Heidelberglaan 25
3584 CS Utrecht
+31 88 972 7272
l.m.wellens@prinsesmaximacentrum.nl

DR.A.C. Rios
Heidelberglaan 25
3584 CS Utrecht
+31 88 972 7272
a.c.rios@prinsesmaximacentrum.nl

<p>Principal Investigator M.H.W. Wijnen, MD, PhD Princess Máxima Center Department of Solid Tumors 3584 CS Utrecht Phone +31 88 972 7272 m.h.w.wijnen-4@prinsesmaximacentrum.nl</p>	<p>Co Investigators A.C. Rios, MD, PhD Princess Máxima Center Imaging Princess Maxima Center 3584 CS Utrecht Phone +31 88 972 7272 a.c.rios@prinsesmaximacentrum.nl</p>	<p>Study Coordinator L.M. Wellens, MD Princess Máxima Center Department of Surgical Oncology 3584 CS Utrecht Phone +31 88 972 7272 l.m.wellens@prinsesmaximacentrum.nl</p>
<p>Co-investigator Pathology P. van Diest, MD, PhD University Medical Center Utrecht Department of Pathology 3584 CS Utrecht Phone +31 88 972 7272 p.vandiest@umcu.nl</p>	<p>Co-investigator Pathology R. de Krijger, MD, PhD Princess Máxima Center Department of Pathology 3584 CS Utrecht Phone +31 88 972 7272 r.r.dekrijger@prinsesmaximacentrum.nl</p>	<p>Co-investigator Solid Tumors A. van der Steeg, MD, PhD Princess Máxima Center Department of Clinical Pharmacy 3584 CS Utrecht Phone +31 88 972 7272 a.f.w.vandersteeg@prinsesmaximacentrum.nl</p>
<p>Statistician M. Fiocco, PhD Princess Máxima Center Department of Statistics 3584 CS Utrecht Phone +31 88 972 7272 M.fiocco@prinsesmaximacentrum.nl</p>	<p>Chair Neuroblastoma Group M. van Noesel, MD, PhD Princess Máxima Center 3584 CS Utrecht Phone +31 88 972 7272 m.m.vannoesel@prinsesmaximacentrum.nl</p>	<p>Trial Pharmacist <i>To be announced</i> Princess Máxima Center Department of Clinical Pharmacy 3584 CS Utrecht Phone +31 88 972 7272</p>
<p>Supervisor Trial & Data center M.P. van Dierselhuis, MD, PhD Princess Máxima Center Department of Statistics 3584 CS Utrecht Phone +31 88 972 7272 m.p.dierselhuis@prinsesmaximacentrum.nl</p>	<p>Study Coordinator - 2 B. Jeremiase, MD Princess Máxima Center Department of Surgical Oncology 3584 CS Utrecht Phone +31 88 972 7272 b.jeremiase-4@prinsesmaximacentrum.nl</p>	

TABLE OF CONTENTS

1. OBJECTIVES	5
1.1 Primary Objectives	5
1.2 Secondary Objectives	5
1.3 Trial Endpoints	5
2. BACKGROUND	6
2.1 Study Disease	6
2.2 Background Therapeutic Information	7
2.3 Correlative Studies Background	8
3. PATIENT SELECTION	9
4. REGISTRATION PROCEDURES	10
5. TRIAL DESIGN	10
5.1 Dosing / Imaging Schedule	10
5.2 Methods and Endpoints	12
Analysis of Primary Endpoints	12
6. TREATMENT AND IMAGING PLAN	13
6.1 Treatment Administration	13
6.2 Acquisition of imaging data	14
6.3 General Concomitant Medication and Supportive Care Guidelines	14
6.4 Dosing Delays/Dose Modifications and Adverse Event Management	15
6.5 Duration of Follow Up	15
6.6 Criteria for Removal from Study	15
7. ADVERSE EVENT REPORTING REQUIREMENTS	16
7.1 Expected Adverse Events using Qarziba-IRDye800CW	16
7.2 Adverse Event Characteristics	16
7.3 Routine Adverse Event Reporting	17
8. PHARMACEUTICAL and IMAGING AGENT INFORMATION	17
8.1 Investigational Agent(s)	17

CHAPTER 7

9. STUDY CALENDAR	18
9.1 Baseline/Pre-Study Evaluations	18
9.2 During Treatment	19
9.3 Follow-up Evaluation	19
9.4 Summary Table	20
10. DATA REPORTING / REGULATORY REQUIREMENTS	20
Data Reporting	21
11. STATISTICAL CONSIDERATIONS	21
11.1 Study Design/Endpoints	21
11.2 Sample Size/Accrual Rate	22
11.3 Stratification Factors	22
11.4 Analysis of Secondary Endpoints	22
12. QUALITY ASSURANCE	23
12.1 Control of Data Consistency	23
12.2 Central Review of Pathology	23
13. ETHICAL CONSIDERATIONS	24
13.1 Patient Protection	24
13.2 Subject Identification	24
13.3 Informed Consent	24
14. PUBLICATION POLICY	25
15. REFERENCES	26

1. OBJECTIVES

1.1 PRIMARY OBJECTIVES

- To establish an effective dose of anti-GD2-IRDye800CW for intra-operative detection of neuroblastoma using near-infrared fluorescence

1.2 SECONDARY OBJECTIVES

- To assess the safety, pharmacodynamic and pharmacokinetic characteristics of an intravenous injection of the conjugate anti-GD2-IRDye800CW
- To describe the pharmacokinetics of anti-GD2-IRDye800CW
- To assess the efficacy of the conjugate for intra-operative detection of anti-GD2-IRDye800CW for neuroblastoma.
- To describe the toxic effects of anti-GD2-IRDye800CW

1.3 TRIAL ENDPOINTS

Primary endpoints:

- **Tumor to background ratio (TBR)** of at least 2.0 in vivo during surgery. TBR is established by dividing the mean fluorescence signal of the tumor by the mean fluorescence signal of the background. Background is determined by fluorescence intensity in healthy kidney, liver and surrounding background tissue.
- **Pathologic status of removed fluorescent tissue and of removed non-fluorescent tissue.** After surgery, the ex-vivo resected specimen fluorescence hotspots will be marked within the same day. Pathologic analysis based on morphological characteristics, between 1 – 10 days after surgery, will differentiate between different neuroblastoma stages and/or necrosis. The pathology morphology report of these samples will be compared with the microscopic mean fluorescence intensity.

Secondary Endpoints:

- **Treatment related adverse events** after injection of the conjugate anti-GD2-IRDye800CW
- **Changes in serum pharmacokinetics;** blood samples will be taken just before infusion (t=0h), after infusion (t=60min and t=120min, t=24h, t=72h), immediately before surgery (t=96h) and 24hr after surgery (t=120h). Blood samples can be taken 10 min before or after the indicated timepoint.
- **The optimum dose** is defined as the lowest dose of the administered immunoconjugate giving an adequate TBR of >2.0.

2. BACKGROUND

2.1 STUDY DISEASE

Neuroblastoma surgery is a challenge for the surgeon

Neuroblastoma is the most commonly diagnosed extracranial solid tumor in young children. Patients diagnosed with high risk neuroblastoma – approximately 50% of all neuroblastoma patients – currently have a survival chance of only 50% despite intensive therapy. Children with high risk neuroblastoma are generally treated with induction chemotherapy, followed by surgery, high dose chemotherapy with stem cell rescue, additional radiotherapy and immunotherapy with *Dinutuximab* (anti-GD2 antibodies)¹. Tumor resection remains technically challenging because of its encasement of blood vessels and nerves, and the involvement of lymph-nodes. *Ex vivo*, the International Neuroblastoma Pathology Classification (INPC) describes four neuroblastoma subtypes, including neuroblastoma (NB), ganglioneuroblastoma-nodular (GNB-N) subtype, ganglioneuroblastoma-intermixed (GNB-I), and ganglioneuroma. The first is considered most malignant, while ganglioneuroma's are favorable tumors with excellent outcome². Most neuroblastomas contain these subtypes heterogeneously distributed. For the surgeon, it is impossible during surgery to differentiate between different subtypes. Furthermore, the percentages of complications (e.g. bleeding or unplanned nephrectomy) during neuroblastoma surgery is high (40%)³.

The presence of residual tumor cells after resection is considered a strong predictor of tumor recurrence. Many studies in adult cancers, including breast, lung, prostate, bladder and colorectal cancers, show that positive margins, defined as the identification of tumor cells at the margin of a surgical specimen, are associated with local recurrence and indicate a poor prognosis. For children with neuroblastoma, the objective benefit of surgery is difficult to evaluate. A recent review on the role of surgery in high-stage neuroblastoma performed by the Children's Oncology Group (COG) shows a beneficial effect of radical surgery in decreasing the cumulative incidence of local relapse⁴. It has been established that a surgeon-assessed resection extent $\geq 90\%$ of tumor significantly improves the event free survival of patients with neuroblastoma⁵.

To assist the surgeon in decision making during neuroblastoma debulking surgery, to reduce the number of surgical complications and to make sure the undifferentiated neuroblastoma cells can be visualized and resected during surgery, new intra-operative visualization tools need to be developed.

Fluorescence imaging

Recently, novel intra-operative imaging modalities have been developed to assist surgeons to identify cancerous tissue and delineate tumor margins, which helps to reduce damage to important structures such as nerves, blood vessels and increase the extend of tumor surgery. The most promising methodology is Fluorescence-guided surgery (FGS), which offers the benefit of high contrast and sensitivity and the absence of ionizing radiation (e.g. intraoperative computed tomography and/or radioactive colloids). In addition, it is easy to use and does not disrupt the normal workflow of the surgical procedure, with the use of a single portable instrument. Most advanced FGS are based on near infrared (NIR) light that has proven its value for multiple surgical procedures⁶. The advantages of NIR light (wavelengths of 700-900 nm) are (1) avoiding tissue autofluorescence which emits in the visible spectrum (400-550 nm) and (2) a relatively high tissue penetration capacity (5-10mm), which enables detection of targets even if they are covered with blood vessels or a thin layer of tissue.

The challenge for this technology is developing tumor-specific fluorescence imaging probes to target cancerous tissue. The first-in-human proof of principle of using FGS tumor-specific probe was provided in 2011. Tumor-specific fluorescence imaging of the folate receptor α using folate-FITC, was proven to be a specific and sensitive method for real-time identification of peritoneal carcinomatosis during surgery in patients with ovarian cancer⁷. Later, the therapeutic antibody bevacizumab that binds to VEGF-A, an angiogenesis receptor, was conjugated to the NIR fluorophore IRDye800CW and showed to be efficient for intraoperative breast cancer⁸. Since then, only a few tumor-targeted techniques to visualize tumor cells using fluorescence labelled ligands have been described in *in vivo* studies in adult patients for different types of tumors^{9,10}. So far, in pediatric oncology FGS and the use of targeted-fluorescent probes have not been implemented.

Glycodisianganglioside 2 (GD2)

GD2 is part of a family of gangliosides containing 2 N-Acetylneuraminic acids¹¹. GD2 is expressed by neuroblastomas, most melanomas and some other tumors¹². In normal human tissues, GD2 expression is expressed on neurons, skin melanocytes, and peripheral sensory nerve fibers¹³. Immunotherapy with *Dinutuximab* has shown to improve event-free and overall survival among children with high-risk neuroblastoma¹⁴. Currently, in Europe a similar product has been approved by EMA for the treatment of neuroblastoma, *Dinutuximab-beta* or Qarziba®. In high-risk treatment of neuroblastoma immunotherapy with the Qarziba, targeting the tumor-associated antigen disialoganglioside GD2 is now part of the standard therapy. IRDye800CW has previously been conjugated to other immunotherapy antibodies, such as cetuximab and bevacizumab^{15,16}. In our preclinical studies, we developed

and validated a clinical translatable GD2-specific NIR fluorescent imaging probe that can be used to visualize Neuroblastoma, anti-GD2-IRDye800CW. Based on the preclinical assessment, we hypothesize that GD2 could be a potential tumor-specific marker for FGS. This study will be the first to determine the recommended dose for anti-GD2-IRDye800CW in pediatric patients with neuroblastoma.

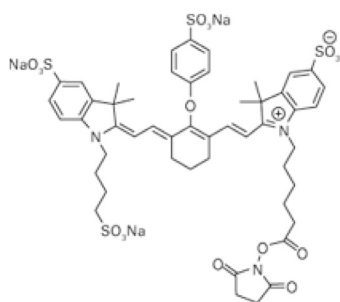
2.2 BACKGROUND THERAPEUTIC INFORMATION

Anti-GD2

Anti-GD2, or *Dinutuximab-Beta* is a chimeric (human-murine) IgG1 κ monoclonal anti-GD2 antibody similar to *Dinutuximab*, the anti-GD2 immunotherapeutic known to improve the survival of high-risk neuroblastoma¹⁴. Its molecular weight is approximately 148 kDa. Anti-GD2 binds to cell surface glycolipid GD2 expressed on many neuroblastoma cells as well as on many normal cells in the central nervous system and peripheral nerves and induces lysis of the GD2-expressing cells. The supposed mechanisms of cell lysis are antibody-dependent cell-mediated cytotoxicity (ADCC) and complement-dependent cytotoxicity (CDC).

IRDye-800CW

The Fab fragment of anti-GD2 is in our study conjugated to a dye, IRDye 800CW, which is a near-infrared (NIR) fluorophore. IRDye800CW has an absorption and emission wavelength in the NIR spectrum, at 778nm and 794 nm, respectively. Preclinical studies proved IRDye800CW is not immunogenic and the no adverse effect level (NOAEL) according to rats is 20mg/kg¹⁵. The NHS ester of the dye reacts with a primary aliphatic amine. Dye label is attached through an amide bond.



IRDye® 800CW NHS Ester



Exact Mass: 1165.20291

Mol. Wt.: 1166.20297

Figure 1. Structural formula of IRDye 800CW.

2.3 CORRELATIVE STUDIES BACKGROUND

Preclinical data

In preclinical work our group has evaluated the NIR fluorescence tracer anti-GD2-Beta-IRDye800CW in an *in vivo* mouse model¹⁷. First, a dose escalating cohort study was performed. Because the TBR was optimal at a dose of 1,0 nmol, this was chosen for further examinations. The human-derived relapsed neuroblastoma cell line KCNR, known to be overexpressing GD2, was subcutaneously transplanted into immunocompromised mice. After intravenous tail injection of 1.0 nmol anti-GD2-IRDye800CW, fluorescence was measured in different tumors on mouse models using the PEARL *in vivo* imager and the QUEST fluorescence near-infrared camera system. Tumor tissue was clearly identified in mouse models. Optimal TBR was obtained after 96 hours. Microscopic evaluation using the fluorescence microscopy identified a strong fluorescence signal in the tumor, with clear demarcation of tumor tissue¹⁷.

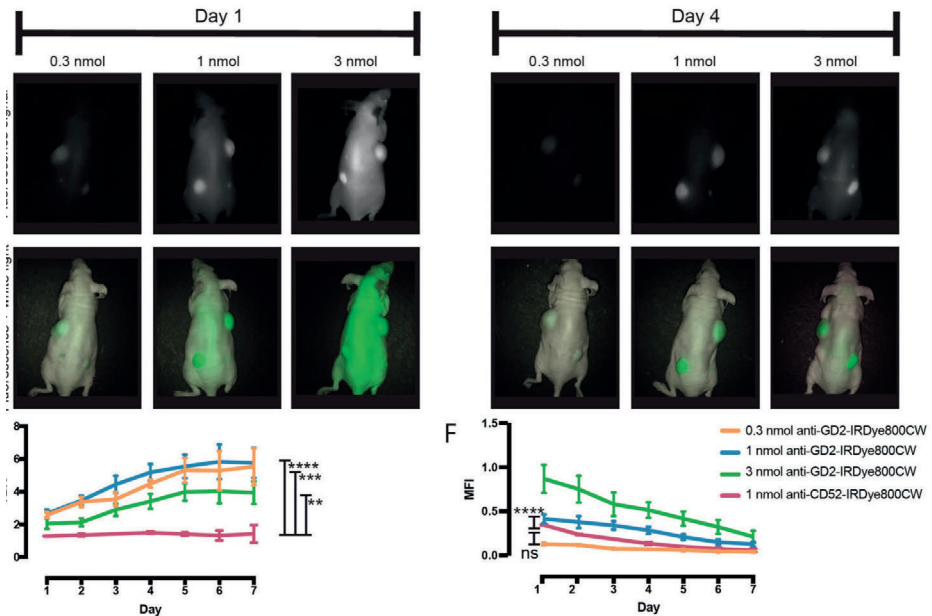


Figure 2. Identification of tumor tissue in a neuroblastoma mouse model.

After venous tail injection of 0.3, 1.0 and 3.0 nmol anti-GD2-IRDye800CW, the GD2 overexpressed in the tumors could be clearly identified. TBR was reached at maximum of 96 hours after injection with an optimal dose of 1nmol, as seen in the figure.

3. PATIENT SELECTION

3.1 SUBJECT INCLUSION CRITERIA

- Diagnosis of neuroblastoma as defined by histopathology (confirmed by the PMC Department of Pathology)
- Patients older than 1 year of age and not older than 18 years.
- Hemoglobin >6,0 mmol/L, leukocyte count >2,0 x10⁹/L; neutrophil count ≥0,5x10⁹/L; thrombocyte count >20x10⁹/L
- No anti-GD2 immunotherapy prior to the administration of anti-GD2-IRDye800CW
 - o Patients that received prior treatment with antibodies must have HAHA antibody titer <1300 Elise units/ml. This to confirm that the patient is not forming antibodies against the immunotherapy antibody treatment. Human anti-mouse antibody positivity is allowed.
- Signed informed consent indicating awareness of the investigational nature of this program.
 - o absence of any psychological, familial, sociological or geographical condition potentially hampering compliance with the study protocol and follow-up schedule; those conditions should be discussed with the patient before registration in the trial
 - o before patient registration, written informed consent must be given according to ICH/GCP, and local regulations.

4. REGISTRATION PROCEDURES

Eligible patients will be entered on study centrally at the Princess Máxima Center by the Study Coordinator. Following registration, patients should begin protocol treatment depending on the date of the scheduled surgery. Issues that would cause treatment delays should be discussed with the Principal Investigator. If a patient does not receive protocol therapy following registration, the patient's registration on the study may be canceled. The study coordinator should be notified of cancellations as soon as possible.

To register a patient, the following documents should be completed by the Study Coordinator:

- Copy of required laboratory tests
- Signed patient consent form

The study coordinator will then verify eligibility. To complete the registration process, the coordinator will

- assign a patient study number
- register the patient on the study
- assign the patient a dose

5. TRIAL DESIGN

This is a pilot, non-randomized, single center study in neuroblastoma patients, consisting an initial pharmacokinetic (PK) study of anti-GD2-IRDye800CW in patients with neuroblastoma undergoing surgery. The aim of the study is to measure the fluorescence signal of the tumor during surgery. Based on PK data and the level of TBR (>2.0), an optimal dose will be determined.

Since this is a pilot, first-in-child, study, we will use a 3+3 design. Other than to test the efficiency of the fluorescence, we will not plan further dose escalation steps. Our main endpoint is to achieve effective imaging. Instead, we will act by an adaptive recruitment strategy (**figure 3**). It will be studied, but we do not expect any new adverse effects since we will be using maximally the dose of the antibody anti-GD2 that is currently used for immunotherapy for 24 hours, compared to 240 hours in a therapeutic setting. Therefore, the Maximum Tolerated Dose which has been defined for anti-GD2 treatment will not be reached and not be assessed in this study^{18,19}.

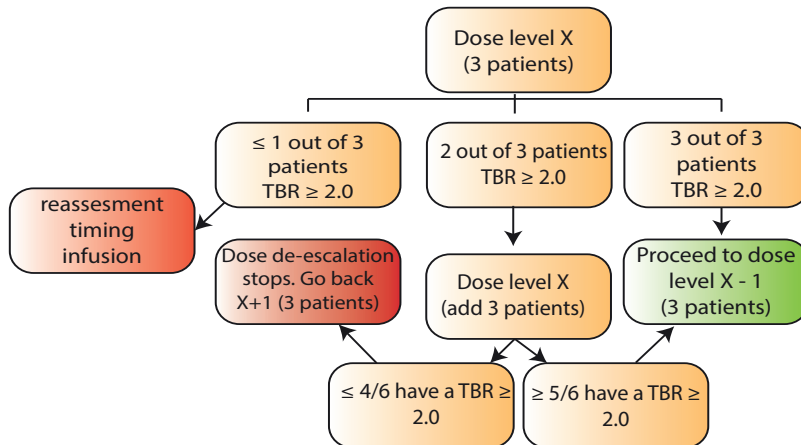


Figure 3. Workflow of the alternative 3+3 strategy. Based on the efficacy of the dose for the imaging during surgery per patient, it will be decided to move to a next, lower dose.

5.1 DOSING / IMAGING SCHEDULE

Rationale for the starting dose

The optimal biologic dose of anti-GD2-IRDye800CW will be determined using doses of 10 mg/m², 3 mg/m² and 1 mg/m² in groups of 3 patients, based on the experience in clinical and preclinical studies. Since we are looking for an effective dose, with the least toxicity possible, we will be scaling down our dose levels after the starting dose.

A preclinical study in our institute in a mouse model with an injected anti-GD2-IRDye800CW dose of 1.0 nmol showed that an optimal TBR was reached after 96 hours, after which the signal in the tumor remained high in comparison to the background¹⁷. Microscopic examination of the tumors showed a good demarcation of tumor borders. Based on the optimal dose of 1nmol (0.15 mg anti-GD2-IRDye800CW) in mice, we expect the dose of 0.9 mg/kg (22mg/m²) to be effective in humans according to the human equivalent dose (HED)²⁰. This dose is above the dose of 20mg/m² that is reported to have minimal toxicity in children²¹ and needs severe supportive care. Therefore, we choose to start with a lower dose of 10 mg/m². According to our study results, a dose of 0.3 nmol in mice (0.045mg anti-GD2-IRDye800CW) should still generate a TBR > 2.0 at 96 hours after infusion. The HED of this dose is 6.75 mg/m² in children, lower than our starting dose. In clinical trials with a comparable antibody fragment, the injected dose is 10 mg/m² per cycle and is feasible when supportive care is given using adequate pain relieve.

To follow the protocol of the immunotherapy schedule, infusion of the antibody will be 10 mg/m² per 24 hours. Ninety-six hours after start of the infusion, the surgery will take place. We expect the time of imaging to be similar to our preclinical experiments. The time of administration for similar size antibodies in other fluorescence guided surgery literature usually correlated to the preclinical experiments^{7,22}. However, if we see no fluorescence signal with our starting dose, we will have to reconsider our administration time point before surgery.

Dose level	Dose of anti-GD2-IRDye 800 CW
X	10 mg/m ²
X - 1	3 mg/m ²
X - 2	1 mg/m ²
RP2D	10 or 3 or 1 mg/m ²

Imaging Schedule

During surgery and during pathology examination, there will be multiple time points where the fluorescence signal will be measured and afterwards analyzed (See section 6.2, **figure 4**).

Alternative 3+3 Strategy

The starting dose of anti-GD2-IRDye800CW will be 10 mg/m² (see section 5.1). This dose is based on preclinical animal experiments (see section 2.3) and lower than the minimal toxicity dose for Dinutuximab (20mg/m²).

We will test this dose first in 3 patients. However, if after 3 patients the fluorescence signal is absent in 2 or 3 of the patients, we will reassess the timing of the infusion based on the PK data we will collect at time point t(0), t(1), t(2), t(24), t(72), t(96) and t(120).

If we find our 10 mg/m² effective in our first 3 patients, both *in vivo* and *ex vivo* (see section 6.2), we will continue to dose X - 1, which is 3 mg/m² dose. If this dose is still considered effective, we will continue to the X - 2, which is 1 mg/m², to see if an effective fluorescence *in vivo* and *ex vivo* signal can be established.

Recommended Phase II Dose

The recommended Phase II (RP2D) dose will be the lowest dose where $\geq 5/6$ patients in the cohort have a mean TBR > 2.0 (see section 5.2) with a variation (SEM) no more than 10% without DLTs. If the groups are alike, the lowest dose with the TBR > 2.0 will be chosen as the RP2D.

5.2 METHODS AND ENDPOINTS**Analysis of Primary Endpoints**

- **Tumor to background ratio (TBR)**

Regions of Interest (ROIs; intermittent circle) (**figure 2**) will be drawn to quantify fluorescent signal in a tumor and a background area. Fluorescence quantified value of tumor and background region will be divided from each other to obtain a TBR. The background is defined as normal kidney/liver or surrounding tissue, adjacent to tumor tissue.

- **Pathologic status of removed fluorescent tissue and removed non-fluorescent tissue.**

After surgery, the ex-vivo resected specimen fluorescence hotspots will be marked within the same day. Pathologic analysis based on morphological characteristics, between 1 - 10 days after surgery, will differ between different neuroblastoma stages and/or necrosis. The pathology morphology report of these samples will be compared with the microscopic mean fluorescence intensity.

Standard operating procedure for ex vivo processing of surgical specimen will be performed. Upon excision during surgery, the entire fresh specimen will be cut into slices and imaged by the optical imaging system in overlay images of white light and fluorescence mode. Next, tissue will be embedded into paraffin blocks and overlay images of white light and fluorescence will be taken. H&E staining will be performed, and the morphology of the sections will be assessed by an experienced pediatric oncology pathologist according to the INPC classification.

6. TREATMENT AND IMAGING PLAN

6.1 TREATMENT ADMINISTRATION

Treatment will be administered on an *inpatient* basis. After the infusion ends (24hr), and if the patient is pain-free for 1 hour, the patient can be discharged from the hospital and return for the blood samples and 1 day prior to surgery. Reported adverse events and potential risks are described in Section 7. No investigational or commercial agents or therapies other than those described below may be administered with the intent to treat the patient's malignancy.

Regimen Description					
Agent	Premedication; Dose Precautions	Dose	Route	Infusion time	Schedule
Anti-GD2-IRDye800CW	Administer adequate opioid dose 10 minutes prior to anti-GD2-IRDye800CW	** in 500 cc NS	IV (10 mg/m ² over 24 hours, infusion)	10 mg/m ² over 24 hours, infusion (lower doses in same rate, less infusion time, so 0,42mg/m ² per hour)	96 hours before surgery
**Doses as appropriate for assigned dose level.					

Pain and allergic reactions are clinically significant in the short term, since GD2 is expressed in healthy tissue on pain fibers. To limit the side-effects of the anti-GD2 (pain, urticaria), patients shall receive opiates and/or antihistamines similar to standard immunotherapy treatment protocol.

6.2 ACQUISITION OF IMAGING DATA

The fluorescent camera system will be used to record tumor tissue identified under normal light (non-fluorescence) and under fluorescence prior to surgical excision, and again under fluorescence after surgical excision tumor tissue. After the tumor specimen has been resected, a third image will be obtained to measure the background after the debulking surgery has taken place (**figure 4**). Implementation of this research during surgery will extend the complete operation time with approximately 15 minutes. Switching from the normal light modus (“white light”) to fluorescent light modus can be done within seconds. Fluorescent detection of tumor tissue can thus be performed quick, although visualization of the tumor and its adjacent tissue is needed to ensure all possible fluorescent signals of the surrounding organs are being obtained and measured. During surgery, when the fluorescent light modus is turned on, a video will be recorded. Postoperatively, these images will be assessed to determine the TBR.

Postoperatively, fluorescence signal of multiple histological slides will be detected by fluorescence microscopy.

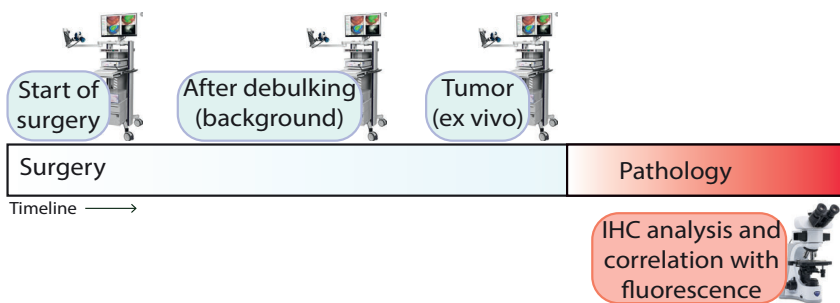


Figure 4. Three images to capture the intensity of the fluorescence signal will be captured with the Quest camera at different time points during surgery. During pathology assessment, a fluorescence microscope will quantify the fluorescence signal ex vivo.

Analysis

The fluorescence intensity of all images will be quantified measuring the mean fluorescence intensity (MFI) of the Quest Artemis Imaging System (Quest Medical Imaging, Middenmeer, The Netherlands) and the corresponding software. The MFI of the tumor and the MFI of the background area will be calculated. Also, the MFI of the kidney and liver will be collected.

To get the TBR, the MFI of the tumor will be divided by the MFI of the background.

6.3 SUPPORTIVE CARE GUIDELINES

The supportive care guidelines will be carried out as described in the long-term infusion protocol for immunotherapy:

A pediatric oncologist, specialized nurse practitioner or a nurse specialist will be involved during the infusion. Pain and allergic reactions are clinically significant in the short term, since GD2 is expressed in healthy tissue on pain fibers. It is thought that complement activity is primarily responsible for pain side effects²³. To limit the side-effects of the anti-GD2 (pain, urticaria), patients will receive analgesia and/or antihistamines according to standard treatment protocol starting 1 hour before infusion of anti-GD2. The standard supportive care protocol in the Princess Máxima Center contains paracetamol oral (60mg/kg/day), bolus injections of morphine and levocetirizine oral, 2 times a day, dose based on age.

Children will be monitored during infusion. Blood pressure and heart rate are to be assessed every 30min for the first 2 hours, after that every 5 hours during the 24-hour infusion.

6.4 DOSING DELAYS/DOSE MODIFICATIONS AND ADVERSE EVENT MANAGEMENT

The infusion will be stopped in case of any severe adverse events, graded according to the CTCAE as \geq grade 3 or upon the opinion of the treating physician. The amount of anti-GD2-IRDye800CW administered at that point, will be calculated and documented. Dose adjustments are to be made according to the greatest degree of toxicity but are not to be expected giving the results of the anti-GD2 immunotherapy protocol (see 6.6). Adverse events will be graded using the NCI Common Terminology Criteria for Adverse Events Version 5.0 (CTCAE).

Adverse events known from anti-GD2 infusion studies are:

- Cytokine release syndrome (fever, hypotension, urticaria)
- Anaphylactic reaction
- Capillary leak syndrome (hypotension, tachycardia, oedema)
- Decreased diuresis
- Bladder retention (as a side effect from the morphine)
- Visual problems (In case of less sight: discuss with the oncologist)
- Peripheral neuropathy, transverse myelitis, unknown neurological complaints
- Systemic infections
- Hematological toxicity
- Liver- and electrolyte irregularities

These toxicities are merely present at administration of higher dosis of *Dinutuximab* than 10mg/m²/day.

6.5 DURATION OF FOLLOW UP

All patients participated in this study will be followed for 30 days after surgery.

6.6 CRITERIA FOR REMOVAL FROM STUDY

Adverse Events

In case of severe adverse events during administration, the infusion of the anti-GD2-IRDye800CW will be stopped. The dose that is administrated will be calculated after the stop of iv infusion. Since the patients will not receive a second dose, the patients will not be removed from the protocol. During surgery, it will be investigated if the amount of dose that reached the patient is sufficient for imaging the tumor. Patients with adverse events will be treated and followed according to established, acceptable medical practice. The adverse events and the adjusted dose must be documented in the Case Report Form.

Withdrawal of consent

The patient's desire to withdraw from the study may occur at any time. The investigator should carefully consider whether the patient's withdrawal of consent is due to an adverse event, and if so, record the adverse event as the reason for withdrawal.

Withdrawal by the physician

For clinical reasons not related to study drug treatment in the absence of an adverse event.

7. ADVERSE EVENT REPORTING REQUIREMENTS

Any serious adverse event must be reported to the EMA as soon as possible but no later than 5 calendar days.

7.1 EXPECTED ADVERSE EVENTS USING ANTI-GD2-IRDYE-800CW

This is a first-in-human study of the conjugate anti-GD2-IRDye800CW. Separately, anti-GD2 and IRDye800CW are cGMP products and have been clinically tested. Therefore, we do not expect new adverse events other than reported for *Dinutuximab* (anti-GD2). However, we will monitor closely for adverse events.

7.2 ADVERSE EVENT CHARACTERISTICS

- **CTCAE term (AE description) and grade:** The descriptions and grading scales found in the revised NCI Common Terminology Criteria for Adverse Events (CTCAE) version 4.0 will be utilized for AE reporting. All appropriate treatment areas should have access to a copy of the CTCAE version 4.0. A copy of the CTCAE version 4.0 can be downloaded from the CTEP website:
http://ctep.cancer.gov/protocolDevelopment/electronic_applications/ctc.htm.

- **For expedited reporting purposes only:**
 - AEs for the agent that do not require expedited reporting are defined in Section 7.1.
 - Other AEs for the protocol that do not require expedited reporting are outlined in section 7.3.

- **Attribution of the AE:**
 - Definite – The AE *is clearly related* to the study treatment.
 - Probable – The AE *is likely related* to the study treatment.
 - Possible – The AE *may be related* to the study treatment.
 - Unlikely – The AE *is doubtfully related* to the study treatment.
 - Unrelated – The AE *is clearly NOT related* to the study treatment.

- An adverse event is considered **serious (SAE)** if it results in **ANY** of the following outcomes:
 - Death

- o A life-threatening adverse event
- o An adverse event results in inpatient hospitalization or prolongation of existing hospitalization for ≥ 24 hours
- o A persistent or significant incapacity or substantial disruption of the ability to conduct normal life functions
- o Important Medical Events (IME) that may not result in death, be life threatening, or require hospitalization may be considered serious when, based upon medical judgment, they may jeopardize the patient or subject and may require medical or surgical intervention to prevent one of the outcomes listed in this definition.

7.3 ROUTINE ADVERSE EVENT REPORTING

All Adverse Events **must** be reported in routine study data submissions.

8. PHARMACEUTICAL AND IMAGING AGENT INFORMATION

A list of the adverse events and potential risks associated with the investigational agent administered in this study can be found in Section 7.1.

Source and Pharmacology: Anti-GD2 is a chimeric monoclonal antibody of the IgG1 subclass. It is purified by affinity and ion exchange chromatographies and filtered to remove pathogens, included viruses. The final product is tested to assure that it is free of nucleic acid, viruses, bacteria, fungi, mycoplasm and pyrogens.

Supplier: Anti-GD2-IRDye800CW will be manufactured under GMP conditions by a contracted manufacturer as an investigational agent for the Princess Máxima Center.

Route of administration: IV infusion

8.1 INVESTIGATIONAL AGENT(S)

Confidential

Pharmaceutical information for investigational study agents supplied by CTEP will be provided as attachments to the approved Letter of Intent (LOI) response and will be inserted once finale approval of our GMP product is arranged.

Agent Ordering and Agent Accountability

NCI-supplied agents may be requested by the Principal Investigator (or their authorized designee). Pharmaceutical Management Branch (PMB) policy requires that agent be shipped directly to the institution where the patient is to be treated. PMB does not permit the transfer of agents between institutions (unless prior approval from PMB is obtained). The CTEP-assigned protocol number must be used for ordering all CTEP-supplied investigational agents. The responsible investigator in case of multiple participating institutions at each participating institution must be registered with CTEP, DCTD through an annual submission of FDA Form 1572 (Statement of Investigator), Curriculum Vitae, Supplemental Investigator Data Form (IDF), and Financial Disclosure Form (FDF). If there are several participating investigators at one institution, CTEP-supplied investigational agents for the study should be ordered under the name of one lead investigator at that institution.

Active CTEP-registered investigators and investigator-designated shipping designees and ordering designees can submit agent requests through the PMB Online Agent Order Processing (OAOP). Access to OAOP requires the establishment of a CTEP Identity and Access Management (IAM) account and the maintenance of an “active” account status and a “current” password.

Agent Inventory Records – The investigator, or a responsible party designated by the investigator, must maintain a careful record of the inventory and disposition of all agents received from DCTD using the NCI Drug Accountability Record Form (DARF). (See the NCI Investigator’s Handbook for Procedures for Drug Accountability and Storage.)

9. STUDY CALENDAR

9.1 BASELINE/PRE-STUDY EVALUATIONS

Visit 1: Screening, Day -28 to day 0

During Visit 1/Screening (up to 4 weeks prior to surgery), subjects who provide written informed consent, and who have an established diagnosis of neuroblastoma will undergo

- Complete medical history and physical examination
- Vital signs and weight
- Clinical chemistry, hematology, and urinalysis laboratory assessments
- Evaluation of inclusion and exclusion criteria
- Collection of concomitant medication information.

This population of patients can consist of patients that already underwent a pre-operative biopsy.

9.2 DURING TREATMENT

Visit 2: 72 – 96 hours prior to surgery

Eligible subjects will have the following procedures performed:

- Any changes in concomitant medications will be recorded and AEs will be collected. Medical history and physical examination will be updated as needed. During and post-infusion of the anti-GD2-IRDye800CW, AEs and ADEs will be collected.
- A single dose of anti-GD2-IRDye800CW will be administered IV (over 24 hours or less) to each subject starting 96 hours prior to surgery. The dose will be assigned by the Trial Pharmacy.
- Vital signs will be taken every 1 hour during infusion for the first 2 hours and followed up daily until surgery is initiated. Patients will be monitored during the full infusion time.
- Blood samples will be taken at 0, + 60, + 120min, +24 hours and immediately prior to surgery to assess serum fluorescence intensity. A time range of +/- 10 min is approved.
- Urinalysis will be performed at 0, 2, 24 and 96 (prior to surgery) hours to measure fluorescence intensity (surrogate measure of anti-GD2-IRDye800CW).

Visit 3: Time of surgery

- AE's will be collected 24 hours before surgery
- Vital signs will be taken prior to surgery
- Blood samples will be taken to assess serum fluorescence intensity.
- Urinalysis will be performed and checked for fluorescence intensity.

9.3 FOLLOW-UP EVALUATION

Visit 4 (Follow-up, Day 14 \pm 3, this can be planned together with the follow-up appointment to the clinician)

Subjects will return to the site and the following information will be recorded:

- Vital signs
- AE-assessments
- Concomitant medications
- Blood samples for clinical laboratory assessments and serum anti-GD2-IRDye800CW level
- Urinalysis

o Summary Table

All indicated times are in a time range of +/- 10 min. The exact timing of the measurement should be written on the CRF.

Table 1. Schedule of study procedures

	Pre- Study	Base- line	Dose	+1 h	+2 h	+24 h	+ 96 h	+14 days
Anti-GD2-IRDye800CW			X					
Informed consent	X							
Demographics	X							
Medical history	X							
Concurrent meds		X						X
Physical exam	X	X					X	X
Vital signs	X	X	X	X	X	X	X	X
Height	X							
Weight	X	X						X
Performance status	X							
Serum chemistry ^a	X	X	X	X	X	X	X	X
Adverse event evaluation		X						X
B-HCG	X ^b							
Surgery and fluorescent imaging							X	
Urinalysis	X	X			X	X	X	X

a: Albumin, alkaline phosphatase, total bilirubin, bicarbonate, BUN, calcium, chloride, creatinine, glucose, LDH, phosphorus, potassium, total protein, SGOT [AST], SGPT [ALT], sodium.

b: Serum pregnancy test (women of childbearing potential).

10. DATA REPORTING / REGULATORY REQUIREMENTS

Adverse event lists, guidelines, and instructions for AE reporting can be found in Section 7.0 (Adverse Events: List and Reporting Requirements).

Data Reporting

- The Trial Data Center (TDC) from the Princess Máxima Center will be the Data Centre for this trial. The Data Centre will be responsible for registration

- of patients, supply of Case Record Forms (CRFs), receipt of CRF pages, and creation of Clean File.
- Anonymized copies of correspondence / reports concerning efficacy endpoints will be gathered.
 - The CRFs must be completed and signed by the surgeon or one of his/her authorized staff members as soon as the requested information is available. In all cases it remains the responsibility of the investigator to check that original CRFs are sent to the Data Centre and to verify that they are completed and filled out correctly.
 - The CRF will have the form of a booklet that can serve as source document. After completion, the original pages must be sent to the Data Centre. The CRF copy must be kept together with the patient's records. If information is not known, this must be clearly indicated.
 - To enable peer review and/or inspections from Health Authorities, the investigator must agree to keep records, including the identity of all participating subjects (sufficient information to link records, e.g., CRFs and hospital records), all original signed Informed Consent Forms, copies of all CRFs. To comply with international regulations, the records should be retained by the Investigator for 15 years.

11. STATISTICAL CONSIDERATIONS

11.1 STUDY DESIGN/ENDPOINTS

Alternative 3 + 3 Recruitment Strategy

This study is a proof-of-concept study. Pharmacokinetic characteristics of anti-GD2-IRDye800CW will be assessed to draw a decision, together with the optimal TBR, on what an efficient dose of the conjugate should be.

Mean TBR's will be compared using the non-parametric Mann-Whitney U test. TBR data will be presented as mean TBR with standard deviation for all dose groups. Additionally, this will be shown in a chart.

The anti-GD2-IRDye800CW will be administered in cohorts of 3 patients. During and after surgery, fluorescent signals will be assessed by the Quest camera system or by fluorescence microscopy at the pathology department. Of every lesion, the mean fluorescence intensity (MFI) and the fluorescence status (yes/no) and tumor status (y/n, golden standard pathology analysis) will be assessed.

First, three patients will be administered with the first dose. The TBR of the first three patients will be determined. If the fluorescence signal is < 2.0 or absent, the infusion time window will be reassessed (96 hours). If the first dose is sufficient in 2/3 or 3/3 patients, the 2nd dose will be administered in the second 3 patients (3mg/m²). When 2/3 or 3/3 patients have a TBR > 2.0 , another cohort of 3 patients will be administered with the 3rd dose (1mg/m²). After these TBR's have been established, the recommended phase 2 dose will be determined, and three extra patients will be administered with that dose.

What we suggest is an alternative 3+3 dose escalation approach. However, since we want to establish the lowest dose that is still efficient and minimal dose toxicity of anti-GD2 (10 mg/m²) has been established in this patient cohort, we do believe this is the most ethical and efficient way to approach this research question.

11.2 SAMPLE SIZE/ACCRUAL RATE

Since this is a proof-of-principle study, first to be ever performed in children, we have chosen to use an adaptive recruitment strategy and test three different set doses in groups of a maximum of three patients, where we will add +3 patients in the dose group that looks the most optimal. The sample size of this feasibility study will be 12 patients. Currently, in the Princess Máxima Center, between 10 - 15 patients will undergo debulking surgery for High-Risk neuroblastoma per year. We expect to achieve this number of potential candidates in one year.

11.3 STRATIFICATION FACTORS

Dose escalation and the Maximal Tolerated Dose determination will not be performed for this study.

12.5 ANALYSIS OF SECONDARY ENDPOINTS

- Treatment related adverse events after injection of the conjugate anti-GD2-IRDye800CW
- Changes in serum pharmacokinetics; blood samples will be taken at t=0 (just before infusion), t=60min (after infusion), t=120min (after infusion), t=24h, t=72-84hr (at intake before surgery), immediately before surgery (t=96h) and 24hr after surgery (t=96). Blood samples can be taken 10 min before or after the indicated timepoint.
- The optimum dose is defined as the lowest dose of the administered immunoconjugate giving an adequate TBR of >2.0 .

We will compare the mean of the different groups with the Mann-Whitney U test. In case we find the same TBR's for different dose cohorts, we will choose the lowest dose with the highest TBR (minimal > 2.0) for the recommended phase II dose.

Negative predictive value will be determined by the true negative lesions divided by the sum of the true negative lesions and the false negative lesions according to the pathologist.

The positive predictive value will be determined by the true positive lesions divided by the sum of the true positive and the false positive lesions according to the pathologist.

AEs and treatment-emergent adverse events (TEAEs) will be summarized by body system and presented by severity and causal relationship to study drug. AE's will be coded using the Medical Dictionary for Regulatory Activities and listed.

Subjects experiencing serious AEs will be listed and summarized in tabular format.

Patient characteristics and vital signs will be summarized using descriptive statistics. Pathology and immunohistochemical results will be listed per subject.

13. QUALITY ASSURANCE

Registration reports will be generated by the Study Coordinator to monitor patient accruals and completeness of registration data. Routine data quality reports will be generated to assess missing data and inconsistencies. Accrual rates, accuracy of evaluations and follow-up will be monitored periodically throughout the study period and potential problems will be brought to the attention of the study team for discussion and action.

Random-sample data quality and protocol compliance audits will be conducted by the study team on an ongoing basis.

13.6 CONTROL OF DATA CONSISTENCY

A Research Nurse will be assigned to the study. The responsibilities of the Research Nurse include project compliance, data collection, abstraction and entry, data reporting, regulatory monitoring, problem resolution and prioritization, and coordinate the activities of the protocol study team. The data collected for this

study will be entered into a secured database. Source documentation will be available to support the computerized patient record.

13.7 CENTRAL REVIEW OF PATHOLOGY

Data of histology relevant to this study will be collected by the Study Coordinator, reviewed by pediatric oncology pathologists, and stored at the Pathology Department of the Princess Máxima Center.

14. ETHICAL CONSIDERATIONS

14.1 PATIENT PROTECTION

The responsible investigator will ensure that this study is conducted in agreement with either the Declaration of Helsinki (Tokyo, Venice, Hong Kong, Somerset West and Edinburgh amendments) or the laws and regulations of the country, whichever provides the greatest protection of the patient.

The protocol has been written, and the study will be conducted according to the ICH Harmonised Tripartite Guideline for Good Clinical Practice (ref: http://www.ich.org/fileadmin/Public_Web_Site/ICH_Products/Guidelines/Efficacy/E6_R1/Step4/E6_R1_Guideline.pdf).

The protocol will be approved by the Local Ethics Committees.

14.2 SUBJECT IDENTIFICATION

All patients enrolled will be pseudo-anonymized and given a study-number. The study-coordinator will be the only one having access to the encryption key making it possible to relate the study data to the clinical outcome.

14.3 INFORMED CONSENT

All patients will be informed of the aims of the study, the possible adverse events, the procedures and possible hazards to which she/he will be exposed, and the mechanism of treatment allocation. They will be informed as to the strict confidentiality of their patient data, but that their medical records may be reviewed for trial purposes by authorized individuals other than their treating physician. An example of a patient informed consent statement is given as an appendix to this protocol.

It is the responsibility of the individual investigator to translate the enclosed informed consent document. The translated version should be dated, and version controlled.

The bold sections of the enclosed informed consent document are the sections that **must** appear in the translation.

The translated informed consent form is part of the documents to be submitted to the ethics committee for approval. The competent ethics committee for each institution must validate local informed consent documents before the center can join the study. It is the responsibility of the Local Ethical Committee to guarantee that the translation is conforming to the ICH-GCP guidelines.

It will be emphasized that the participation is voluntary and that the patient is allowed to refuse further participation in the protocol whenever he/she wants. This will not prejudice the patient's subsequent care. Documented informed consent must be obtained for all patients included in the study before they are registered or randomized in the study. This must be done in accordance with the national and local regulatory requirements.

For European Union member states, the informed consent procedure must conform to the ICH guidelines on Good Clinical Practice. This implies that "the written informed consent form should be signed and personally dated by the patient or by the patient's legally acceptable representative".

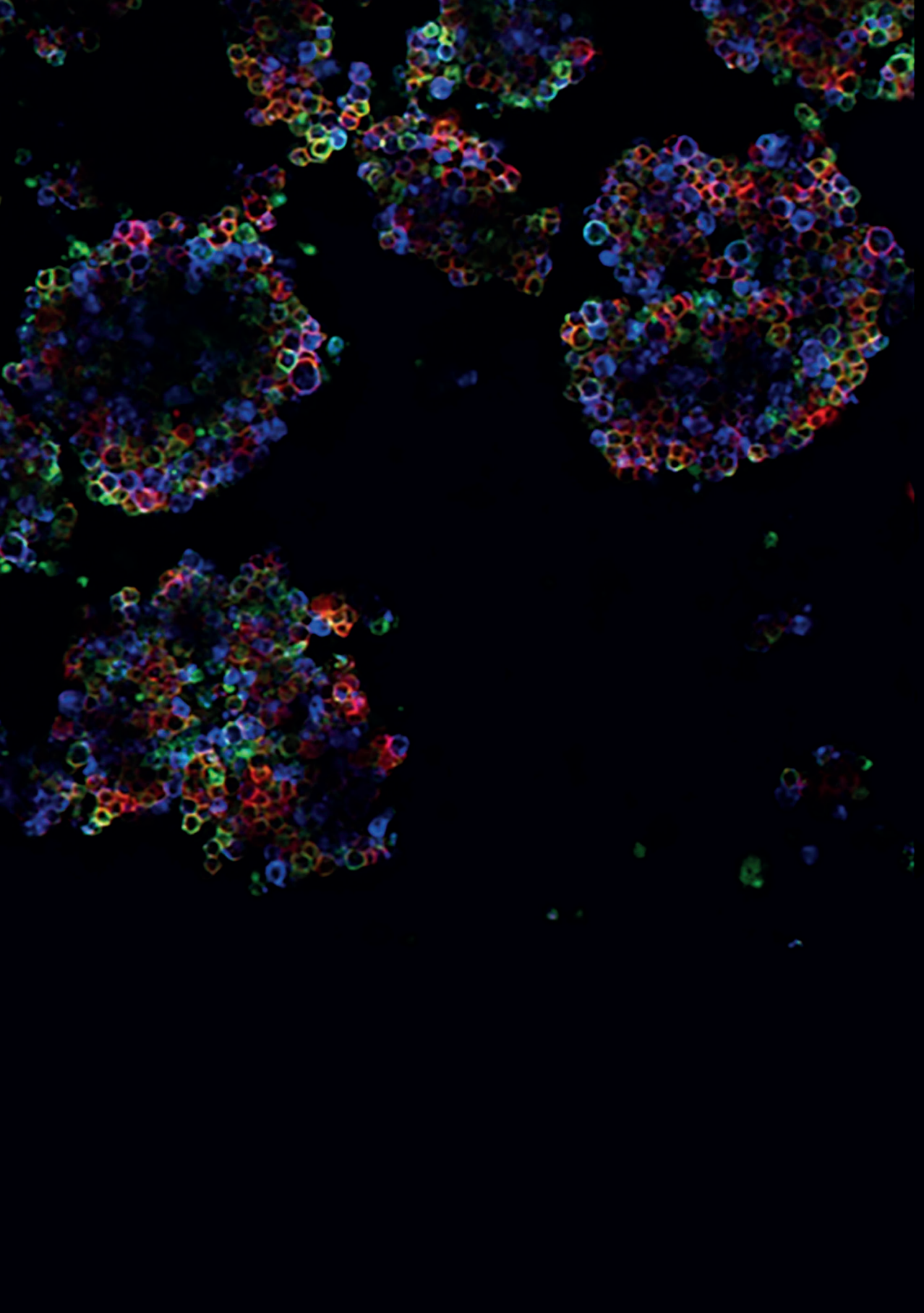
15. PUBLICATION POLICY

Regardless the outcome, results will be submitted to a peer reviewed journal. Results will be published after the inclusion of all patients, pathological assessment and statistical analyses are finalized. The study coordinator will be the (co)first author, the trial-coordinator will be the final author. All persons contributing to the trial will be co-authors or named in the acknowledgements, depending on their efforts.

REFERENCES

- 1 Louis, C. U. & Shohet, J.M. Neuroblastoma: molecular pathogenesis and therapy. *Annu Rev Med* 66, 49-63, doi:10.1146/annurev-med-011514-023121 (2015).
- 2 Shimada, H. et al. Terminology and morphologic criteria of neuroblastic tumors: recommendations by the International Neuroblastoma Pathology Committee. *Cancer* 86, 349-363 (1999).
- 3 Jans M., W.M., Van De Ven C., Van Baren R., Tytgat G., Zwaveling S. . *Analysis of Surgery for Neuroblastoma in The Netherlands* (Catalogue No. S5-S321 (abstr O-155), SIOP 2016 Scientific Programme+Index).
- 4 Irwin, M.S. & Park, J.R. Neuroblastoma: paradigm for precision medicine. *Pediatr Clin North Am* 62, 225-256, doi:10.1016/j.pcl.2014.09.015 (2015).
- 5 von Allmen, D. et al. Impact of Extent of Resection on Local Control and Survival in Patients From the COG A3973 Study With High-Risk Neuroblastoma. *J Clin Oncol* 35, 208-216, doi:10.1200/JCO.2016.67.2642 (2017).
- 6 Nagaya, T., Nakamura, Y.A., Choyke, P.L. & Kobayashi, H. Fluorescence-Guided Surgery. *Front Oncol* 7, 314, doi:10.3389/fonc.2017.00314 (2017).
- 7 Harlaar, N.J. et al. Molecular fluorescence-guided surgery of peritoneal carcinomatosis of colorectal origin: a single-centre feasibility study. *Lancet Gastroenterol Hepatol* 1, 283-290, doi:10.1016/S2468-1253(16)30082-6 (2016).
- 8 Lamberts, L.E. et al. Tumor-Specific Uptake of Fluorescent Bevacizumab-IRDye800CW Microdosing in Patients with Primary Breast Cancer: A Phase I Feasibility Study. *Clin Cancer Res* 23, 2730-2741, doi:10.1158/1078-0432.CCR-16-0437 (2017).
- 9 Olson, E.S. et al. Activatable cell penetrating peptides linked to nanoparticles as dual probes for in vivo fluorescence and MR imaging of proteases. *Proc Natl Acad Sci U S A* 107, 4311-4316, doi:10.1073/pnas.0910283107 (2010).
- 10 Weissleder, R., Tung, C. H., Mahmood, U. & Bogdanov, A., Jr. In vivo imaging of tumors with protease-activated near-infrared fluorescent probes. *Nat Biotechnol* 17, 375-378, doi:10.1038/7933 (1999).
- 11 Aaboud, M. et al. Electron efficiency measurements with the ATLAS detector using 2012 LHC proton-proton collision data. *Eur Phys J C Part Fields* 77, 195, doi:10.1140/epjc/s10052-017-4756-2 (2017).
- 12 Cheresh, D.A., Harper, J.R., Schulz, G. & Reisfeld, R.A. Localization of the gangliosides GD2 and GD3 in adhesion plaques and on the surface of human melanoma cells. *Proc Natl Acad Sci U S A* 81, 5767-5771 (1984).
- 13 Svennerholm, L. et al. Gangliosides and allied glycosphingolipids in human peripheral nerve and spinal cord. *Biochim Biophys Acta* 1214, 115-123, doi:10.1016/0005-2760(94)90034-5 (1994).
- 14 Yu, A.L. et al. Anti-GD2 antibody with GM-CSF, interleukin-2, and isotretinoin for neuroblastoma. *N Engl J Med* 363, 1324-1334, doi:10.1056/NEJMoa0911123 (2010).
- 15 Ter Weele, E.J. et al. Development, preclinical safety, formulation, and stability of clinical grade bevacizumab-800CW, a new near infrared fluorescent imaging agent for first in human use. *Eur J Pharm Biopharm* 104, 226-234, doi:10.1016/j.ejpb.2016.05.008 (2016).

- 16 Gao, R.W. *et al.* Safety of panitumumab-IRDye800CW and cetuximab-IRDye800CW for fluorescence-guided surgical navigation in head and neck cancers. *Theranostics* 8, 2488-2495, doi:10.7150/thno.24487 (2018).
- 17 Wellens, L.M. *et al.* Anti-GD2-IRDye800CW as a targeted probe for fluorescence-guided surgery in neuroblastoma. *Sci Rep* 10, 17667, doi:10.1038/s41598-020-74464-4 (2020).
- 18 Ozkaynak, M.F. *et al.* Phase I study of chimeric human/murine anti-ganglioside G(D2) monoclonal antibody (ch14.18) with granulocyte-macrophage colony-stimulating factor in children with neuroblastoma immediately after hematopoietic stem-cell transplantation: a Children's Cancer Group Study. *J Clin Oncol* 18, 4077-4085, doi:10.1200/JCO.2000.18.24.4077 (2000).
- 19 Gilman, A.L. *et al.* Phase I study of ch14.18 with granulocyte-macrophage colony-stimulating factor and interleukin-2 in children with neuroblastoma after autologous bone marrow transplantation or stem-cell rescue: a report from the Children's Oncology Group. *J Clin Oncol* 27, 85-91, doi:10.1200/JCO.2006.10.3564 (2009).
- 20 Reagan-Shaw, S., Nihal, M. & Ahmad, N. Dose translation from animal to human studies revisited. *FASEB J* 22, 659-661, doi:10.1096/fj.07-9574LSF (2008).
- 21 Yu, A.L. *et al.* Phase I trial of a human-mouse chimeric anti-disialoganglioside monoclonal antibody ch14.18 in patients with refractory neuroblastoma and osteosarcoma. *J Clin Oncol* 16, 2169-2180, doi:10.1200/JCO.1998.16.6.2169 (1998).
- 22 Lu, G. *et al.* Tumour-specific fluorescence-guided surgery for pancreatic cancer using panitumumab-IRDye800CW: a phase I single-centre, open-label, single-arm, dose-escalation study. *Lancet Gastroenterol Hepatol*, doi:10.1016/S2468-1253(20)30088-1 (2020).
- 23 Navid, F. *et al.* Phase I trial of a novel anti-GD2 monoclonal antibody, Hu14.18K322A, designed to decrease toxicity in children with refractory or recurrent neuroblastoma. *J Clin Oncol* 32, 1445-1452, doi:10.1200/JCO.2013.50.4423 (2014).




A large white circle is centered on a black background. The text "PART 4" is written in bold, black, sans-serif capital letters inside the circle. At the bottom of the page, there are several clusters of small, colorful, abstract shapes in shades of blue, green, red, and yellow, resembling microscopic cells or particles.

PART 4



CHAPTER 8



**General Discussion
& Future Perspectives**

Pediatric oncologic surgery can be improved by bringing novel imaging strategies from the scientific bench to the operation room. This thesis focusses on 3D imaging innovation in surgery for children with neuroblastoma and Wilm's tumors. By combining the latest 3D visualization developments with implemented imaging modalities for Wilms' tumors (**chapter 2**), reviewing the literature on complications of neuroblastoma surgery (**chapter 3**), and by exploring the possibilities for new scientific visualization techniques during surgery of neuroblastoma (**chapter 4**) and using the latest 3D in vitro modelling technology (**chapter 5 and 6**), the first results were used to generate a protocol for a phase I clinical trial (**chapter 7**) using a near-infra red fluorescence antibody during surgery in pediatric oncology.

PRE-OPERATIVE 3D IMAGING CAN ASSIST THE SURGEON AND SHOULD BE DEVELOPED FURTHER TO BE USED DURING THE SURGICAL PROCEDURE.

State of the art preoperative imaging is of paramount importance in achieving good results during oncological surgery. **Chapter 2** shows that novel 3D visualization techniques could be a useful assisting tool in planning and performing nephron sparing surgery in Wilms Tumors. Personalized 3D models of pediatric WT in children were constructed to function as training objects for preoperative planning. This chapter indicates that preoperative 3D imaging strategies help increase the surgeons' knowledge on the patient specific anatomy of the kidney, consistent with data in adult surgery¹⁻³. 3D models can be useful for improving the planning of tumor resection and optimizing the procedure of choice; nephron sparing surgery or total nephrectomy. This could potentially improve the radicality of tumor resection and spare healthy tissue, thereby preserving long-term renal function. However, effectiveness of this approach still needs to be confirmed and this study is primarily based on the surgeon's opinion. Therefore, more research needs to be performed to objectively establish the value of these new imaging modalities in pediatric surgery.

High quality conventional imaging (MRI or CT) is key for obtaining useful pre-operative 3D reconstructions. For further objective and accurate conversion of these imaging data into 3D prints or AR holograms, research should focus on creating standardized algorithms. There is a need for more research into standardizing the optimal imaging method (MRI, CT or CT-angiogram), slice thickness and timing for contrast enhancement, specifically in children of different ages.

With the development of standardized algorithms in mind, another challenge for the clinical application of the proposed novel 3D visualization techniques is

the conversion of the radiology data into 3D segmentations. The large amount of information produced by CT or MRI requires the interpretation of experienced radiologists. In **chapter 2**, the segmentation of CT and/or MRI scans to 3D models is performed manually in close collaboration between an information technology expert, pediatric radiologist and pediatric surgeon. When the standardization of this process is obtained, it would save valuable time for these experts. But again, high quality of the segmentation process for the 3D visualizations and accuracy of interpretation needs to be guaranteed when developing standardized algorithms and before expanding its clinical use in pediatric oncological surgery. As a future perspective, the 3D generated hologram developed in **chapter 2**, should be used during the surgery. When the anatomy of the hologram correlates perfectly to the real-life situation in the individual patient, the complete resection of the tumor could be guided by the generated hologram in a live setting.

COMPLICATIONS IN NEUROBLASTOMA SURGERY SHOULD BE REPORTED IN A STANDARDIZED WAY.

In the early nineties, neuroblastoma surgery had a complication rate between 5 and 25%^{4,5}. The risk of complications associated with the surgical resection of neuroblastoma depends on the location of the tumor, the risk-assessment of the surgeon and the timing of the procedure. **Chapter 3** reviewed the number of complications published in the last three decades. Our results showed a wide variety of complication rates reported, of which the most common found complications were (major) hemorrhage and unplanned nephrectomies, mainly the result of encasement of the vasculature and surgeons striving for complete resection of neuroblastoma⁶⁻⁸. When comparing the results in the Netherlands retrospectively and prospectively, a complication rate of 40% was found⁹. This indicates that there is a discrepancy between our complication rate and the lower reported rate in literature. Underreporting of complications in the existing literature using retrospective studies and the lack of standardization on registration of complications may have contributed to this huge difference. In **chapter 3**, we refer to a new way to report complications that we believe should be used by all pediatric surgeons performing neuroblastoma surgery¹⁰.

FLUORESCENCE GUIDED SURGERY HAS THE POTENTIAL TO LOWER COMPLICATIONS DURING THE DEBULKING OF NEUROBLASTOMA

In **chapter 4**, the first pediatric FGS-target is investigated, showing the feasibility of intraoperative fluorescence imaging of neuroblastoma with anti-GD2-IRDye800CW in a mouse model. As described in **chapter 3**, due to encasement of

important vasculature and the surgeon's challenge to discern tumor from healthy tissue, resection is almost never complete and has a high risk for complications¹¹. The additional survival benefit of a gross total resection remains controversial^{8,12,13} and some studies claim no survival benefit¹⁴. Also, the extent to which tumor resection was complete is determined by the subjective impression of the surgeon, which is known to have a poor correlation with the results of post-operative imaging¹⁵. Using fluorescence guided surgery for neuroblastoma resection, will provide a tool to inform the surgeon on what tissue she/he is actually removing and guide them through resection. The extent of resection can thereby be more accurately determined. The results generated in **chapter 4** could open new possibilities to reliably assess the effect of surgery on overall survival. But most importantly, by providing a precise surgery tool to resect tumoral tissue with higher confidence, the number of complications could decrease together with chances of local recurrence due to remaining tumor. In the future, a more accurate quantification of remaining tumor tissue will help the clinician in decision making on post-surgery treatment and be useful in studies of the potential benefit of anti-GD2 immunotherapy in particular.

Before testing efficacy in phase II/III clinical trials, phase I clinical trials will be required to determine the safety of anti-GD2-IRDye800CW. Future research should be focused on merging augmented reality as described in **chapter 2** with fluorescence vision *during* surgery. When looking ahead, it should be within reach to correlate the anatomy of conventional imaging scans (CT and/or MRI) with real-time fluorescence signal taken up by near-infrared camera systems, as is currently being investigated in neurosurgery¹⁵. This way, a surgeon can operate on tumor tissue, while seeing fluorescence with an augmented reality visualization system. In conclusion, **chapter 4** presents the first pediatric cancer specific tracer with potential for the vast majority of high-risk neuroblastoma patients to guide tumor resection with greater accuracy, and thereby has the potential of lowering the risk of surgical complications and reducing the incidence of local recurrence. The transformation of these results into a clinical trial are presented in **chapter 7**.

THE ORGANOID IMAGING PLATFORM IS A HIGH-THROUGHPUT TECHNIQUE TO GENERATE FAST RESULTS ON THE EFFICACY OF FLUORESCENCE PROBES.

Although GD2 has proven to be a very successful preclinical target as described in **chapter 4**, it is not uniformly expressed in all patients with neuroblastoma. Therefore, there is a need to investigate more candidate targets suitable for fluorescence guided surgery. The existing ways of investigation are time and material consuming, requiring laborious *in vitro* and *in vivo* experiments. In

chapter 6, we took a combined organoid and 3D imaging approach, to establish a new pipeline for developing and testing suitable probes for the future use of FGS in Neuroblastoma. Here, the protocol described in **chapter 5** was leading to generate high quality microscopic images. By using 3D-rendering of confocal- or multiphoton- microscopy data, the specificity and discriminative potential of probes could be studied in organoid models and effectively quantified and compared, in order to select the most promising candidates for further *in vivo* validation in an efficient way. **Chapter 6** shows that 3D imaging with the organoid platform generates adequate information on the cellular composition and potential of fluorescence antibodies. Furthermore, the fluorescence signal of the 3D images of the organoids shows a correlation with the results of the *in vivo* fluorescence signal. This could mean that 3D imaging of organoids is similarly effective in predicting the efficiency of fluorescence and has the potential to replace *in vivo* experiments with mice. The platform implicates higher throughput and generates faster results. With its use, it could contribute to the reduction and welfare of animals in science by reducing the need of animal experiments⁶. A platform like this can be useful for all sorts of tumors, with now a high number of organoids available¹⁷⁻²¹. In this chapter, we screened for potential fluorescence guided surgery probes, but with the right microscopy techniques, it can also be of use for drug screening or testing for cancer targeting therapies. The protocol as described in **chapter 5** and referred to in the above, was used to establish the high-throughput organoid imaging platform. However, for these organoid imaging platforms to be widely used to assess multiple tumors in a personalized matter, it should be taken into account that this complex technology requires advanced microscopes and the knowledge and training to use them.

Another future perspective, given the time window of multiple months in between the diagnosis of neuroblastoma and the debulking surgery, is that organoids can be grown from the primary biopsy of neuroblastoma. When the organoids are generated, *in vitro* experiments can be performed to test the efficacy of different fluorescent tracers using the organoid platform, ideally without the use of an animal model. This way, the generated organoids can be used to predict the efficiency of NIR fluorescence intra-operatively in a personalized approach. Even multiple probes could be administered to incorporate a personalized fluorescence approach of combined targets. This would lead to the optimal fluorescence strategy for the specific surgical procedure of every individual child undergoing neuroblastoma surgery.

RESULTS GENERATED IN THIS THESIS CREATED THE FIRST FGS CLINICAL PHASE I TRIAL IN CHILDREN

Based on the results of **chapter 4**, we created a protocol for a clinical phase I trial in **chapter 7**. By using anti-GD2-IRDye800CW as a clinical approved antibody combined with a NIR fluorophore – we are on a fast track for getting this tumor-specific tracer in a first-in-child Phase I Trial. The Phase I trial could start after the conjugate anti-GD2-IRDye800CW will receive the Good Manufacturer Practice (GMP) approval, QC release and IRB approval. With anti-GD2 alone already being a GMP approved product used in the clinic, it should be possible to achieve this within a year from now. Important end points will be 1) the establishment of an effective clinical dose to give an adequate fluorescence signal intraoperatively and 2) the fluorescence of the tumor specimen compared to the different morphology stages based on the Shimada classification²² as scored by the pathologist.

CENTRALIZATION OF RESEARCH AND CLINICAL CARE IN PEDI- ATRIC ONCOLOGY IS KEY TO PERFORM OPTIMAL RESEARCH.

In this thesis, basic laboratory techniques were explored to potentially improve surgery. To achieve this, close collaboration between scientists and clinicians was necessary and achieved. To bridge the gap between translational science and clinical healthcare, it is highly important to optimize communication and collaboration between preclinical research and clinical healthcare to maintain a symbiotic research environment. This has been the aim of the Princess Maxima Center. In accordance with other institutes with the same mission in pediatric oncology, such as st. Jude's Children's hospital in Memphis, the Princess Máxima Center houses clinicians and scientist in the same building. This allows for closer collaborations and is one of the reasons this thesis could originate.

IN CONCLUSION

This thesis explored the possibility to bring new imaging techniques to the surgical theatre. 3D visualizations such as augmented reality and 3D printing should be implemented in the preoperative planning of bilateral Wilms tumors in assisting nephron sparing surgery. Implementation of FGS as a precision tool could establish tumor resection of neuroblastoma with greater confidence, a lower risk of surgical complications and unbiased evaluation of the extent of tumor removal, thereby guiding the post-surgery course of treatment. This would fulfill an unmet need in high-risk neuroblastoma that could benefit a wide range of patients. Moreover, the comprehensive preclinical evaluation pipeline, encompassing organoid technology and multiple imaging techniques, can be applied towards the development of

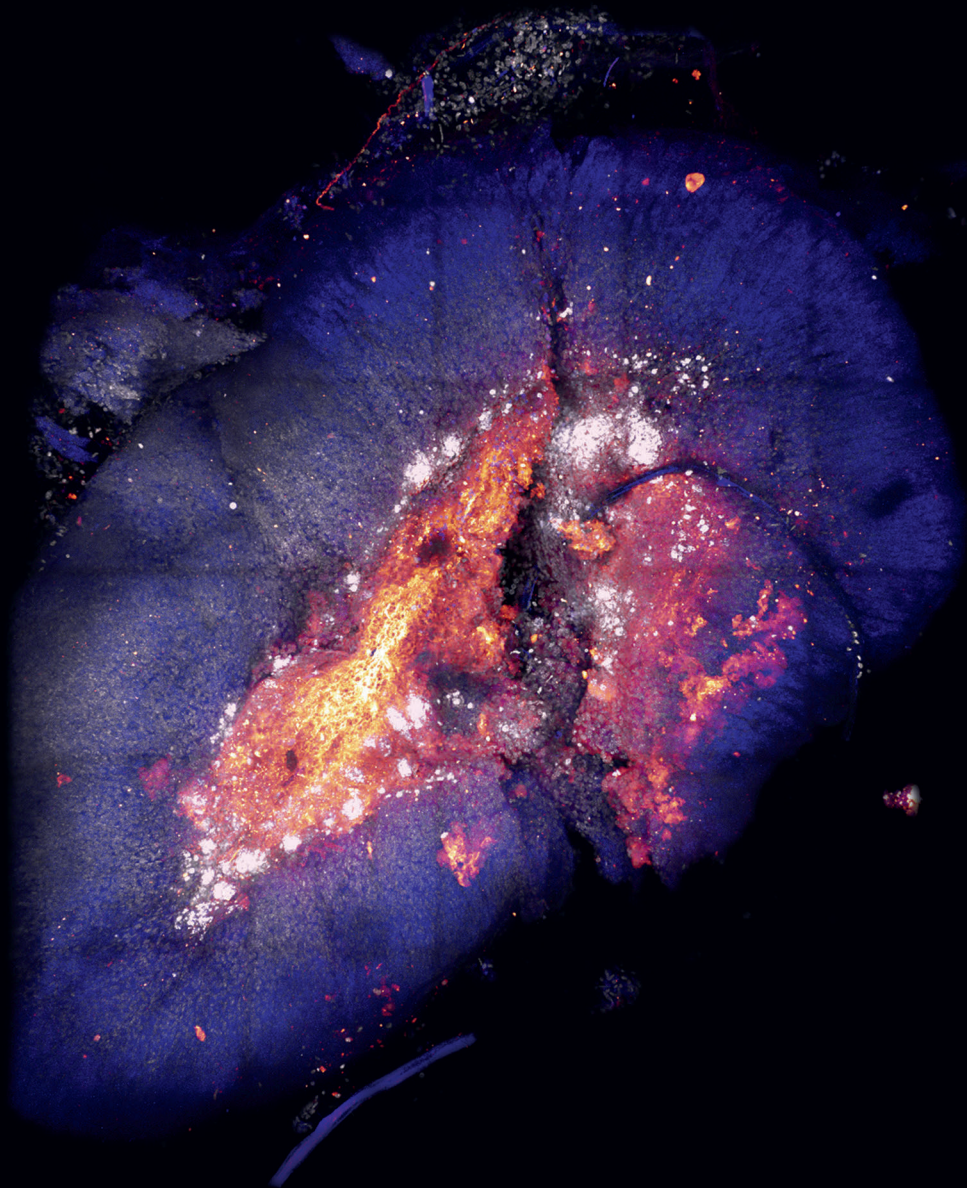
other targeted probes for fluorescence guided surgery. In this thesis, accurate quantification of fluorescence of the investigated probes was described and thereby tumor-specific labeling functionality *in vitro* and preliminary predictive *in vivo* potential was shown. In addition, future research can focus on merging the techniques described in this thesis; using augmented reality to visualize real-time tumor-specific fluorescence intra-operatively. In an ideal situation, all 3D visualization modalities will be combined during surgery. When it will be possible to accurately derive 3D visualizations from conventional imaging, the visualizations can be related to the individual anatomy of the patient. Eventually, augmented reality could combine the personalized anatomy with a fluorescence overlay with NIR-imaging with cellular preciseness and the future will shine bright for surgery in pediatric oncology.

Overall, to improve surgical outcome and to decrease the complication rate in the surgery of pediatric oncology, two main points are to be considered:

1. Investments in new visualization techniques providing real time feedback on cancerous tissue should be made to more accurately remove tumor tissue and decrease surgical related morbidity. It is worth investing further in these visualization techniques and assessing their synergy, when combined.
2. Collaboration between clinicians and scientist is essential, as created in the Princess Máxima Center and the reason behind originating the research described in this thesis. The centralization of surgery and having a specialized surgical team operating all pediatric solid tumors, is key to combine the best possible care with optimal research strategies.

- 1 Wake, N., Bjurlin, M.A., Rostami, P., Chandarana, H. & Huang, W. C. Three-dimensional Printing and Augmented Reality: Enhanced Precision for Robotic Assisted Partial Nephrectomy. *Urology* 116, 227-228, doi:10.1016/j.urology.2017.12.038 (2018).
- 2 Knoedler, M. et al. Individualized Physical 3-dimensional Kidney Tumor Models Constructed From 3-dimensional Printers Result in Improved Trainee Anatomic Understanding. *Urology* 85, 1257-1261, doi:10.1016/j.urology.2015.02.053 (2015).
- 3 Maddox, M. M. et al. 3D-printed soft-tissue physical models of renal malignancies for individualized surgical simulation: a feasibility study. *J Robot Surg* 12, 27-33, doi:10.1007/s11701-017-0680-6 (2018).
- 4 Losty, P., Quinn, F., Breatnach, F., O'Meara, A. & Fitzgerald, R.J. Neuroblastoma--a surgical perspective. *Eur J Surg Oncol* 19, 33-36 (1993).
- 5 Azizkhan, R.G., Shaw, A. & Chandler, J. G. Surgical complications of neuroblastoma resection. *Surgery* 97, 514-517 (1985).
- 6 Rich, B.S. et al. Resectability and operative morbidity after chemotherapy in neuroblastoma patients with encasement of major visceral arteries. *J Pediatr Surg* 46, 103-107, doi:10.1016/j.jpedsurg.2010.09.075 (2011).
- 7 Rich, B.S., McEvoy, M.P., LaQuaglia, M.P. & Wolden, S.L. Local control, survival, and operative morbidity and mortality after re-resection, and intraoperative radiation therapy for recurrent or persistent primary high-risk neuroblastoma. *J Pediatr Surg* 46, 97-102, doi:10.1016/j.jpedsurg.2010.09.068 (2011).
- 8 La Quaglia, M.P. et al. The impact of gross total resection on local control and survival in high-risk neuroblastoma. *J Pediatr Surg* 39, 412-417; discussion 412-417, doi:10.1016/j.jpedsurg.2003.11.028 (2004).
- 9 Jans M., W.M., Van De Ven C., Van Baren R., Tytgat G., Zwaveling S. . *Analysis of Surgery for Neuroblastoma in The Netherlands* (Catalogue No. S5-S321 (abstr O-155), SIOP 2016 Scientific Programme+Index).
- 10 Matthyssens, L.E. et al. A Novel Standard for Systematic Reporting of Neuroblastoma Surgery: The International Neuroblastoma Surgical Report Form (INSRF): A Joint Initiative by the Pediatric Oncological Cooperative Groups SIOPEN*, COG**, and GPOH**. *Ann Surg*, doi:10.1097/SLA.0000000000003947 (2020).
- 11 Cecchetto, G. et al. Surgical risk factors in primary surgery for localized neuroblastoma: the LNESG1 study of the European International Society of Pediatric Oncology Neuroblastoma Group. *J Clin Oncol* 23, 8483-8489, doi:10.1200/JCO.2005.02.4661 (2005).
- 12 Vollmer, K. et al. Radical Surgery Improves Survival in Patients with Stage 4 Neuroblastoma. *World J Surg* 42, 1877-1884, doi:10.1007/s00268-017-4340-9 (2018).
- 13 von Allmen, D. et al. Impact of Extent of Resection on Local Control and Survival in Patients From the COG A3973 Study With High-Risk Neuroblastoma. *J Clin Oncol* 35, 208-216, doi:10.1200/JCO.2016.67.2642 (2017).
- 14 von Schweinitz, D., Hero, B. & Berthold, F. The impact of surgical radicality on outcome in childhood neuroblastoma. *Eur J Pediatr Surg* 12, 402-409, doi:10.1055/s-2002-36952 (2002).

- 15 Incekara, F., Smits, M., Dirven, C. & Vincent, A. Clinical Feasibility of a Wearable Mixed-Reality Device in Neurosurgery. *World Neurosurg* 118, e422-e427, doi:10.1016/j.wneu.2018.06.208 (2018).
- 16 Fenwick, N., Griffin, G. & Gauthier, C. The welfare of animals used in science: how the "Three Rs" ethic guides improvements. *Can Vet J* 50, 523-530 (2009).
- 17 Sachs, N. et al. A Living Biobank of Breast Cancer Organoids Captures Disease Heterogeneity. *Cell* 172, 373-386 e310, doi:10.1016/j.cell.2017.11.010 (2018).
- 18 Schutgens, F. et al. Tubuloids derived from human adult kidney and urine for personalized disease modeling. *Nat Biotechnol* 37, 303-313, doi:10.1038/s41587-019-0048-8 (2019).
- 19 Huch, M. et al. Long-term culture of genome-stable bipotent stem cells from adult human liver. *Cell* 160, 299-312, doi:10.1016/j.cell.2014.11.050 (2015).
- 20 Sato, T. et al. Single Lgr5 stem cells build crypt-villus structures in vitro without a mesenchymal niche. *Nature* 459, 262-265, doi:10.1038/nature07935 (2009).
- 21 Drost, J. & Clevers, H. Organoids in cancer research. *Nat Rev Cancer* 18, 407-418, doi:10.1038/s41568-018-0007-6 (2018).
- 22 Shimada, H. et al. The International Neuroblastoma Pathology Classification (the Shimada system). *Cancer* 86, 364-372 (1999).



APPENDICES

Dutch Summary

Nederlandse Samenvatting

Contributing Authors and Affiliations

List of Publications

Review committee

Acknowledgements – Woord van Dank

Curriculum Vitae Auctoris

NEDERLANDSE SAMENVATTING

Binnen de medische wetenschap worden nieuwe beeldvormingstechnieken veelvuldig onderzocht ter innovatie en verbetering van operaties. Enkele voorbeelden van nieuwe technieken die zijn ontwikkeld in het laatste decennium, zijn het gebruik van 3D printing en augmented reality. Deze technieken kunnen helpen bij het voorbereiden en plannen van een operatie. Ook fluorescentie geassisteerde chirurgie is een nieuwe, opkomende techniek welke het mogelijk maakt tijdens de operatie tumorweefsel te detecteren door kankercellen te laten oplichten. Beide voorbeelden zijn veelvuldig onderzocht bij volwassenen, maar nog nooit bij kinderen. Dit proefschrift beschrijft de toepassing van deze technieken voor het eerst in de kinderchirurgie.

Een operatie welke veel wordt uitgevoerd door de oncologische kinderchirurg is de resectie van de Wilms tumor. Wilms tumoren komen voor in de nieren van kinderen. De overlevingskans van kinderen met een Wilms tumor is > 90%. Veruit de meeste kinderen met een Wilms tumor, hebben een tumor in 1 van beide nieren. In dit geval wordt de totale nier verwijderd. Een kleine groep (5%) van deze kinderen krijgt echter een Wilms tumor in beide nieren. Bij deze kinderen kunnen niet beide nieren worden verwijderd, dus zal de chirurg altijd proberen de tumoren te verwijderen terwijl zij/hij zoveel mogelijk gezond nier weefsel spaart. Dit gaat vaker gepaard met complicaties tijdens en na de operatie, dan het verwijderen van de nier in zijn geheel. Wanneer patiënten in beide nieren tumoren hebben, gebeurt het ook vaker dat de tumor niet volledig kan worden verwijderd. Om de beste operatie-strategie te ontwikkelen per patiënt, creëerden we in **hoofdstuk 2** gepersonaliseerde, 3D geprinte modellen en augmented reality hologrammen van de nieren van patiënten met een Wilms tumor. Daarna vroegen we chirurgen of zij zich beter vonden voorbereid op de operatie vergeleken met de zwart-witte 2D afbeeldingen van een CT of MRI-scan. Uit dit onderzoek bleek dat de 3D modellen een toegevoegde waarde hadden voor het begrip van de kinderchirurgen op de gepersonaliseerde anatomie.

Een andere tumor die vaak voorkomt bij kinderen is de Neuroblastoom. Deze vaak zeer agressieve tumor komt voor bij ongeveer 7-10% van de kinderen met kanker en groeit vaak vanuit de bijnieren. De classificatie kan worden verdeeld van *laag risico* tot *hoog risico* waar de laag-risicopatiënten een goede overlevingskans hebben. De hoog-risicopatiënten hebben echter maar een 5-jaars overleving van < 50%. Deze kinderen krijgen een uitgebreide behandeling van chemotherapie, chirurgie, stamceltransplantatie, radiotherapie en sinds kort ook immunotherapie. Het volledig verwijderen van de tumor na chemotherapie lukt vaak niet aangezien de tumor langs slagaders en rondom organen kan groeien. Het is daarom een

uitdaging voor de chirurg om zoveel mogelijk tumorweefsel weg te halen, zonder al te veel schade aan gezonde organen te brengen. In **hoofdstuk 3** worden de meest voorkomende complicaties van neuroblastoomchirurgie in de afgelopen dertig jaar beschreven. De resultaten van dit hoofdstuk laten zien dat complicaties vaak niet, of zeer gevarieerd, worden beschreven in de literatuur. In dit hoofdstuk refereren we naar een gestandaardiseerde manier van het beschrijven van deze complicaties, om discrepanties in de literatuur te voorkomen en zo verschillende operaties en onderzoeken beter te kunnen vergelijken.

Fluorescentie-geassisteerde chirurgie is een techniek waarbij anatomische structuren of individuele cellen oplichten tijdens operaties. Hierbij wordt fluorescerend contrastmiddel toegediend aan de patiënt om de tumor te visualiseren en daarmee te laten oplichten. Dit kan aspecifiek door fluorescerend contrastmiddel te injecteren in bloedvaten of schildwachtklieren, of specifiek door het toedienen van fluorescerende antilichamen die specifiek binden aan receptoren op tumorcellen. Deze fluorescente middelen zenden een nabijinfrarode golflengte (650 en 800nm) uit en kunnen daardoor diep in weefsels penetreren (ongeveer 1cm). De aspecifieke methode bestaat al een decennium, maar de tumor-specifieke methode welke individuele kankercellen laat oplichten, is vrij nieuw en nog niet geïmplementeerd in de medische zorg. Voor kankersoorten die voorkomen bij volwassenen bestaan er een aantal specifieke contrastmiddelen, maar bij kinderen zijn deze tot voor kort niet onderzocht. In **hoofdstuk 4** beschrijven we het eerste tumor-specifieke fluorescente contrastmiddel binnen de kinderoncologische chirurgie. Hier wordt een fluorescente tracer aan een antilichaam gekoppeld, genaamd *dinutuximab-beta*, om neuroblastoomcellen te laten oplichten. *Dinutuximab-beta* bindt aan de GD2 receptor, een receptor die tot over expressie komt (lees: veel meer aanwezig is) in het merendeel van neuroblastoom cellen ten opzichte van gezonde cellen.

Een andere techniek die het laatste decennium een grote opmars heeft gemaakt, is het maken van organoiden. Organoiden zijn 3D groeiende mini-tumoren waarbij kanker op een patiënt-specifieke manier bestudeerd kan worden. Van de originele tumor van de patiënt wordt weefsel afgenomen, welke in het lab wordt opgekweekt tot levende tumoren in miniatuur. Hiervoor werden er voornamelijk gekloonde cellijnen gebruikt, waarbij de kenmerken van de originele tumoren niet altijd meer intact waren. Ook betrof het dan vaak 1 soort cel, waarbij in de organoiden er verschillende tumorcellen naast elkaar een organoid kunnen vormen. Met microscopische 3D (live) beeldvorming als aanvulling, kan de cellulaire organisatie van deze organoiden tot in de kleinste details worden afgebeeld. In **hoofdstuk 5** beschrijven we een gedetailleerd protocol hoe organoiden van verschillende vormen, grootte en origine in 3D afgebeeld kunnen worden met cellulaire resolutie.

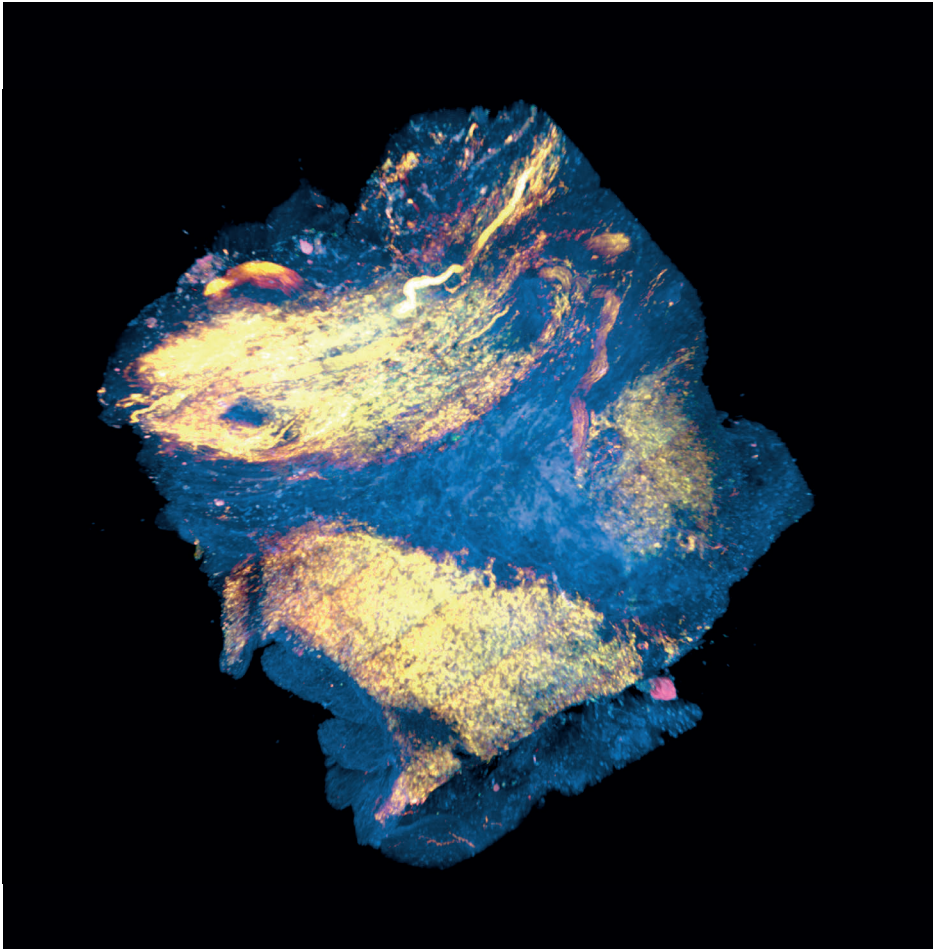
In **hoofdstuk 4** komen we er echter achter dat GD2 niet bij elke neuroblastoom tot expressie komt. Daarnaast staan neuroblastomen erom bekend om hun heterogeniteit aan verschillende soorten tumorcellen. Dit zou kunnen betekenen dat de fluorescente marker *dinutuximab-beta* dan alleen zal werken in een bepaalde subgroep van patiënten. Om deze potentiële variëteit in expressie te ondervangen, ontwikkelden we een gepersonaliseerde strategie om andere fluorescente tracers te testen in **hoofdstuk 6**. Hier testen we meerdere nieuwe tracers op neuroblastoom organoiden tegelijkertijd en creëerden daarmee een efficiënte pijpleiding voor de ontwikkeling van nieuwe fluorescente tracers, hopelijk in de toekomst toepasbaar op alle verschillende neuroblastoom tumoren.

Dit proefschrift onderzocht de mogelijkheid om nieuwe onderzoekstechnieken te implementeren in de kinderchirurgie met als doel het risico op complicaties te verkleinen. Basale laboratoriumtechnieken werden gebruikt om de klinische zorg te verbeteren. Om dit te bereiken, werkten biomedische wetenschappers zeer nauw samen met chirurgen. Om een brug te slaan tussen de basale wetenschap en de medische praktijk, was het van optimaal belang om goed te communiceren en samen te werken. Het oprichten van het Prinses Máxima Centrum maakte deze nauwe samenwerking tussen dokters en wetenschappers mogelijk.

Concluderend, 3D visualisaties, zoals 3D prints en augmented reality, hebben de potentie om de patiënt specifieke voorbereiding op chirurgie te verbeteren. Daarnaast kan fluorescentie geassisteerde chirurgie de resectie (het verwijderen) van neuroblastomen verbeteren en mogelijk de kans op complicaties verkleinen. Hier moet echter meer onderzoek naar gedaan worden om dit te bewijzen. De organoiden techniek en de 3D beeldvorming van deze mini-tumoren, kan hierbij helpen. Deze techniek kan naast neuroblastomen, ook toegepast worden op allerlei verschillende tumoren waardoor de ontwikkeling van andere fluorescente tracers ook mogelijk is. In de toekomst zal onderzoek zich moeten richten op het samenvoegen van deze technieken; het gebruik van augmented reality om tumoren tijdens de operatie met fluorescentie te visualiseren.

Kortom, om de chirurgie bij kinderen met kanker te verbeteren en de kans op complicaties te verkleinen, zijn twee punten van belang:

1. Nieuwe visualisatietechnieken moeten verder onderzocht worden om de chirurgie te verbeteren.
2. Samenwerking tussen wetenschappers en doktoren was in het genereren van de resultaten voor dit proefschrift essentieel en mogelijk gemaakt door de centralisatie van kideroncologische zorg in het Prinses Maxima Centrum.



Een gedeelte van een neuroblastoom tumor na chirurgie, waar de marker GD2 in het geel de neuroblastoomcellen kleurt. 40x vergroot.

CONTRIBUTING AUTHORS AND AFFILIATIONS

Princess Máxima Center for Pediatric Oncology, Utrecht, The Netherlands.

Department of Surgery

Ceder H. van den Bosch, MD, PhD candidate

Alida F.W. van der Steeg, MD, PhD

C.E.J. (Sheila) Terwisscha van Scheltinga, MD

Cornelis P. van de Ven, MD

Marc H.W.A. Wijnen, MD, PhD

Rios Research group

Cancer Genomics, Oncode Institute, Utrecht, The Netherlands

Maria Alieva, PhD

Hendrikus C.R. Ariese

Johanna F. Dekkers, PhD

Fatima de la Jara – Ortiz, Msc, PhD candidate

Hannah R. Johnson – Leferink

Anne C. Rios, PhD

Ellen J. Wehrens, PhD

Molenaar group

Waleed M. Kholosy, Msc, PhD candidate

Jan J. Molenaar, MD, PhD

Department of clinical oncology

Martha Fiocco, PhD

Martine van Grotel, MD, PhD

Marry M. van den Heuvel-Eibrink, MD, PhD

Department of Pathology

Ronald R. de Krijger, MD, PhD

Department of Radiology

Annemieke S. Littooi, MD, PhD

Leiden University Medical Center, Leiden, The Netherlands

The Molecular-Targeted Precision Surgery lab

Victor M. Baart, Msc
Shadvhi S. Bhairosingh
Marion M. Deken, MD
Ruben Houvast, Bsc
Cornelis F.M. Sier, PhD
Alexander L. Vahrmeijer, MD, PhD

**Hubrecht Institute, Royal Netherlands Academy of Arts and Sciences (KNAW) and
University Medical Centre (UMC) Utrecht**

Hans Clevers lab

Oncode Institute, Department of Cancer Research

Hans Clevers, MD, PhD
Huili Hu, PhD

University Medical Center Utrecht, Utrecht, The Netherlands

**Department of Pediatric Respiratory Medicine, Wilhelmina Children's Hospital
Regenerative Medicine Center Utrecht**

Jeff M. Beekman, MD, PhD
Annelotte M. Vonk, Bsc
Gimano D. Amatngalim, PhD

Molecular Cancer Research, Center for Molecular Medicine - Snippert group

Oncode Institute, Department of Cancer Research, Netherlands Cancer Institute.

Koen C. Oost, PhD
Hugo J.G. Snippert, PhD

Wilhelmina Children's Hospital, Utrecht, The Netherlands

Clinical Research Department

J. Tjomme van den Bruggen, MD, PhD
Florine N.J. Frakking, MD, PhD
Yvette G.T. Loeffen, MD

Radboud University Medical Center, Nijmegen, The Netherlands

3D lab Nijmegen

Thomas Maal, PhD
Jene W. Meulstee, Msc

CONTRIBUTING AUTHORS AND AFFILIATIONS

Maasstad Ziekenhuis, Rotterdam, The Netherlands

Department of Surgical Oncology

Annique M.M.J Pieters, MD, PhD

Walter and Eliza Hall Institute, Melbourne, Australia

Department of Medical Biology, The University of Melbourne, Australia.

Cancer Biology and Stem Cells Division

Jane Visvader, PhD

LIST OF PUBLICATIONS

Kholosy WM, Derieppe M, van den Ham F, Ober K, Su Y, Custers L, Schild L, van Zogchel LM, **Wellens LM**, Ariese HC, Szanto CL, Wienke J, Dierselhuis MP, van Vuurden D, Dolman E, Molenaar JJ. Neuroblastoma and DIPG organoid coculture system for personalized assessment of novel anticancer immunotherapies. *Journal of Personalized Medicine*. 2021 aug; Aug 30;11(9):869.

Wellens LM, Deken MM, Sier CFM, Johnson HR, de la Jara Ortiz F, Bhairosingh SS, Houvast RD, Kholosy WM, Baart VM, Pieters AMMJ, de Krijger RR, Molenaar JJ, Wehrens EJ, Dekkers JF, Wijnen MHWA, Vahrmeijer AL, Rios AC. Anti-GD2-IRDye800CW as a targeted probe for fluorescence-guided surgery in neuroblastoma. *Scientific Reports*. 2020 Oct 19;10(1):17667.

Dekkers JF, **Wellens LM**, Alieva M, Ariese HCR, Jamieson PR, Vonk AM, Amatngalim GD, Hu H, Oost KC, Snippert HJG, Beekman JM, Wehrens EJ, Visvader JE, Clevers H, Rios AC. High-resolution 3D imaging of fixed and cleared organoids. *Nature Protocols*. 2019 June;14(6):1756-1771.

Wellens LM, Meulstee J, van de Ven CP, Terwisscha van Scheltinga CEJ, Littooij AS, van den Heuvel-Eibrink MM, Fiocco M, Rios AC, Maal T, Wijnen MHWA. Comparison of 3-Dimensional and Augmented Reality Kidney Models With Conventional Imaging Data in the Preoperative Assessment of Children With Wilms Tumors. *JAMA Network Open*. 2019 April 5;2(4):e192633.

van den Bosch CH, van der Bruggen JT, Frakking FNJ, Terwisscha van Scheltinga CEJ, van de Ven CP, van Grotel M, **Wellens LM**, Loeffen YGT, Fiocco M, Wijnen MHWA. Incidence, severity and outcome of central line related complications in pediatric oncology patients; A single center study. *Journal of Pediatric Surg*. 2019 Sep;54(9):1894-1900.

Roorda D, Witvliet MJ, **Wellens LM**, Schulten DV, Sloots CEJ, de Blaauw I, Broens PMA, Oosterlaan J, van Heurn LWE, van der Steeg AFW. Long-term outcome and quality of life in patients with total colonic aganglionosis in the Netherlands. *Colorectal Disease*. 2018 Aug;20(8):719-726.

Kremer ME, **Wellens LM**, Derikx JP, van Baren R, Heij HA, Wijnen MH, Wijnen RM, van der Zee DC, van Heurn LW. Hemorrhage is the most common cause of neonatal mortality in patients with sacrococcygeal teratoma. *Journal of Pediatric Surgery*. 2016 Nov;51(11):1826-1829.

REVIEW COMMITTEE

Prof. dr. M.M. van den Heuvel

Professor of Translational Pediatric Oncology
Princess Máxima Center for Pediatric Oncology, Utrecht, The Netherlands

Prof. dr. I.H.M. Borel Rinkes

Professor of Surgical Oncology
University Medical Center Utrecht, The Netherlands

Prof. dr. N.D. Bouvy

Professor of Innovative Surgical Techniques
Maastricht University Medical Center, Maastricht, The Netherlands

Prof. M. van Egmond

Professor of Oncology and Inflammation
Amsterdam University Medical Center, Amsterdam, The Netherlands

Dr. M.P. van den Tol

Medical doctor in Surgical Oncology
Medical Center Leeuwarden, Leeuwarden, The Netherlands

WOORD VAN DANK

Dit proefschrift had onmogelijk tot stand kunnen komen zonder de hulp van velen. Een goede relatie is communicatie. Graag wil ik een aantal personen in het bijzonder bedanken.

Prof. dr. M.H.W.A. Wijnen, beste Marc, ons contact begon met een email en een week later een promotie-traject van vier jaar. Ik wil je bedanken voor al het vertrouwen dat je in mij hebt en voor de vrijheid en middelen die je me gaf om nieuwe projecten op te zetten. Je hebt me in contact gebracht met de grootste bollebozen van de kinderoncologie waardoor de samenwerkingen in dit proefschrift tot stand zijn gekomen. Dankjewel Marc, voor je humor, sarcasme, professorische wijsheden en af en toe gedateerde grappen waar ik dan hoofdschuddend op mocht reageren.

Dr.A.C. Rios, dear Anne, thank you for the amazing years and your patience in training me to become a scientist. With your strong passion for the beauty of science and your sparkling personality, you are a true inspiration for everyone that is lucky enough to get to work for you. Since day one, you encouraged me to explore science and surgery. You challenged my own capabilities to the maximum, which made me sometimes uncomfortable during the process, but in the end successful and stronger. Thank you for becoming my mentor and very close friend.

Dr.A.L. Vahrmeijer, beste Lex, veel dank voor mijn opname in het Greenlight team. Vanaf het eerste moment heb je me vol enthousiasme ontvangen (samen met prof. dr. **Koos** Burggraaf) en onbaatzuchtig begeleid als vijfde wiel in jullie hoogwaardige researchgroep waardoor het opnieuw-uitvinden-van-het-wiel mij bespaard is gebleven. Dank voor alle mogelijkheden in het LUMC, de gezelligheid met de Greenlighters in Amerika en alle gesprekken over de luchtvaartindustrie.

Leden van de beoordelingscommissie, **prof. dr. van den Heuvel**, **prof. dr. I. Borel Rinkes**, **prof. dr. N. Bouvy**, **prof. dr. M. van Egmond** en **dr. Dr. M.P. van den Tol**, hartelijk dank voor jullie interesse en de tijd die jullie genomen hebben in het beoordelingsproces van mijn onderzoek. Ik kijk ernaar uit om met jullie van gedachten te wisselen over de inhoud van dit proefschrift.

Dr. Ronald van Dam, **prof. dr. Ernst van Heurn**, **dr. Lideke van der Steeg**, **dr. Joep Derikx**, **dr. Marijke Kremer**, dank voor het aanwakkeren van mijn enthousiasme voor de (kinder)chirurgie tijdens mijn studentenjaren. Ik heb ontzettend veel geleerd van mijn tijd als student onderzoeker onder jullie hoede.

Prof. dr. J. Molenaar, beste Jan. Dank voor het vele Neuroblastoom-sparsessies en je onuitputtelijke energie en enthousiasme. Het was een feestje om met jou en **de Molenaargroep** te mogen samenwerken en de ANR in Australië te bezoeken. Tot op Lowlands!

Drs. C.P. van de Ven, Drs. C. Terwisscha van Scheltinga, Drs. C Hulsker, Lieve Kees, Sheila & Caroline. Veel dank voor jullie interesse en bijdrage aan dit proefschrift, en het mogen assisteren van operaties in de eerste fase van het Máxima. Jullie optimisme en humor binnen de chirurgie werkt zeer motiverend. Dank voor het gezellige samenwerken de afgelopen jaren!

Prof.dr. Thomas Maal & Jene Meulstee, dank voor al jullie hulp en expertise rondom de Hololens. **Dr. Annemiek Littooi**, dank voor je radiologische kennis en inzichten. **Prof. dr. Ronald de Krijger**, dank voor alle scholing en hulp rondom het pathologisch classificeren van neuroblastomen. **Dr. Annique Pieters**, dank voor de chirurgische tips voor een cel-biologische promotie, de perfecte hulp tijdens mijn start in het Prinses Maxima Centrum.

Beste **Kika** en **Villa Joep**, dank voor het vertrouwen en de financiering van de projecten in dit proefschrift.

Rios group, Dream-team, heart and braino's, many thanks for all your patience and all that you taught this medical doctor. Everything you do has clinical relevance and I hope we can connect the science and surgery for a very long time together. **Maria**, thank you for coaching me in my first imaging experiments and your trust on leaving me Celine Dion style (all by myself) during our first mice surgery. **Ravi**, thank you for your patience on how to use the 880 and explaining it about 880 times again. **Riri**, thank you for teaching me how to make washing buffers and especially to not forget putting them back in the fridge. **Hannah**, thank you for all your wisdom on the mice trainings. Your wedding was one of the highlights of my Phd-time. **Ellen**, word-magician, if I had quotes in this thesis, one of them would be that every PhD student deserves an Ellen. Thank you for upgrading my written sentences. **Fati-fati-flow**, thank you for all studentic enthusiasm, and making me even more feministic. **Gerard**, thank you for all your dedicated hard work.

Onderzoekers van de Wijnen groep, **Bernadette, Merel, Matthijs, Tim, Myrthe**, en ook **Floor**, veel dank voor jullie gezelligheid! **Lieve Ceder**, dank voor je aanstekelijke enthousiasme, dat je mijn eerste student wilde zijn en we dat heel snel inwisselden voor een ongelooflijk vrolijke en hopelijk levenslange vriendschap. **Lieve Bas**, ik mis onze Amsterdamse koffie's nu al. Veel dank voor je vriendschap die we hebben overgehouden aan afgelopen jaren & de goede gesprekken. We vechten nog wel uit

wie er burgemeester van Amsterdam wordt. Lieve **Michelle**, ook eigenlijk onderdeel van alle gezamenlijke onderzoeksgroepen, dank voor je vriendschap en je lieve, attente en creatieve support. Je wordt een fantastische kinderarts. Ik weet het zeker!

Greenlight team, uit het LUMC, veel dank voor jullie adoptie in de groep en de introductie in de wondere wereld van de image-guided surgery. Dank ook voor alle mooie avonden aan de andere kant van de oceaan op de WMIC. **Marion & Hein** in het bijzonder. Zonder jullie enthousiasme, lering en het en aan-de-hand-nemen was een groot deel van dit proefschrift niet geschreven. **Kees, Victor & Shadhvi**, onwijs veel dank met de hulp rondom het koppelen en onderzoeken van de fluorescente markers vanuit het LUMC.

Allerliefste en beste vrienden & huisgenoten van de hele wereld, dank voor jullie ongeëvenaarde interesse, sociale opvang, borrels, bubbel-momenten, schouders-om-op-te-huilen, knuffels, grappen en steun de afgelopen jaren! Ik ben ongelooflijk dankbaar voor zo'n mooie groep mensen die ik mag liefhebben en die mijn wereld zo vrolijk en gezellig maakt. **Lieve Audrey**, dank voor je fantastische, onvoorwaardelijke, blijde, vreugdevolle vriendschap en emotionele cheerleading de afgelopen jaren, en voor de hulp met het doorlezen van mijn stukken en grants. **Lieve Bar**, dank voor alle submitted-bubbels die we samen hebben opengemaakt, snel voordat de artikelen weer werden afgewezen, en voor het samen aangaan van de New York Kika Marathon. **Lieve Pien & Pam**, dank voor de gedeelde-smart-is-halve-smart-werksessies in de woonkamer. **Liz, Kifah, Hein, Kim, Ded, Fabiola, Jordana, Lavinia & Lena** dank voor de feestelijke momenten, vakanties, weekenden weg en de zeer zeer welkome ontspanning tijdens dit traject.

Daarnaast wil ik iedereen bedanken die heeft geholpen aan het feestelijk en sprankelijk maken van mijn leven als onderzoeker. **Lieve onderzoekers** van het Maxima, **promovendi, assistenten** en **stafleden** van het **UMC Utrecht**, onderzoekers van de **AmsterdamUMC Oncogenomics** met in het bijzonder de mannen van **R2** en **Peter van Sluis**, assistenten & stafleden van **het Meander**, Carpoolgroep '**de Vroem Vroem-ers**', cabaret en band van het **regio V Cinque du Soleil Cabaret**, veel dank voor alle gezellige momenten. Dank aan de **Jaap Eden baan**. Dank **Anass** voor het oneindig afbreken van Eva en mij, samen met alle trainers van en bij **Eastbound**. **Badeta** koffiebranders voor alle shotjes additionele energie. **Cafe Buhrs**, voor alle Ajax wedstrijden op groot scherm. **Dirty Needles** en **Blues zweet en tranen**, dank voor de muzikale hoogtepuntjes. **Thijs Sins**, dank voor al je reflectie en filosofische wijsheden. **Paul Rigter** en AVROTROS, dank voor het zeer mooie vastleggen van mijn onderzoek. Zonder al deze extraatjes waren de afgelopen 5 jaar een saaie bedoening geweest.

Lieve Paranimfen Florijn & Eva, dankjulliewel dat jullie op 11 maart 2022 aan mijn zijde willen staan. **Lieve Flop**, je bent mijn grootste inspiratie binnen de wetenschap. Ik bewonder je intelligentie, je analytisch vermogen en je efficiëntie. Je werk combineer je met veel passie voor het klimaat, humor en uitzonderlijke anatomische tekenkunsten. Je bent een verademing tussen alle biologische (veelal mannelijke) wetenschappers en ik wil je onwijs bedanken voor al je hulp de afgelopen jaren. Ik ben er trots op jou als vriendin te mogen rekenen. **Lieve Eef**, dank voor al het filosofische sparren over de chirurgie, alle fijne sportsessies en alle grote levensevents die we met elkaar mogen delen. Ik bewonder je humor (vooral de woordgrappen), je rechtvaardigheid, je loyaliteit, je avontuurlijke instelling en ik kijk uit naar oneindig veel jaren heerlijke vriendschap.

Lieve Car & Rob, dank voor alle fijne gesprekken aan de eettafel in Loosdrecht en politieke uitleg over het systeem der wetenschap en ziekenhuizen. Jullie liefdevolle adviezen en vertrouwen voelt alsof ik me rijk mag rekenen met een extra paar ouders. Dank Rob, voor je bereidheid mijn stukken te bekritisieren waardoor alles net wat (lees: heel veel) beter en gestructureerder werd. Pas als een stuk langs jou was gegaan, had ik het vertrouwen dat ik niets gemist had. Dank voor al je vertrouwen en mogelijkheden die je me hebt laten inzien.

Lieve Mariska & Henk, dankjewel dat jullie me zo welkom laten voelen in de familie. Dank ook aan **Eva, Jaco, Sven en Daniël** voor alle fijne dagen samen.

Lieve Eline & Lieuwe, dank voor jullie bijstand en oprechte belangstelling. Ik hoop dat we heel snel samen dit proefschrift kunnen vieren Pien! **Mart & Sas**, dank voor jullie gekkigheid en warme aandacht. **Lieve oma**, dank voor alle lieve zorgen!

Lieve Bart & Emma, dankjulliewel voor alle gezelligheid die we samen als gezin mogen ervaren en dat ik altijd met mijn kletspraat bij jullie terecht kan. **Lieve Bro**, ik zeg het je niet vaak genoeg, maar je bent een grote inspiratiebro(n) voor me en ik bewonder je relaxte, rechtvaardige en stabiele levensstijl. Ik ben trots op je.

Lieve ouders, Harry & Hedwig, wat mogen Bart en ik ons gelukkig prijzen dat we van alle ouders ter wereld juist jullie hebben gekregen. Jullie leerden me dat ik alles wat ik maar wil kan bereiken en stonden altijd op drie plekken klaar om me te aan te moedigen. Wanneer het iets te zwaar werd voor de schouders onder dit rode haar, remden jullie me vaak net op tijd af. Ik ben ontzettend dankbaar met jullie liefde en steun. **Dit proefschrift is voor jullie.**

Allerliefste Tim, dankjewel voor alles wat je bent en wat ik voor jou mag zijn. De heerlijke tijd die we hebben, staat hopelijk model voor wat we allemaal nog mogen meemaken.

CURRICULUM VITAE

After obtaining her medical degree, Lianne started as a PhD candidate at the Princess Máxima Center focusing on new imaging strategies that could improve surgery in pediatric oncology, under the supervision of Professor Marc Wijnen. She organized an ongoing collaboration with Anne Rios, molecular biology imaging specialist, and Alexander Vahrmeijer, leader of the image-guided surgery group from the Leiden University Medical Center. For her work, she received two major grants from the Villa Joep foundation for Neuroblastoma research and the Children Cancer Free foundation, known as KiKa. In 2019 Lianne's work got selected to join the 22nd workshop on Methods in Clinical Cancer Research (MCCR) to create a clinical trial design based on her study results.



During her PhD, Lianne developed a special interest in science communication. In 2017 she won the Breaking Science Competition from the University of Utrecht and participated in the (inter)national science pitch competition Fame Lab, from the British Embassy. In 2018, she became a writer for the Faces of Science of the Royal Netherlands Academy for Arts and Sciences (KNAW). In the summer of 2018, a documentary was broadcasted on Dutch NPO1 by AVROTROS where the work of Lianne was recorded for one year. In 2020, Lianne started working as a resident not-in-training at the department of surgery at the Meander Medical Center (Amersfoort). She is currently working as a surgical resident not-in-training at the University Medical Center Utrecht.

In her spare time, Lianne loves to make music and to practice sports with friends. She finished the New York Marathon in 2017 for KiKa. Lianne is currently living in Amsterdam.

